**PETROLOGY OF THE PHLOGOPITE-BEARING
ULTRAMAFIC-MAFIC PLUTONIC ROCKS
WITHIN CENTRAL ANATOLIAN CRYSTALLINE COMPLEX, TURKEY**

**A THESIS SUBMITTED TO
THE GRADUATE SCHOOL OF NATURAL AND APPLIED SCIENCES
OF
THE MIDDLE EAST TECHNICAL UNIVERSITY**

BY

FATMA (TOKSOY) KÖKSAL

IN PARTIAL FULFILLMENT OF THE REQUIREMENTS FOR THE DEGREE OF

DOCTOR OF PHILOSOPHY

IN

THE DEPARTMENT OF GEOLOGICAL ENGINEERING

AUGUST 2003

Approval of the Graduate School of Natural and Applied Science.

Prof. Dr. Canan ÖZGEN
Director

I certify that this thesis satisfies all the requirements as a thesis for the degree of Doctor of Philosophy.

Prof. Dr. Asuman G. TÜRKMENOĞLU
Head of Department

This is to certify that we have read this thesis and that in our opinion it is fully adequate, in scope and quality, as a thesis for the degree of Doctor of Philosophy.

Prof. Dr. Roland OBERHAENSLI   Prof. Dr. M. Cemal GÖNCÜOĞLU
Co-Supervisor   Supervisor

Examining Committee Members

Prof. Dr. M.Cemal GÖNCÜOĞLU

Prof. Dr. Roland OBERHAENSLI

Prof. Dr. Asuman G. TÜRKMENOĞLU

Assoc. Prof. Dr. Cüneyt ŞEN

Assoc. Prof. Dr. M. Kenan YALINIZ

ABSTRACT

PETROLOGY OF THE PHLOGOPITE-BEARING
ULTRAMAFIC-MAFIC PLUTONIC ROCKS
WITHIN CENTRAL ANATOLIAN CRYSTALLINE COMPLEX, TURKEY

(TOKSOY) KÖKSAL, Fatma

Ph.D., Department of Geological Engineering
Supervisor: Prof. Dr. M. Cemal Göncüoğlu
Co-Supervisor: Prof. Dr. Roland Oberhaensli
August 2003, 274 pages

The aim of this study is to define mineralogical and geochemical characteristics of phlogopite-pargasite enriched ultramafic-mafic cumulate rocks from Kurançalı (Kırşehir) and their implications for petrology and regional geological setting.

The Kurançalı rocks, found within an allochthonous sliver, are representative for the isolated members of the Central Anatolian Ophiolites, derived from closure of İzmir-Ankara-Erzincan branch of Alpine Neotethys. The rocks overthrust the Metamorphic Ophiolitic Mélange (the uppermost part of the Central Anatolian Metamorphics) and cut by felsic dykes of the Late Cretaceous Central Anatolian Granitoids.

The Kurançalı rocks are unusually enriched in phlogopite and pargasite with varying crystal sizes. They are also composed of diopsidic augite, plagioclase, rutile, ilmenite, sphene, apatite and pyrite. The rocks are divided into six types;

clinopyroxenite, clinopyroxenite-with-hydrous minerals-plagioclase, phlogopitite, hornblendite, layered gabbro and diorite.

Evaluation of detailed EMP data from constituent minerals of different rock types showed that phlogopite with high Fe^{2+}-Fe^{3+}-$Al^{[6]}$-Ti, diopsidic-augite with high Ca-$Al^{(t)}$-Ti, Si-undersaturated pargasite with high $Al^{[4]}$-K-Na-Ti-contents and intercumulus plagioclase with a wide range of composition (an%=40.61-98.58) display unusual compositions. Substitution mechanisms and elemental variations of the minerals suggest crystallization from hydrous metasomatized mantle, high water pressure and oxygen fugacities during formation of the Kurançalı rocks.

Major oxide, trace and rare earth element abundances of the rock units were used to evaluate petrological characteristics. Chemical and tectonic discrimination diagrams, and parallel multi-element and REE patterns with highly enriched in LILE and LREE relative to HREE and HFSE show strong calc-alkaline affinity with slight alkaline features. Troughs at Nb-Ta and Ti characterize the rocks but these elements are slightly enriched than N-MORB. The rocks show high LREE/HREE ratios.

Both unusual mineralogical and geochemical features of the rocks show that the rocks were generated in an arc environment. Moreover, they require a mantle wedge source strongly influenced by metasomatic components (fluid/melt) derived from subducting slab and/or OIB-like alkaline melt.

Comparison of the rocks with tectonically well-defined rocks displays that they are generated in an intra-oceanic arc environment, but owe a comparison with fore-arc back-arc Central Anatolian Ophiolites within supra-subduction zone environment revealed that Kurançalı rocks are different and generated in an arc basement.

Keywords: Kurançalı, phlogopite, pargasite, mafic-ultramafic cumulates, mineral chemistry, geochemistry, petrology, intra-oceanic arc, mantle metasomatism.

ÖZ

**ORTA ANADOLU KRİSTALEN KOMPLEKSİNDEKİ
FİLOGOPİTLİ ULTRAMAFİK-MAFİK PLUTONİK
KAYAÇLARIN PETROLOJİSİ, TÜRKİYE**

(TOKSOY) KÖKSAL, Fatma

**Doktora, Jeoloji Mühendisliği Bölümü
Tez Yöneticisi: Prof. Dr. M. Cemal Göncüoğlu
Ortak Tez Yöneticisi: Prof. Dr. Roland Oberhaensli
Ağustos 2003, 274 sayfa**

Bu çalışmanın amacı Kurançalı (Kırşehir) bölgesindeki filogopit ve pargasitçe zenginleşmiş ultramafik-mafik kumulat kayaçlarının mineralojik ve jeokimyasal karakterlerini belirleyerek petrolojik ve bölgesel jeolojiye katkılarını araştırmaktır.

Tektonik dilim içersinde bulunan Kurançalı kayaçları, Alpin Neotetis'inin İzmir-Ankara-Erzincan kolunun kapanması sırasında türeyen Orta Anadolu Ofiyolitlerinin izole birimlerinden birini temsil eder. Kumulat kayaçlar Orta Anadolu Metamorfiklerinin en üst kısmı olan Metamorfik Ofiyolitli Melanjını tektonik dokanakla üzerlemiş ve Orta Anadolu Granitoyidlerine ait felsik dayklar bu iki birimi kesmiştir.

Kurançalı kayaçları, yaygın olmayan bir şekilde değişken kristal boyutlarında filogopit ve pargasitçe zenginlik sunarlar. Kayaçlar ayrıca diyopsidik ojit, plajiyoklas, rutil, ilmenit, sfen, apatit ve pirit içermektedirler. Kayaçlar altı gruba

ayrılmıştır: klinopiroksenit, sulu mineraller ve plajiyoklaslı klinopiroksenit, filogopititit, horblendit, tabakalı gabro, diyorit.

Minerallerin detaylı EMP verilerinin değerlendirilmesi, filogopitin yüksek Fe^{2+}-Fe^{3+}-$Al^{[6]}$-Ti bileşimli, diyopsidik ajutin yüksek Ca-$Al^{(t)}$-Ti bileşimli, Si-fakir pargasitin yüksek $Al^{[4]}$-K-Na-Ti içerikli ve interkumulus plajiyoklasın geniş kompozisyonal aralıklı (an%=40.61-98.58) özellikleri ile olağan olmayan içerikler sergilediklerini göstermiştir. Yerdeğişim vektörleri ve element değişim diyagramları Kurançalı kayaçlarının yüksek su basıncı ve oksijen fugasitesi etkisi altında sulu metasomatizmaya uğramış kaynaktan türediğini göstermiştir.

Kayaçların ana, iz ve nadir toprak element içerikleri petrolojik özellikleri belirlemek için kullanılmıştır. Kimyasal ve tektonik tanımlama diyagramları, ve HFSE ve HREE'ye göre zenginlik gösteren LILE ve LREE ile karakterize olan birbirine parallel çoklu element değişim ve REE profilleri zayıf alkalin karakterde kalk-alkalin özellik gösterirler. N-MORB'a göre hafif zenginlik sunan kayaçlar Nb-Ta ve Ti'ce diğer elementlere göre fakirdirler. Kayaçların LREE/HREE oranları yüksektir.

Mineralojik ve jeokimyasal veriler, kayaçların yay bölgesinde gelişmiş olduğunu göstermektedir. Bununla birlikte kayaçların, batan dilimden türeyen metasomatik akışkan/ergiyik ve/veya OIB-tipi alkalin ergiyik tarafından etkilenmiş manto kaması kaynak kayasından türediğini ortaya koymuştur.

Kayaçların, tektonik ortamları iyi tanımlanmış kayaçlar ile yapılan karşılaştırmaları okyanus içi yay bölgesinde geliştiklerini gösterirken, dalma-batma zonu bölgesinde gelişen, yay-önü yay-arkası Orta Anadolu Ofiyolitleri ile yapılan karşılaştırmalar Kurançalı kayaçlarının farklı özellikler sunduğunu ve yay baseninde geliştiğini ortaya koymuştur.

Anahtar Kelimeler: Kurançalı, filogopit, pargasit, mafik-ultramafik kumulatlar, mineral kimyası, jeokimya, petroloji, okyanus içi yay, manto metasomatizması.

To my husband Serhat KÖKSAL

ACKNOWLEDGMENTS

TABLE OF CONTENTS

LIST OF TABLES

TABLE

LIST OF FIGURES

FIGURE

xvii

xix

xx

LIST OF ABBREVIATIONS

ROCKS:

clinopyroxenite	CPXnite
clinopyroxenite with hydrous minerals and plagioclase	CPXnite WHMP
phlogopitite	PHLtite
hornblendite	HBdite
layered gabbro	LG
diorite	DIO

MINERALS:

acmite	ac
actinolite	act
aegerine	ae
albite	ab
aluminum pargasite	Al-parg
amphibole	amph
andesine	and
annite	ann
anorthite	an
apatite	ap
augite	aug
barite	bar
biotite	bio
bytownite	by
calcite	cc
carbonate	carb
Ca-tschermak pyroxene	cats
celadonite	cel
celestite	cels
chlorite	chl
clinopyroxene	cpx
diopside	di

dolomite	dol
eastonite	east
eckermannite	ek
edenite	ed
enstatite	en
epidote	ep
esseneite	es
feldspar	feld
ferrosilite	fs
fluorite	fl
garnet	gr
glaucophane	gl
hastingsite	hs
hedenbergite	hd
hematite	hem
hornblende	hb
ilmenite	İlm
jadeite	jd
jadeite	jd
jervisite	je
johannsenite	jo
kaersutite	kaer
kaonite	ka
K-feldspar	K-feld
kosmochlor	ko
labradorite	labr
leucite	leu
magnetite	mt
Mg-tschermakite pyroxene	Mgts
muscovite	musc
Na-Ti tschermakite	Nat
Na-Ti-Al tschermakite	Natal
olivine	ol
orthoclase	orth

orthopyroxene	opx
pargasite	parg
periclase	peric
petedunnite	pe
phengite	phen
phlogopite	phl
plagioclase	plag
pumpellyite	pump
pyrite	pyr
pyroxene	py
quartz	qt
rhodonite	rhon
richterite	rich
richterite	rc
riebeckite	rb
rutile	rt
sanidine	san
sericite	ser
siderophyllite	side
sphene	sph
spinel	sp
Ti-Al tschermakite	Tal
tremolite	tr
tschermakite	ts
tugtupite	tugt
ursinite	ur
vermiculite	verm
wollostonite	wo
zircon	zrc

I hereby declare that all information in this document has been obtained and presented in accordance with academic rules and ethical conduct. I also declare that, as required by these rules and conduct, I have fully cited and referenced all material and results that are not original to this work.

CHAPTER 1

INTRODUCTION

1.1. Purpose and Scope

Geology of Turkey occupies a critical segment in the Alpine-Himalayan orogenic system. Series of narrow oceanic seaways and microcontinents, developed during fragmentation of the northern part of Gondwana during early Mesozoic, were largely closed by convergence of Africa and Eurasia during Late Cretaceous (Robertson, 2002 and references therein). An allochthonous ophiolitic assemblage derived from İzmir-Ankara-Erzincan branch of the Alpine Neotethys crops out in central Turkey. The assemblage (Central Anatolian Ophiolites (CAO), Göncüoğlu et al., 1991, 1992), in overall, has been investigated as product of an intra-oceanic subduction zone during the closure of the İzmir-Ankara-Erzincan seaway (e.g. Yalınız et al., 1996, 2000a; Floyd et al., 2000). Despite the more or less ordered ophiolitic bodies with preserved magmatic pseudostratigraphy (e.g. Sarıkaraman Ophiolite, Yalınız et al., 1996, 1999, 2000b; Floyd et al., 1998; and Çiçekdağ Ophiolite, Yalınız et al., 2000a), many ultramafic and mafic plutonic units also occur as isolated outcrops (Yalınız and Göncüoğlu, 1998; Göncüoğlu et al., 1998).

Ultramafic-mafic plutonic rocks exposed as an allochthonous unit in the Kurançalı area (Kaman-Kırşehir) differ from other ultramafic and mafic rocks of the CAO by their mineral contents (Toksoy, 1998). The rocks from the Kurançalı area are characterized by unusual enrichment in hydrous minerals,

phl and parg. The rocks are also composed of cpx, plag as major minerals, and rt, ilm, sph, ap, pyr as accessory phases.

Several studies suggest that occurrence of phl and parg is generally due to mantle metasomatism caused by silica-rich fluids or hydrous melts, derived from the subducting slab and/or the hanging wall mantle in a subduction zone environment (e.g. Sekine and Wyllie, 1982; Hawkesworth and Norry (eds.), 1983 and references therein; Arculus, 1994 and references therein; Johnson et al., 1996 and references therein; Brandon et al., 1999, Zanetti et al., 1999). These studies were mainly focused on phl-bearing xenoliths in volcanic rocks, whereas, the hydrous minerals found in the Kurançalı area are not from volcanic xenoliths but they occur in well-exposed ultramafic-mafic plutonic rocks within a tectonic sliver. Moreover, these minerals are pegmatitic in size unlike many other occurrences. Considering their proposed tectonic setting in previous studies, the Kurançalı rocks may provide a rare opportunity to investigate the compositional effects imparted to mantle lithosphere by subduction-derived components in a compressional environment.

A further question is whether subduction mechanism is developed within oceanic or continental environment. In previous studies (Kadıoğlu, 1996; Kadıoğlu and Güleç, 1996; Kadıoğlu et al., 1998; Güleç and Kadıoğlu, 1998; Yılmaz-Şahin and Boztuğ, 1997; Erdoğan et al., 1996; Tüysüz and Dellaloğlu, 1995) it has been suggested that continental arc related granitoids and gabbroic rocks were formed by subduction of Neotethyan oceanic lithosphere beneath the continental crust of the Kırşehir Block. Regional geology constraints, described in detail by Göncüoğlu et al. (1992, 1998) and overall geochemical features of the CAO units (e.g. Yalınız et al., 1996, 2000a; Floyd et al., 1998, 2000) argue against a continental arc origin and favour a supra-subduction zone (SSZ) origin developed during closure of İzmir-Ankara-Erzincan branch of Neotethys. However, remarkable differences in the geochemical characteristics of different isolated outcrops suggest differences in the source area and tectonic setting within intra-oceanic subduction.

Nevertheless, occurrence of phl and parg does not alone put constraints for source or process because phl does not only originate in metasomatized mantle in a subduction zone environment, but also crystallize from intraplate continental alkaline basaltic and carbonatitic melts (e.g. Waters and Erlank, 1988; Beard et al., 1996; Verhulst et al., 2000; Morbidelli et al., 1995; Larsen and Rex, 1992; Dalton and Presnall, 1998). Therefore, the phl-parg enriched Kurançalı rocks were chosen to contribute for a better understanding of the processes and products of these very complex mechanisms. The aim of this thesis is to define the composition and origin of the phl-parg enriched ultramafic-mafic plutonic rocks from Kurançalı, and their implications for regional geology. The hydrous plutonic rocks seem to illustrate an unusual phenomenon of metasomatism. The main points to be addressed are; (1) which kind of metasomatic processes pervasively enriched the source in incompatible elements, and resulted in SiO_2 undersaturation, Al_2O_3-CaO-alkali-TiO_2 enrichment in both mineral and whole-rock chemistry, (2) the origin and composition of the metasomatic agent(s).

For this purpose, this thesis mainly concerns mineralogy of the constituent phases and whole-rock geochemistry, and their implications for petrology and tectonic setting from which metasomatic component was derived. The layout of the thesis is given as below:

- Introduction (Chapter 1) including purpose and scope, geographic setting, method of study and a review of metasomatism.

- Geology (Chapter 2) comprises of a review of regional geological setting of ophiolites in central Anatolia, and geology of the Kurançalı area.

- Petrography (Chapter 3) mentioning textural and mineralogical features of the studied rocks.

- Mineral Chemistry and Petrogenetic Implications (Chapter 4) including mineralogical features of the constituent phases of the rocks, nomenclature of

the minerals, their implications on petrology, tectonic setting and physicochemical conditions, and their geothermobarometric constraints.

- Whole-Rock Chemistry and Petrogenetic Implications (Chapter 5) interpreting major and trace element characteristics of the studied rocks and their implications.

- Discussion on the Geneses of the Kurançalı Rocks (Chapter 6) based on mineralogical and whole-rock geochemical characteristics implying metasomatism in mantle wedge, source of metasomatizing component, and their indications on tectonic setting and regional geological setting.

- Conclusions (Chapter 7) summarizing the results of the study.

1.2. Geographic Setting

The study area is just at south of the Kurançalı town of Kırşehir. It is located in J31-b3 quadrangle of the 1:25 000 scaled topographic map of Turkey within latitudes 39°17'41"-39°19'17" N and longitudes 33°53'33"-33°55'39" E in the central Anatolia (Figure 1).

Traveling from Ankara to Kurançalı town is easy along Ankara - Kırıkkale - Keskin - Akpınar - Sofular - Kurançalı or Ankara - Kırıkkale - Keskin - Hamitköy - İsahocalı - Sofular - Kurançalı with a distance of about 180 km. The distance of the town to Kırşehir is about 43 km.
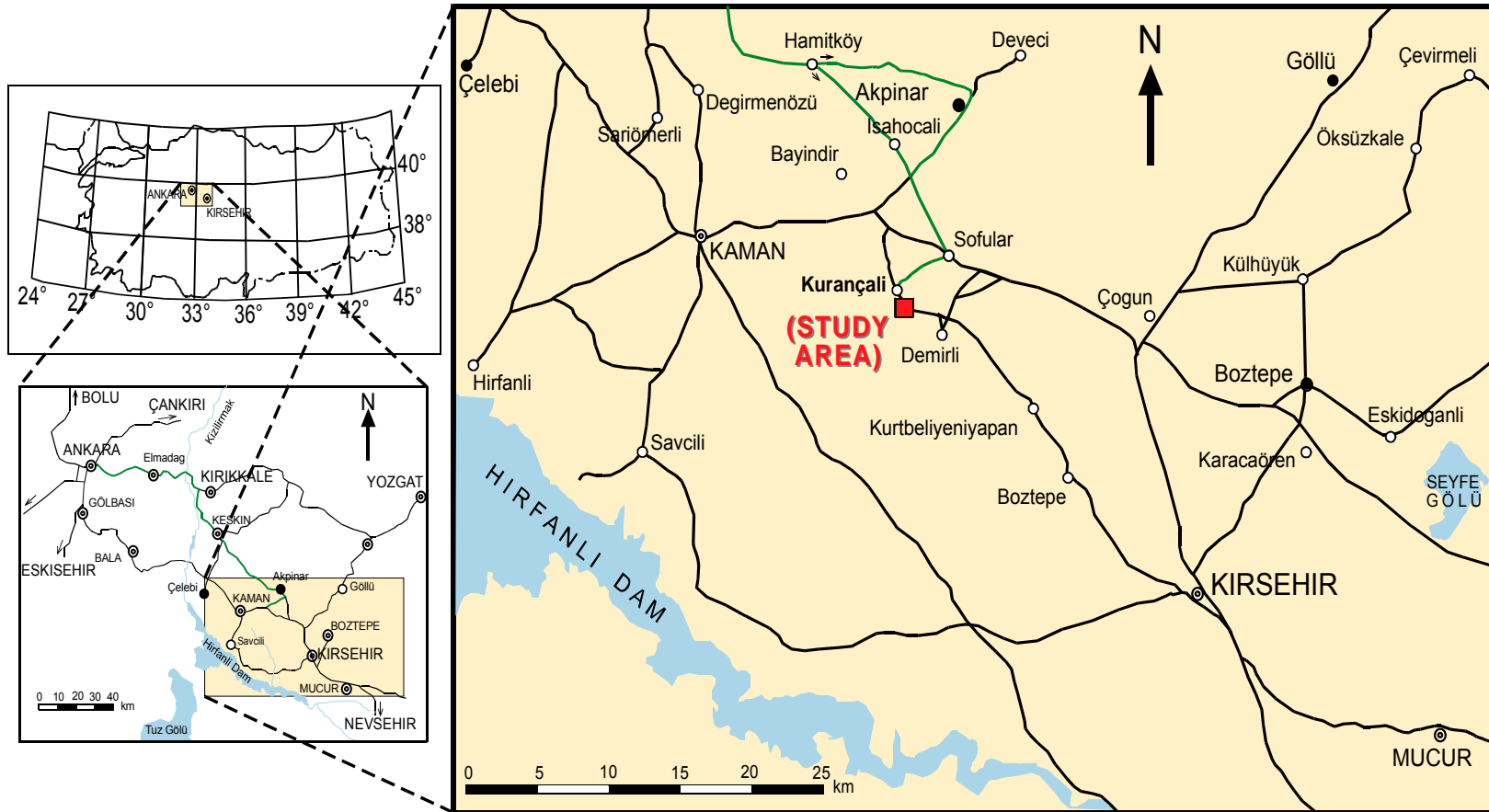
Figure 1. Location map of the study area.

1.3. Methods of Study

This study was mainly performed in two major steps; field and laboratory studies.

1.3.1. Field Work

The field work was mainly performed for sampling from the ultramafic-mafic plutonic rocks in the study area since geological mapping was previously done on the 1:25 000 scale topographic map of Kırşehir sheet by Toksoy (1998).

1.3.2. Laboratory Work

68 samples of hydrous phases-rich mafic-ultramafic plutonic rocks were collected from the Kurançalı body. Size of the samples was a function of the crystal size varying from millimetric to pegmatitic size, i.e. the greater crystal size, the greater sample size up to 2-3 kg. At least 2-3 slices for petrographic thin sections, polished-thin sections were cut off from each sample. Representative pieces of the samples were kept for further reference and the rest of the samples were crushed and powdered for geochemical analysis. Petrographic thin sections of all samples were studied using transmitting light microscopy.

1.3.2.1. Mineralogical Analyses

Major and minor element compositions of the minerals of the concerned mafic-ultramafic plutonic rocks were determined by using non-destructive in-situ microanalysis method, electron microprobe (EMP). 45 mm x 27 mm size of the polished-thin sections for the analyses were prepared at Institut für Geowissenschaften, Universitat Potsdam, Germany. Coating of well-polished sections with a 20 nm layer of carbon and the analyses were carried out at

GeoForschungsZentrum Potsdam (GFZ), Germany. The analyses on the minerals including major rock forming minerals, accessories, subsolidus and alteration product minerals, were performed for ca. 3000 points using a fully automated CAMECA SX-100 electron microprobe. The instrument, operating in wavelength-dispersion mode, was accelerated to 15 kV electron-beam at 20 nA beam current for all minerals except for ap. The beam current used for ap was 10 nA. The applied beam (spot) size was 5 µm for py, amph, mica, ep, oxides; and 10 µm for feld, carb and ap. Variable beam diameters from 10 µm to 30 µm on the glassy material of the quenched magmatic enclave from HBdite were applied to get accurate compositions.

A variety of natural and synthetic standards were used for calibration. The following elements of silicates, oxides and sulphides have been analyzed using the standards: Fe_2O_3 for Fe; NiO for Ni, di and wo for Ca and Si; orth and san for K and Al; rt for Ti; Cr_2O_3 for Cr; rhod for Mn; ab for Na; di, peric SCOli, MgO for Mg; fl for F; $SrSiO_3$ for Sr; Bora, tugt for Cl; bar for Ba; YPO_4 for P. The standards used for carbonate analyses are; Fe_2O_3 for Fe; $Ca_1C_1O_3$ for Ca; rhod for Mn; ab for Na; dol for Mg; $SrSiO_3$ for Sr; $BaAl_2Si_2O$ for Ba. The compositions of ap are determined using the following standards; Fe_2O_3 for Fe; di for Ca and Si; rhod for Mn; ab for Na; di for Mg; fl for F; cels for Sr; Bora for Cl; bar for Ba; YPO_4 for P and Y; $CePO_4$ for Ce; $LaPO_4$ for La. Matrix corrections were performed by the PAP procedure in the CAMECA software.

$K_2Cr_2O_7$ titration method was applied on mica separates to determine Fe^{2+} and Fe^{3+} of mica since the iron value obtained by EMP represents the total FeO. 8 samples were ground in an agate mortar, and sieved to the range of 63-150 µm. Mica was separated from rest of the rock samples by use of frictional electricity feature of mica on paper. Last purification was done by hand picking under binocular microscope. At the end of separation, 100% pure mica samples were obtained. After completing purification, samples were reground to <63 µm to use in $K_2Cr_2O_7$ titration method at Institut für Geowissenschaften, Universitat Potsdam. Measurements were done after dissolution of the separates at room temperature in HF and oxidation with NH_4VO_3.

1.3.2.2. Whole-Rock Analyses

Whole-rock samples for the chemical analyses were chosen after examining the thin sections of the samples in terms of mineralogical compositions, very low grade metamorphism and degree of iron oxidation due to surface alteration. 52 representative and fresh samples (50 ultramafic, 1 layered gabbro and 1 diorite) were selected for analysis. Since the rocks in concern are too variable from fine-grained to pegmatitic in size, at least 600-800 g of hand specimens were used for whole-rock analyses to provide homogenization and to represent the lithologies in the best way. The rock samples were crushed and ground at the Department of Geological Engineering of Middle East Technical University. Firstly samples were crushed to small chips, less than 1 cm size, in a Spex 4200 model jaw crusher. Altered chips were eliminated by hand picking, then the rest of the samples were ground in Bico LC-115 shatter box and sieved to grain size of less than 63 μm. The sample powder was dried at 105°C overnight before all analyses.

Compositions of the whole-rock samples including major, minor and trace elements were determined by wavelength dispersive X-ray fluorescence spectrometry (WD-XRF), inductively coupled plasma - mass spectrometry (ICP-MS) and inductively coupled plasma - atomic emission spectrometry (ICP-AES). Analyses were performed for 49 samples at laboratories of GeoForschungsZentrum Potsdam (GFZ) and Institut für Geowissenschaften, Universitat Potsdam, Germany, for 5 samples at Acme Analytical Laboratories, Canada. 2 of the samples were analyzed both at laboratories in Germany and Canada to make crosscheck between the results (Appendix A).

For 49 whole-rock samples, major, minor and some of trace elements (Ba, Cr, Ni, Rb, Sr, V, Y, Zn, Zr) were acquired by Bruker-axs SRS303-AS XRF with a Rh X-ray tube at standard running conditions at GeoForschungsZentrum Potsdam (GFZ), Germany. International and internal reference samples were used for calibration. Analyses for major and minor elements, and for trace elements were carried out on fused glass and pressed powder discs, respectively. Both of the discs were prepared at Institut für

Geowissenschaften, Universitat Potsdam, Germany. The glass discs were made by fusing the powdered sample (exactly 1 g) using exactly 6 g Spetromelt A12 (66% Li-tetraborate - 34% Li-metaborate) and approximately 0.5 g NH_4NO_3 in Pt-crucible. Fusion of the samples was done by 4-step procedures at temperatures starting at 400°C through 500, 600 and 1150°C to form a homogeneous melt. Each step takes 6 minutes. The melt was then poured into a preheated mold to chill to a glass disc.

Ferrous iron, CO_2 and H_2O^+ for whole-rock samples were measured at Institut für Geowissenschaften, Universitat Potsdam. Volatile components (CO_2 and H_2O^+) were analyzed using Vario EL. Data for ferrous iron was obtained by $K_2Cr_2O_7$ titration after dissolution at room temperature in HF and oxidation with NH_4VO_3.

Measurements of trace elements including Li, Sc, Co, Cu, Ga, Nb, Cd, Sn, Sb, Cs, Ta, Tl, Pb, Th, U for 15 representative whole-rock samples, were performed at the ICP-MS laboratory equipped with a VG Elemental Plasma Quad System PQ2+ in GeoForschungsZentrum Potsdam (GFZ), Germany. Samples were dissolved with a mixture of concentrated $HF-HClO_4-HNO_3$ in the same laboratory using the following procedure: Savillex-Teflon beaker was cleaned in mixture of HCl_{conc}:H_2O_{bidist} (5:1). Accurately weighted 250 mg of powdered sample was put into beaker and shaken after addition of few drops of H_2O_{bidist}. HF_{conc} (4 ml) and mixture of HCl_{conc} (3 ml) + HNO_3 (1 ml) was added to sample. After completeness of reaction, lids of beaker were tightly closed and put into oven at a temperature of 160°C at least for 10 hours. After cooling, $HClO_{4\ conc}$ (1 ml) was added to sample and evaporated at 180-190°C to near dryness, redissolved with H_2O_{bidist} (2 ml) - $HNO_{3\ conc}$ (1 ml) and dried again. Then HNO_3 (1 ml) - H_2O_{bidist} (5 ml) was added to sample, treated as lids of beaker were closed at 100°C at least for 10 hours. After cooling, clean solutions were poured into 50 ml volumetric flasks and diluted to 50 ml with H_2O_{bidist} and transferred into 50 ml sample bottles. The sample solution is introduced to the instrument dispersed in an argon gas stream using a nebuliser. All samples were analyzed for four times and results of these were averaged. JGb-1 (gabbro) provided by Japanese Geological Survey was used

as reference rock. Precision and accuracy of the analyses were evaluated from four times repeated analyses of standards. In general, precision was better than 5–8%.

Rare earth element (REE), Y, Sc, Ba analyses of 17 whole-rock samples were carried out using a Scanni VARIAN Vista MPX ICP-AES at Institut für Geowissenschaften, Universitat Potsdam, Germany. Standards used for the analyses were JG1-b (gabbro), JB-1b (basalt), BM (basalt), 6450 (basalt) provided by the Japanese Geological Survey. Precision and accuracy of the analyses was determined as done for ICP-MS analyses. Sample dissolution for ICP-AES analyses was made following procedures outlined in Zuleger and Erzinger (1988) in which REE, Y, Ba and Sc were separated and concentrated from the Na_2O_2 sinter-dissolved sample using ion-exchange chromatography. A mixture of Na_2O_2 (5 g) and powdered sample (exactly 1 g) in a nickel crucible was covered with 1 g Na_2O_2. The crucible with closed lib was waited in a muffle furnace 480°C for 1.5 hr. After cooling down to room temperature, distilled water was added to the sinter-cake and waited overnight. Sinter-cake was mixed with 40 ml distilled water and centrifuged. After pouring off the solution, sinter-cake stirred up with 40 ml distilled water and centrifuged again. This step is repeated at least three times. 8.2 ml of HCl was added to residue of the sinter-cake and stirred to dissolve. Solution was transferred into a 100 ml PE-bottle and distilled water (41.8 ml) was added to this solution. The solution was completed to 100 ml by adding of HCl and waited at 50°C overnight as the lib of the bottle is closed. After this step, concentration and separation of REE was done chromatographically using an ion-exchange method. The resin in borosilicate glass ion-exchange column with sinter-disc was washed with 1N HCl. The sample solution was poured into the exchange column. The solution was filtered from the resin to hold REE and some of the traces in the resin and to remove the major and most of the trace elements. 550 ml of 1.7N HCl was put into the exchange column and filtered to leave only REE, Ba, Sc and Y in the resin. Finally, 550 ml of 4N HCl was filtered from the resin to transfer REE, Y, Ba, Sc from the resin into solution in a clean beaker. This last solution composed of only REE, Y, Sc, Ba was waited over a hotplate at 80-90°C overnight to evaporate HCl and leave a residue with REE,

Ba, Y and Sc. This residue was redissolved with 10% HCl (exactly 10 ml). Measurements by ICP-AES were made from the last solution. From each sample, measurements were repeated for four times and average of the results were used.

The elements, Ba, Sc and Y, were analyzed by three of the methods (XRF, ICP-MS, ICP-AES). There is good agreement among the methods. Ba and Y values from XRF analyses, and Sc values from ICP-MS measurements were used in this study.

Five of the samples were analyzed at Acme Analytical Laboratories, Canada. 2 of these 5 samples were also analyzed in Potsdam to make crosscheck (Appendix A). In general, there is excellent agreement between the results obtained from different laboratories on the same samples. In Acme Laboratories, major and minor elements as well as Ba, Ni and Sc were measured by ICP-AES from 0.2 g sample dissolved by $LiBO_2$ fusion. REE and Co, Cs, Ga, Hf, Nb, Rb, Sn, Sr, Ta, Th, U, V, Zr, Y of the $LiBO_2$ fused samples were determined by ICP-MS.

1.4. Phlogopite Generation by Metasomatism

1.4.1. Subduction Related Metasomatism

The hydrous mineral enriched ultramafic-mafic rocks from the Kurançalı area was previously studied in terms of a completely different aspect concerning alterations in the rocks and verm formation by Toksoy (1998), Toksoy and Öner (1997) and Toksoy-Köksal et al. (1999, 2001b). Early in this study, dark mica (phl) was assumed to be a secondary mineral due to K-metasomatism, related to the intrusion of K-rich granitic dikes of the granitoids in central Anatolia. However, further study showed that phl is the primary magmatic phase. The rocks enriched in phl and parg were described to be originated in an initial arc next to other (IAB and IAB/BABB (IAB: island arc basalts, BABB: back-arc basin basalt)) in SSZ environment based on data

from few samples (Toksoy-Köksal et al., 2001a, 2002) and indicative of mantle metasomatism.

Mantle metasomatism is divided into two types depending on mode of occurrence (Menzies et al., 1987): (a) cryptic metasomatism: characterized by enrichment in trace elements without clear evidence of changes of texture, mode or major element compositions, (b) modal metasomatism: characterized by changes in major, minor and trace element concentrations and modal mineralogy. Modal metasomatism is further subdivided into two such that (a) silicate melt metasomatism (alkaline melt) (i.e. Fe-Ti-rich metasomatism) is characterized by kaer, parg, high-Ti phl, di, ap, carb and mt-ilm, (b) hydrous fluid (rich in H_2O and CO_2) metasomatism (i.e. K-rich metasomatism) is characterized by rich, parg, low-Ti phl, di, rt, ilm, ap. Moreover, carbonatitic melts also result in mantle metasomatism producing second generation in cpx, ol, sp, and minerals (e.g. ap, phl, amph, cc) enriched in light rare earth elements (LREE) (e.g. Dautria et al., 1992; Rudnick et al., 1993; Ionov, 1998; Yaxley et al., 1991).

Studies on mantle metasomatism are mainly from xenoliths of metasomatized peridotites (e.g. Litasov et al., 2000; Maury et al., 1992) or at contacts with hornblendite and/or pyroxenite layers in peridotite massifs (e.g. Zanetti et al, 1996; 1999). Cryptic metasomatic enrichment for amph and phl is quite common (e.g. Bodinier et al., 1988; McPherson et al., 1996; Zanetti et al., 1996). However, modal mantle metasomatism causing pervasive enrichment in phl, amph, cpx and locally in ap and carb is observed often in kimberlite-transported mantle xenoliths (e.g. Erlank et al., 1987; Hawkesworth et al., 1990; van Achterbergh et al., 2001) and in mantle xenoliths which interacted with alkaline melts (e.g. Fabriès et al., 1989; Zinngrebe and Foley, 1995; Wulff-Pedersen et al., 1996) and carbonatite-like alkaline metasomatism at subduction zone (Zanetti et al., 1999).

In subduction zones, material transport from subducting slabs into the overlying mantle wedge is a fundamental process that leads to melting, basalt and andesite production, and chemical heterogeneity in the upper mantle

(Arculus, 1994 and references therein). Alkalis and lithophile elements, derived from dehydrating and/or melting of slabs due to break down of amph, are transferred into the hanging wall mantle (Tatsumi, 1989; Arculus, 1994; Tatsumi and Kogiso, 1997). A significant portion of these elements may not be retained in the mantle wedge for long periods of time (e.g. Gill et al., 1993; Arculus, 1994) and are transferred to the arc crust by arc lavas that are generated in the mantle wedge in response to the influx of this hydrous fluid (Arculus, 1994 and references therein). In this process, the volatile and K-rich fluids/melts infiltrating in the hanging wall result in hybridization (Fyfe and McBirney, 1975) and may directly induce melting in the mantle wedge by lowering of the peridotite solidus in hotter portions (Kushiro, 1972; Nicholls and Ringwood, 1973; Mysen and Boettcher, 1975a,b). In cooler portions of the mantle wedge, the infiltration of slab fluids/melts results in modal metasomatism with addition of hydrous phases to the hanging wall mantle (Fyfe and McBirney, 1975; Sekine and Wyllie, 1982). Fluids stabilize amph in the shallow regions of the mantle wedge beneath the fore-arc, and phl at higher pressures beneath the arc front and in the back arc region (Sekine and Wyllie, 1982; Wyllie and Sekine, 1982). If this metasomatized, but often melt depleted peridotite is then convected by corner flow into hotter regimes within the mantle wedge, it may melt or dehydrate and contribute to arc and back-arc magmatism (Wyllie and Sekine, 1982). Phl may also replace amph if the metasomatized, amph-bearing peridotite in the hanging wall is dragged downward along with the slab as the result of corner flow in the mantle wedge.

Brandon et al. (1999) explained a multi-stage metasomatic model in light of isotopic data. In the first stage, fluids/melts derived from subducting slab are transferred into the overlying hanging wall mantle and react with it (hybridization after Wyllie and Sekine, 1982). In the second stage, the hybridized hanging wall mantle is remobilized as melt or fluid. In the third stage, this fluid/melt migrates upward to temperatures greater than 1200°C in the mantle wedge and acts as a metasomatic agent that subsequently interacts with the overlying mantle lithosphere. Metasomatism by the K-rich melt takes place resulting in reaction with the peridotite and the precipitation of phl at 900-1000°C.

Actually, the multi-stage model of Brandon et al. (1999) is the same as the model of Wyllie and Sekine (1982) for the generation of arc and back-arc magmas and their relationship to the hybridized hanging wall over slabs where material transport from the slab into the hanging wall produces a hybridized peridotite, followed by melting of this hybridized peridotite.

In collisional zones, the slab melts thought to be effective in metasomatism of mantle wedge in an arc environment is collectively known as adakitic melts (Defant and Drummond, 1990). Adakites result from wet melting of garnet-amphibolite or basaltic eclogite (Green, 1982; Rapp et al., 1991; Sen and Dunn, 1994) if; (1) subducting slab is young and relatively hot (Defant and Drummond 1990), or (2) older and colder slab display flat subduction mechanism (Gutscher et al., 2000), (3) the edge of a torn old oceanic slab is exposed to mantle flow, it results in slab ablation, heating, and eventually melting lithosphere (Yogodzinski et al., 2001). The compositional contribution of fluid/melt derived from subducting slab in metasomatism of sub-arc mantle peridotite is severely shown either by experimental studies (e.g. Sekine and Wyllie, 1983; Carroll and Wyllie, 1989; Sen and Dunn, 1994; Rapp et al., 1999), or from peridotitic xenoliths in nature (e.g. Batan and Negros in the Philippines: Sojana et al., 2000).

Phl, the most obvious indicator of metasomatism, is found in association with silica and alkali-rich glasses in many sub-arc mantle peridotite xenoliths (e.g. from arc lavas in the Philippines: Schiano et al., 1995; Maury et al., 1998; Sajona et al., 2000, and from Simcoe in USA: Ertan and Leeman, 1996; Brandon et al., 1999). Hydrous, high silica and alkaline glasses from mantle xenoliths infer that alkaline melts result from low-degree melting of the subducted oceanic crust and cause metasomatism in sub-arc mantle. Alkaline metasomatism crystallizes opx, cpx, amph and phl in peridotite. On the contrary, it is well known that infiltrating alkaline melts dissolve opx at lithospheric mantle depth (Fabriès et al., 1989; Zinngrebe and Foley, 1995). Draper and Green (1997) experimentally showed that such water-bearing alkali- and silica-rich glasses will be saturated with cpx and phl at pressures and temperatures of 850 to 1100 °C and 1-2 Gpa, and such melts may act as

agent resulting in metasomatism. These melts are enriched in LILE and alkalis relative to typical basaltic melts (e.g. Schiano et al., 1995; Draper and Green, 1997; Brandon et al., 1999).

Zanetti et al. (1999) proposed an alternative possibility for alkaline/carbonate-rich melts as metasomatic agents from subduction zones, in which carbonatite-like metasomatism does not necessarily imply mantle-derived carbonatite components, but may result from the evolution of a silicate liquid containing some CO_2 derived from melting subducting slab. According to Zanetti et al. (1999) slab derived melt is composed of CO_2 and H_2O. Crystallization of anhydrous mineral (mostly cpx) increases H_2O/CO_2 ratio in the system and then hydrous minerals start to crystallize using H_2O of the system. Use of H_2O by hydrous minerals increases CO_2 in the system, and ap-bearing, -rich domains and secondary cpx crystallizes. This model requires melting of subducting slab and resulting melt should include H_2O and CO_2. Presence of H_2O and CO_2 is evidenced from fluid inclusions and brines in eclogite-facies rocks (Philippot, 1993; Andersen et al., 1993; Philippot and Scambelluri, 1995).

1.4.2. Other Modes of Occurrences

Volatile bearing minerals, phl and amph in metasomatized mantle xenoliths are not only from arc related settings but also from intraplate settings in continental and oceanic environments. Metasomatism results from reactions between wall-rock mantle peridotites and alkaline basaltic or carbonatitic melts that lead to the formation of such as amph, phl and ap (e.g. Lloyd and Bailey, 1975; Wass, 1979; O'Reilly and Griffin, 1988; Ionov et al., 1993; Ashchepkov et al., 1994; Hirschmann and Stolper, 1996; Chalot-Prat and Boullier, 1997; Litasov et al., 2000). They are commonly related to rifts or to doming, and form provinces of clustered intrusions, especially in continental plate. Best examples of metasomatized peridotite xenoliths are common in many kimberlite pipes in the Archaean cratons in Southern Africa (e.g. Erlank et al., 1987; Waters and Erlank, 1988) and Kola Peninsula, Russia (e.g. Beard et al.,

1996; Verhulst et al., 2000), south Brazil (Morbidelli et al., 1995), Greenland (Larsen and Rex, 1992). Dalton and Presnall (1998) demonstrated that very low-degree partial melting (between 0.3 and 1.1) can generate carbonatite to kimberlite melts at pressures between 5 and 7 GPa (about 170-230 Km), i.e. at the lithosphere/asthenosphere transition below continental shields. Moreover, Coltorti et al. (2000) also interpreted based on geochemical features of mantle glasses occurring together with hydrous phases that there are different types of metasomatizing agents such as carbonatite, Na- and K-alkaline silicate basic melts originated by very small degrees of partial melting in the deepest portions of the lithospheric mantle, or at the lithosphere/asthenosphere transition.

Physical separation from mantle rocks, fluidization of mantle rocks and rapid ascent of carbonatitic and alkaline melt are probably accounted by CO_2 exsolution, a factor that is responsible for deep explosivity (e.g. Bailey, 1985). During the rise, carbonatitic and alkaline liquid become immiscible at pressures between 10 and 20 kbar and tend to separate (e.g. Kjarsgaard and Hamilton, 1989). This may cause instability and turbulence of magma column and form a fine dispersion of carbonatite and alkaline droplets having sufficient strength to carry mantle xenoliths. Chemical interaction of mantle peridotite with CO_2 rich melts has often invoked to explain trace element enrichment in alkalic magmas and mantle peridotite xenoliths carried by them (e.g. O'Reilly and Griffin, 1988). Carbonatitic melts can percolate easily through ol rich rocks (Hunter and McKenzie, 1989) and signature of enrichment in REE without contaminant enrichment in high field strength elements (HFSE: Ti, Zr, Hf, Ta, Nb) in mantle derived peridotites have been interpreted as reflecting chemical interaction with such melts (e.g. Yaxley et al., 1991).

CHAPTER 2

GEOLOGY

2.1. Introduction

Ultramafic-mafic plutonic rocks, which are enriched in phl and parg, crop out in the Central Anatolian Crystalline Complex (CACC), central Turkey (Göncüoğlu et al., 1991, 1992). The CACC, an assemblage of magmatic and metamorphic rocks, has been the topic of numerous studies (Göncüoğlu et al., 1991, 1992, 1993, 1998; Göncüoğlu and Türeli, 1993; Yalınız et al., 1996, 1999, 2000a,b; Floyd et al., 1998, 2000; Toksoy-Köksal et al., 2001a,b, 2002). According to these authors, the CACC consists of three main units; Central Anatolian Metamorphics (CAM), Central Anatolian Ophiolites (CAO) and Central Anatolian Granitoids (CAG). The metamorphic rocks present in the CACC are overthrusted by the ophiolitic units, and both units are cut by the granitoids.

The CACC, is composed of many isolated outcrops of ultramafic rocks, as well as massive and layered gabbroic rocks (e.g. Yalınız and Göncüoğlu, 1998; Göncüoğlu et al., 1998). Although, a few of the mafic rocks were interpreted as intrusive assemblages within the CACC continental crust (e.g. Yılmaz-Şahin and Boztuğ, 1997, 1998; Güleç and Kadıoğlu, 1998; Kadıoğlu and Güleç, 1996; Kadıoğlu et al., 1998), most of the ultramafic-mafic rocks were described as dismembered parts of an allochthonous ophiolitic assemblage of Late Cretaceous, part of CAO (Göncüoğlu et al., 1992; Koçak and Leake, 1994; Yalınız et al., 1996; Yalınız and Göncüoğlu, 1998; Floyd et al., 2000; Toksoy-Köksal et al., 2001a,b, 2002), derived from the northerly located İzmir-Ankara branch of the Alpine Neotethys. The ultramafic-mafic

allochthonous unit from the Kurançalı area (Kaman-Kırşehir), which has been studied in this thesis, is generally considered as a part of the CAO (Göncüoğlu et al., 1992; Toksoy, 1998; Toksoy-Köksal et al., 2001a,b, 2002; Yalınız and Göncüoğlu, 1998).

2.2. Regional Geological Setting

The Tethyan Ocean between Gondwana and Laurasia resulted from rifting of variably sized continental fragments from Gondwana. The oceanic basins, created following a diachronous opening from east to west during the latest Paleozoic to earliest Tertiary, are collectively called Neotethys, the closure of which still continues. The ophiolites of the Mediterranean region, which belong to the long chain of Tethyan ophiolites, were divided into two groups: the western and central area (Alps-Apennines-Carpathians-Dinarides-Hellenides) and the eastern Mediterranean (Cyprus-Turkey-Syria-Oman) (e.g. Nicolas and Jackson, 1972; Rocci et al., 1975; Abbate et al., 1976). Pearce et al. (1984) divided the Tethyan ophiolites into non-subduction influenced (the western Tethyan region) and subduction influenced (eastern Tethyan region) ones. Western and eastern Tethyan regions differ both in age and geodynamic environments. The western realm is represented by Jurassic ages, intra-oceanic slow spreading ocean ridge type, laterally evolving into SSZ-type geodynamic settings, while the eastern areas show Triassic to mainly Cretaceous ages, ocean ridge, sea mount to SSZ-type settings, respectively (Robertson, 2002 and references therein).

The eastern Mediterranean Neotethyan realm indicates that the fragmentation of the northern margin of Gondwana during the Mesozoic resulted in a series of narrow oceanic seaways and microcontinent fragments (Robertson and Dixon, 1984; Robertson, 2002). Openning of the Neotethyan ocean started with rifting of the northern margin of Gondwana during Late Permian-Early Triassic, rifting continued with intrusion/extrusion during Early-Mid Triassic, and continental break-up, initial mid-ocean ridge (MOR) volcanism and initial sea-floor spreading started during Late Triassic (Robertson, 2002). The generated small seaways survived up to Late Cretaceous time and the convergence of Africa and Eurasia largely closed this

segment via northwards subduction under the Pontide active margin of Eurasia (Livermore and Smith 1984; Yılmaz et al., 1997). Due to the closure of Neotethyan oceans during the end of Mesozoic (Robertson and Dixon, 1984), a number of distinct episodes of subduction and obduction activities have taken place throughout the Eastern Mediterranean region, as reflected by traces of the Neotethyan evolution.

The Turkish sector of the Neotethys, occupying a critical segment in the Alpine-Himalayan orogenic system, is characterized by two major east-west trending belts of variably disrupted fragments of ophiolites (Figure 2) (Şengör and Yılmaz 1981). Each belt records closure and destruction of a separate branch of the Neotethyan ocean: (a) the northern branch located at north of the Anatolide-Tauride microplate is comprised of Intra-Pontide ocean and İzmir-Ankara-Erzincan (İAE) ocean (although Görür et al. (1984) suggest an additional derivation, the Inner Tauride Belt), (b) the southern branch (Southeast Anatolian Suture) (Şengör and Yılmaz, 1981) or the Peri-Arabic Belt (Ricou, 1971), represented by well documented ophiolite bodies such as Troodos, Hatay, Guleman and Cilo, is located between the Arabian Platform and the Anatolide-Tauride microplate.

Şengör and Yılmaz (1981) stated that the İAE ocean originated as a marginal basin separating the Anatolides from the Sakarya Microcontinent during the Jurassic time. This is indicated by an association of alkali ocean island basalt (OIB) type metabasites and MOR basalt (MORB) (Floyd et al., 2000). Both, İAE and Intra-Pontide oceans of the northern Neotethys, reaching their maximum size during early Cretaceous, were distrupted and consumed by northward subduction beneath Eurasia and Sakarya continents giving rise to widespread southwergent obduction of ophiolite (Şengör and Yılmaz, 1981).

The dismembered ophiolites in central Anatolia (CAO; e.g. Göncüoğlu et al., 1991, 1992), and the unfragmented Pozantı-Karsantı Ophiolite (Parlak et al., 2000, 2002) and the ophiolite fragments in the Ankara Mélange, which were derived from destruction of İAE ocean, were exposed as allochthonous blocks on the passive margin of the Anatolide-Tauride microplate during Late Cretaceous (e.g. Göncüoğlu et al., 1991, 1992, 1996-1997, 1998; Parlak et al.,
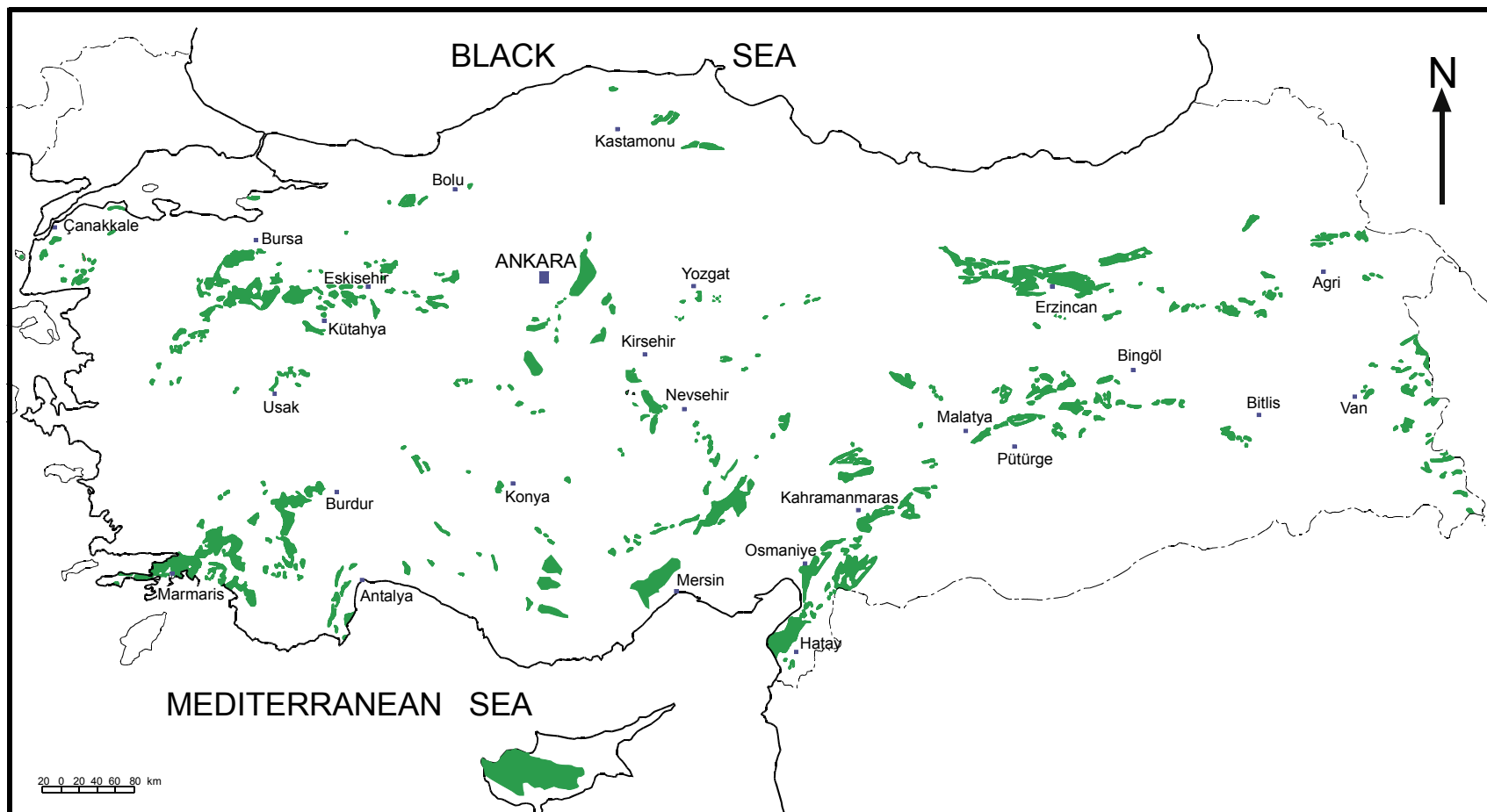
Figure 2. The map showing Turkish ophiolites (compiled from 1:2.000.000 scaled geological map of Turkey; Bingöl, 1989).

2000, 2002). However, Şengör and Yılmaz (1981), Görür et al. (1984), and Robertson (2002) suggest an alternative model for the origin of the Pozantı-Karsantı and Mersin ophiolites. According to these authors, these ophiolites were derived from the Inner-Tauride ocean (ITO) that separated the Kırşehir block (the present CACC) from the Tauride platform. Görür et al. (1984) proposed that ITO was consumed during Late Cretaceous, and final collision between the Kırşehir and Tauride blocks occurred during the latest Paleocene - Early Eocene resulting in subduction of the ITO lithosphere beneath the Kırşehir Massif and the formation an Andean-type continental arc plutonism in western CACC. Kadıoğlu (1996) suggested that granitoids and petrologically related gabbros in central Anatolia formed with a similar mechanism.

The detailed geological and petrological studies in CACC (Kırşehir block of Görür et al., 1984) put forward that CACC consist of polyphase metamophic platform sequences (CAM), overthrust by ophiolitic complexes (CAO) with metaophiolites and subophiolitic metamorphics, and intruded by granitoids (CAG) cutting both the CAM and the CAO (Göncüoğlu, 1977, 1981, 1986; Göncüoğlu et al., 1991, 1992). Based on crystallization ages of the granitoids Göncüoğlu (1986) suggested that the main metamorphism and ophiolite emplacement in CACC occurred during pre-Cenomanian times. This idea constrasts with Seymen (1984)'s interpretations suggesting that granitoids also cut Uppermost Cretaceous-Lower Paleocene sediments, and with the model of Görür et al. (1984) proposing that the granitoids (younger than sediments) must be related to subduction of the speculative IOT in the western part of CACC. Morever, the comparison of the CAM in CACC with the weakly metamorphosed Kütahya-Bolkardağ Belt (Özcan et al., 1980) (belonging to Tauride platform of Görür et al., 1984) showed that both are quite similar at least up to early Cretaceous in stratigraphic successions and geological events (Göncüoğlu, 1986). The pre-Cenomanian obduction of İAE ophiolites on the the CAM, deep burial polyphase metamorphism resulted in high temperature-low pressure metamorphism. Therefore Göncüoğlu (1986) infers that the Anatolide (Kırşehir block of Görür et al., 1984) and the Tauride blocks were not separated by IOT, and Anatolide and Tauride actually formed a single platform (Tauride-Anatolide plate).

The studied ultramafic-mafic plutonic rocks, enriched in hydrous minerals (parg, phl), belong to the CAO (Göncüoğlu et al., 1992; Toksoy, 1998; Toksoy-Köksal et al., 2001a,b, 2002; Yalınız and Göncüoğlu, 1998) which will be emphasized in the following review.

The CAM mainly exposed in the center and along the western and eastern-northeastern parts of the CACC (Figure 3) were divided into three groups from bottom to top (Göncüoğlu, 1977, 1981, 1986; Göncüoğlu et al., 1991, 1992, 1993a, 1998) (Figure 4): (a) Gümüşler Formation: containing well-foliated gneisses with marble interlayers and amphibolite bands. (b) Kaleboynu Formation: composed of pure marbles interbeded with calcsilicate marble, calcsilicate, mica-schist, gneiss, and bands of amphibolite and calcsilicate amphibolites. (c) Aşıgediği Formation: consisting of massive marbles with cherty-marbles and amphibolite alternations. A metamorphic ophiolite-bearing sedimentary mélange developed during the emplacement of the CAO onto the CAM appears in the uppermost part of the Aşıgediği Formation. This unit, mainly composed of schist, gneiss and amphibolite is typical for a sedimentary complex with blocks of ophiolites and marbles. In addition, serpentinites, metagabbros, amphibolites and marble blocks within hb-bio gneissic matrix are also present in the mélange. The age of the metamorphic ophiolitic mélange is post-Cenomanian - Turonian to pre-Upper Campanian (Göncüoğlu et al., 1998). The unit experienced the same deformation and metamorphism as CAM.

The CAO in central Anatolia, are exposed as allochthonous dismembered and scattered bodies (e.g. Sarıkaman and Çiçekdağ ophiolites, and various isolated units) (Figure 3). The contacts of these bodies with the CAM are always a thrust fault. A thin tectonic sliver of sub-ophiolitic amphibolites locally occurs in the thrust zone (Figure 4). The ophiolitic bodies partially preserved a magmatic pseudostratigraphy, thus an overall ophiolite succession can be reconstructed based on the relations of the units. The lowermost units are serpentinized ultramafic rocks that only occur in limited extend. They are overlain by layered, and isotropic gabbros, followed by plagiogranite, dolerite dykes and pillow basalts and finally late dykes cutting the lavas (e.g. well-defined Sarıkaraman Ophiolite: Yalınız, 1996; Yalınız et al.,
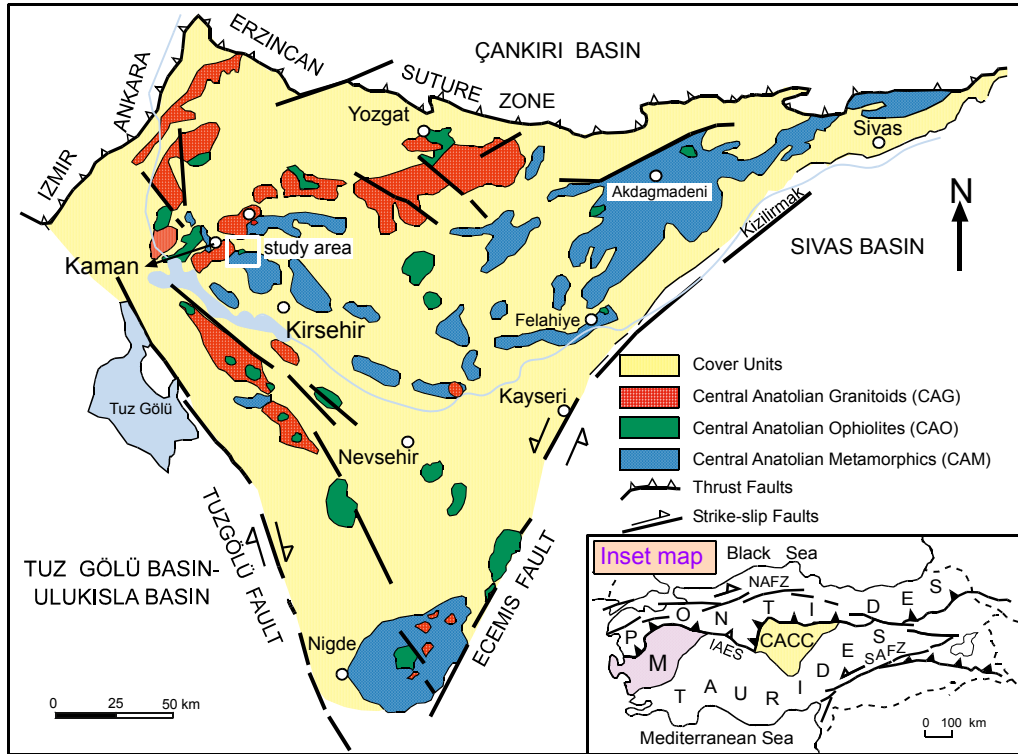
Figure 3. Simplified geological map of the CACC showing the geological settings of the main units and location of the study area (In inset map: CACC: Central Anatolian Crystalline Complex, M: Menderes Massif, NAFZ: North Anatolian Faults Zone, SAFZ: South Anatolian Fault Zone, İAES: İzmir-Ankara-Erzincan Suture (after Göncüoğlu et al., 1991; Yalınız and Göncüoğlu, 1998).

23

AGE & FORMATION	LITHOLOGY	EXPLANATIONS

Latest Cretaceous - Lower Paleocene — Olistostromal clastics

Unconformity

Upper Cretaceous (Turonian-Santonian)

A — Stratiform ophiolite

Amphibolitic ophiolitic sole

Upper Cretaceous — Metamorphosed ophiolitic mélange

MESOZOIC

CENTRAL ANATOLIAN METAMORPHICS

ASIGEDIGI FORMATION

granite, syenite, monzonite, monzogranite (S: S-type, H: H-type, A-type)

Pelagic cherty marbles & mudstones

H

Calcitic & dolomitic marble

KALEBOYNU FORMATION

Amphibolitic schists & amphibolites

Marbles, calc-silicates, mica schists

Quartzite

S — Unconformity

PALEOZOIC

GÜMÜSLER FORMATON

Mica, sillimanite, corderite paragneisses & garnet quartzites

Amphibolites & amphibole gneisses

Marbles & calcsilicates

NOT TO SCALE

Figure 4. Generalized columnar section of the CACC (modified from Göncüoğlu et al., 1991).

1996, 1998). The basic volcanic sequence (pillow lavas, massive flows and sheeted dykes) is aphyric and mainly ol-poor plag-cpx pyric tholeiitic in composition indicating island arc environment. The late-stage MOR-like dykes represent rifting in a marginal basin (Yalınız et al., 1996; Floyd et al., 1998). The whole-rock and mineral data from gabbros indicate that the occurrence of a high-Mg and low-Ti magma constrains the formation of the Sarıkaraman ophiolitic gabbro to a SSZ environment (Yalınız and Göncüoğlu, 1999).

The high-level gabbros are intruded by net-vein trondjemites and numerous dykes (Floyd et al., 1998; Yalınız et al., 2000a). Plagiogranite dykes, correlating with acidic extrusives higher in the succession, were interpreted to feed extrusive silicified rhyolites. They are typical for SSZ plagiogranites and probably derived from the roof section of a dynamic and evolving magma chamber.

The other well-defined part of the CAO is the Çiçekdağ Ophiolite which partially preserved its magmatic pseudostratigraphy (Yalınız et al., 2000). The units are: layered gabbro, isotropic gabbro, plagiogranite, dolerite dyke complex, basaltic volcanic sequence and sedimentary cover. The basic rocks have similar petrographical and chemical characteristics as those of the Sarıkaraman Ophiolite summarized above.

In addition to ophiolitic bodies with preserved magmatic pseudostratigraphy (e.g. Sarıkaraman and Çiçekdağ ophiolites), many isolated bodies of ultramafic rocks and massive/layered gabbroic rocks are found as tectonic slivers having field characteristics of ophiolitic units in the CAO (Göncüoğlu et al., 1998; Yalınız and Göncüoğlu, 1998). Ophiolitic ultramafic rocks (peridotite), which are found generally at contacts of the CAO and the CAM, are completely serpentinized. These serpentinized rocks generally alternate with bands of cumulate gabbros although they tectonically overly the gabbros at some locations. The gabbros, ranging from fine-grained to pegmatitic with variable compositions (leuco to melano), are extensively exposed in the CAO. The epi-ophiolitic sedimentary cover of the CAO is generally characterized by pillows lavas, epiclastic volcanogenic deep sea-sediments and debris flows intercalated with pelagic units (Yalınız et al.,

2000b,c). The richest and most significant planktonic foraminiferal association recorded from the lowest pelagic members infers a formation of age of early-middle Turonian to early Santonian. K/Ar ages of post-collisional granitoids (81-65 Ma of Yalınız et al., 1999), which intruded the basement rocks as well as the CAO, suggest a post-early Santonian to pre-middle Campanian emplacement. The time interval between the formation and emplacement ages of the SSZ-type rocks in the CACC is very short. This is a typical feature of all fore-arc type Eastern Mediterranean Ophiolites (Yalınız et al., 1999). This helps to explain the short time-span between ophiolite generation in the İAE Ocean and initial emplacement onto the southern passive margin, the CAM of the CACC.

In contrast to the suggestions mentioned above, some of the gabbroic rocks in CACC were interpreted as magmatic bodies that intrude the CAM as members of the Late Cretaceous continental arc magmatism (Kadıoğlu, 1996; Kadıoğlu et al., 1998; Yılmaz-Şahin and Boztuğ, 1997).

The units of the CAG, cutting through all units of the CAM and the CAO, represent the youngest intrusive rocks within the CACC. They show an Upper Cretaceous intrusion age (Ataman, 1972; Erkan and Ataman, 1981; Göncüoğlu, 1986; Yalınız et al., 1999; Köksal et al., in rev). They are variable in composition such as leucogranite, bio-hb granite, K-feld megacrystic granite, granodiorite and aplitic K-feld granite in general. Among them, leucogranites and bio-hb granites intrude mafic rocks. Aplitic granitoids are generally found as dykes. The granitoids are classified as S-type syn-collision granitoids formed just after the climax of a collision of the CACC with the Sakarya microcontinent, H-type post-collision granitoids evolved from underplating mantle-derived mafic magma formed due to the crustal thickening followed by lithospheric delamination, and A-type granitoids represent advanced and final stages of the post-collisional period (e.g. Göncüoğlu et al. 1991, 1992, 1993, 1997; Göncüoğlu and Türeli, 1993, 1994; Aydın et al., 1998; Düzgören-Aydın et al., 2001; Yalınız et al., 1999; Floyd et al., 2000).

2.3. Geology of the Kurançalı Area

The ultramafic-mafic rocks from the Kurançalı area to the east of Kaman (Kırşehir) are considered as one of the isolated bodies of the CAO that is exposed as a tectonic sliver (Göncüoğlu et al., 1992; Yalınız and Göncüoğlu, 1998; Toksoy, 1998; Toksoy and Göncüoğlu, 1998; Toksoy-Köksal et al., 1999, 2000, 2001a,b, 2002) (Figure 3). In the study area, Metamorphic Ophiolitic Mélange (the uppermost part of the CAM), tectonically overlying ultramafic-mafic cumulates (lower units of the CAO) and felsic dykes (representative of the CAG) cutting the first two units are exposed.

The ultramafic-mafic rocks overthrust the uppermost unit of the CAM from north to south with an intervening E-W trending shear zone (Figures 5, 6). The underlying metamorphic rocks belong to Metamorphic Ophiolitic Mélange with blocks of meta-ophiolitic rocks and meta-carbonates. This unit is dominated by irregular bands and lenses of calcsilicate amphibolites, calcsilicate marbles, cherty marbles, amphibolites and serpentinites within a matrix dominated by calcsilicate bio-gneisses and amph-bio-gneisses. The amount of the calcsilicate rocks diminishes while the amph-bio-gneisses increases away from the underlying meta-carbonate contact. The intervening shear zone, between the cumulate rock sliver and the Metamorphic Ophiolite Mélange, is characterized by the presence of sheared boudins of cumulates, amphibolites and serpentinites.

The observed tectonic contact for the Kurançalı rocks is characteristic for the CAO units in the CACC. There is no other ophiolitic unit exposed together with these cumulate rocks (cumulate texture is petrographically defined in Chapter 3). The field characteristics of the studied rocks differ from those of intrusive assemblages within the CACC continental crust, i.e. there are no signs of intrusive contact.

All units (Metamorphic Ophiolitic Mélange, shear zone and ultramafic-mafic plutonic rock sliver) are cut by NW-SE trending CAG leucocratic felsic dykes. The dykes with width of 10-25 cm have sharp contacts with their host rocks, and are moderately sheared (Figure 7). They vary in grain size from
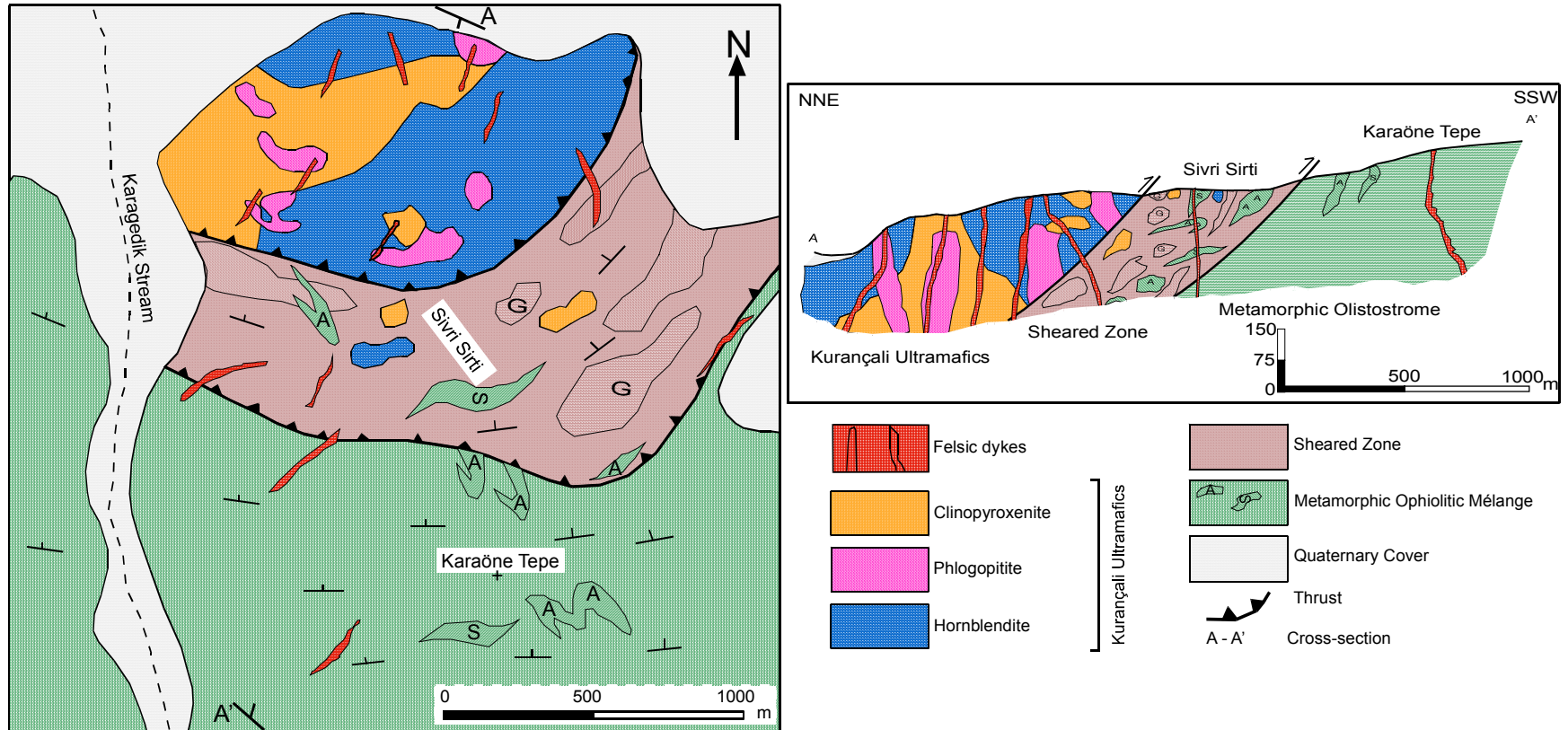
Figure 5. Geological map and cross-section of the study area showing the rock units and their contact relationships.
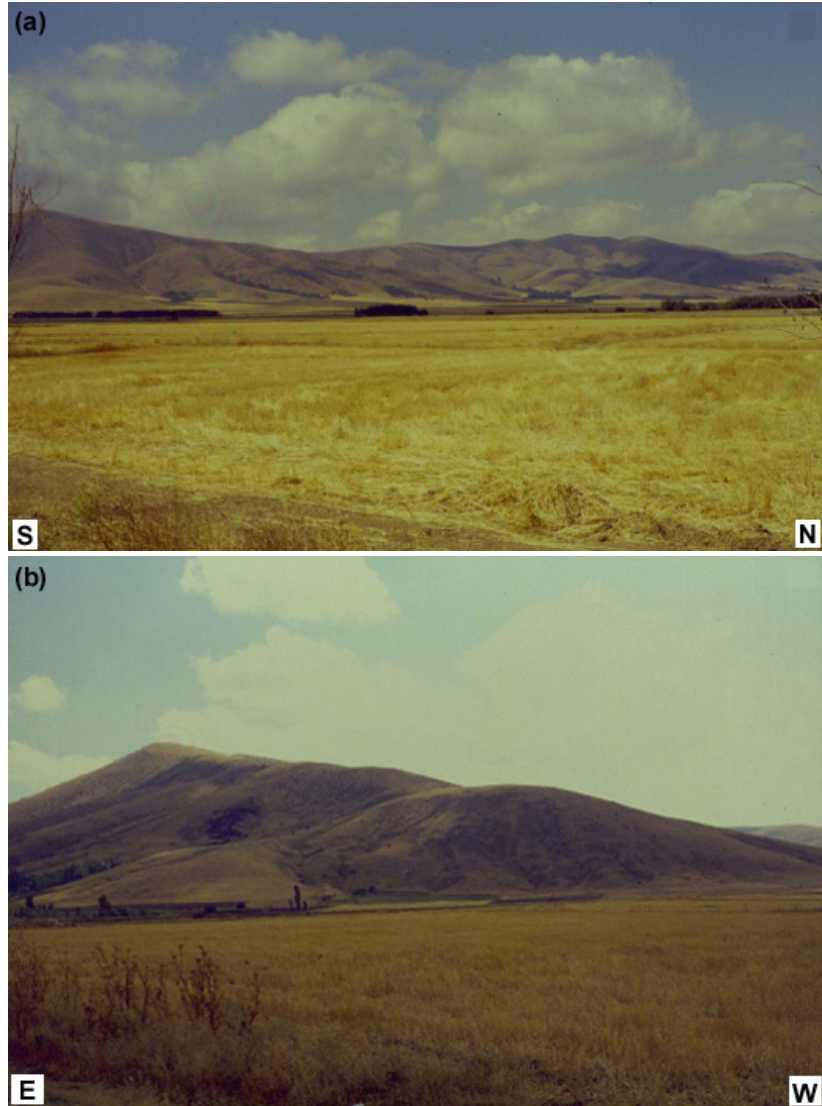
Figure 6. General field view of the study area showing positions at; (a) south-north direction, (b) east-west direction.

very fine to medium. The dykes, not homogeneous in composition, are made up of K-feld granite, qt syenite and K-feld syenite (Toksoy, 1998).

Figure 7. Felsic dykes of the CAO cutting HBdite.

This study focuses on the allochthonous body of the ultramafic-mafic cumulates of the CAO exposed in the Kurançalı area. This unit is characterized by enrichment in dark mica (phl) and magmatic amph (parg). This is a unique feature in the CAO. The studied rocks were previously called Kurançalı metaophiolitic peridotite (Yalınız and Göncüoğlu, 1998) and Kurançalı Metagabbro (Toksoy, 1998; Toksoy and Göncüoğlu, 1998; Toksoy-Köksal et al., 1999, 2000, 2001a,b, 2002). But further detailed studies showed that cumulate ultramafics, layered gabbros and diorites occur within this tectonic sliver. Thus previously used terms are left behind in this study.

The ultramafic-mafic rocks are composed of cpx, phl, parg and plag. They show heterogeneity in both composition (leuco to melano) and grain size (fine-grained to pegmatitic). The ultramafic cumulate rocks can be divided into four groups based on their modal compositions of mafic minerals: (a) clinopyroxenite (CPXnite), (b) clinopyroxenite with hydrous minerals and plag

(CPXnite WHMP), (c) phlogopitite (PHLtite), (d) hornblendite (HBdite) (Figure 5). Rocks composed of cpx, plag, and low but variable amount of hydrous minerals, and showing rhythmic layering are called layered gabbro (LG). Rocks composed of phl and plag (with relict cpx from petrographical observation) are called diorite (DIO). Exposures of ultramafic-mafic rocks are highly dissected. Therefore contact relationships of the rock types could not be traced accurately. LG shows many outcrops, but generally they are not exposed in situ. DIO shows a very small outcrop that is not mapable. Therefore both LG and DIO were not shown in the map (Figure 5). In general, all rock types show quite irregular outcrops.

CPXnite consists mainly of green-prismatic cpx crystals variable in size. It is dark green in color (Figure 8). It is characterized by lack of plag and primary prismatic amph. CPXnite shows phl flakes ranging in size from few mm to 1-2 cm. Phl bearing CPXnite is generally found close to PHLtite with increasing phl amount.

Figure 8. Field view of CPXnite with few plag.

CPXnite WHMP is made up mainly of cpx. In addition, it has varying amounts of fine-grained to pegmatitic sized plag, amph and phl. This rock type is found close to the PHLtite and HBdite where amph-plag pods are common in cpx-plag rich rocks (Figure 9).

Irregular masses of pegmatitic PHLtite consist mainly of phl with lesser amount of cpx. Phl crystals are brittle and dark brownish in color. Crystal sizes are variable up to 2-2.5 cm in diameter. Almost no plag is present in PHLtite (Figure 10a,b). In addition, the presence of amph is restricted to PHLtite outcrops neighboring HBdite (Figure 10b) and generally found in small amph-plag veins. PHLtite is generally fresh; however, in some outcrops phl is altered to gold-yellow colored verm in trace amounts.

HBdite is mainly composed of amph with low amounts of plag (Figure 11). Black colored amph crystals are highly variable in size from few mm to pegmatitic size prismatic crystals (up to 20 cm in length) (Figure 12). HBdite is divided into two groups based on crystal size, such as fine-grained HBdite and pegmatitic HBdite (Figure 13). While fine-grained HBdite contains very limited plag and cpx (less than 5%), pegmatitic HBdite contains plag up to 10-15% but lacks cpx. In pegmatitic HBdite, plag is generally found as aggregates forming leucocratic parts. This is interpreted as being due to strong magmatic filter pressing (Figure 14). Plag from leucocratic parts is usually characterized by well-defined irregular to angular margins (Figure 14a).

The small outcrops of LG showing compositional and grain size variations are distributed among the other outcrops in the study area. LG with varying grain size of 3-5 mm to 1-1.5 cm are marked by variations of modal proportions of mainly cpx and plag (Figure 15). In coarser grained parts amph crystals are present, and crystals of both plag and amph are coarse-grained. These parts may represent re-injection of plag-amph liquid into cpx-plag layering (Figure 16). This is inferred from the pothole-like structures and regular/irregular layers filled by pegmatitic amph and plag within LG and CPXnite WHMP (Figures 9,15,16,17). Moreover, small veins of plag-amph in CPXnite, CPXnite WHMP and PHLtite also support this idea.
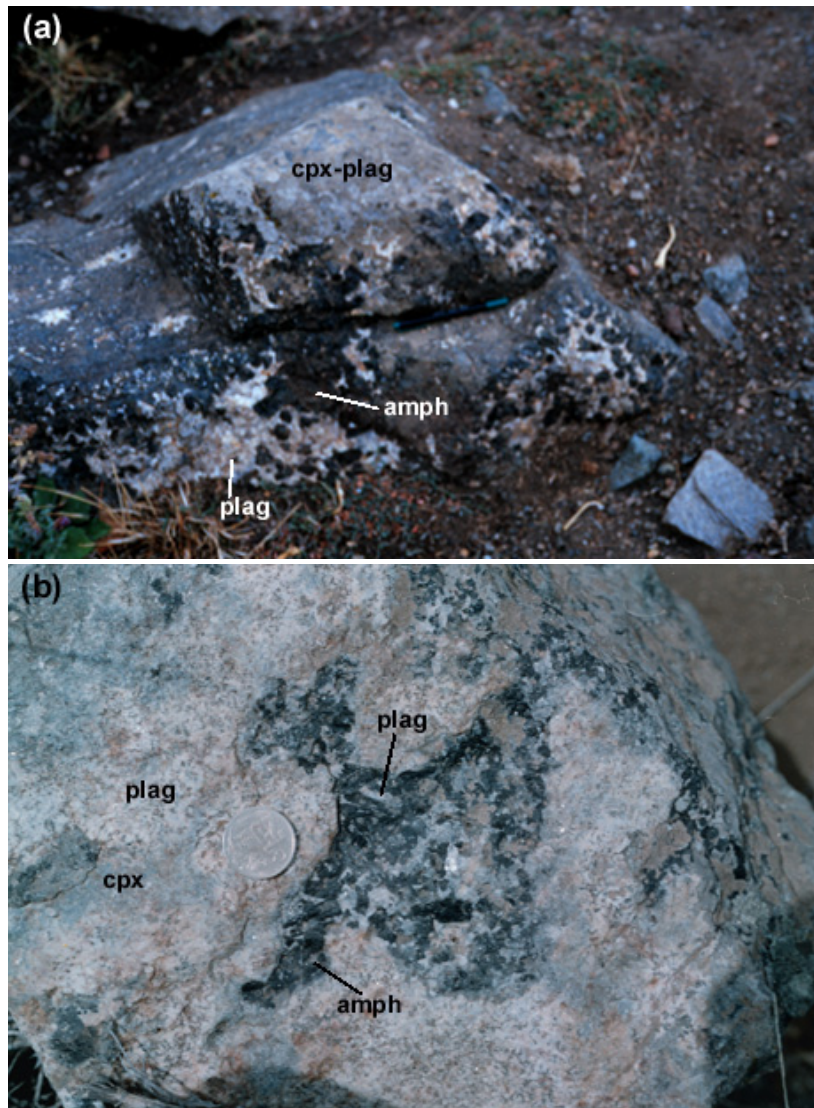
Figure 9. Field views of CPXnite WHMP with enrichment of pegmatitic plag and amph in irregular pothole-like structure.
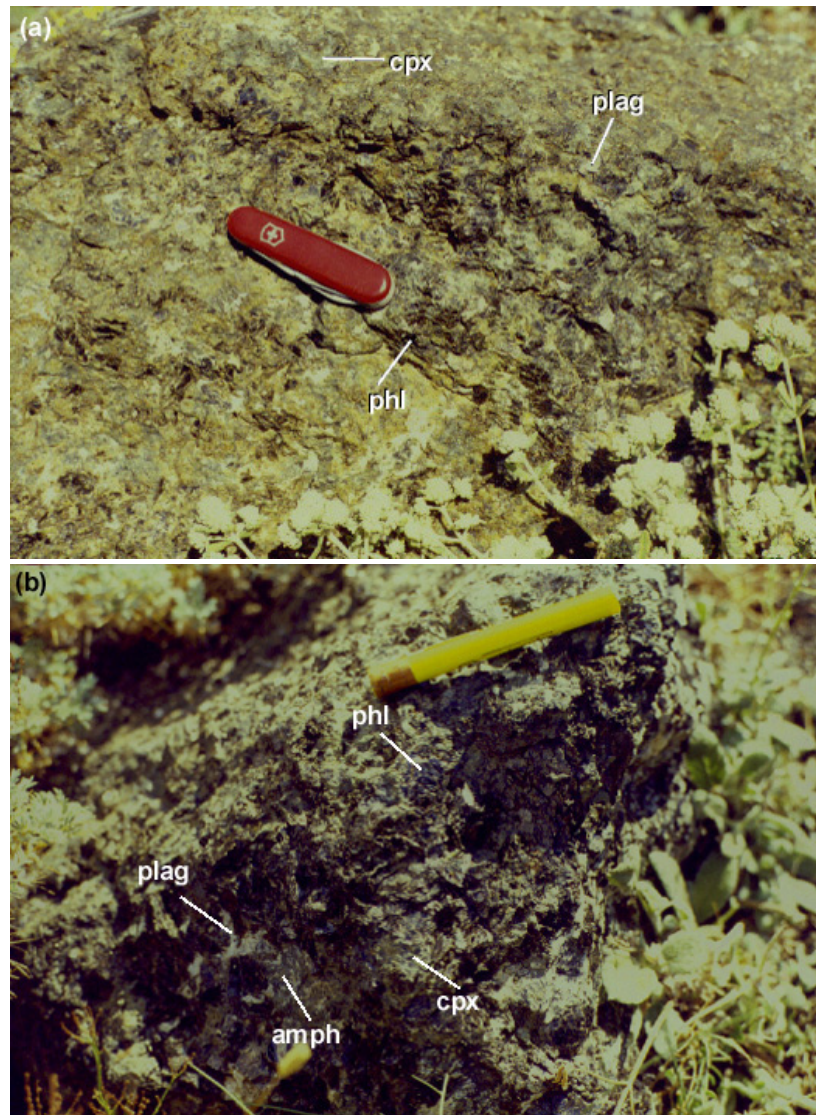
Figure 10. Field views of PHLtite (a) with few plag, (b) contact with pegmatitic HBdite.
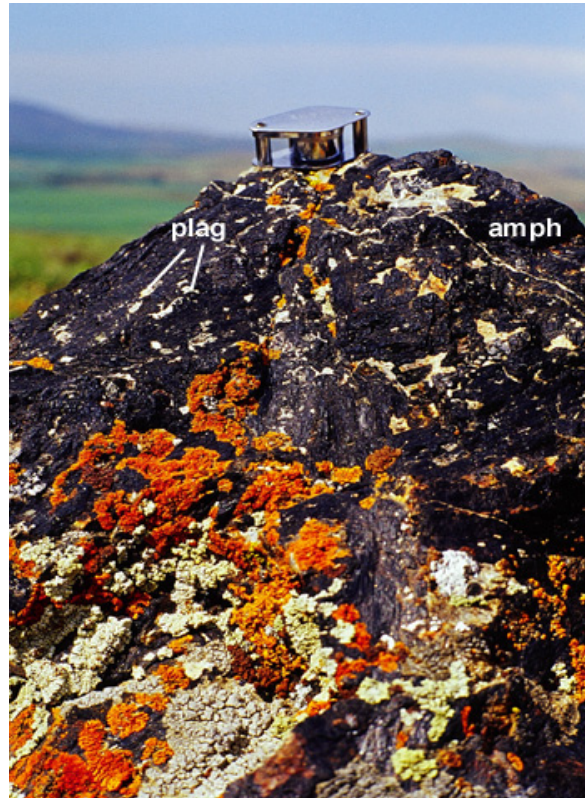
Figure 11. Field view of HBdite composing of mainly black prismatic amph and few plag.
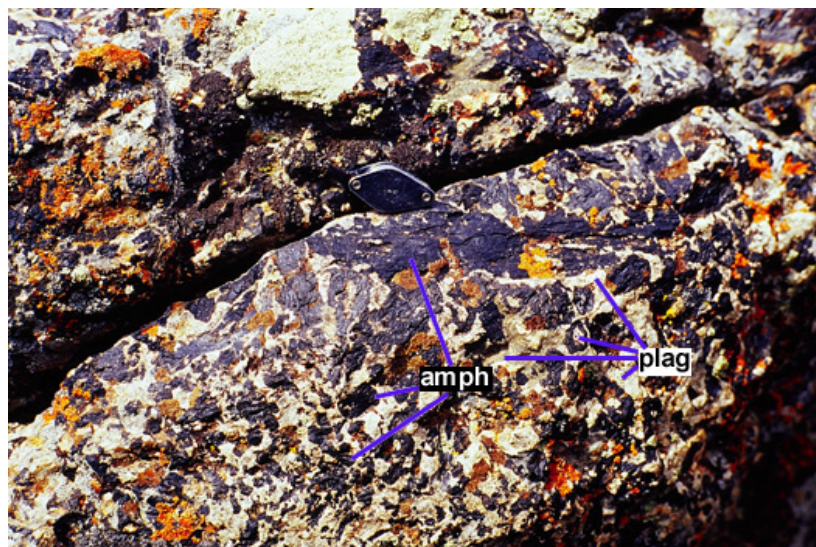
Figure 12. Field view of HBdite with variable sized crystals.
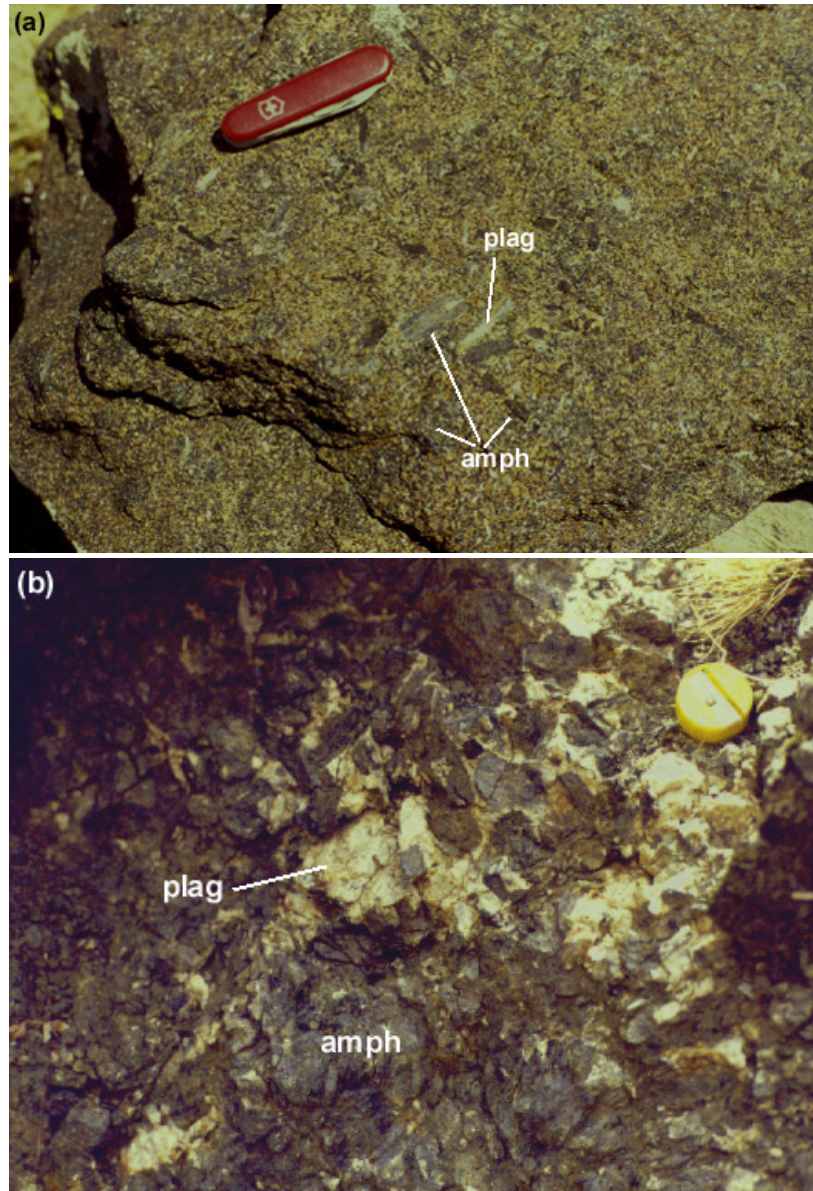
Figure 13. Field views of HBdite (a) fine-grained HBdite, (b) pegmatitic HBdite.
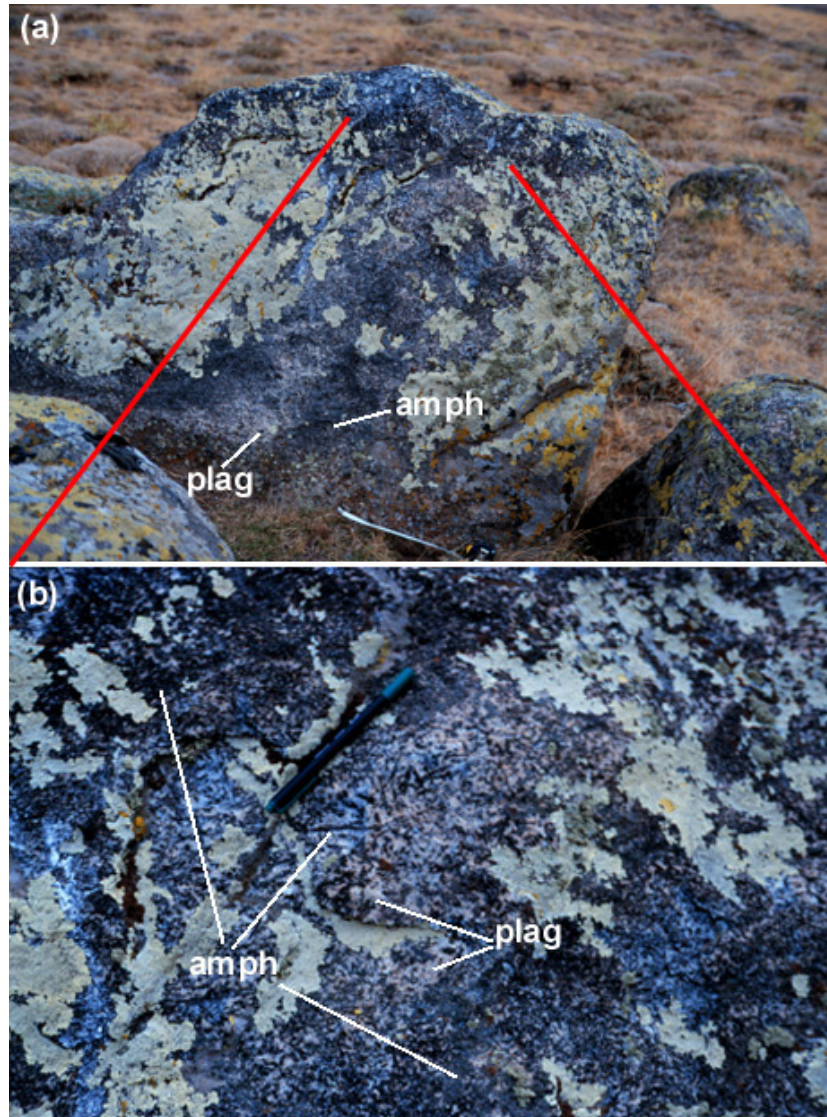
Figure 14. Field view of pegmatitic HBdite having plag-enriched leucocratic parts; (a) general view, (b) close up view of (a) showing long prismatic amph crystals disseminated in leucocratic parts.
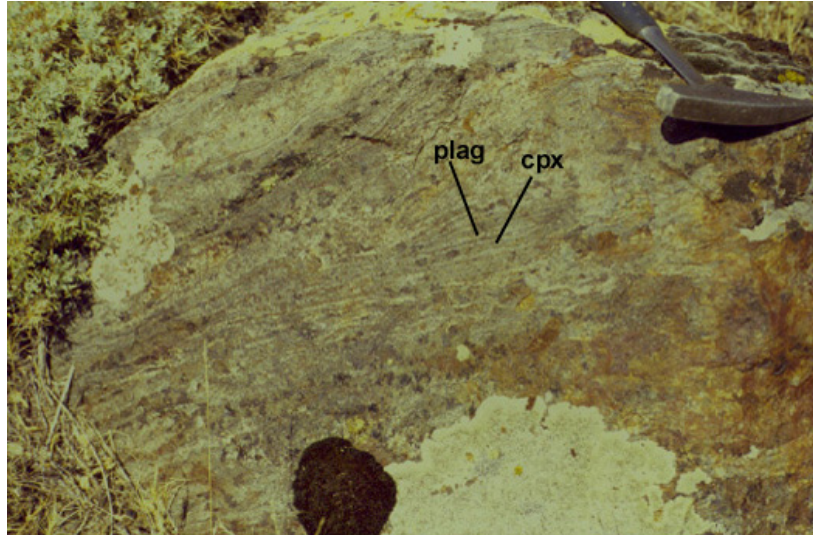
Figure 15. Field view of LG with alternating layers of plag and cpx.
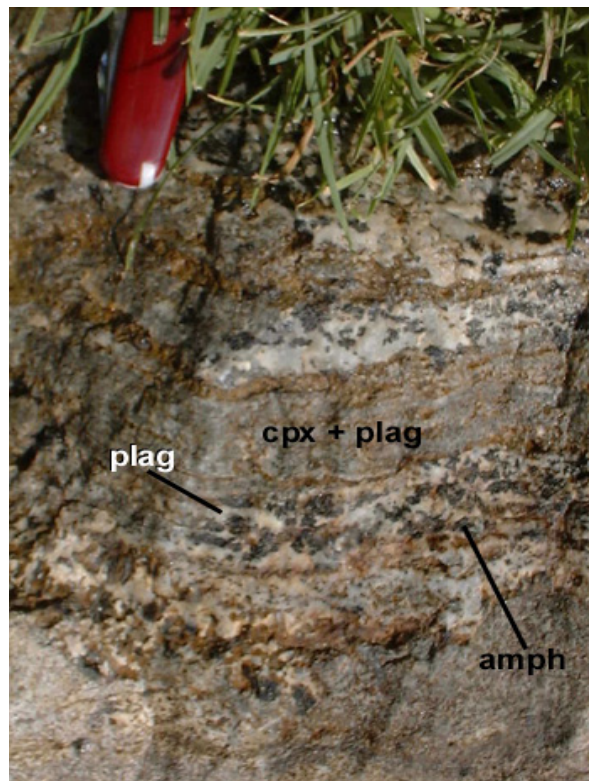
Figure 16. Field view of LG with alternating layers of fine-grained plag and cpx (very thin), and layers of pegmatitic amph and plag.

DIO occurring only in small exposure contains dominantly light brownish phl and plag. It shows a quite homogeneous mineral and grain size distribution.

Figure 17. Field views of LG with plag-cpx and pegmatitic plag-amph layers.

CHAPTER 3

PETROGRAPHY

3.1. Introduction

A petrographic study for the ultramafic-mafic rocks was carried out on 75 samples. Since the rocks are heterogeneous in both crystal size and mineral modes, at least 2 thin-sections were examined for each sample. Most of the samples are too coarse-grained for point counting to provide accurate modal proportions of the minerals; therefore modal proportions were calculated using major element compositions. For this purpose, many normative programs were used but unfortunately neither of them gave reliable results due to the high amounts of hydrous minerals in the rocks. Thus no accurate mode determination and so no further classification for the studied rocks was possible. Therefore, the same nomenclature has been used for the rock types defined by mineral modes in the field, such as CPXnite, CPXnite WHMP, PHLtite, HBdite, LG and DIO.

All rock types are composed essentially of cpx, dark mica (phl), amph (parg) and plag in varying amounts. The rocks rarely show act, chl, pump, ep due to low grade metamorphism. In addition, little amounts of surface alteration products (verm, ser, cc) are present. The accessory minerals are mainly Ti-rich phases (sph, rt, ilm), ap and pyr.

3.2. Texture

The rocks exhibit well-preserved igneous textures, despite signs of low grade metamorphism, surface alteration and cataclastic deformation. They are characterized by cumulate textures. CPXnite and PHLtite display orthocumulate textures (Figure 18) while CPXnite WHMP, HBdite, LG, DIO has adcumulate textures (Figure 19). The cumulate minerals are cpx, phl and amph while the intercumulate phase is plag. Cumulate textures infer that the first crystallizing phase was cpx. Phl crystallized after cpx, and then amph appeared. Plag crystallized last as an intercumulus phase. In this study, crystallization of phl before amph was observed, and therefore the interpretation in previous studies (phl replacing amph; Toksoy, 1998; Toksoy and Göncüoğlu, 1998; Toksoy-Köksal et al., 2001) was corrected. Appearance of phl before amph indicates crystallization from a magma with high H_2O content (Maaloe and Wyllie, 1979).
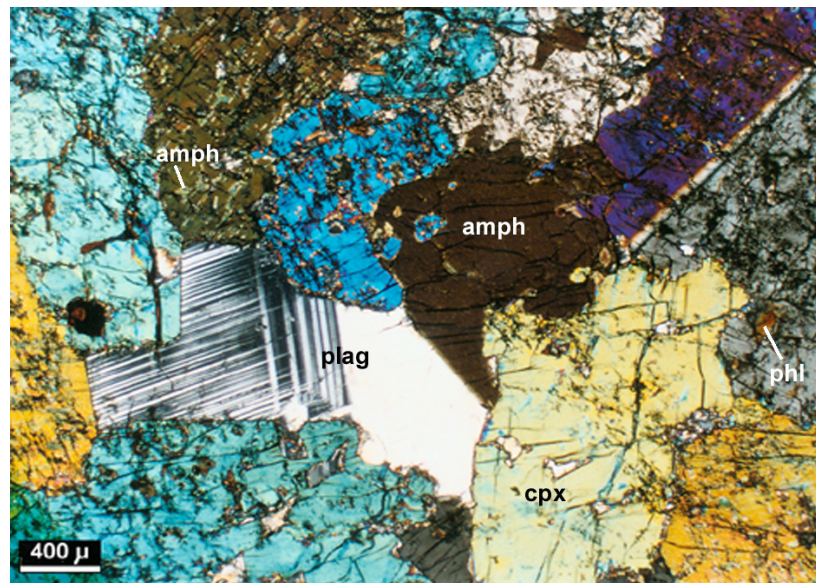
Figure 18. Photomicrograph showing orthocumulate texture from a CPXnite sample (analyzer in position).
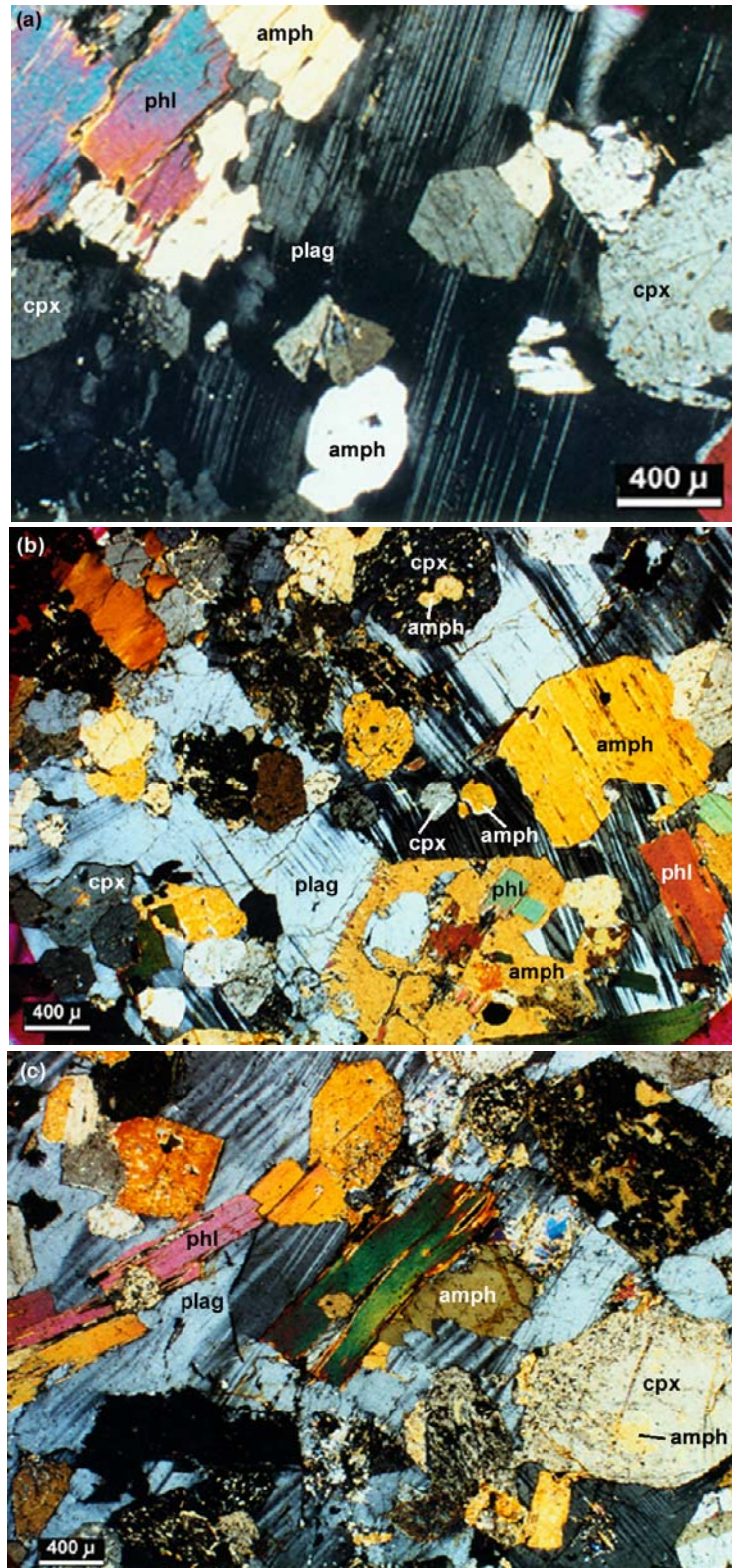
Figure 19. Photomicrograph showing adcumulate texture from CPXnite WHMP samples where plag is intercumulus phase (analyzer in position).

3.3. Major Minerals

The first crystallizing phase, cpx, is the most abundant mineral in the studied rocks. It is found in varying amounts. CPXnite is composed of almost 100% cpx while CPXnite WHMP, PHLtite and LG are composed of 20 to 60% modes of cpx. DIO shows only minor amounts of cpx (less than 3-4%). While fine-grained HBdite is composed of 3-4% cpx, pegmatitic HBdite is characterized by very little cpx (0.5-1%) that is found as tiny relict grains. Relict cpx in pegmatitic amph suggests that amph replaced primary cpx.

Petrographical features of cpx display a composition of diopsidic aug with an extinction angle of 40°-45° and interference colors of middle to upper second order. Cpx is colorless to pale green - pale grayish green and shows very weak pleochroism. Cpx crystals are found as very fresh, euhedral, short prismatic grains (Figure 19) to intensely altered, fractured and fragmented anhedral ones (Figure 20). Cataclastic deformation is recognized mainly at grain boundaries of cpx crystals, and fracturing is also intense in cpx-rich rocks (CPXnite, CPXnite WHMP and PHLtite) (Figure 20). Cpx is commonly replaced by amph and dark mica at rims, along cleavage and fracture planes, in cataclastically fragmented parts (e.g. Figure 20). These parts show a spongy appearance. Cpx crystals, highly variable in grain size from few mm to pegmatitic size, generally display sutured boundaries with coexisting crystals, either cpx or other phases of the rocks (Figure 21). Cpx rarely exhibits zoning (Figure 21a).

The dark mica (phl) with variable crystal size (few mm to 2-2.5 cm) is found in all rock types in varying amounts from about 1% to 80%. It is the essential mineral of PHLtite (up to 80%) and DIO (up to 60-70%). It does not coexist with plag in PHLtite whereas it is found together with plag in DIO. Phl is commonly found in association with cpx. Large crystals of phl poikilitically enclose cpx (Figures 22, 23). In CPXnite, the amount of phl is generally reduced and replaces cpx as tiny needles or patches (e.g. Figure 21a). However, in CPXnite WHMP and LG phl occurs as fine to medium sized euhedral to subhedral crystals in varying amounts (Figure 19). It is commonly

found as relict in amph crystals of the pegmatitic HBdite while there is no phl in fine-grained HBdite.
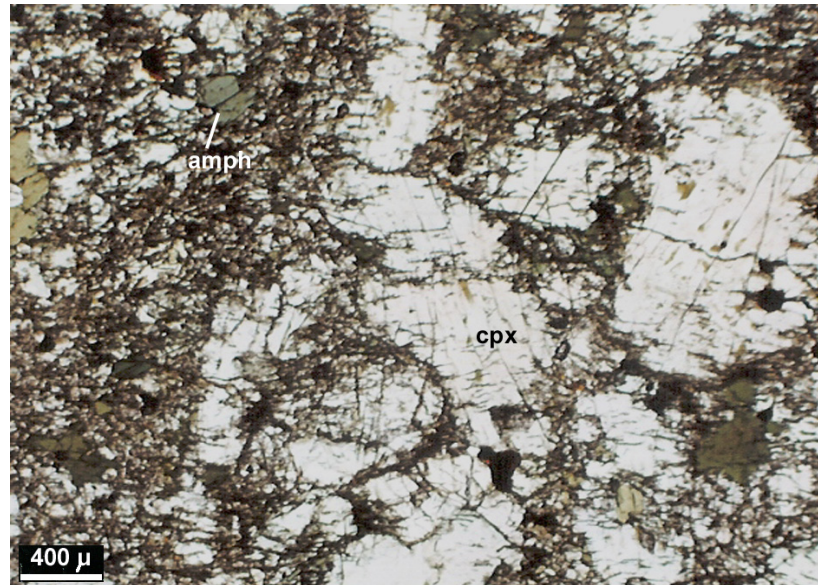
Figure 20. Photomicrograph showing cataclastic deformation on cpx crystals from a CPXnite sample (analyzer out position).

Phl having pegmatitic size is developed in form of plates with some degree of ragged terminations (Figures 23, 24). Such phl crystals show a strong pleochroism from light yellowish brown to reddish brown, purplish to greenish brown. The crystals show bright interference colors of second and third orders, and a low 2V of 2-8°. Crystals commonly display kink bands and bending due to magmatic deformation (Figures 19c, 25). There is no zoning in the crystals. In general, the crystals are fresh except for a limited degree of alteration to chl and verm.

Amph, one of the major phases in the rocks shows both, primary and late magmatic origins. Primary magmatic amph, either fine-grained or pegmatitic, is the essential mineral of HBdite (Figure 26). However, amph occurs in minor amounts as late magmatic phase in the forms of blebs,
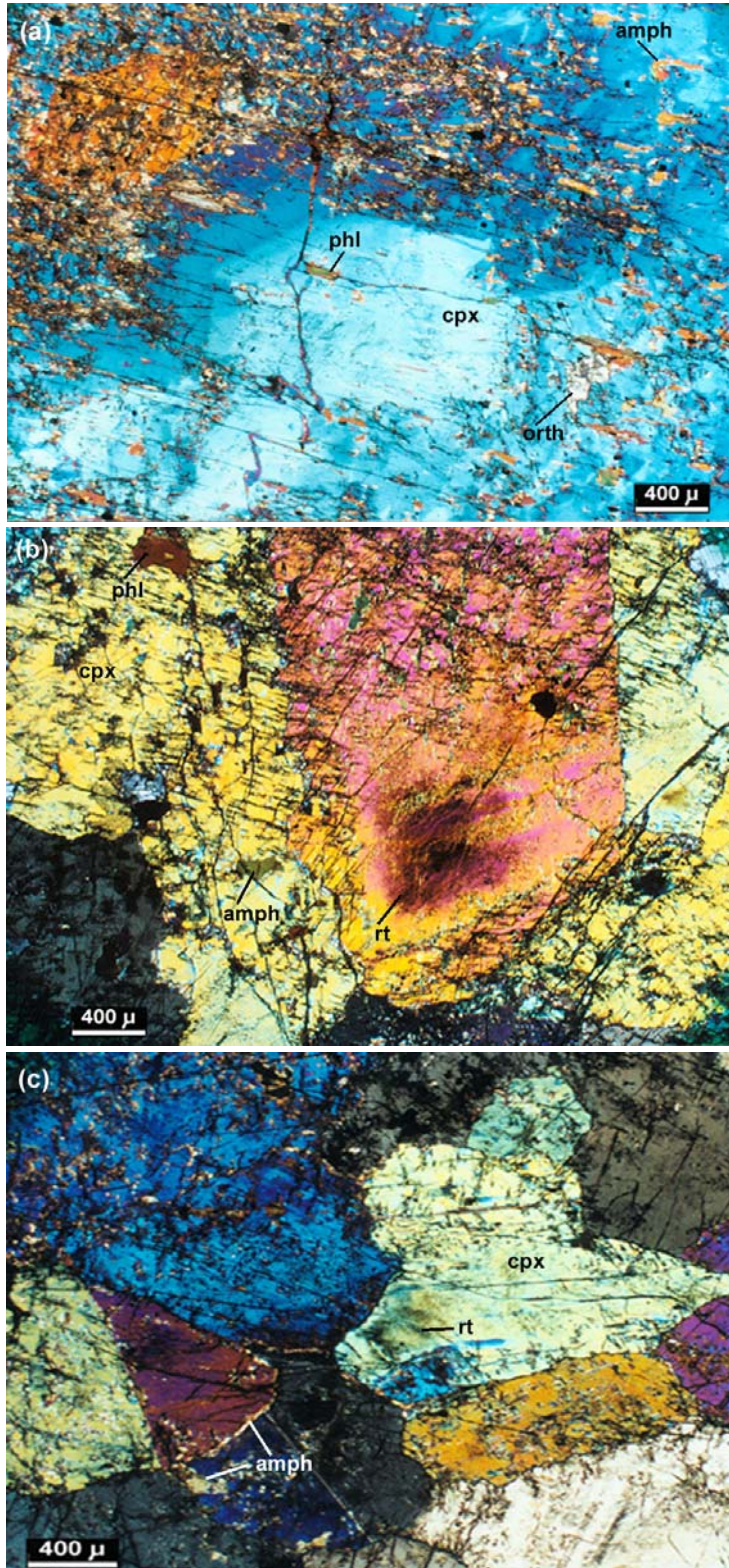
Figure 21. Photomicrograph showing variable sizes of cpx crystals from CPXnite samples (analyzer out position).

45
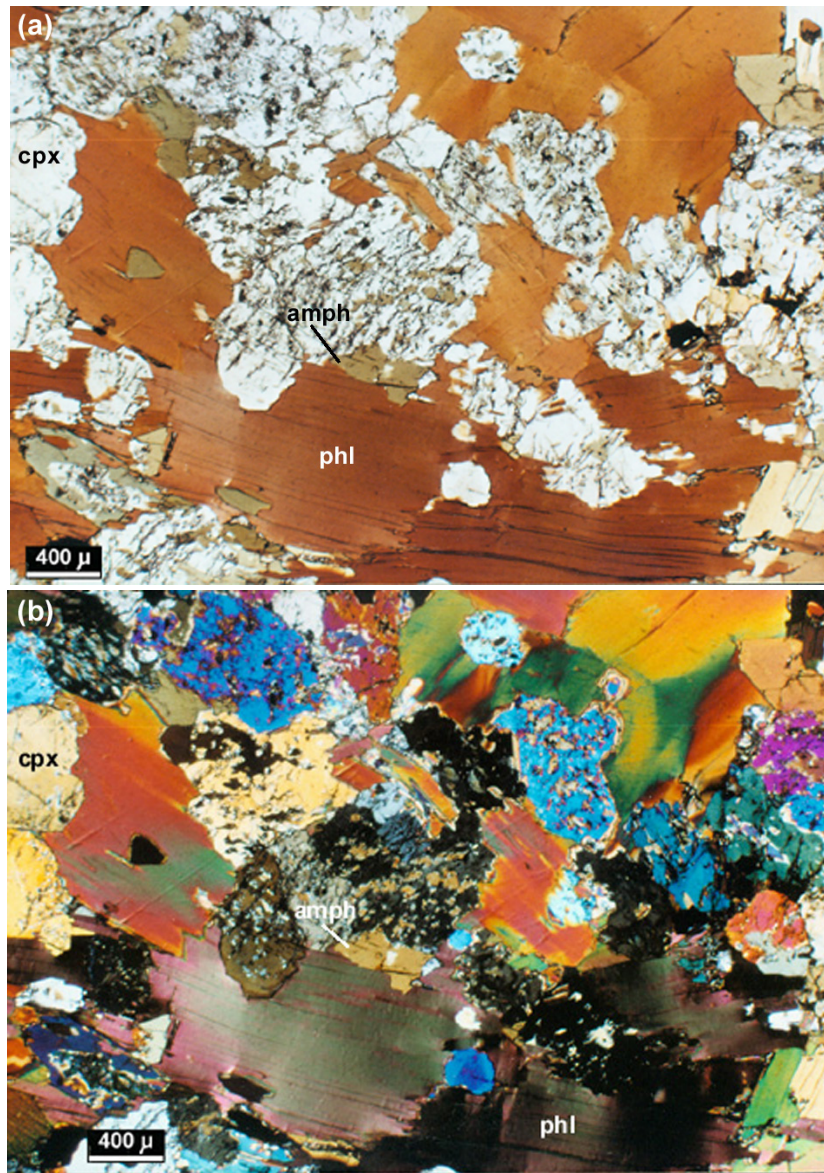
Figure 22. Photomicrograph showing phl enclosing cpx from finer grained and cpx enriched PHLtite sample (a) analyzer out position, (b) analyzer in position.

lamellae or rims on cpx crystals, and as interstitials between cpx crystals in CPXnite, CPXnite WHMP, PHLtite, LG (e.g. Figures 18, 19c, 20, 21). Moreover, late magmatic amph is also found as pseudomorph after cpx in CPXnite WHMP in variable amounts. Neither primary nor late magmatic amph is present in DIO. In general, primary euhedral amph and pseudomorph amph crystals are not found in association with phl while late stage magmatic amph blebs, lamellae or patches coexist with phl (Figure 22). Late phase magmatic amph appears as an overgrowth on cpx that formed by reaction between a melt (residual or infiltrating) and cpx. This partial replacement texture grades into complete replacement, where amph forms pseudomorphs after cpx (Figure 19b). Partial and complete replacement of cpx by amph is a common occurrence in CPXnite, CPXnite WHMP, PHLtite and LG. Crosscutting amph-plag rich veins display a relative enrichment in late phase magmatic amph developed coexisting with phl.
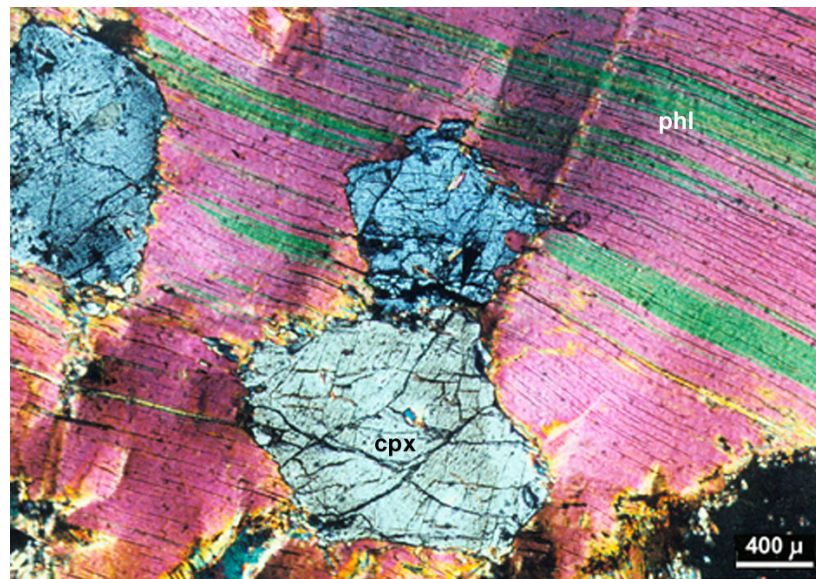
Figure 23. Photomicrograph showing phl enclosing cpx from a coarse-grained PHLtite sample (analyzer in position).
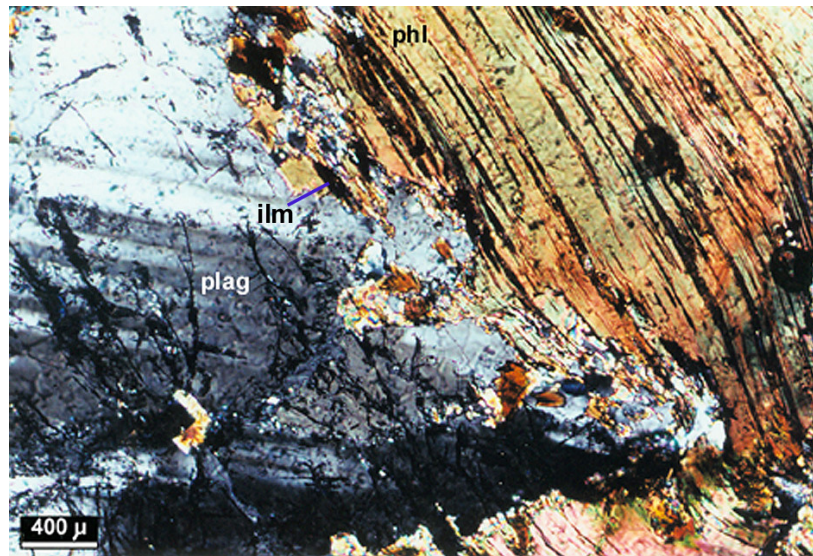
Figure 24. Photomicrograph showing contact relation of phl with plag from a DIO sample (analyzer in position).

Figure 25. Photomicrograph showing kink banding in phl crystal from a PHLtite sample (analyzer in position).
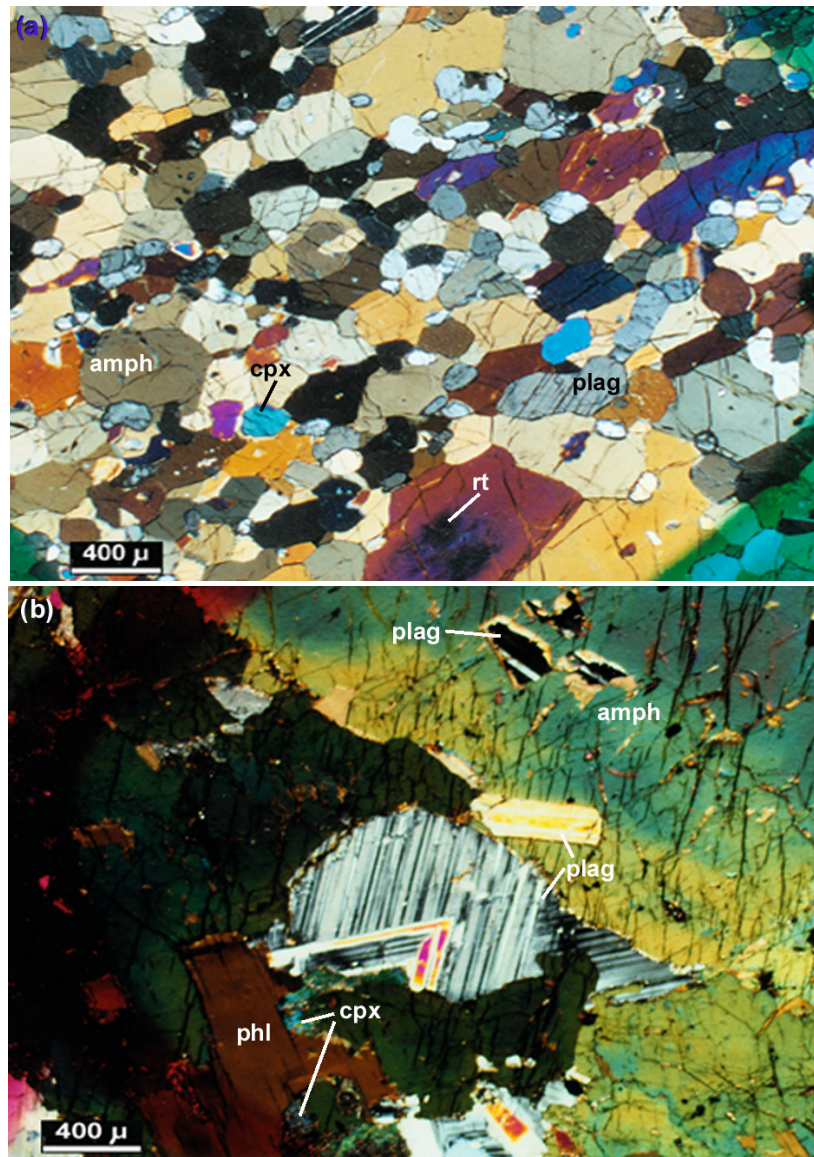
Figure 26. Photomicrograph showing (a) fine-grained HBdite sample, (b) pegmatitic HBdite (analyzer in position).

Primary amph crystals, which are highly variable in size (from few mm to pegmatitic size (up to about 20 cm) are usually euhedral long prisms. Rarely amph crystals showing faint optical zoning and twinning (Figure 26b) are found. Prismatic crystals show brownish green colors with strong pleochroism. Pseudomorphs after cpx are also brownish green and resemble primary prismatic ones. However, the rest of late phase magmatic occurrences are green colored.

Plag exists almost in all rock types in varying amounts. It is very limited in PHLtite, CPXnite with a mode of up to 3-4% and found as intercumulus phase between cpx crystals (Figure 18). However, it is found in higher amounts in CPXnite WHMP, LG, DIO and HBdite (Figure 19). It accounts for 85% of the modal mineralogy in leucocratic parts of HBdite. Plag crystals are usually anhedral to euhedral. They rarely show weak zoning.

Neither ol nor opx was observed in the studied samples. The absence of these two minerals is a characteristic feature of the studied ultramafic-mafic rocks.

3.4. Quenched Magmatic Enclave

Three small quenched magmatic enclaves were petrographically identified in one of the pegmatitic HBdite specimens (sample no: KK-34). They are placed between plag and amph crystals (Figure 27) and show sharp resorbed boundaries with the surrounding crystals. Generally the outer parts of the enclaves are detached from the matrix, leaving empty spaces. Amph is the only mineral observed that is enclosed in the glassy matrix of enclaves. Crystallites and microcrysts of amph (e.g. 3 to 200 μm in size) dominate the enclaves.

3.5. Accessory Minerals

The rocks are composed accessorily of Ti-rich phases (sph, rt, ilm), ap and pyr. The most common accessory mineral is sph either as post-cumulus phase or as exsolution in cpx. It is generally found between interstices of large crystals or as small inclusions within cpx crystals from cpx and phl rich rocks.

Anhedral to euhedral crystals of sph show strong pleochroism indicating a high Ti-content. rt is found as very tiny needles in amph and cpx. Blackish tiny crystals of rt form aggregates giving a dirty appearance to amph and cpx (Figures 21b,c, 26, 27). Ilm rarely occurs as small grains at boundary of phl crystals (Figure 24). Sporadic occurrence of ap domains are rarely observed. Pyr occurs as tiny crystals.
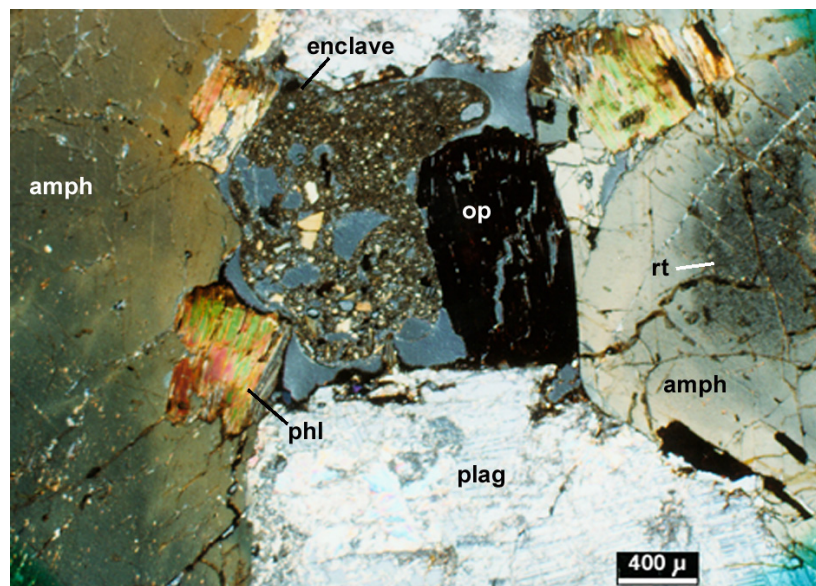
Figure 27. Photomicrograph showing quenched magmatic enclave in pegmatitic HBdite (analyzer in position).

3.6. Low Grade Metamorphism and Surface Alteration Products

Petrographic studies allowed to identify rare cc, verm and ser as surface alteration products, and act, chl, pump, ep as low grade metamorphic phases.

Replacement of phl to verm is poorly developed at rims and along cleavage planes due to surface alteration (Toksoy, 1998; Toksoy-Köksal et al., 1999, 2000, 2001b). Verm replacing phl plates shows optical continuity with the parent mineral. It is colorless to pale yellow with very weak pleochroism. cc

is rarely observed as filling the interstices between the main minerals, and in plag crystals. Ser is common in plag crystals.

The most common low grade metamorphic mineral is act. It is developed on cpx and late stage magmatic amph. It rarely progresses into plag. Chl, ep, pump are very rarely observed.

CHAPTER 4

MINERAL CHEMISTRY AND PETROGENETIC IMPLICATIONS

4.1. Introduction

Chemical analyses on the minerals of the rocks were carried out using electron microprobe (EMP). The details about the conditions of the analysis are given in Section 1.3.2.1. The oxide values obtained by EMP were converted to cations per formula unit (pfu) for each mineral based on the crystal chemistry of the minerals. For the major minerals of the studied rocks, py, mica, amph and feld, the calculations were based on the following features: For py having 6 oxygen atoms and 4 cations, cation totals were normalized to stoichiometric values (Vieten and Hamm, 1978). For mica having 24 oxygens and 4 OH groups, cations were calculated on anhydrous basis using 23 oxygens (Deer et al., 1992; Rieder et al., 1998). For amph having 46 negative charges (22 oxygen and 2 OH groups), calculations were based on anhydrous form with 23 oxygens and subtotals of cations rather than cation totals that were normalized to stoichiometric values (Leake et al., 1997), and so 13eCNK (13 cations excluding Ca, Na, K) correction (cation subtotal of Si through Mn excluding Ca, Na and K) was used. For feld, 8 oxygen atoms (Deer et al., 1980) were taken as the base. It is important to note that chemical formula of the hydrous minerals (mica, amph) were calculated based on anhydrous form since H_2O, F, and Cl determinations by EMP are not possible or not so precise.

Recalculations of mineral analyses (oxides) into cations pfu were carried out using the formulations prepared under Microsoft Excel program during this study on the basis of hints given in literature (e.g. Deer et al., 1980; Vieten and

Hamm, 1978; Droop, 1987; Schumacher, 1991; Morimoto, 1989; Leake et al., 1997; Rieder et al., 1998; etc), and the results from them were used in this study. Classifications and site allocations were done according to recommendations of the International Mineralogical Association (IMA) for the mafic minerals, py, amph and dark mica (Morimoto, 1989; Leake et al., 1997; Rieder et al., 1998, respectively) and Lindsley (1983) for py. The results obtained were crosschecked by various mineral chemistry related programs working under Windows and DOS. For the same analyses, cation calculations by various programs fitted without any problem.

The results depend on the normalization scheme that is used to estimate ferric and ferrous iron, and to estimate hydroxyl concentrations of hydrous minerals as well. The biggest problem in determination of chemical formulae is to derive Fe^{2+} and Fe^{3+} since all the iron is treated as FeO ($FeO^{(t)}$) by EMP. Estimation of ferric iron from the $FeO^{(t)}$ can be established through two ways of the same basic method; oxygen-based formulae (Droop, 1987) and cation-based formulae (Schumacher, 1991). In this study, the second way was used to estimate Fe^{2+} and Fe^{3+} where oxygen deficiency was determined following Droop (1987) as proposed by Schumacher (1991). After cation-based calculation, an oxygen sum is obtained which is less than ideal. This oxygen deficiency is compensated by converting ferrous iron to ferric iron using the equation 4 of Droop (1987) ($Fe^{3+} = 2 *$ (ideal oxygen – normalized oxygen sum), $Fe^{2+} = Fe^{(t)} *$ (normalized) – Fe^{3+}). Ferric- and ferrous-iron of py and amph are determined following the above estimation. However, this stoichiometric calculation is not applicable to mica because of probability of vacancies in both interlayer and octahedral sites resulting in excess cations exceeding stoichiometric limits if total iron is treated as $FeO^{(t)}$ (Guidotti, 1984). Therefore, instead of stoichiometric calculations $K_2Cr_2O_7$ titration method was carried out on mica separates to determine ferric- and ferrous-iron.

4.2. Mica

Chemical properties of the dark micas of the plutonic mafic-ultramafic rocks from the Kurançalı area were studied to infer evidences about the system from which they were crystallized. However, Speer (1984) and

Feldstein et al. (1996) explained that micas from plutonic rocks are not as valuable as those from fresh volcanic rocks. Because mineral alteration, that is absent in phenocrysts of young lavas, is common in plutonic rocks due to interaction with meteoric water (Taylor, 1977; Criss and Taylor, 1986). Moreover, subsolidus re-equilibration is common in plutonic rocks while it is minimal in the volcanics due to rapid cooling (Speer, 1984; Feldstein et al., 1996).

Chemical compositions of the dark micas, compiled in Appendix B, were determined for each type of the rocks in the study area. Several analyses (about 500 point analyses) were performed on both large and micro crystals. Anhedral crystals either within cpx, amph or micro-fractures were also analysed. Major and minor element analyses were performed on 17 specimens. Moreover, mica separates from 8 of the specimens analyzed by EMP were also used to determine ferrous and ferric iron by $K_2Cr_2O_7$ titration. From the titration results, the standard equation; $Fe_2O_3 = 0.225024 * FeO^{(t)}$ was derived and the equation of $FeO = FeO^{(t)} - Fe_2O_3 * 0.8998$ was used to estimate ferric- and ferrous-iron, respectively.

4.2.1. Compositional Variations

Chemical compositions of the dark mica were examined separately for each rock types. It was observed that there is a compositional variation not only between several samples but also within a single sample. The dark mica, key mineral for the petrogenesis of the studied rocks, displays a gradational change in chemistry from ultramafic to mafic rocks. It is generally characterized by moderately high MgO and low $FeO^{(t)}$ with $Mg/(Mg+Fe^{(t)})$ ratios ranging from 0.43 to 0.71 and $Mg/(Mg+Fe^{2+})$ ratios ranging from 0.49 to 0.75 (Appendix B). Major and minor oxide values range within the same limits for micas of all ultramafics while micas from LG and DIO have relative differences in oxide compositions.

The dark mica crystals from ultramafic rocks are characterized by variable Mg# ($=Mg/(Mg+Fe^{2+})$) ranging from 0.52 to 0.75, where the anhedral patchy and/or small needle like crystals display the lowest values. Micas from

all ultramafics have similar compositions in SiO_2, Al_2O_3, TiO_2 and K_2O contents ranging between 34.65-36.62, 14.39-17.91, 1.76-4.30, and 6.68-9.66 in weight percentage (wt%), respectively. The highest TiO_2 values are found in micas from HBdite. Cr_2O_3 contents are very low, with a maximum of 0.12 wt%. BaO is also present and ranges from 0.01 to 0.88 wt%. The Na_2O contents are very low ranging between 0.06 and 0.46 wt%.

Mg-numbers of micas (0.56-0.60) from LG are relatively low but within the range of those of the ultramafics. SiO_2 contents vary similar to those of the ultramafics within the range of 34.99 and 36.77 wt%. Variations in Al_2O_3, TiO_2 and K_2O contents, within the ranges of 14.49-15.16, 3.60-4.61, 8.95-9.67 wt%, respectively, are not so wide as those for micas of the ultramafics. Cr_2O_3 contents of micas (<0.06 wt%) from LG are lower than those of micas of the ultramafics. Na_2O and BaO contents are also very low and within the ranges of 0.061-0.180, 0.036-0.483 wt%, respectively.

Chemistry of the dark micas from DIO with Mg# ranging between 0.49 and 0.54 is different from those of micas in the ultramafics and LG. SiO_2 content is higher and varies from 35.51 to 37.70 wt% while the range of Al_2O_3 content between 13.79 and 16.60 wt% is relatively lower than that of others. TiO_2 content is higher and varies from 2.54 to 5.62 wt%. K_2O contents vary from 8.05 to 9.49 wt%, similar to those in micas of LG. Cr_2O_3, Na_2O and BaO contents are <0.05, 0.072-0.201 and 0.090-0.474 wt%, respectively.

It is likely that the host magmas from which micas of PHLtite and CPXnite crystallized had higher MgO and Al_2O_3 concentrations relative to those of mafic rocks, which in turn were enriched in $FeO^{(t)}$ and TiO_2. Micas of PHLtite and CPXnite are highly aluminous (15.21-17.20 wt% Al_2O_3) with high Mg# (0.58-0.75) relative to micas in other rocks even those in the ultramafics. CPXnite WHMP overlapping the compositional field of HBdite and LG shows transitional compositions to micas of DIO. TiO_2 behaving similar to $FeO^{(t)}$ increases in micas from CPXnite through PHLtite, CPXnite WHMP, HBdite, LG to DIO. The lowest TiO_2 concentration for micas of the ultramafics can be explained by the presence of free Ti-rich phases such as rt, ilm and sph.

The best way to show chemical changes in the compositions of micas from different rock types is to identify the distribution of cation pfu against Mg# for each major and minor element (Figure 28), although oxide (wt%) vs. Mg# plots display the same patterns as well. The used cation values were calculated based on the method given in Section 4.2.2. Micas show a general pattern of decreasing Si, Ti and $Fe^{(t)}$ (also Fe^{2+} and Fe^{3+} separately) (Figure 28a,c,d), and increasing $Al^{(t)}$ (also $Al^{[4]}$ and $Al^{[6]}$, separately), Mg, Na (Figure 28b,e,g) with the increasing Mg# in the sequence of DIO-LG-HBdite-CPXnite WHMP-CPXnite-PHLtite. The largest compositional changes are shown by Mg, Fe^{2+}, Ti, Si and Al through micas of ultramafic to mafic rocks. Lower Al content of micas from LG and DIO may be explained by high amounts of plag present in mafic rocks, i.e. higher preference of Al into plag rather than mica. However, plag content is the least in the ultramafics, generally less than 2-3% except for HBdite. Although the major element compositions of dark mica are comparable among different crystals and give good relation among the rocks, minor elements (particularly Ca, Ba, Mn, Cr and Ni) are highly variable and scatter in the plots (Figure 28h,i,j,k,l). These relations may reflect different melt/crystal reaction proportions as suggested by Costa et al. (2001). Although there seems to be a too broad reverse relation between Mg# and K (pfu) except for micas of DIO, there is no systematic change in mineral chemistry in terms of K (Figure 28f).

The behaviour of OH against Mg# seems to be reversely controlled by F content (Figure 28m,n) and OH content varies broadly within the ultramafics themself in a negative way. Micas of DIO with the lowest Mg# and the highest Fe^{2+} content have the lowest OH and the highest F contents. Cl shows a broad reverse relation to Mg# except for most of the data from micas of CPXnite WHMP where plag is an intercumulus phase (Figure 28o). The Cl and F concentrations for the hydrous phases of the rocks with Cl=0.00-0.05 wt%, F=0.00-0.08 wt% for mica, and Cl=0.00-0.06 wt%, F=0.00-0.16wt% for amph are within the range of those for hydrous phases of kimberlites despite relatively lower values (Dawson and Smith, 1977; Erlank et al., 1987). Low amount of deficiency is present in OH sites of both mica and amph structures. The hydrogen deficiencies can be explained by their halogen contents (0.22
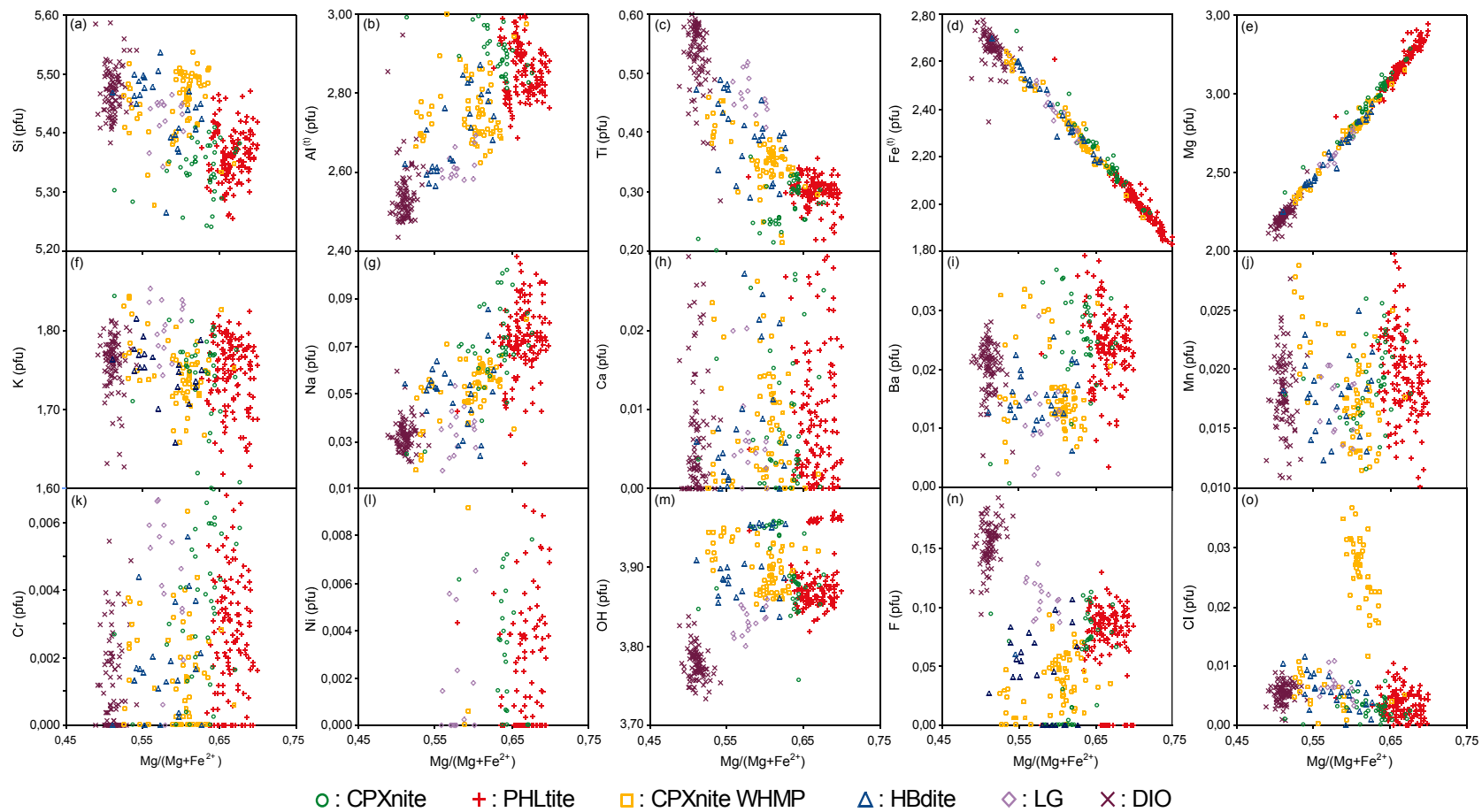
Figure 28. The behaviour of major and minor elements (cation pfu) against Mg# for micas.

wt% max) and/or as a characteristic feature of mantle minerals (Erlank et al., 1987; Dawson and Smith, 1977).

Tiny needle-, lath-like and/or anhedral mica crystals present in cpx crystals, uralitic amph and microfractures especially within CPXnite WHMP and HBdite, have lower Mg#, $Al^{(t)}$ and Mg (pfu) contents than large mica crystals, and approach the composition of micas found in LG and DIO. They are relatively enriched in $Fe^{(t)}$ and OH, and, may be related to late-magmatic or post-magmatic processes resulting from evolved, water rich liquids comparable to large crystals in the ultramafics, especially LG and DIO (Figure 28n). The lowest Cr (pfu) values, even 0.00 are from small patchy mica crystals (Figure 28g). The higher Cr content of the large crystals, even not so high, relative to small patchy crystals may be a result of reaction between the first crystallizing phase (i.e. py) and evolved melt(s).

Na# (Na/(Na+K)) varies between 0.010 and 0.071. Even though the Na# values are too low, there is a broad positive correlation between Na- and Mg-numbers (Figure 29). Na- and Mg-numbers of dark micas from the ultramafics are higher than those of micas from DIO. That means, the higher $Mg/Fe^{(t)}$, the higher substitution of Na for K. There is a crystal-chemical compositional control for the incorporation of Na in mica structure as suggested by Volfinger and Robert (1980), Volfinger et al. (1985) and Costa et al. (2001).

4.2.2. Nomenclature and Substitution Mechanisms with their Implications

Chemistry of mica as well as other minerals is best defined by cation pfu as mentioned above. Cation pfu in mica structure for each element was calculated by normalizing the sum of the atomic proportion of oxygen from each oxide to a positive charge of 44 based on anhydrous form as recommended by the IMA (Rieder et al., 1998), since there is no accurate determination of H_2O (wt%) by EMP. In theory, cation totals should be 16, however, the totals of the calculated cations are less than 16 for all of mica analyses in this study. This deficiency is the result of vacancies in both the octahedral and the interlayer sites as explained below. It is difficult to get correct structural formula for the studied dark micas because of vacancies in

the structure, impossibility of direct measurements of Fe_2O_3 and FeO, and H_2O by EMP as discussed by many authors (e.g. Hewitt and Abrecht, 1986; Schumacher, 1991; Feldstein et al., 1996).
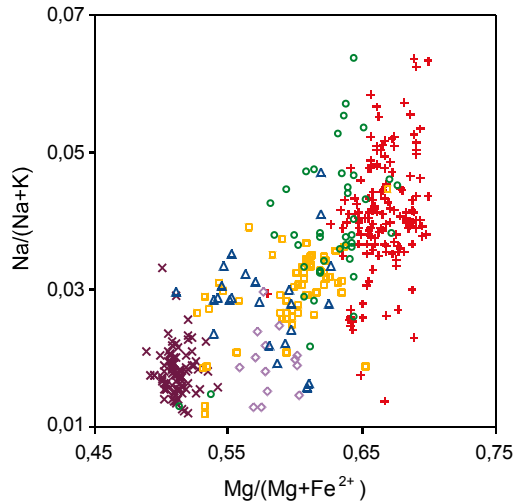
Figure 29. The broad linear correlation of Na# with Mg# (the symbols are as in Figure 28).

Because of complexities of solid solution in micas, description of natural micas is possible if at least five or six independent components are used (Foster, 1960; Guidotti, 1984; Rieder et al., 1998). The IMA recommended a simplified half cell formula, I M_{2-3} ()$_{1-0}$ T_4 O_{10} A_2, in which assignments of the elements to the sites are suggested as following; I (interlayer site) is filled by K, Na, Ba, Ca (sum to 1); M (octahedral site) is filled by Mg, Fe^{2+}, Fe^{3+}, Al, Ti, Cr, Mn (sum to 3); ()[6] (vacancy in octahedral site after allocation of all the elements), T (tetrahedral site) is filled by Si, Al (sum to 4); and A is representative of OH^-, F^-, and Cl^- anions (sum to 2). Based on this site allocation, the range of the average structural formula (half cell) for micas of ultramafic and mafic rocks is the following:

$$K_{0.9}(Mg_{1.6-1.1}Fe^{2+}_{0.8-1.0}Al_{0.0-0.1}Ti_{0.2-0.3}Fe^{3+}_{0.2-0.3}()_{0.1-0.3})(Si_{2.7}Al_{1.3})O_{10}(OH_{2.0-1.9}F_{0.1-0.0})$$

60
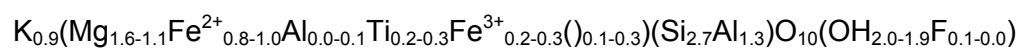
The studied dark micas having univalent interlayer cations greater than 80% are true micas according to the definition of IMA (Rieder et al., 1998) in which more than 50% of interlayer cations should be univalent. Micas exhibiting >0.85 interlayer cations are not interlayer deficient because interlayer cations should be <0.85 for being interlayer deficient. Based on the definition of the IMA, they are trioctahedral with their octahedral site cations approximating to 3.00 as well as vacancies in varying amounts ($I_{0.91-0.93}$ $M_{2.73-2.86}$ ()$_{0.27-0.14}$ T_4 O_{10} A_2). The formula given above shows that trivalent cations (Fe^{3+}, Al, Ti) are also present as well as divalent cations (Mg, Fe^{2+}) in the octahedral site of these micas. It is clear that as the percentage of trivalent cations increases in the octahedral site, occupancy decreases (i.e. vacancy increases) (Figure 30a). As seen from the Figure 30, occupancy in the octahedral site is the highest for micas from PHLtite having the highest MgO (wt%) and the lowest for those from DIO with the lowest MgO. Micas from the rest of the rocks are transitional through those of PHLtite and DIO. Some of the data for micas of CPXnite overlap the field of PHLtite. The relation of each trivalent cation and vacancy in octahedral site (Figure 30b,c,d) shows that positive correlation of vacancy and total of trivalent cations is extensively controlled by Fe^{3+} and Ti. However, there is a reverse relation between $Al^{[6]}$ and vacancy (Figure 30d). The control of divalent cations on the vacancy is also idenfied and it is seen that Fe^{2+} correlates positively with the vacancy in octahedral site while there is a reverse relation between Mg and vacancy (Figure 30e,f). In summary, the main control on vacancy in octahedral cation is dominated by Fe^{3+}, and also by Ti, Fe^{2+}. There is a linear relation between amounts of Fe^{2+} and R^{3+} (trivalent cations) in octahedral site, i.e. with increasing Fe^{2+}, R^{3+} also increases through PHLtite to DIO (Figure 31). This relation is mainly controlled by reverse relation of Mg and $Fe^{(t)}$ of micas.

The total number of octahedral cations ranges between 5.46 and 5.72 with need of a high amount of vacancy to fill the octahedral site to 6. The high amount of vacancy gives rise to departure from the ideal trioctahedral mica plane (Guidotti, 1984) (Figure 32). This may be caused by several reasons. For example, analytical procedures, especially failure for measurements of minor elements, may be one of these reasons. Actually, this can be best explained by a deviation toward a dioctahedral sheet due to solution between
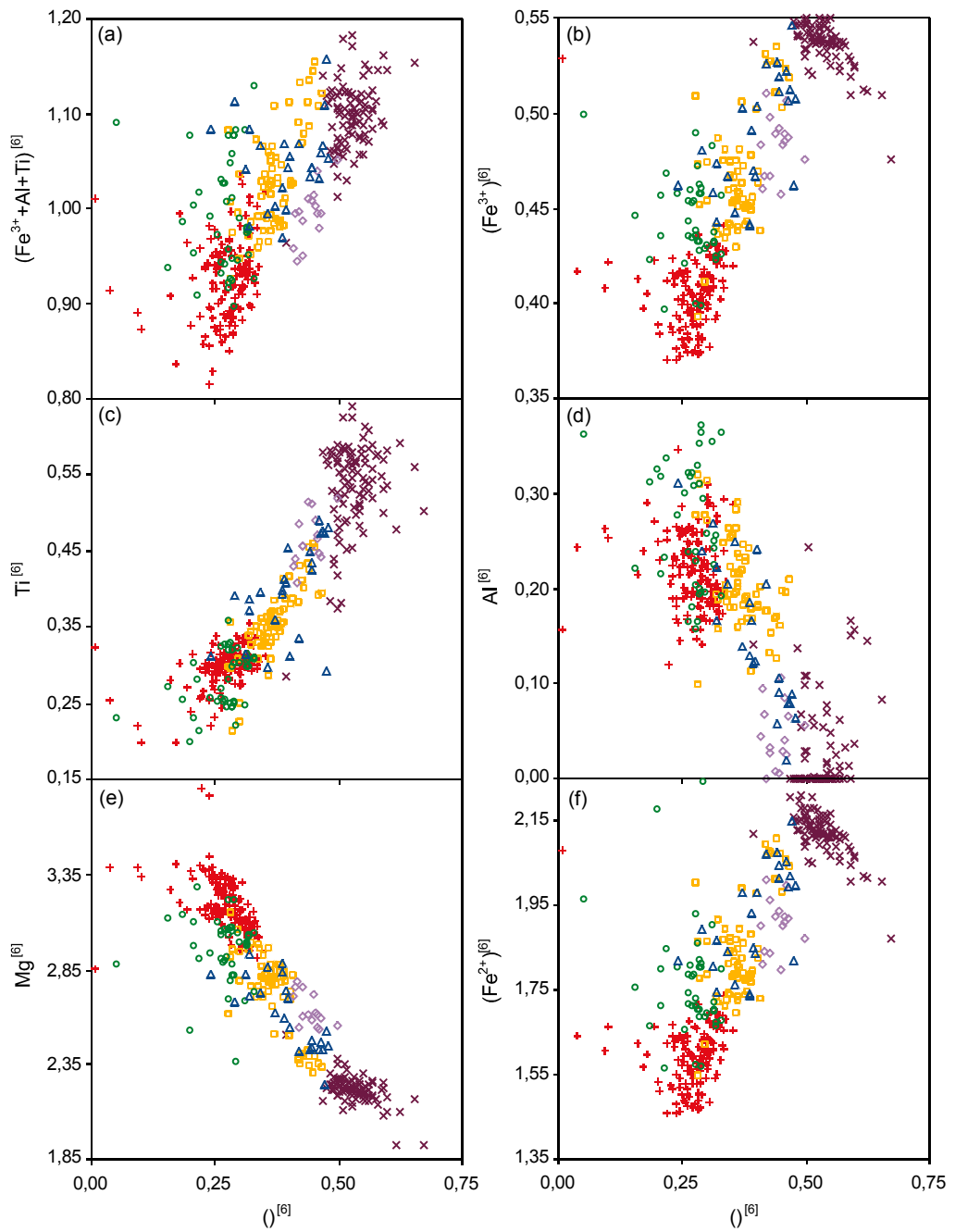
Figure 30. Effect of elements occupying the octahedral site on vacancy in the octahedral site (the symbols are as in Figure 28).

bio (in general sense) and musc. The hypothetical solid solutions between phl-musc, and between ann-musc, with substitution mechanisms of $3Mg^{[6]} \Leftrightarrow 2Al^{[6]}+()^{[6]}$ (Robert, 1976a), and $3(Fe^{2+})^{[6]} \Leftrightarrow 2Al^{[6]}+()^{[6]}$ (Rutherford, 1973) (Figure 33a,b), respectively, were defined to create vacancy in the octahedral site. Either mechanism is not very effective by itself. The first mechanism seems to be slightly more effective for micas of PHLtite, CPXnite and CPXnite WHMP while the second one slightly affects micas of HBdite, LG and DIO. Instead of a single hypothetical mechanism, the combination of these mechanisms, $3(Mg+Fe^{2+})^{[6]} \Leftrightarrow 2Al^{[6]}+()^{[6]}$ (Figure 33c), seems to be more effective to create vacancy and deviation toward the dioctahedral micas. For the studied trioctahedral micas, the well-defined mechanism $2Mg^{[6]}+Al^{[6]} \Leftrightarrow 2(Fe^{2+}+Fe^{3+}+Ti)^{[6]}+()^{[6]}$ (Figure 33d), may best explain the presence of vacancy in octahedral site and deviation from the ideal mica plane. The total number of the octahedral cations of the studied micas (5.46-5.72) may reflect a solution greater than 6.6% according to the calculations of Guidotti (1984).
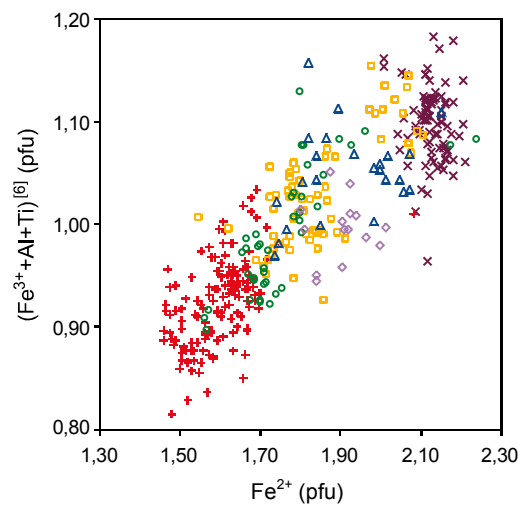
Figure 31. Linear relation of trivalent cations with Fe^{2+} within the octahedral site (the symbols are as in Figure 28).
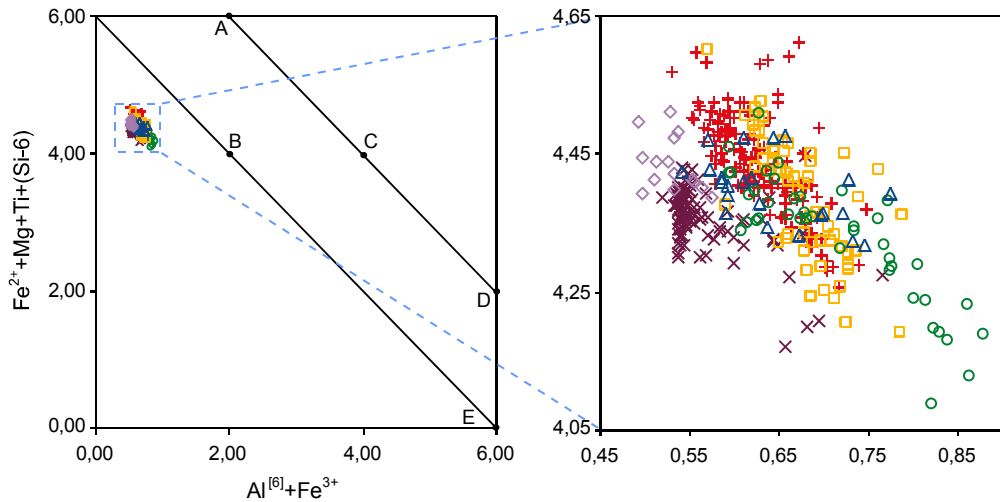
Figure 32. The plot showing the position of the studied micas on the ideal mica planes after Guidotti (1984) where A: $K_2(Mg,Fe^{2+})_6(Al_2Si_6O_{20})(OH)_4$ (bio) B: $K_2R^{3+}_2(Mg,Fe^{2+})_2(Si_8O_{20})(OH)_4$ (cel), C: $K_2Al(Mg,Fe^{2+})_5(Al_3Si_5O_{20})(OH)_4$ (east), D: $K_2Al_2(Mg,Fe^{2+})_4(Al_4Si_4O_{20})(OH)_4$, E: $K_2Al_4(Al_2Si_6O_{20})(OH)_4$ (musc) (the symbols are as in Figure 28).

In addition to the effect of vacancy on deviation from ideal mica plane, the presence of very high $Al^{[4]}$ content with depleted Si in the tetrahedral site and existence of Al in the octahedral site are assumed to be other reasons.

Compositions of the dark micas, rich in Mg, Fe^{2+} and Al in decreasing order, plot close to ann/phl corner on the side-musc-phen-ann/phl quadrilateral proposed by Deer et al. (1992) (Figure 34). Although mica compositions of the studied rocks are close to the phl/ann corner, they depart from the ideal phl/ann join shown by the relation of $Al^{[4]}/(Al^{[4]}+Si)$ (Al#) to $Fe^{2+}/(Fe^{2+}+Mg)$ (Fe#) due to the high $Al^{(t)}$ content (Figure 35) (Parsons et al., 1991), presence of Ti and Fe^{3+}, substitutition of F and Cl for OH, presence of vacancies both in octahedral and interlayer sites. Despite the departure from the ideal phl-ann join, mica compositions are more close to the phl end-member on the join (Figure 35). There is a reverse relation between Al# and Fe#, i.e. the highest Al# and the lowest Fe# are found in micas of PHLtite while the lowest Al# and the highest Fe# are typical for those of DIO. There is a decrease in Al# with increasing Fe# in micas from PHLtite through CPXnite, CPXnite WHMP, HBdite, LG and DIO. The data of micas from CPXnite WHMP, HBdite and LG
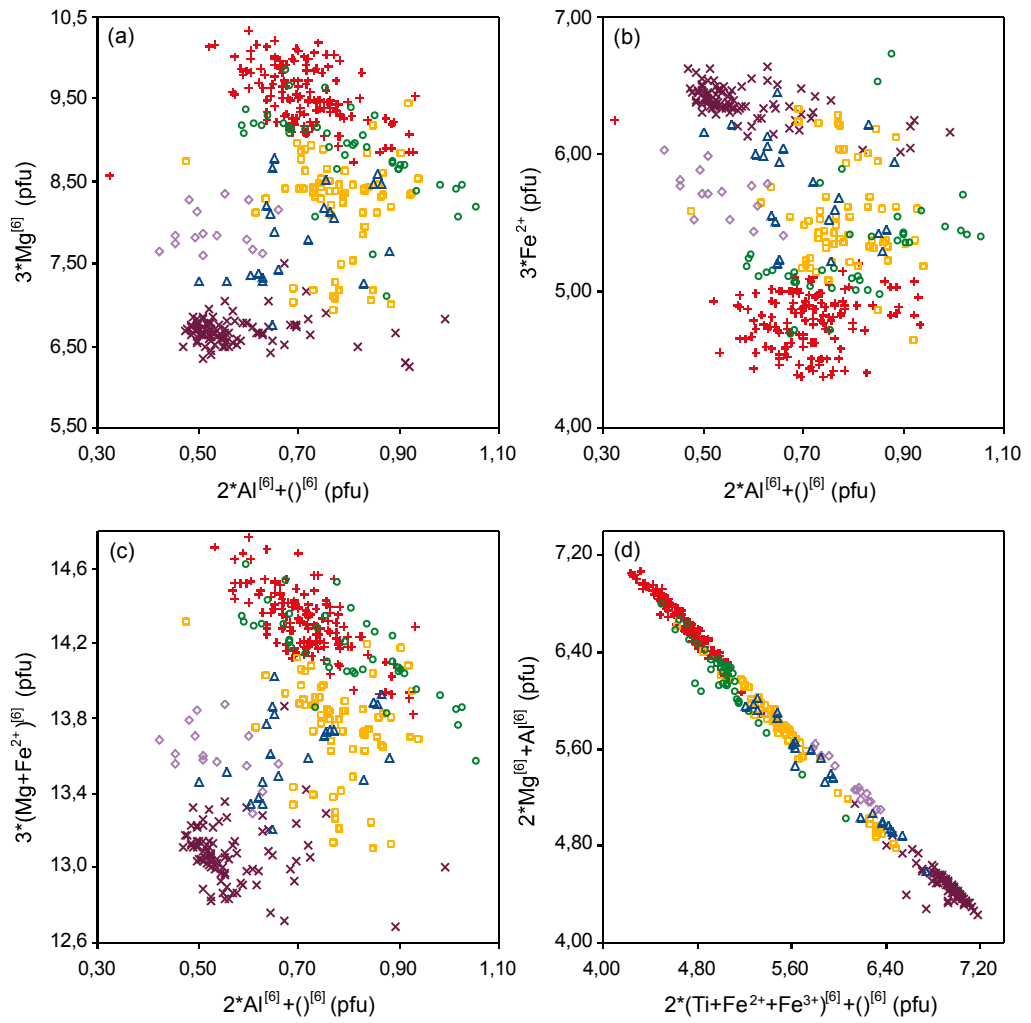
Figure 33. The substitution mechanisms showing the presence of solid solution between trioctahedral and dioctahedral micas creating vacancy in the octahedral site (the symbols are as in Figure 28).

overlap eachother. Some of micas from ultramafic rocks, tiny-andhedral-patchy, plot closer to DIO micas.
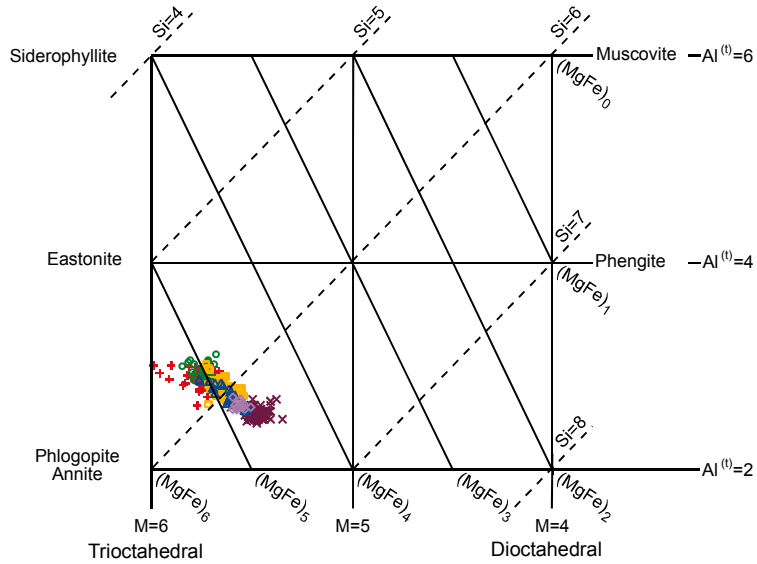
Figure 34. Plots of micas on Si-Al[^(t)]-M diagram of Deer et al. (1992) (the symbols are as in Figure 28).
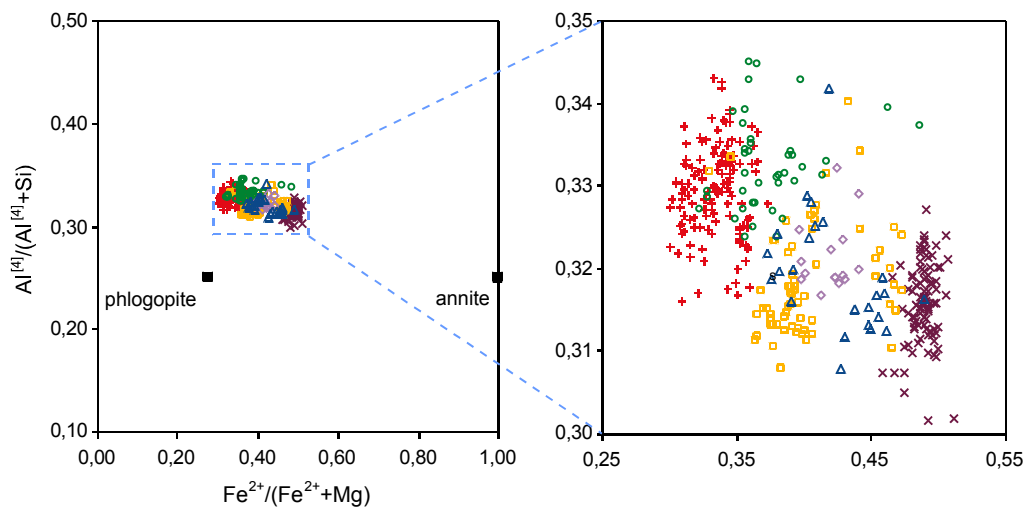
Figure 35. Plots of micas on phl-ann join given by $Al^{[4]}/(Al^{[4]}+Si)$-$Fe^{2+}/(Fe^{2+}+Mg)$ relation after Parsons et al. (1991) (the symbols are as in Figure 28).

66

The comparison of the structural formulae ($R^{3+}_{0.38-0.65}Fe^{2+}_{0.80-1.06}Mg_{1.60-1.11}$)($Si_{2.74-2.68}Al_{1.32-1.25}$)) of the studied micas with those of phl ($R^{3+}_{<0.50}Fe^{2+}_{<0.50}Mg_{3.00-2.00}$)($Si_{3.00-2.70}Al_{1.00-1.30}$)) and bio ($R^{3+}_{0.35-1.00}Fe^{2+}_{0.50-1.75}Mg_{1.75-0.75}$)($Si_{3.00-2.50}Al_{1.00-1.50}$)) of Foster (1960) supposes that the studied micas are closer to phl end member in terms of R^{3+} and $Al^{[4]}$ contents. It is important to note that Foster (1960) used only the perfect data without vacancy for his end member formula. The end member phl of Foster (1960) has Mg cation 90% of the octahedral position, and replacement of Mg up to 30% by most commonly Fe^{2+}, Mn and R^{3+} ($Al^{[6]}$, Fe^{3+} and Ti) results in all the other trioctahedral micas considered to be members of a system. The inter-element relation of Mg-(Fe^{2+}+Mn)-($Al^{[6]}$+Fe^{3+}+Ti) within octahedral site for the studied micas are shown in a ternary diagram (Figure 36). Based on the octahedral-site occupancy, the studied micas are within the Mg-bio field of Foster (1960) (Figure 36a) and mainly within the east field of Jiang et al. (2002 after Foster, 1960) (Figure 36b). The data line is inclined to the (Fe^{2+}+Mn) apex, and few of the analyses of tiny, anhedral patchy micas from the ultramafics and DIO, plot within the Mg-bio field of the later classification.

The classification of the dark micas, either as phl or as bio follows the Fe# (Fe^{2+}/(Fe^{2+}+Mg)) vs. $Al^{[4]}$ diagram of Deer et al. (1980) and the compositional limits of Rieder et al. (1998). All micas plot in the phl field of the diagram (i.e. Fe#<0.5) (Figure 37a). There are no important differences in the compositions of micas among the rock types except for DIO. It is clear that micas from DIO with the highest Fe# values fall very close to the phl-bio boundary and some of them lie on the boundary. However, micas of PHLtite with the lowest Fe# and the highest $Al^{[4]}$ are away from the boundary (Figure 37a). Although there is no significant change in Fe# and $Al^{[4]}$ content, it is obvious that $Al^{[4]}$ decreases with increasing Fe# through PHLtite to DIO. Thus it can be assumed that they record significant changes in crystallization history.

The plot of micas on a diagram with $Al^{[6]}$ against Mg# shows the relation of trioctahedral micas on an ideal bio plane (i.e. phl, ann, east, side quadrilateral) (Guidotti, 1984), high $Al^{[6]}$ micas lay close to the phl end-member (Figure 37b) while low $Al^{[6]}$ micas plot closer to the bio-phl boundary. In detail,
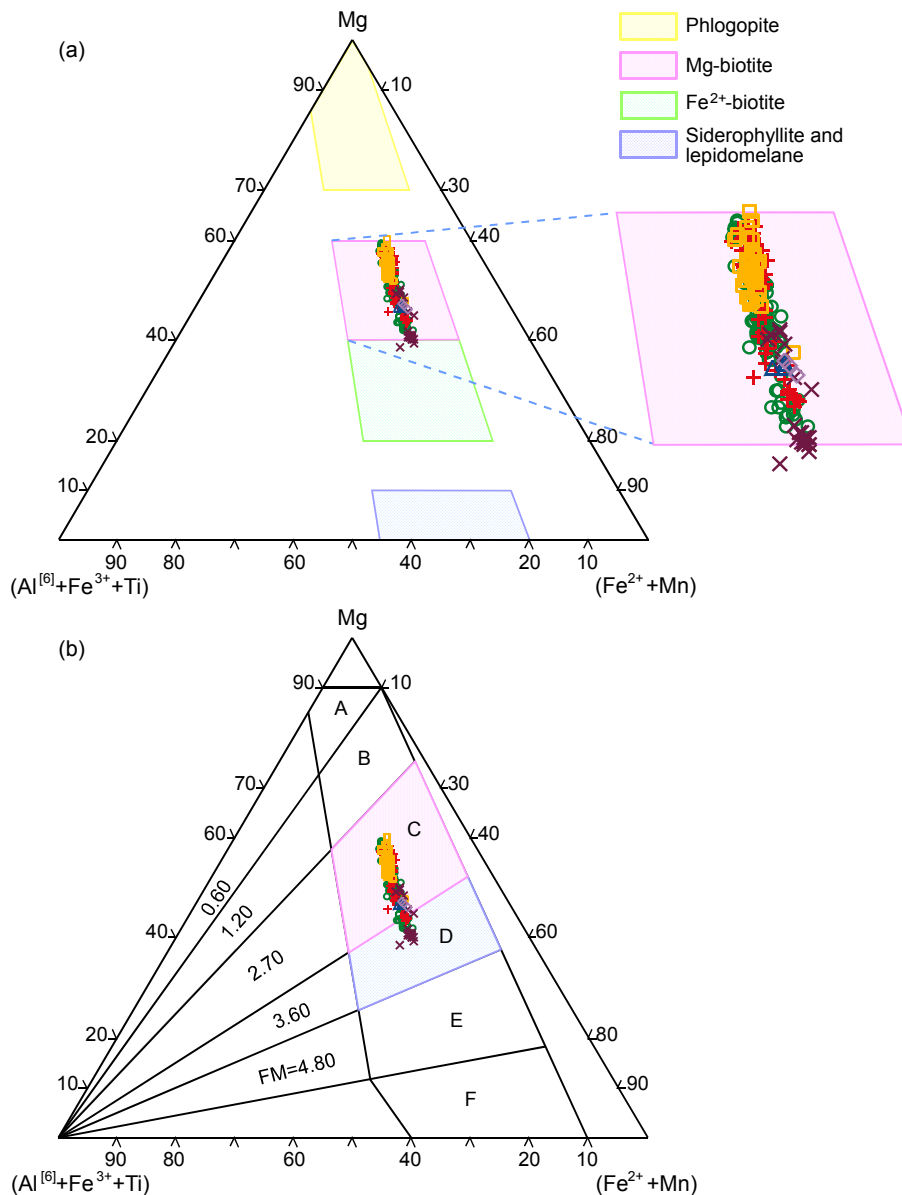
Figure 36. The position of the micas within the classification diagrams based on Mg-(Fe^{2+}+Mn)-(Al$^{[6]}$+Fe^{3+}+Ti) relation. (a) classification of Foster (1960), (b) classification of Jiang et al. (2002 after Foster, 1960) where A: phlogopite, B: Fe–phlogopite, C: eastonite, D: Mg-biotite, E: ferribiotite, F: siderophyllite and lepidomelane (the symbols are as in Figure 28).
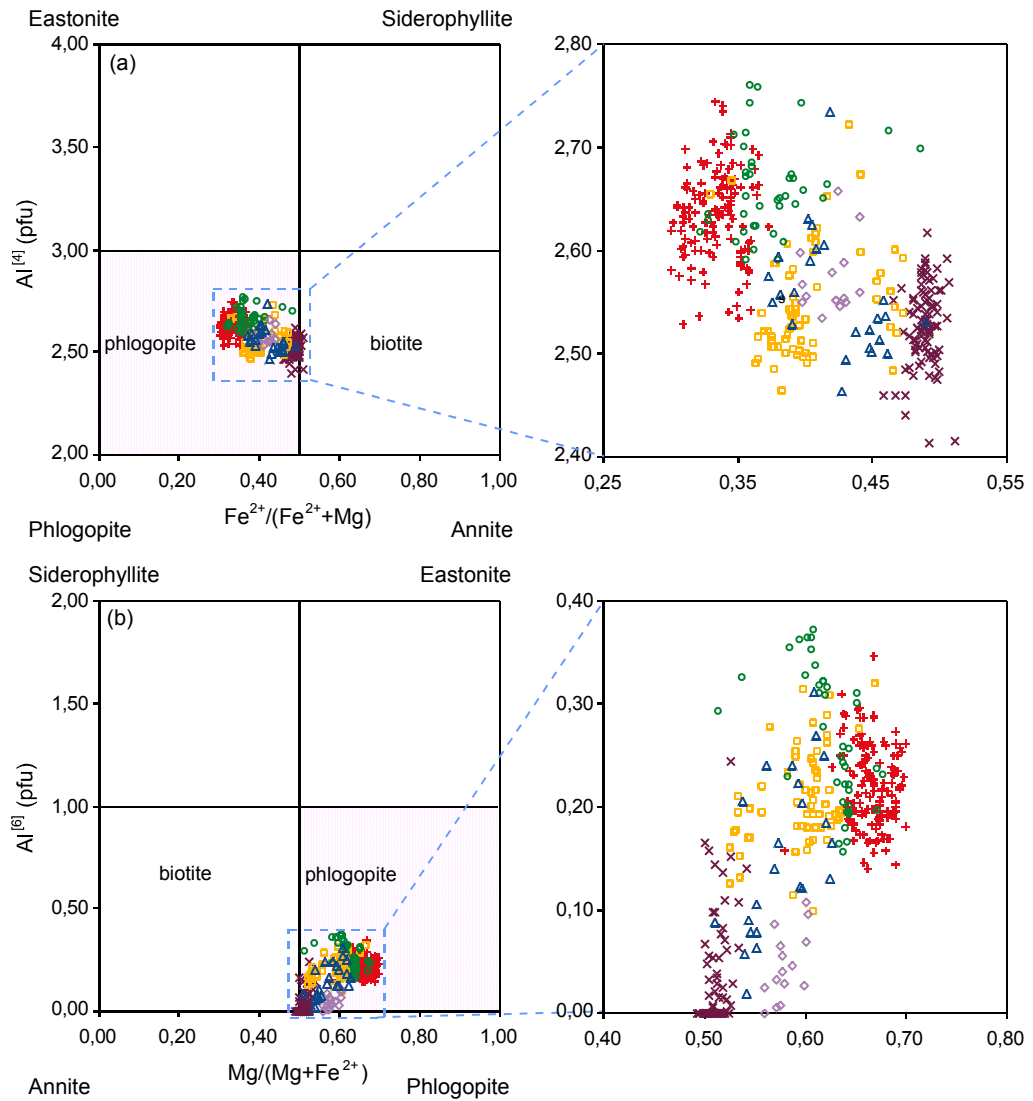
Figure 37. The places of micas on the ideal trioctahedral mica plane being based on ts and Mg-Fe^{2+} exchanges; (a) Al$^{[4]}$-Fe# from Deer et al. (1980) after Rieder et al. (1998), (b) Al$^{[6]}$-Mg# from Guidotti (1984) (the symbols are as in Figure 28).

those from the ultramafics except for HBdite show higher $Al^{[6]}$ values with a range between 0.1-0.37 than those from LG and DIO which range between 0.00 and 0.24. HBdite having 0.02-0.31 plots between these two groups (Figure 37b). Micas with Ti<0.54 and $Al^{[6]}$<0.40 (pfu) deviate from the ideal tetrahedral $Si/Al^{[4]}$ ratio of 3.0 as in phl or ann (Figures 37b and 38). All micas plot in a field indicating Si deficency and $Al^{[4]}$ excess compared to ideal phl (Figure 38) as discussed by Seifert et al. (2000) and Guidotti (1984). Besides $Al^{[6]}$, it is evident from Figure 38a that the studied micas approximate the ideal $Si/Al^{[4]}$ ratio of ann-phl with decreasing Mg from the ultramafics to the mafics. This is due to tschermakitic substitution in which for $Al^{[4]}$>2 charge balance is maintained by substituting $Al^{[6]}$ for Fe^{2+} in the octahedral site (Guidotti, 1984) where $Al^{[6]}$ is exchangeable with Ti as well (Figure 41d).
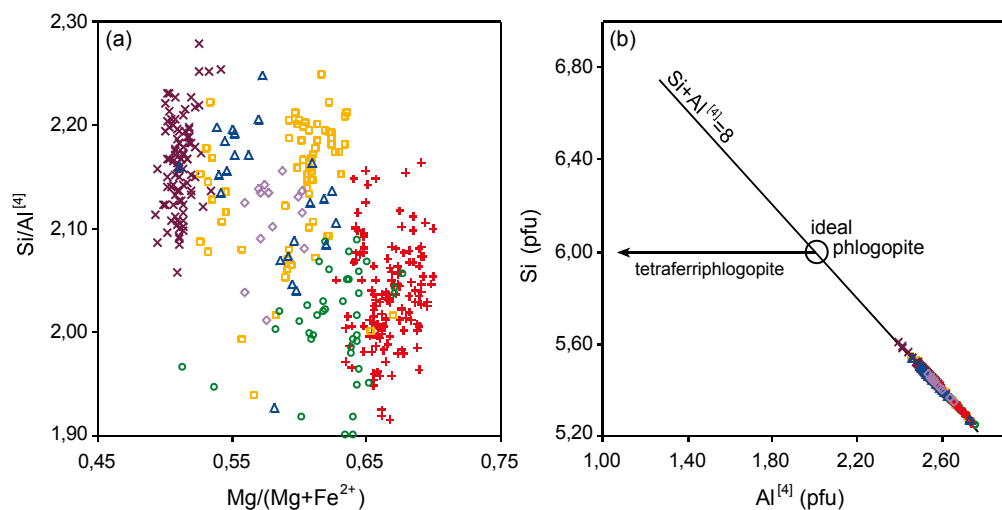
Figure 38. (a) The change in $Si/Al^{[4]}$ ratio (<3.0) with $Mg/(Mg+Fe^{2+})$, (b) Position of micas on $Si-Al^{[4]}$ diagram showing ideal position of phl composition (after Seifert et al., 2000) (the symbols are as in Figure 28).

Activity calculations using Holland and Powell (1990) displayed that activity of phl (0.020-0.171) is higher than those of east (0.000-0.041) and ann (0.000-0.039) (Figure 39). There is a well-defined correlation between phl activity (a_{phl}) and Mg#, where micas of DIO have the lowest a_{phl} while those of

PHLtite show the highest acitivity. east activity (a_{east}), which has lower values, behaves like that of phl with a larger spread. While a_{phl} and a_{east} show a positive correlation with the Mg#, a_{ann} correlates negatively.
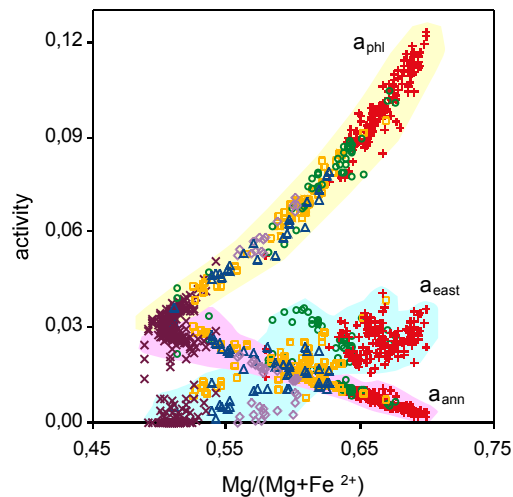
Figure 39. The Mg# control on the activities of end members for micas where a_{phl}, a_{east} and a_{ann} abbreviations for the activities for phl, east and ann, respectively (the symbols are as in Figure 28).

Following the discussions above, the final nomenclature and classification for mica was done according to IMA recommendations (Rieder et al., 1998). Although mica compositions are close to phl end-member, they can be defined as solid solution products between phl, east and their ferrous equivalents due to their high Al-content. They can be called aluminous. In spite of the presence of Fe^{2+}, Fe^{3+}, $Al^{[6]}$, Ti as well as higher proportion of Mg in the octahedral site, "**phlogopite**" is preferred as the name for the studied trioctahedral dark micas. Because the use of end-member names with or without modifiers and suffixes is suggested by the IMA instead of using series names associated with varietal modifiers (e.g. bio). Phl is preferred as name of micas as clearly shown in various classification diagrams in which all plots approximate the phl end-member.

Compositional changes in mica, which can be representative of differences in rock composition, can best be explained by substitution mechanisms. There are several substitution mechanisms in trioctahedral micas. The principal differences in the compositions of the studied micas are best expressed in terms of the exchange reaction, $Fe^{2+} \Leftrightarrow Mg$ (Figure 40) where Fe^{2+} increases with decreasing Mg from PHLtite through CPXnite, CPXnite WHMP, HBdite, LG to DIO. Micas of CPXnite WHMP, HBdite and LG overlap each other. For these micas, broad reverse relation of $Al^{[6]}$ to $Fe^{(t)}\#$ $(Fe^{(t)}/(Fe^{(t)}+Mg))$ is well-defined while this relation is not present for $Al^{[6]}+Ti$ against $Fe^{(t)}\#$ due to the stronger positive correlation of Ti with $Fe^{(t)}\#$ (Figure 41a,c,e). Moreover, this is also evident from the clear relation of Ti to $Fe^{(t)}$ (Fe^{3+} and Fe^{2+}) (Figure 41b). Ti showing strong reverse relation to $Al^{[6]}$ and Mg (Figure 41d,g) seems to substitute for both $Al^{[6]}$ and Mg, but the range in Mg cations (1.92-3.80) far exceeds that of Ti (0.20-0.64). In accordance with these elemental relations, substitution mechanism in the octahedral site can be generalized as $(Mg+Al)^{[6]} \Leftrightarrow (Ti+Fe^{2+}+Fe^{3+})^{[6]}\pm()^{[6]}$ (Figure 42).
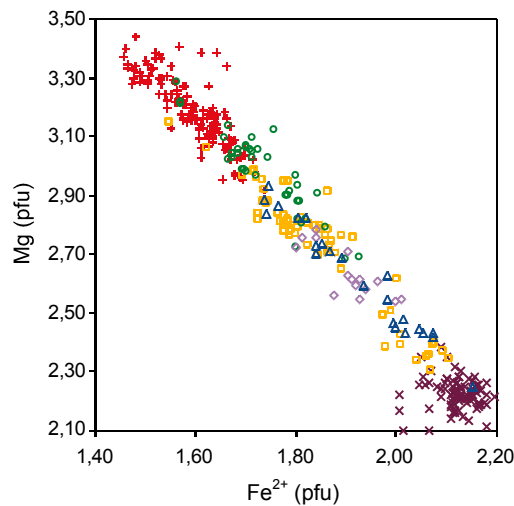
Figure 40. The diagram showing Mg-Fe^{2+} exchange reaction and its relation to rock compositions from PHLtite through DIO (the symbols are as in Figure 28).
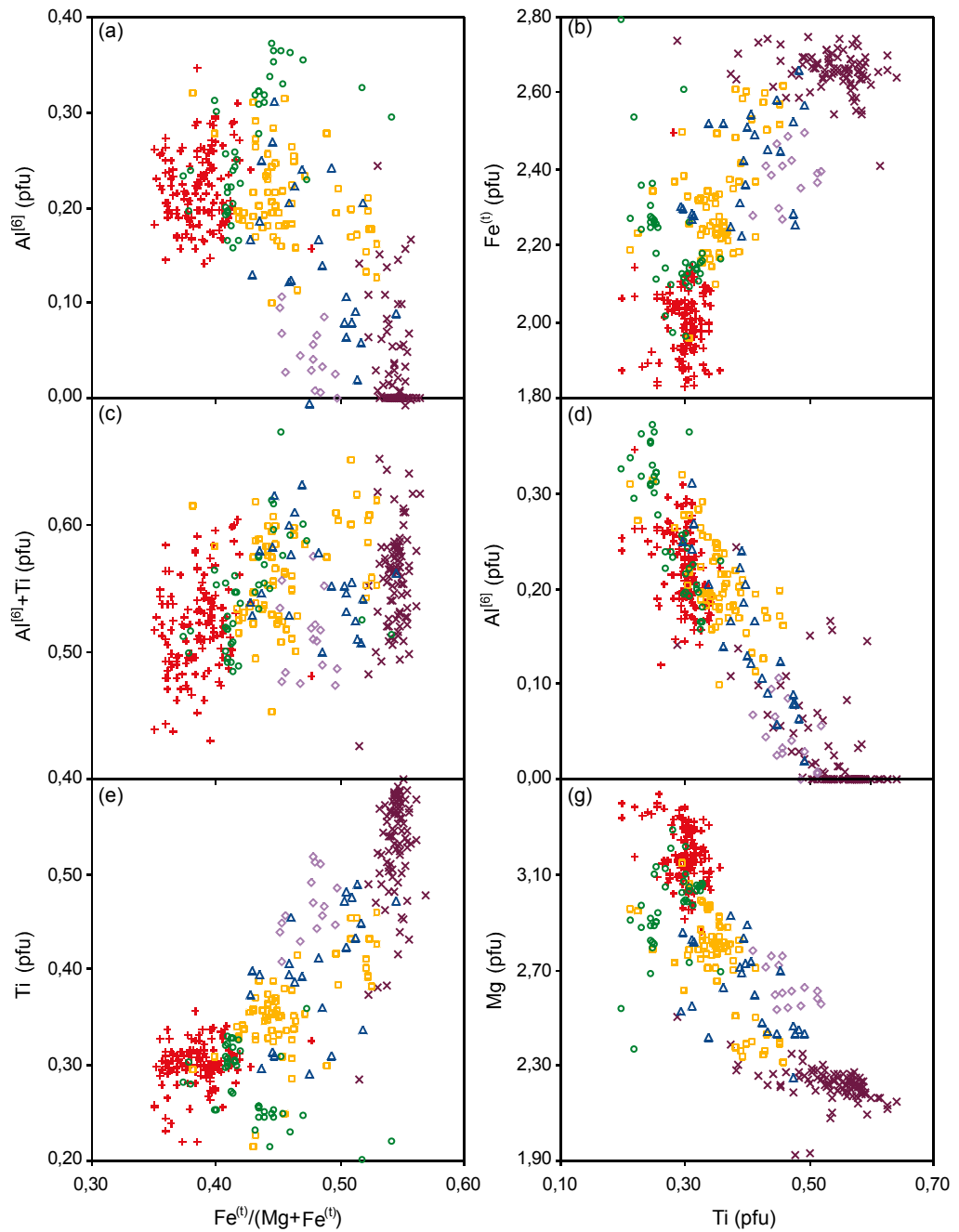
Figure 41. The behavior of Al[6] and Ti againts Fe(t)#, and relations of elements occupying into the octahedral site with Ti (pfu). Observed elemental relations show that they are controlled by rock compositions from PHLtite through DIO (the symbols are as in Figure 28).

73

In addition to substitution mechanisms in the octahedral site, the best-coupled substitution mechanism was proposed based on the theoretical coupled substitution mechanisms. Many authors (Robert, 1976a,b; Guo and Green, 1990; Righter and Carmichael, 1996 and references therein) showed that coupled substitution of cations among tetrahedral [4], octahedral [6], and interlayer [12] sites are complicated for trioctahedral micas. The control of various theoretical mechanisms for the studied micas revealed that incorporation of Al, Ti and Fe^{3+} into trioctahedral mica structure can be achieved by the coupled substitutions, $Si^{[4]}+(Mg+Fe^{2+})^{[6]} \Leftrightarrow Al^{[4]}+Al^{[6]}$ and $2Si^{[4]}+(Mg+Fe^{2+})^{[6]} \Leftrightarrow 2Al^{[4]}+Ti^{[6]}$ (Robert, 1976a,b; Guidotti, 1984; Hewitt and Abrecht, 1986; Patino Douce et al., 1993), and $Si^{[4]}+(Mg+Fe^{2+})^{[6]} \Leftrightarrow Al^{[4]}+(Fe^{3+})^{[6]}$ (Dymek, 1983), respectively (Figure 43a,b,c). The substitution of Al into the octahedral site is clear within each rock type itself, and it creates broad trends for each rock suite parallel to each other (Figure 43a). The strongest one is observed within micas of PHLtite and CPXnite while the weakest one is that of micas from DIO with the lowest $Al^{(t)}$ and the highest Si. This relation can be explained by substitution of $Al^{[6]}$ for Fe^{2+} instead of Mg where Fe^{2+} is lower than Mg as discussed above. The relation of Fe^{3+} in octahedral site is stronger than that of Al for the given coupled substitution mechanism (Figure 43b). The behavior of Fe^{3+} in this coupled mechanism might be caused by substitution of Fe^{3+} for Mg where Fe^{3+} is very low. Two broad trends, parallel to each other, are obtained for mechanisms including Ti, where micas of PHLtite form one trend and those of rest of the rocks create a second one (Figure 43c). Micas of CPXnite overlap both trends. This relation may be due to the lack of plag within PHLtite and CPXnite despite the presence of plag within the rest of the rocks creating the second trend as well as depleted Si and Al-enriched contents in micas of phl and cpx rich rocks.

An alternative way to show Al and Ti occupancies in the octahedral site is $2(Mg+Fe^{2+})^{[6]} \Leftrightarrow Al^{[6]}+()^{[6]}$ and $2(Mg+Fe^{2+})^{[6]} \Leftrightarrow Ti^{[6]}+()^{[6]}$ (Figure 43d,e) (Guidotti, 1984; Hewitt and Abrecht, 1986; Patino Douce et al., 1993). Similar to coupled substitution mechanisms discussed previously, $Al^{[6]}$ substitution is more likely in rocks with the highest Mg# and the lowest plag content (i.e. PHLtite and CPXnite) (Figure 43d). That means, micas of PHLtite are strongly

depleted in Si and enriched in Al, and Al is mainly partitioned into mica structure. This may be explained by negligible amount of plag in PHLtite. Ti substitution, according to coupled mechanisms given above, is well defined for micas of all rocks (Figure 43e). In detail, there are two trends, which combine PHLtite, CPXnite, CPXnite WHMP, and LG, DIO where HBdite has a transitional character. The strong reverse relation of Ti to (Mg,Fe^{2+}) (Figure 43e) is characteristic as defined by Robert (1976b), Abrecht and Hewitt (1988), Patino Douce (1993), Patino Douce et al. (1993). The Ti saturating phases of the rocks, which are rt, ilm and sph, can explain the high Ti content of these micas. The relation between Al$^{[6]}$ and Ti is best given by a coupled substitution mechanism of Si$^{[4]}$+Al$^{[6]}$ $\Leftrightarrow$ Al$^{[4]}$+Ti$^{[6]}$ (Dymek, 1983) (Figure 43f). It is clear that Al and Ti substitutions into the octahedral site are mainly achieved by coupled mechanisms.
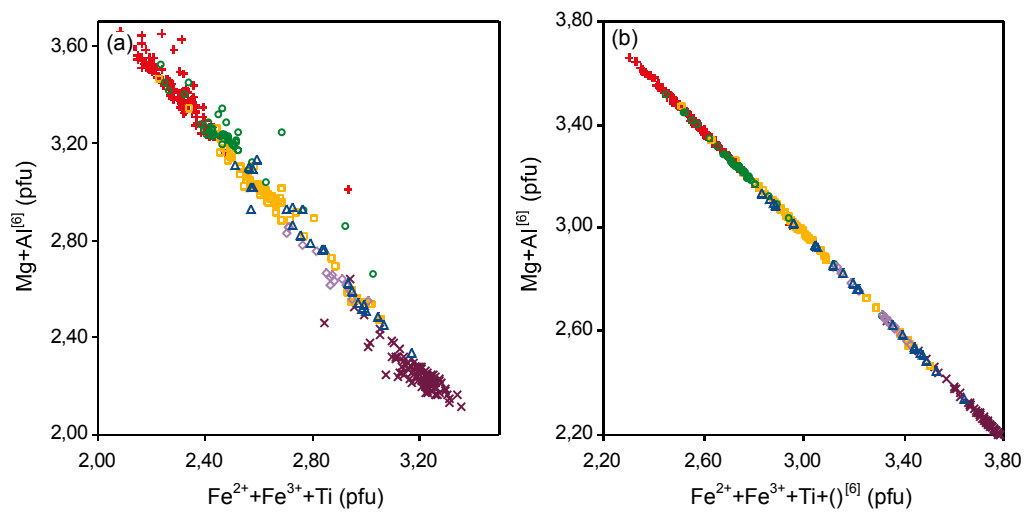
Figure 42. (a) The substitution mechanism giving the best relation for the elements within the octahedral site, and (b) the effect of vacancy on the mechanism given in (a) (the symbols are as in Figure 28).

After examination of various substitution mechanisms above, it is concluded that the presence of Ti, Fe^{3+} and Al in the octahedral site can be explained by the coupled substitution mechanism, 3Si$^{[4]}$+(Mg+Fe^{2+})$^{[6]}$ $\Leftrightarrow$
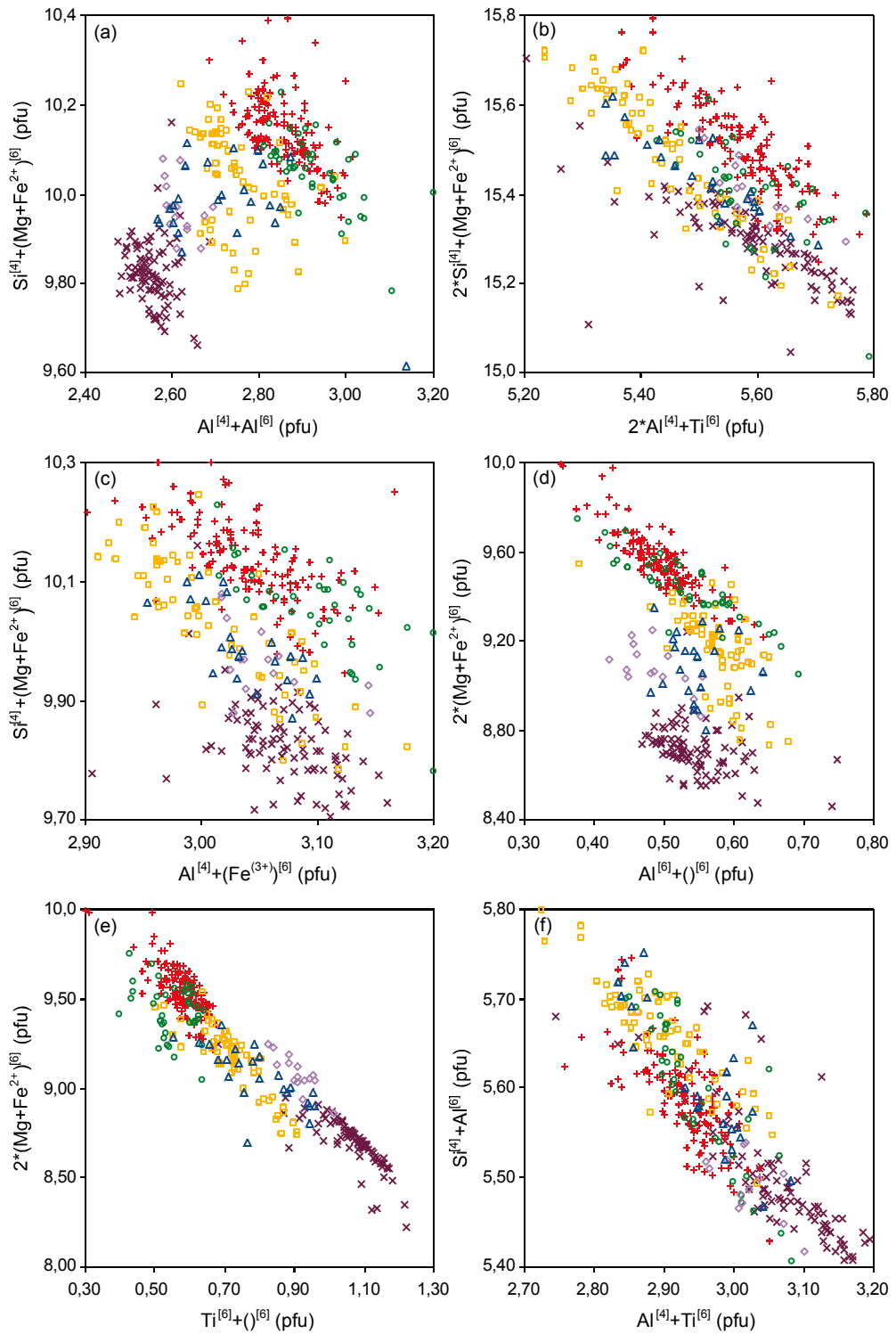
Figure 43. The plots showing various coupled substitution mechanisms and control of rock compositions on mica chemistry (the symbols are as in Figure 28).

$3Al^{[4]}+(Al+Ti+Fe^{3+})^{[6]}$ (Figure 44a) which may be common for micas of magmatic rocks. It is clear that the studied micas are characterized by excess mixing behavior of $Mg-Al^{[6]}-Ti-Fe^{2+}-Fe^{3+}$ in the octahedral site. In other words, contributions of phl, ann, musc, east are effective in bio solid solution where musc-phl, musc-ann and east-phl (Mg-Tschermak's exchange component) solid solutions are considered. Figure 44 shows that micas from different rock compositions give different trends that are parallel to each other in a meaningful way. Micas from PHLtite and CPXnite of the ultramafics display a narrow trend with the highest values, the first trend in Figure 44. Micas of DIO with the lowest values display the bottom most trend, the third trend in Figure 44. The second trend, transitional between the first and the third one, is of micas from CPXnite WHMP, HBdite and LG. The trends given by this substitution mechanism clearly display changes in rock compositions and mineral assemblages, and thus may provide an idea for a crystallization sequence. However, all mechanisms proposed above may not explain the exact relation between exchange relations for the studied micas, therefore a new mechanism has been derived. The best derived substitution mechanism is $3Si^{[4]}+(Mg+Al)^{[6]} \Leftrightarrow 3Al^{[4]}+(Ti+Fe^{2+}+Fe^{3+})^{[6]}+()^{[6]}$ (Figure 44b). It gives perfect exchange relations between elements of octahedral and tetrahedral sites. It is interesting to note that the characteristic relation of $Al^{[6]}$ in the studied mica structure is not common in micas of magmatic rocks as discussed below.

The observed coupled substitution mechanism in the interlayer site, $K^{[12]}+Al^{[4]} \Leftrightarrow ()^{[12]}+Si^{[4]}$, clearly exhibits the presence of two broad trends, which belong to PHLtite plus CPXnite, and CPXnite WHMP, HBdite, LG plus DIO (Figure 45a). Micas of HBLdite show a transitional character between micas of the ultramafics and the mafics, like the mechanisms observed in the octahedral site. K is simply substituted by Ba with a mechanism of $2K^{[12]} \Leftrightarrow Ba^{[12]}+()^{[12]}$ (Figure 45b) (Guo and Green, 1990) but it needs charge compensation due to charge differences of K^+ and Ba^{2+} (Speer, 1984). The substitution of Ba into interlayer site of mica structure has been studied in detail by various investigators (Velde, 1979; Wagner and Velde, 1986; Guo and Green, 1990; Righter and Carmichael, 1996; etc.) which suggested many exchange reactions, e.g. $2K^{[12]}+4(Mg+Fe^{2+})^{[6]}+4Si^{[4]} \Leftrightarrow Ba^{[12]}+3Ti^{[6]}+4Al^{[4]}$,

K[12]+3(Mg+Fe^{2+})[6]+3Si[4] $\Leftrightarrow$ Ba[12]+2Ti[6]+3Al[4], common for magmatic rocks. The mechanisms given as example are valid for the studied micas and define that two broad trends depending on the presence/absence of plag in the rocks (Figure 45c,d). The best fit for the elemental relations between octahedral and tetrahedral sites for the studied micas (Figure 44b), is defined by an exchange of 3Si[4]+(Mg+Al)[6]+K[12] $\Leftrightarrow$ 3Al[4]+(Ti+Fe^{2+}+Fe^{3+})[6]+()[6]+(Ba+Na+Ca)[12] (Figure 45e). This substitution gives the best relation and is quite different from the others proposed for micas of magmatic rocks (e.g. Velde, 1979; Shaw and Penczak, 1996). This behavior is most probably due to the uncommon relation of Al[6] in the octahedral site. The mechanisms characterizing the studied micas are summarized in Table 1.
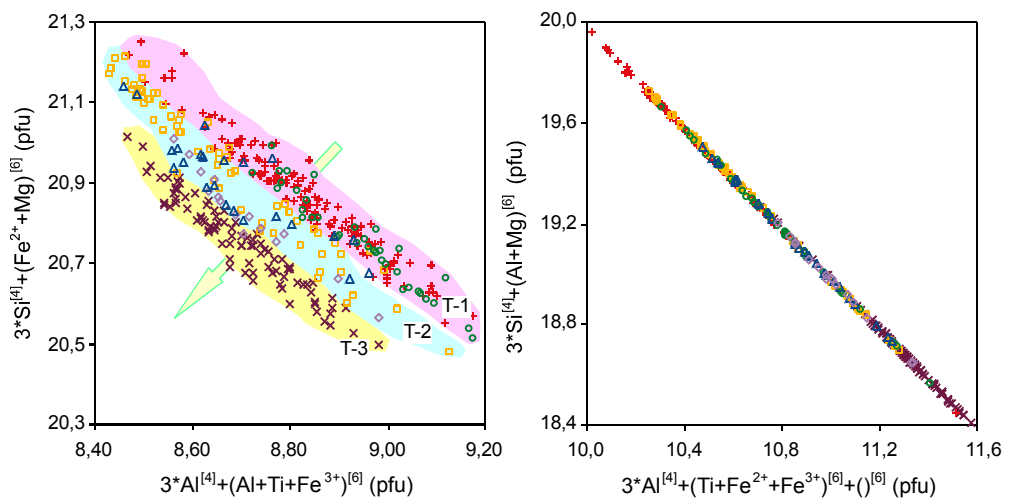
Figure 44. The diagram showing the coupled substitution mechanisms; (a): expressing elemental relations within tetrahedral and octahedral sites. In the diagram; T-1: Trend-1, T-2: Trend-2, T-3: Trend-3 showing control of rock compositions, (b) the best relation of the elements in the mica chemistry (the symbols are as in Figure 28).

The occupancy of Al in the octahedral site is shown by a variety of mechanisms, such as: Si[4]+(Mg+Fe^{2+})[6] $\Leftrightarrow$ Al[4]+Al[6] (Figure 43a), 2Si[4]+(Mg+Fe^{2+})[6] $\Leftrightarrow$ 2Al[4]+Ti[6] (Figure 43b), Si[4]+Al[6] $\Leftrightarrow$ Al[4]+Ti[6] (Figure 43f) and (Mg+Fe^{2+}+Ti)[6] $\Leftrightarrow$ Al[6] (Figure 46a), 2Al[6] $\Leftrightarrow$ 3(Fe^{2+})[6] (Figure 46b) and
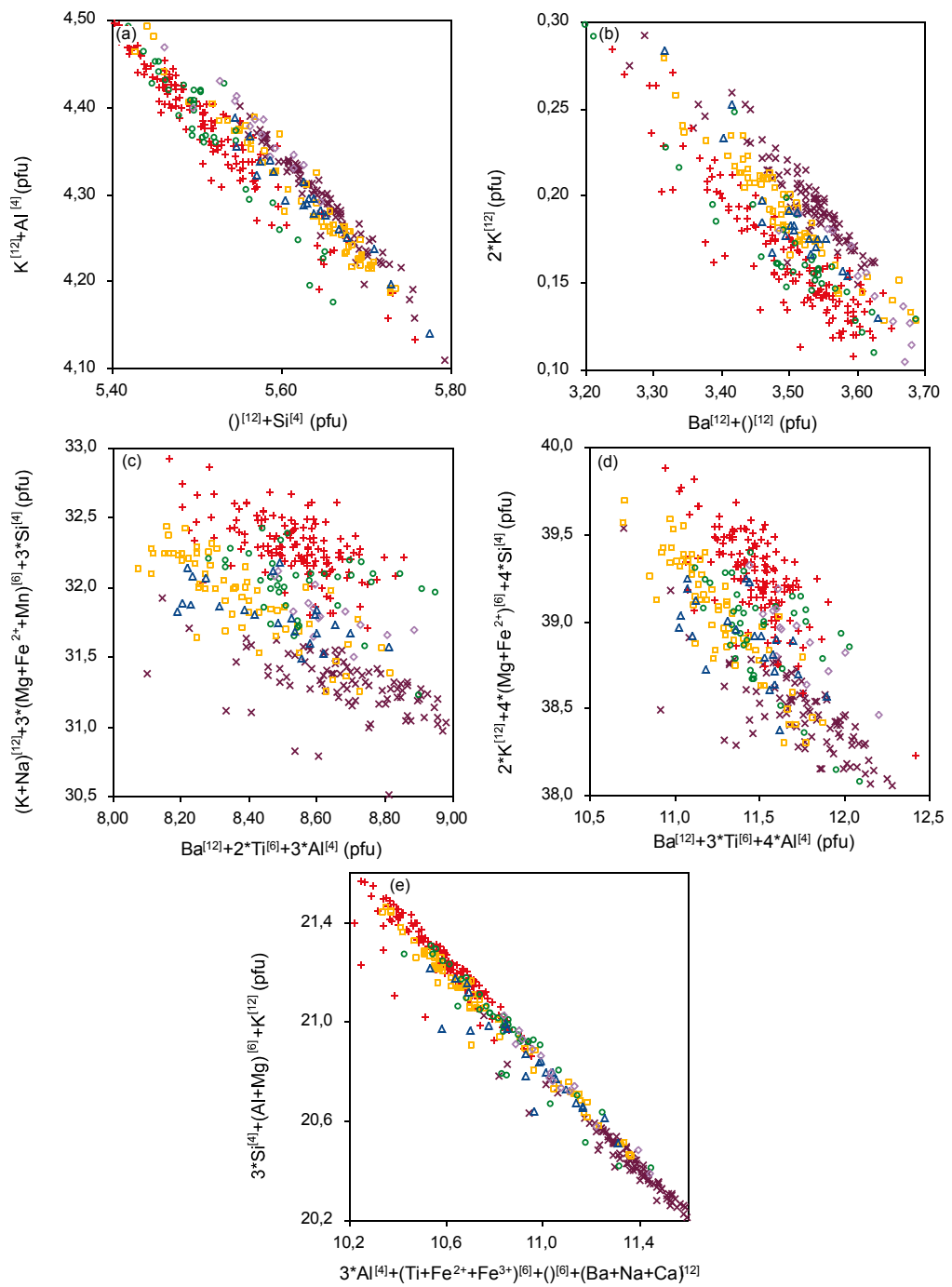
Figure 45. The plots showing the relations in the interlayer site and relations of interlayer elements to those of other sites (the symbols are as in Figure 28).

Table 1. Substitution mechanisms characterizing the studied micas.

$Mg \Leftrightarrow Fe^{2+}$

$Mg \Leftrightarrow Ti$

$Al^{[6]} \Leftrightarrow Ti$

$Fe^{(t)} \Leftrightarrow Ti$

$Mg^{[6]} \Leftrightarrow ()^{[6]}$

$Al^{[6]} \Leftrightarrow ()^{[6]}$

$(Mg+Al)^{[6]} \Leftrightarrow (Ti+Fe^{2+}+Fe^{3+})^{[6]}$

$(Mg+Al)^{[6]} \Leftrightarrow (Fe^{2+}+Fe^{3+}+Ti)^{[6]}+()^{[6]}$

$2Mg^{[6]}+Al^{[6]} \Leftrightarrow 2(Fe^{2+}+Fe^{3+}+Ti)^{[6]}+()^{[6]}$

$(Mg+Al)^{[6]} \Leftrightarrow (Ti+Fe^{2+}+Fe^{3+})^{[6]}+()^{[6]}$

$3Si^{[4]}+(Mg+Fe^{2+})^{[6]} \Leftrightarrow 3Al^{[4]}+(Al+Ti+Fe^{3+})^{[6]}$

$2Al^{[4]}+(Mg+Fe^{2+})^{[6]} \Leftrightarrow 2Si^{[4]}+()^{[6]}$

$3Si^{[4]}+(Mg+Al)^{[6]} \Leftrightarrow 3Al^{[4]}+(Ti+Fe^{2+}+Fe^{3+})^{[6]}+()^{[6]}$

$K^{[12]}+Al^{[4]} \Leftrightarrow ()^{[12]}+Si^{[4]}$

$3Si^{[4]}+(Mg+Al)^{[6]}+K^{[12]} \Leftrightarrow 3Al^{[4]}+(Ti+Fe^{2+}+Fe^{3+})^{[6]}+()^{[6]}+(Ba+Na+Ca)^{[12]}$
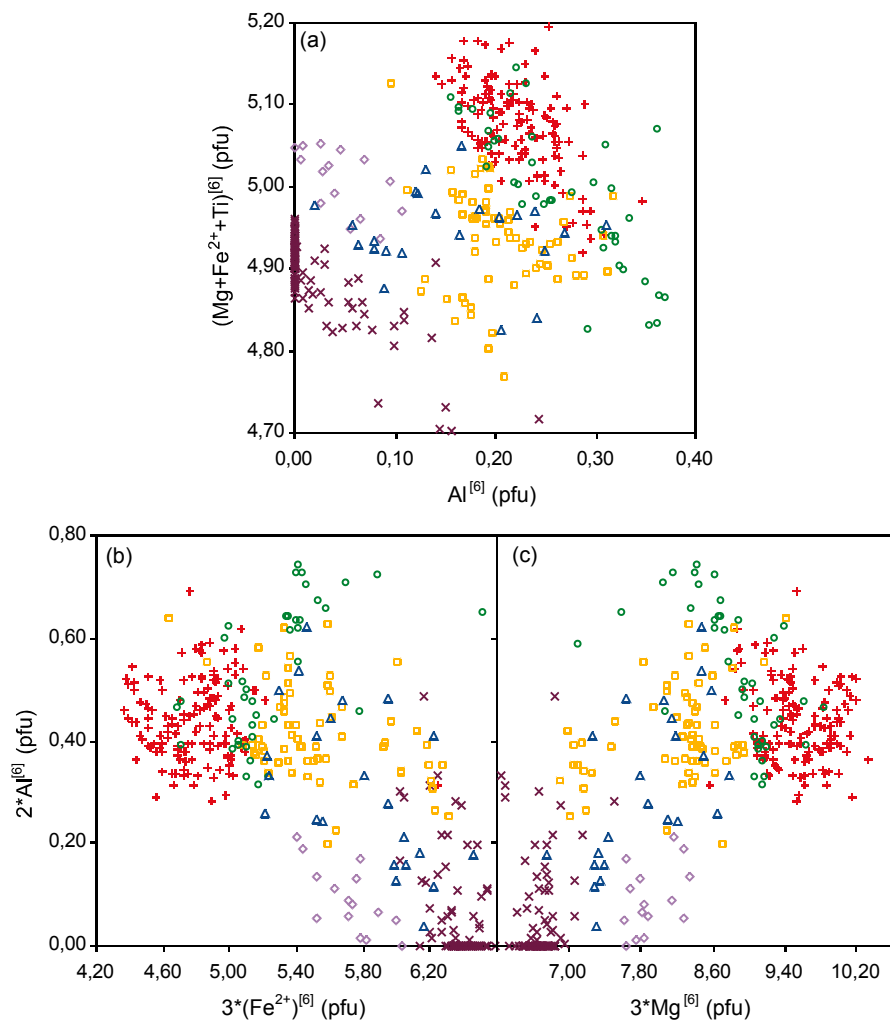
Figure 46. Variable substitution mechanisms for Al[6] (the symbols are as in Figure 28).

$3Mg^{[6]} \Leftrightarrow 2Al^{[6]}$ (Figure 46c) has petrological importance. Since the behavior of Fe and Mg against $Al^{[6]}$ is dependent on various physicochemical conditions including volatiles in the system, the last two substitutions (Figure 46b,c) are characteristic for micas crystallizing from alkaline and calc-alkaline magmas, respectively, additionally both are characterized by $Mg \Leftrightarrow Fe^{(t)}$ substitution as well (Figure 47a) (Abdel-Fattah, 1994, 1996). There is no change in $Al^{[6]}$ as Fe^{2+} increases in micas of PHLtite, CPXnite (Figure 46b). However, $Al^{[6]}$ starts to correlate negatively from CPXnite WHMP through HBdite to LG and DIO. This may be related to presence and/or absence of plag in the rocks. A negative correlation, even though it is weak, of $2Al^{[6]} \Leftrightarrow 3Fe^{2+}$ is representative of alkaline system. However, there is a linear correlation for the mechanism $3Mg^{[6]} \Leftrightarrow 2Al^{[6]}$ (Figure 46c), which is exactly opposed to the $Al-Fe^{2+}$ substitution. There should be a negative relation between Mg and $Al^{[6]}$ to typify the calc-alkaline system. These two mechanisms observed in the studied micas might favor alkaline melt rather than calc-alkaline melt. On the other hand, the observed substitutions, $Mg \Leftrightarrow Fe^{(t)}$ and $(Mg+Fe^{2+})^{[6]}+2Al^{[4]} \Leftrightarrow ()^{[6]}+2Si^{[4]}$ (Figure 47a,b, respectively), and $Si^{[4]}+(Mg+Fe^{2+})^{[6]} \Leftrightarrow Al^{[4]}+Al^{[6]}$ (Figure 43), are characteristic for micas of calc-alkaline systems (Deer et al., 1992; Abdel-Fattah, 1994, 1996). A calc-alkaline character is also clearly demonstrated by the relations of $MgO-FeO^{(t)}$, $Al_2O_3-FeO^{(t)}$, Al_2O_3-MgO and $FeO^{(t)}-MgO-Al_2O_3$ (Figure 48) after Abdel-Fattah (1994, 1996) using mica compositions whose host rocks are tectonically well-defined in literature. Abdel-Fattah (1994, 1996) proposed that physicochemical conditions clearly affect dark mica compositions crystallizing from calc-alkaline and alkaline melts within subduction related and anorogenic environments, respectively.

Mica compositions, from PHLtite and CPXnite are relatively enriched in Al and depleted in Ti and $Fe^{(t)}$ relative to those from DIO, are compared with micas of alkaline rocks (lamproites, kimberlites and melilitites), as well as crustal and peridotitic xenoliths carried by lamproites, silicic alkaline metasomatized oceanic peridotitic xenoliths, and calc-alkaline volcanic rocks (Figure 49). Micas from the Kurançalı rocks show high compositional diversity from the rocks used for comparison. This is due to lower Mg#'s than found in peridotitic xenoliths from either subcontinental or oceanic environments. Ti and

Fe$^{(t)}$, showing similar behaviour in mica structure, decrease with increasing Mg#, like those of micas from peridotitic xenoliths and alkaline rocks. Despite the parallel patterns, the studied micas have lower Mg#'s than those of peridotitic xenoliths and alkaline rocks. They have similar Mg# values to those of crustal xenoliths but their Ti contents are higher than those of crustal xenoliths. Even though Al$^{(t)}$ content is similar for both the studied micas and the compared micas from crustal xenoliths, Al$^{(t)}$ of the studied micas positively correlates to Mg#. However, Al$^{(t)}$ of micas from the crustal xenoliths carried by alkaline rocks correlate negatively with Mg# representative of magmatic differentiation (Hecht, 1994). This reverse relation may be an indication metasomatism as discussed above. The studied micas display similarity to metasomatized peridotitic xenoliths from an oceanic environment in spite of their lower Mg# values. The lower Mg# values of the studied micas are related the host rock composition. The studied micas are similar to micas of calc-alkaline andesitic rocks with low Mg# which are derived from a subduction component enriched subcontinental lithospheric mantle. As a result, it may be suggested that for the Kurançalı magmatic rocks there is a metasomatising agent in an intra-oceanic area.
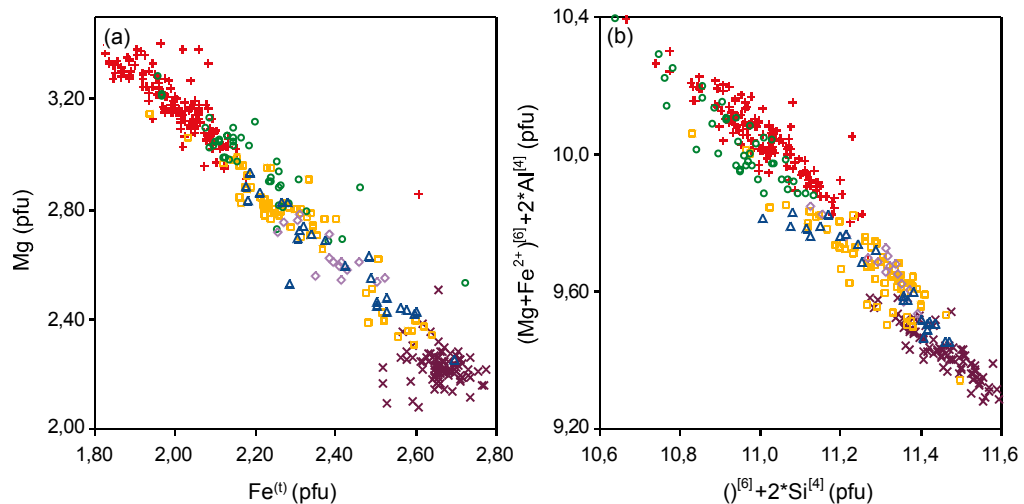
Figure 47. Characteristic mechanisms for micas inferring calc-alkaline affinity of the host rocks (the symbols are as in Figure 28).
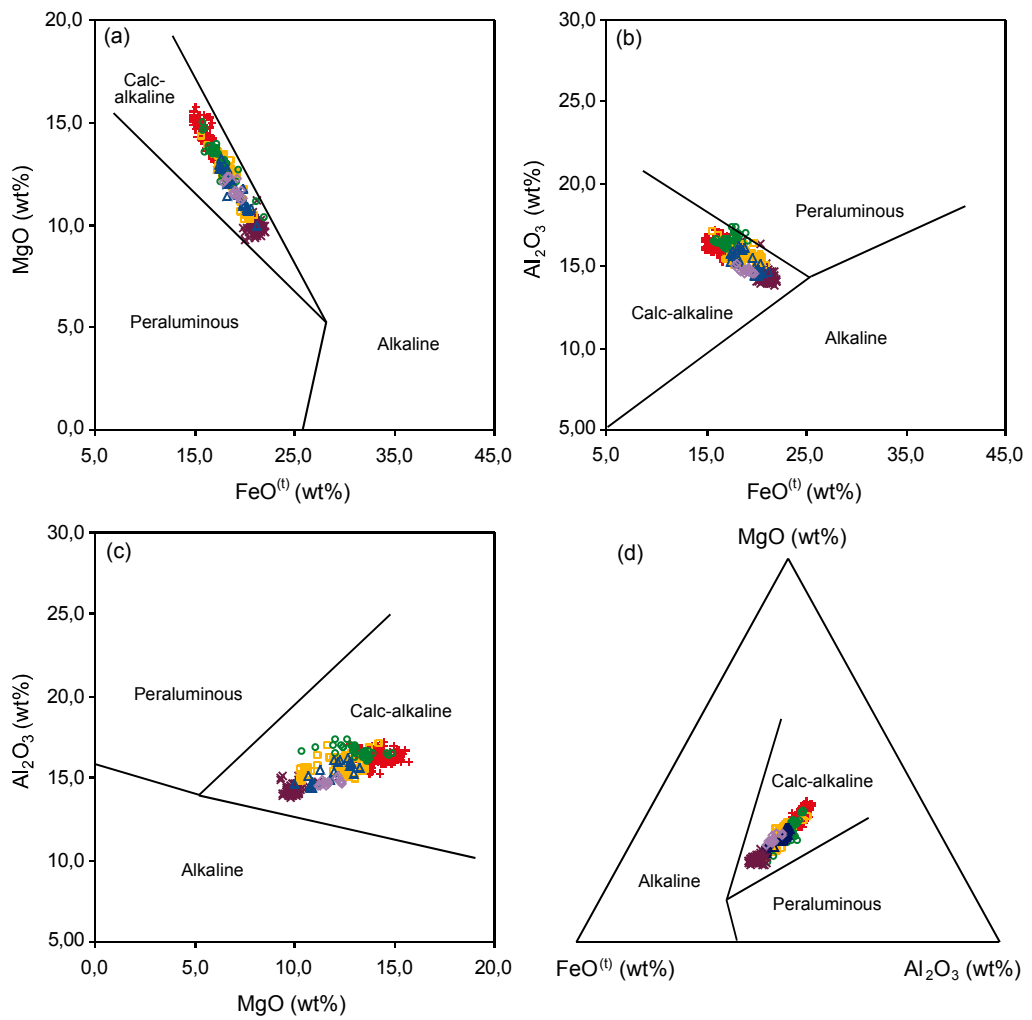
Figure 48. The plots on the oxide variation diagrams to show calc-alkaline character of the system from which the mica is crystallized. The fields for calc-alkaline, alkaline and peralkaline are from Abdel-Fattah (1994, 1996) (the symbols are as in Figure 28).
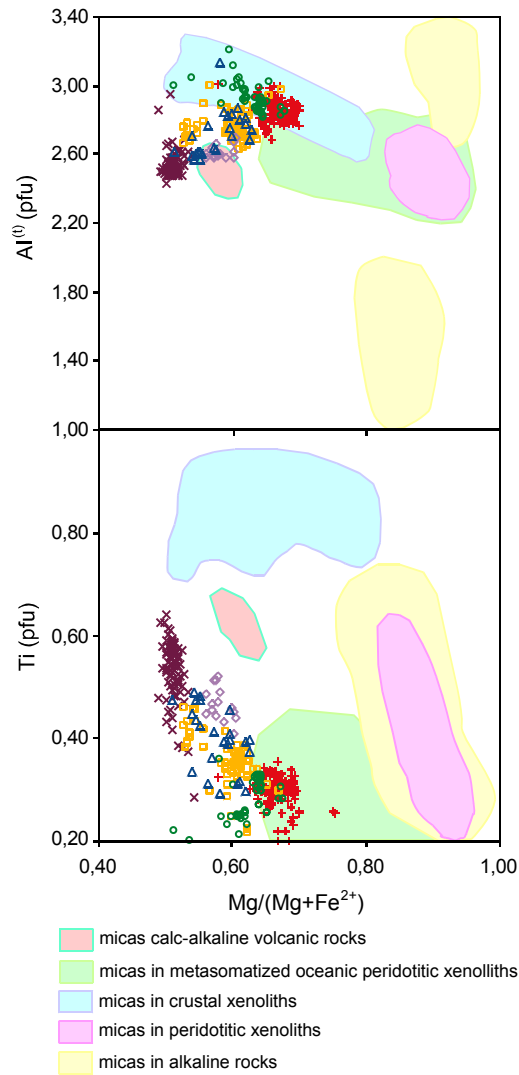
Figure 49. Variations in Ti and Al$^{(t)}$ against Mg# in the studied micas and their comparisons with those of micas from alkaline rock (lamproite, kimberlite and melilitite) and crustal and peridotitic xenoliths carried by many lamproites (data used for comparison from Wagner and Velde, 1986; Mitchell and Bergman, 1991; Cullers et al., 1996; Beard et al., 1998; Conticelli, 1998), silicic-alkaline metasomatized oceanic peridotitic xenoliths (Wulff-Pedersen et al., 1996), and calc-alkaline andesitic volcanic rocks (Yavuz et al., 2002) (the symbol are as in Figure 28).

The studied micas are not tetrahedral cation deficit and they differ from the MARID (mica-amph-rt-ilm-di) type mantle xenoliths carried by kimberlite and related rocks (Dawson and Smith, 1977). Because micas from MARID type xenoliths are tetrahedral cation deficit with total cation sums ≤ 8.00, and with F, Cl in range of 0.07-013 (pfu). The studied micas, however, have halogens ranging 0.00 to 0.143 that is similar to those of micas from xenoliths (Dawson and Smith, 1977; Erlank et al., 1987).

It is clear that some substitution mechanisms and chemical classification diagrams strongly support calc-alkaline magma to form the studied micas although the substitution $2Al^{[6]} \Leftrightarrow 3Fe^{2+}$ (Figure 46b) points to alkaline melts. In addition to a substitution representing alkaline, there is another limitation for calc-alkaline magma. This limitation is presented by the relation of $Al^{[6]}$ to Mg which does not give a magmatic trioctahedral mica differentiation trend as proposed by Hecht (1994) for ultramafic and mafic rocks (Figure 50). The relation for the studied micas exactly opposes the magmatic differentiation trend. Just a weak relation is present for CPXnite, CPXnite WHMP and PHLtite.
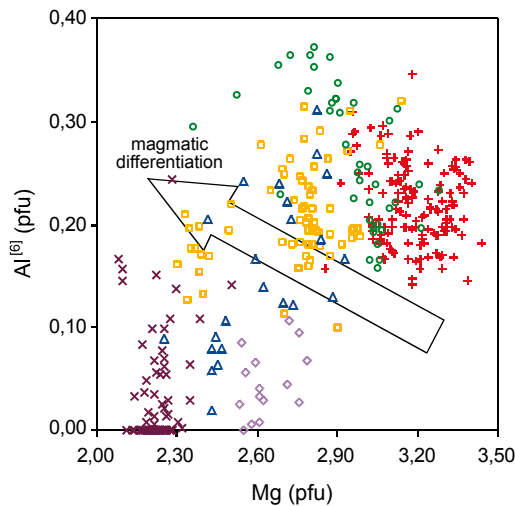
Figure 50. Covariation of $Al^{[6]}$ and Mg (pfu), the trend for magmatic differentiation is from Hecht (1994) (the symbol are as in Figure 28).

These two limitations given by; (a) similarity to micas of alkaline magmas in terms of $2Al^{[6]} \Leftrightarrow 3Fe^{2+}$ substitution and dissimilarity to micas of calc-alkaline magmas by $3Mg^{[6]} \Leftrightarrow 2Al^{[6]}$ mechanism, and (b) opposing relation to the magmatic differentiation trend in $Al^{[6]}$-Mg may indicate source hybridization. Hybridization can be further supported by the relation of MgO-$FeO^{(t)}$-Al_2O_3 (AFM) (Gokhale, 1968; Nockolds, 1947) in which micas show a transitional character between a magmatic and a metasomatic in origin (Figure 51). According to the AFM diagram, micas of the ultramafics and LG show transitional character from metasomatic to magmatic while those of DIO plot within the magmatic field. This may be a clue for mantle metasomatism to the origin of micas of ultramafic and mafic rocks in the Kurançalı area.
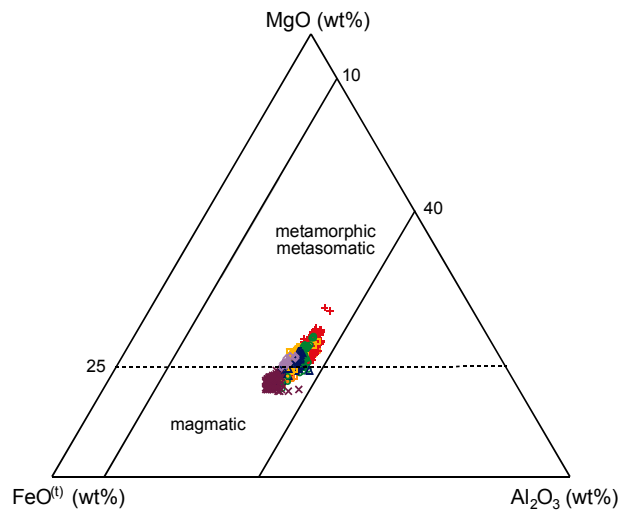
Figure 51. The plots on the MgO-$FeO^{(t)}$-Al_2O_3 diagram, fields from Gokhale, 1968 (dash line); Nockolds, 1947 (solid lines) (the symbol are as in Figure 28).

Micas defined as phl are not pure end-members and relatively enriched in Fe^{2+}, Fe^{3+}, $Al^{[6]}$ and Ti. This is not consistent with phl from continental arc-related magmas as interpreted by Feldstein et al. (1996). Micas may be related to a system generated in an oceanic environment as suggested by Fitton et al. (1991). These authors suggested that oceanic island basalt (OIB) related magmas contain higher $FeO^{(t)}$, TiO_2 and BaO relative to continental arc-related

magmas. However, the system from which mica crystallized may represent an intra-oceanic arc rather than OIB environment because the studied mica compositions, highly OH- and Al-enriched, and Si-depleted, strongly suggest a calc-alkaline character. It is well known that calc-alkaline rocks are typically produced in subduction zone environments where dehydration of a downgoing slab provides water to the melt system. The Kurançalı rocks originated from highly water enriched systems, amph crystallization is after phl, and there is no crystallization of iron oxide minerals neither as early nor as late phase. However, dissociation of H_2O and release of H may enrich the system in oxygen at an early stage and availability of oxygen can cause early crystallization of iron rich-amph and iron oxides (typically mt) in calc-alkaline magmas (Abdel-Fattah, 1994). Thus the absence of iron oxide minerals and crystallization of amph after mica may support mantle metasomatism rather than a magmatic system. Low $Fe^{3+}/Fe^{(t)}$ ratios of micas (0.22) attributed to their higher $Fe^{(t)}$ contents may be another evidence supporting mantle metasomatism (Feldstein et al., 1996).

The substitution Ba into mica structure may be a clue for mantle related origin of the rocks. Ba is strongly incompatible in mantle derived magmas (e.g. lamproites, alkaline potassic rocks). In addition, it may be derived from a subducted slab in a subduction environment due to its strong incompability and added to a previously depleted upper mantle material. On the other hand, it is strongly compatible to mica and easily enters mica structure during the earliest stages of crystallization (Shaw and Penzack, 1996). Mica crystallizing just after cpx from the Kurançalı area, might have taken all Ba into its structure. This is also evident from the whole-rock composition because PHLtite shows the highest Ba content. Presence of Ba may infer that Ba is derived from the subduction component and added to a previously depleted mantle material.

4.2.3. Elemental Variations within Single Crystal

Measurements, along lines within mica crystals from rim to center and rim to rim, show a large variety of element distribution pattern (Figure 52). Profiles for mica crystals in different mineral assemblages show that coexisting minerals slightly affect the elemental changes within a mica crystal. The most
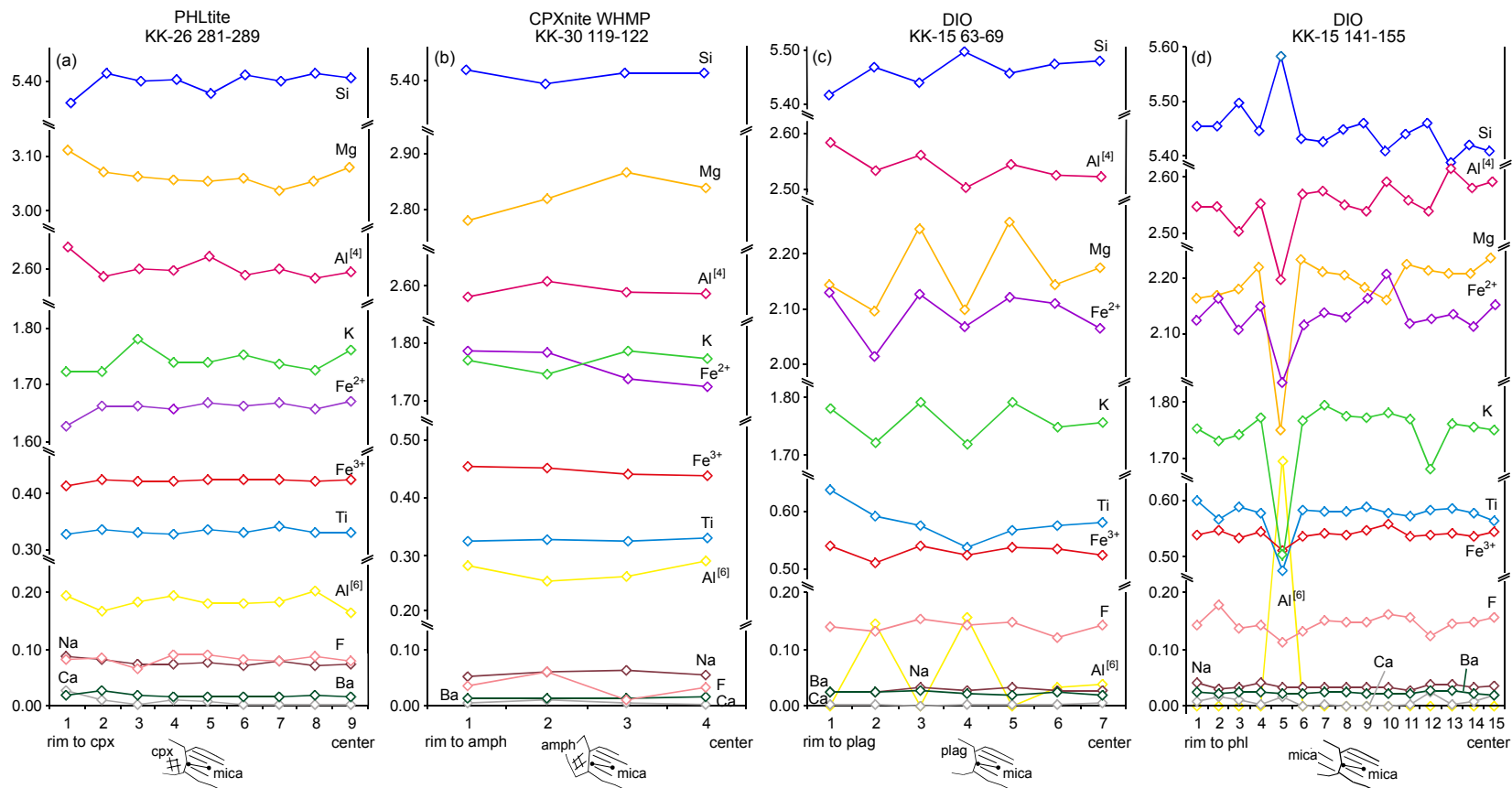
Figure 52. Profiles on mica crystals showing chemical changes across rim to center, rim to rim in different mineral assemblages, and cross-cutting relations of two mica crystal (x: big crystal cut by another small crystal y).
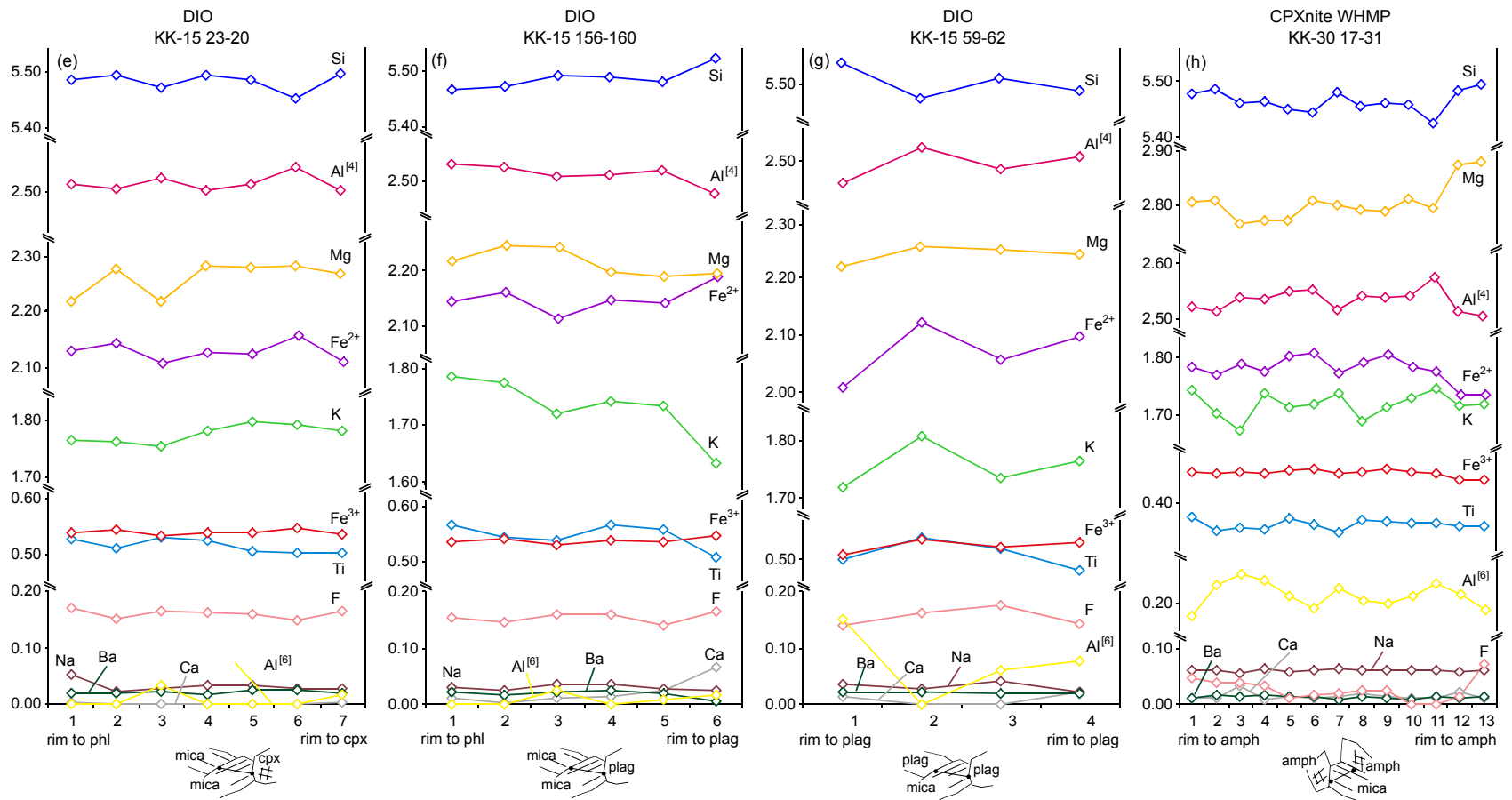
Figure 52 (continued).
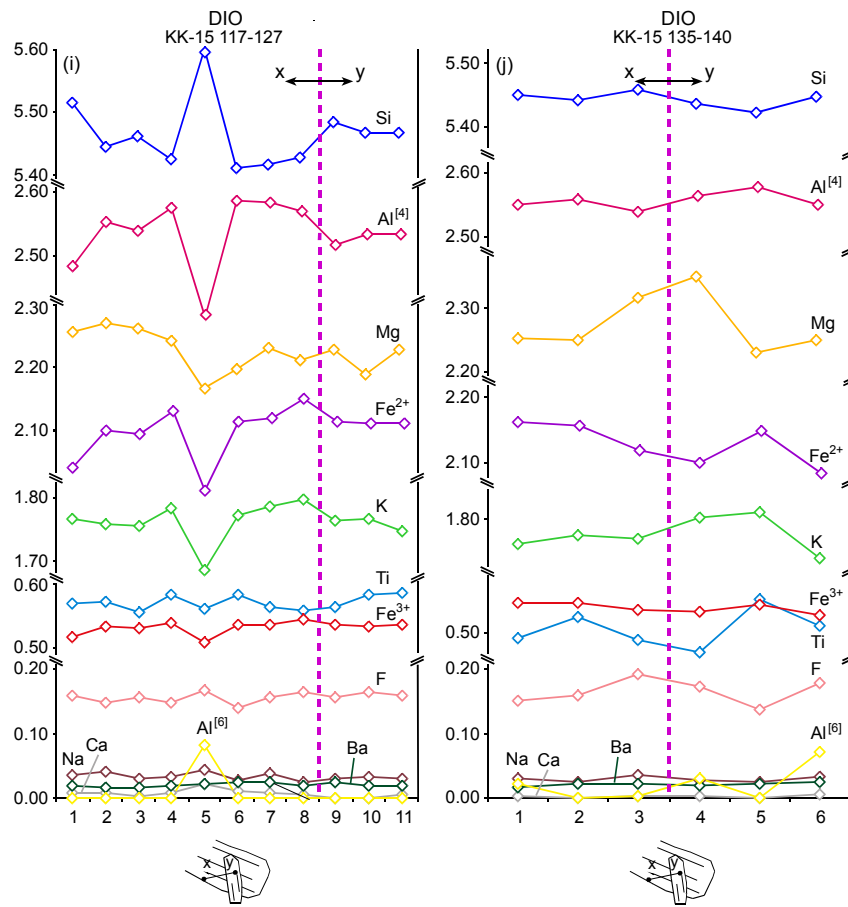
Figure 52 (continued).

obvious changes are of Si, Al[4], Mg and Fe^{2+}. There is a slight decrease in Mg, Ca, Nsa from rim of a mica in contact with cpx through center of a mica of the ultramafics, while Fe^{2+}, Fe^{3+} and Ti are the most constant elements along the profile (Figure 52a). Along the profile from rim of mica crystal in contact with amph, Mg, K increases with a decrease in Fe^{2+} (Figure 52b). The most obvious changes are observed in micas of DIO. From rim of mica in contact with plag to center of mica, Si, Mg show a slight increase (Figure 52c) while a reverse case is observed from associations with other mica crystal through the measured mica (Figure 52d). K as well as Si and Mg decrease from rim to center (Figure 52d). A zigzag like pattern is dominant for Si, Al[4], Mg, Fe^{2+} and K while the rest of the elements scatter more regularly.

Profiles for micas across rim in contact with another mica crystal to rim in contact with cpx are relatively constant while those across a mica rim to a plag rim show slightly increasing Si, Fe^{2+}, Ca contents with decreasing Al[4], Mg, K, Ti (Figure 52e,f). Profiles for micas across rim to rim in contact with plag's at both sides show zigzag patterns for Si, Al[4], Fe^{2+}, K and very slightly convex shaped patterns for Mg, Ti and F (Figure 52g). Moreover, Ca increases towards the rims and decreases at center. Across a mica crystal associated with amph at both sides, Si, Mg, F are higher at rims and become lower towards the center (Figure 52h).

Cross-cutting relationship of mica crystals, i.e. small euhedral crystals cutting larger crystals, was also investigated (Figure 52i,j). There is no obvious regular chemical change and/or definite property, i.e. behaviors of elements are not similar for different crosscutting crystals for one sample.

In summary, there is no regular chemical change for different crystals associated with different minerals, and cross-cutting crystals. Moreover, there is no obvious signature of chemical zoning as well as optical zoning. Absence of zoning may indicate metasomatic origin for micas in the studied rocks because Verhulst et al. (2000) favour magmatic origin rather than metasomatic origin in case of presence of zoning.

Along element profiles in Figure 52d,i, there are few points highly depleted in K, Al[4], Mg, Fe^{2+}, Fe^{3+}, Ti, and enriched in Si, Al[6] relative to ther

points. The enriched and depleted points are most probably representative of vermiculite resulting from weathering as interpreted by Toksoy (1998) and Toksoy-Köksal et al. (1999, 2000, 2001b). Moreover, Pereira et al. (1993) and Bisdom et al. (1982) interpreted that Fe, like K, is one of the first elements to be leached out of dark mica as it weathers, while Al is left behind. In addition to this, Klein and Hurlbut (1985) indicate that Al may enter the Fe site in dark mica structures as it weathers to verm.

4.2.4. Element Partitioning between Mica and Coexisting Phases

Element partitioning between two coexisting crystals provides important tools in igneous petrology, e.g. pressure, temperature, oxygen fugacity. Since the Mg $\Leftrightarrow$ Fe^{2+} exchange reaction is the easiest reaction within the ferromagnesian minerals, partition of these elements between minerals, make data for the crystallization conditions available. The equilibrium constant for the Mg-Fe^{2+} exchange reaction between the trioctahedral mica and coexisting phases such as cpx and amph is (Feldstein et al., 1996) (e.g.):

$$K_{D(cpx\text{-}mica)}^{Mg/Fe2+} = \frac{(X_{Mg}/X_{Fe2+})^{cpx}}{(X_{Mg}/X_{Fe2+})^{mica}}$$

On the basis of complete analyses of mica, amph and cpx (except for ferric and ferrous iron estimations for cpx and amph), $K_D^{Mg/Fe2+}$ values were obtained as 2.11 (±0.31 SD) and 0.79 (±0.15 SD) for mica-cpx and mica-amph pairs, respectively. The $K_D^{Mg/Fe2+}$ values indicate that X_{Mg}/X_{Fe2+} ratios are much more lower in mica than in coexisting cpx but higher and/or similar in mica than in coexisting amph.

The $K_{D(amph\text{-}mica)}^{Mg/Fe2+}$ varies from 0.64 to 1.12, among which the lowest values are from micas of PHLtite. The values are consistent with data of trioctahedral mica-amph pair from a variety of plutonic rocks in literature ($K_{D(amph\text{-}mica)}^{Mg/Fe2+}$=0.6 to 1.4) (Speer, 1984; Feldstein et al., 1996). There is a linear correlation with a slope of 1 between mica and amph for Fe^{2+}/(Fe^{2+}+Mg) (Figure 53a). From Figure 53a, it is clear that rock composition and mineral assemblage are effective on Fe^{2+}/(Fe^{2+}+Mg) and therefore on $K_{D(amph\text{-}mica)}^{Mg/Fe2+}$

values. Micas of HBdite lie on the line with a slope of 1 while micas of PHLtite display deviation from the line. Moreover, micas from CPXnite WHMP show a transitional character between micas of PHLtite with very few amph and HBdite without any cpx. It can be concluded that partitioning of Fe^{2+} into amph becomes higher while that of Mg becomes lower as amph content increases from PHLtite to HBdite. This relation can also clearly be explained from rock composition, i.e. HBdite has higher Fe# than PHLtite, while CPXnite shows intermediate Fe# values. The range of $K_{D(amph-mica)}^{Mg/Fe2+}$ is reversely correlated with $Al^{[4]}$ contents of mica and amph (Figure 53b) where $Al^{[4]}$ concentrations decrease for both of the minerals from PHLtite to HBdite as $K_{D(amph-mica)}^{Mg/Fe2+}$ increases.
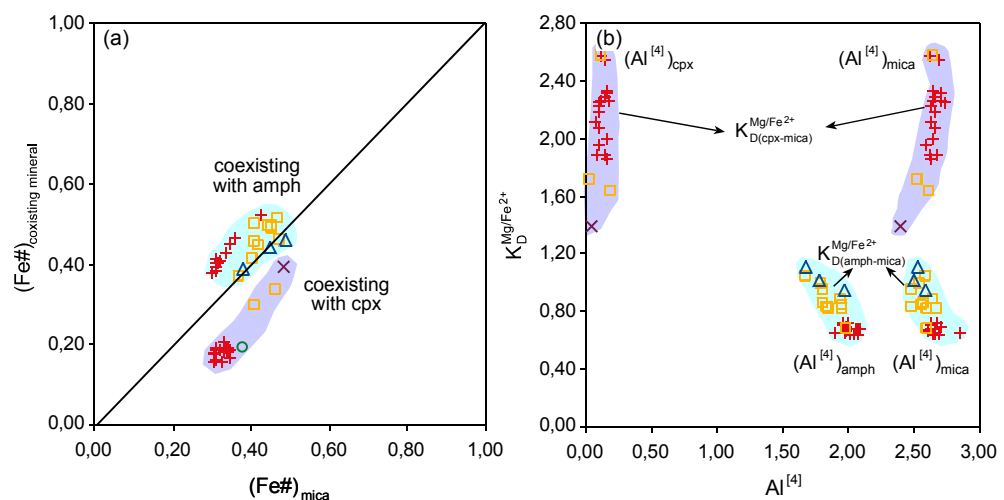
Figure 53. (a) Fe# relations of micas and coexisting mafic minerals (amph, cpx); (b) relations of $K_D^{Mg/Fe2+}$ and $Al^{[4]}$ for micas and coexisting mafic phases (the symbol are as in Figure 28).

$K_{D(cpx-mica)}^{Mg/Fe2+}$ with a range of 1.39-2.58 for mica-cpx are more variable and higher than $K_{D(amph-mica)}^{Mg/Fe2+}$ (Figure 53b). The wide range of variation seems to be due to rock composition and mineral assemblages, which is evident from this figure. It is clear that partitioning of Fe^{2+} into mica is higher

than into cpx (Figure 53a). $K_{D(cpx-mica)}^{Mg/Fe2+}$ slightly correlates with $Al^{[4]}$ of both mica and cpx (Figure 53b). This relation opposes to that for amph-mica pairs.

Partitioning of Fe^{2+} into mica is lower than into amph for PHLtite and CPXnite WHMP while it is almost equal for HBdite (Figure 53a). The relation of the examined mica-amph pairs may specify the crystallization sequence of rocks in the magma in the order of PHLtite-CPXnite WHMP-HBdite. On the other hand, partitioning of Fe^{2+} is higher into mica than cpx where Fe^{2+} partitioning for both increases from CPXnite and PHLtite to CPXnite WHMP, and DIO (Figure 53a). From the combination of the data from mica coexisting with ferromagnesian minerals, the order of crystallization of rocks is assumed as CPXnite - PHLtite - CPXnite WHMP - HBdite - LG - DIO. This data is in accordance with the petrographical observations.

4.2.5. Compositional Relation of Mica to Host Rocks

There is a good correlation between $Fe^{(t)}\#$ for micas and their host rocks (Figure 54a). Despite the presence of a good correlation, there is a deviation from a perfect 1:1 relation towards higher $Fe^{(t)}\#$ of the dark mica. This relation can not be explained by lower MgO wt% of mica. There is a deviation from the 1:1 slope towards higher MgO wt% content of mica compared to its host rock (Figure 54b), although MgO of mica correlates well with that of the host rocks, except for LG with lower MgO wt%. This leads to postulate that $FeO^{(t)}$ wt% of the dark mica is higher than that of its host rock, which may be explained by the absence of iron oxide phases and presence of Ti-rich phases rt, ilm and sph. An increase of mica $Fe^{(t)}\#$ with an increase of its host rock $Fe^{(t)}\#$ is not possible for hem series rocks but is a typical feature of ilm series rocks (Czamanske et al., 1981).

4.2.6. Physicochemical Conditions

It is rather difficult to estimate physicochemical conditions using mica compositions because the compositions are controlled by various factors such as pressure, temperature, oxygen and water fugacities, whole-rock compositions, etc. The Ti-concentration of micas, behaving similar to $Fe^{(t)}$
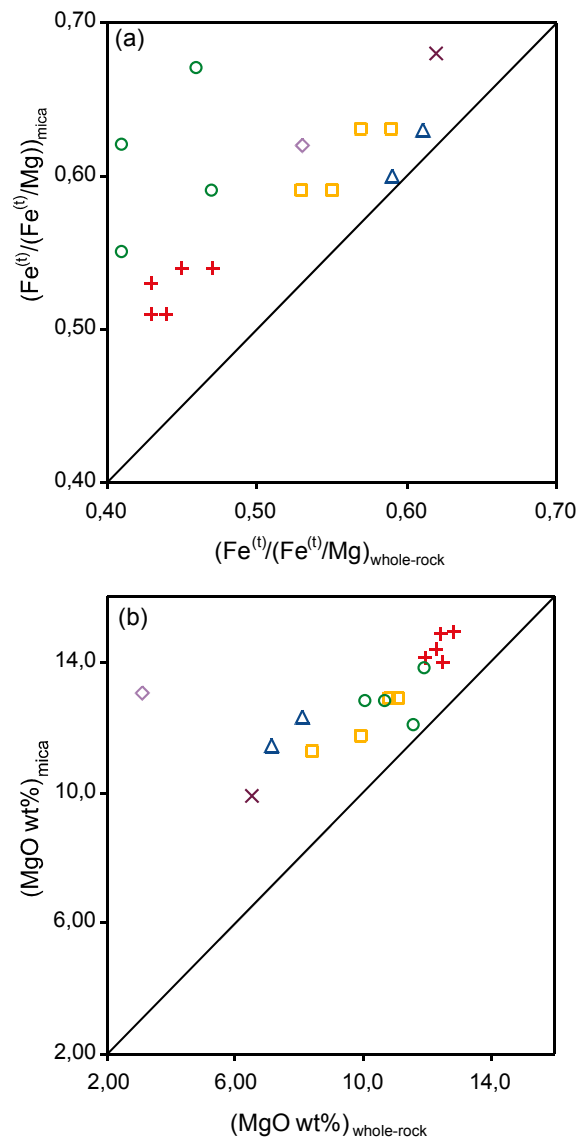
Figure 54. (a) The Fe(t)# relations of micas and their host rocks, (b) MgO (wt%) covariations of micas and their host rocks (the symbol are as in Figure 28).

against Mg#, is clearly defined to decrease with decreasing water content and pressure in the system and, to increase with increasing temperature and oxygen fugacity as discussed in previous and following sections. Micas are interpreted to have crystallized at high temperature, low pressure, high oxygen and water fugacities.

4.2.6.1. Oxygen Fugacity

Phl bearing systems may require high oxygen fugacity and high water activity to stabilize on their liquidus (Esperança and Holloway, 1987). It is possible to estimate either the maximum oxygen fugacity or temperature or the minimum water or hydrogen fugacity by using mica compositions on the base of experimental studies of Wones and Eugster (1965) and Rutherford (1973). Generally, estimates based on experimental studies are limited to felsic rocks since experiments are based on assemblages including bio, K-feld, mt, aluminum silicate, leu or qt, and focus on ann-end member. The mineral assemblages in the studied rocks are not appropriate to estimate magmatic conditions from such experiments. Due to the limitations, it is only possible to make a qualitative assumption for oxygen fugacity from a ternary system of bio solid solutions, which relates mica compositions to the three common oxygen buffers, Fe_2SiO_4-SiO_2-Fe_3O_4 (fayalite-quartz-magnetite, QFM), Ni-NiO (NNO), and Fe_3O_4-Fe_2O_3 (magnetite-hematite, HM), (Wones and Eugster, 1965). The studied micas define buffering conditions between the NNO and HM (Figure 55). Carmichael (1991) indicated that the oxygen fugacities of mantle derived liquids can be as high as those of the HM buffer. Mica compositions run inclined from NNO to HM buffer conditions as their host rock changes from ultramafic to mafic rocks. This may indicate magmatic differentiation since Fe^{3+} content of micas increases as differentiation proceeds. The lower Fe^{3+} content of micas from the ultramafics implies a lower oxygen fugacity than that of the mafics. Micas of the studied rocks seem to be oxidized. This idea is also supported by the presence of the sulphide mineral, pyr, in most of the studied samples, which is an evidence of late oxidation.

Ti content of micas increases from ultramafic to mafic rocks. This may be controlled by oxygen fugacity according to Bachinski and Simpson (1984) and

Guidotti (1984). Constant Mg/Fe$^{(t)}$ ratio of less than 2 for micas of the ultramafics, and greater than 2 for the mafics may infer a slight change in oxygen fugacity. However, Righter and Carmichael (1996) explained that Ti substitution in the octahedral site of trioctahedral micas (discussed in Section 4.2.2) is not related to oxygen fugacity. It is, however, a factor of temperature.
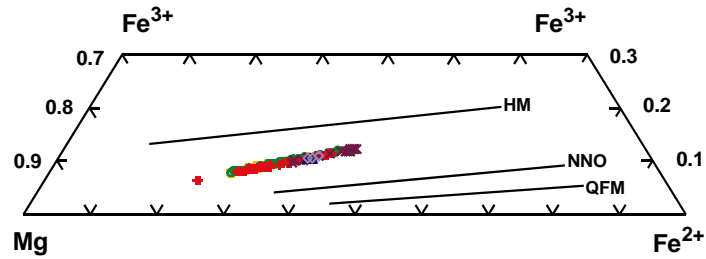
Figure 55. Estimation of redox conditions for micas crystallization in the Fe^{3+}-Mg-Fe^{2+} ternary diagram where QFM: quartz-fayalite-magnetite, NNO: Ni-NiO, HM: hematite-magnetite. Experimentally derived oxygen fugacity buffers after Wones and Eugster (1965) (the symbol are as in Figure 28).

4.2.7. Geothermobarometry

Experimental studies on simple and natural systems have shown that Al, Ti and Ba substitution in trioctahedral micas is dependent on pressure-temperature conditions, and the substitution for phl is maximum at low pressure and high temperature (Edgar et al., 1976; Robert, 1976b; Van Kooten, 1980; Patino Douce and Johnston, 1991; Patino Douce et al., 1993; Righter and Carmichael, 1996). From the hydrous rocks in the Kurançalı area, Si-deficient and Al-enriched phl in both tetrahedral and octahedral sites (as discussed in Section 4.2.2.) might be representative of crystallization at low pressure. The substitution mechanism, $2Mg^{[6]} \Leftrightarrow Ti^{[6]}+()^{[6]}$, shows that there is a negative linear correlation for all rock types except for DIO where micas deviate from the linear trend (Figure 56). This is due to differences in Ti-content of micas of DIO and may favor a slight pressure difference as suggested by Van Kooten (1980). However, Ti-saturation in micas, as

specified by the presence of Ti-phases such as rt, ilm and sph, might be a
function of temperature rather than pressure, and oxygen and H_2O activities
(Righter and Carmichael, 1996).
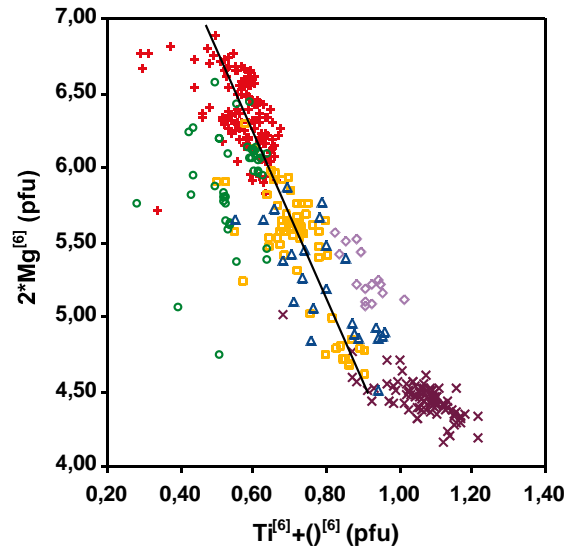
Figure 56. The substitution mechanism, $2Mg^{[6]} \Leftrightarrow Ti^{[6]}+()^{[6]}$, showing deviation
from the main trend for the DIO micas having higher Ti content (the symbol are
as in Figure 28).

As disccused in Section 4.2.2., coupled substitutions of different cations
between sites in phl are complicated, and a substitution mechanism
$Ba^{[12]}+3Ti^{[6]}+4Al^{[4]} \Leftrightarrow 2K^{[12]}+4(Mg,Fe)^{[6]}+4Si^{[4]}$ was proposed to explain
compositional trends in phl's by Guo and Green (1990). Righter and
Carmichael (1996) examined the pressure-temperature dependence of this
coupled mechanism to compare it with the pressure and temperature
dependence of the substitutions, $2K^{[12]} \Leftrightarrow Ba^{[12]}+()^{[12]}$ and $2Mg^{[6]} \Leftrightarrow Ti^{[6]}+()^{[6]}$. At
oxygen fugacities between NNO and HM oxygen buffers, Ti substitution is
dependent on temperature and increases with increasing temperature (Shau et
al., 1991; Righter and Carmichael, 1996) while Ba substitution is a function of
both pressure and temperature, former being more important (Righter and
Carmichael, 1996). Eventhough Ba partitioning into mica decreases with

increasing pressure (Guo and Green, 1990), compositional factors are more efficient (Righter and Carmichael, 1996). Righter and Carmichael (1996) formulated a geothermobarometer based on both mica and liquid compositions. Unfortunately, this formulation could not be used for the studied rocks since liquid composition could not be calculated due to strong disequilibrium compositions of the rocks. Righter and Carmichael (1996) also suggested a qualitative geothermobarometer diagram on which the data of micas for the studied rocks are plotted (Figure 57). The Kurançalı micas plot on the LP trend (low pressure trend), indicating 5-15kbar $\pm$ 4kbar and 1090-1160°C. This is also supported by the estimated high oxygen fugacities of the HM buffer. Low pressure estimation, based on micas being assumed to indicate mantle origin, may infer an intra-oceanic environment.
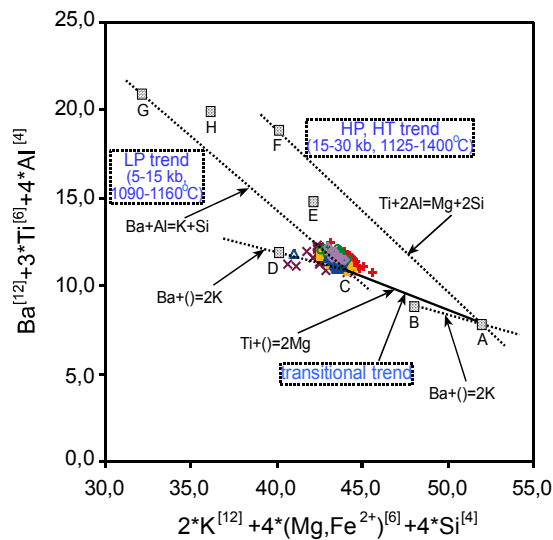
Figure 57. Plots of the micas on the diagram compiled from Righter and Carmichael (1996) who prepared it based on combined substitution mechanism of Guo and Green (1990). End member phl compositions; A: $K_2Mg_6Al_2Si_6O_{20}(OH)_4$, B: $()^{[12]}BaMg_6Al_2Si_6O_{20}(OH)_4$, C: $K_2Mg_4()^{[6]}TiAl_2Si_6O_{20}(OH)_4$, D: $()^{[12]}BaMg_4()^{[6]}TiAl_2Si_6O_{20}(OH)_4$, E: $()^{[12]}KMg_5TiAl_3Si_5O_{20}(OH)_4$, F: $K_2Mg_5TiAl_4Si_4O_{20}(OH)_4$, G: $Ba_2Mg_4()^{[6]}TiAl_4Si_4O_{20}(OH)_4$, H: $()^{[12]}BaMg_5TiAl_4Si_4O_{20}(OH)_4$ (the symbol are as in Figure 28).

4.3. Pyroxene

Py, the first mafic mineral to crystallize in the plutonic mafic-ultramafic rocks of the Kurançalı area, was chemically studied. Chemical compositions of py, given in Appendix C, were achieved for all rock types. The analyses were carried out at center/rim, and along profiles from center to rim of the crystals, and totally 501-point analyses were performed on various crystals of py representing different textural characteristics.

Major and minor element contents of py were determined in oxide form and then the obtained values were converted to cation pfu values based on 6 oxygen atoms and 4 cations following the method given in Section 4.1. Ferric and ferrous iron was derived from $FeO^{(t)}$ based on the Droop equation (1987) (Section 4.1.). Calculated Fe^{2+} and Fe^{3+} values are the same as those estimated by the computer program of Papike et al. (1974) in which calculations are based on charge balance.

4.3.1. Compositional Variations

The first mafic mineral, py, which was examined for each rock type, shows high heterogeneity even in a single sample. Py is, in general, highly magnesian with lower total iron. The ranges of $Mg/(Mg+Fe^{(t)})$ and of $Mg/(Mg+Fe^{2+})=Mg\#$ are 0.56-0.81 and 0.59-0.88, respectively (Appendix C).

Despite the heterogeneous composition, the compositional ranges are similar for py's of all ultramafic rocks, while py's of mafic rocks have similar ranges within themselves. In spite of relatively lower Mg#'s of py from mafic rocks, the values are still within the range of the ultramafics.

Py from all ultramafics with moderately high Mg# (0.64-0.88) are characterized by similar compositional ranges in SiO_2, Al_2O_3, TiO_2, MgO, $FeO^{(t)}$ and CaO contents which are 45.59-53.71, 0.36-8.66, 0.02-1.25, 8.77-14.28, 6.12-12.62 and 21.89-25.12 (wt%), respectively. Although the TiO_2 values of py from HBdite are within the given limit, they have the lowest values. This may be related to micas with the highest TiO_2 values present in HBdite. Na_2O,

K$_2$O, MnO, Cr$_2$O$_3$ and NiO contents of py are very low with the ranges of 0.10-0.97, 0.00-0.38, 0.08-0.46, 0.00-0.12 and 0.00-0.09 (wt%), respectively.

Py of mafic rocks show similar compositional ranges within themselves. However, Mg# of py from LG (0.66-0.71) is relatively higher than that from DIO (0.58-0.62). SiO$_2$, Al$_2$O$_3$, MgO, FeO$^{(t)}$ and CaO contents of py are highly variable with 50.89-53.16, 0.39-3.64, 10.41-12.92, 9.39-14.17 and 21.86-23.85, respectively. The low contents of TiO$_2$, Na$_2$O, K$_2$O, MnO, Cr$_2$O$_3$ and NiO vary with the ranges of 0.04-0.60, 0.13-0.37, 0.00-0.04, 0.31-0.54, 0.00-0.06, and 0.00-0.10 (wt%), respectively. The minor elements of py from the mafics are lower than those from the ultramafics.

Py seems to crystallize from a system having moderately high MgO content. Although Al$_2$O$_3$ is highly variable in py of CPXnite, CPXnite WHMP and PHLtite, Al$_2$O$_3$ and CaO contents of py decrease while MnO increases from the ultramafics to the mafics. These compositional variations were ascribed to igneous differentiation process controlled by the fractionation of cpx and plag (Tiepolo et al., 1997). TiO$_2$ content of py, decreasing from ultramafics to the mafics, opposes to that of the coexisting micas.

Plotting cation pfu against Mg# is the best approach to see compositional changes for py through the ultramafics to the mafics (Figure 58). Si content of py generally increases with decreasing Mg# from the ultramafics to the mafics (Figure 58a). This reverse relation is better constrained for Fe^{2+} and Mn contents (Figure 58e,h). On the other hand, Al$^{(t)}$, Ti, Ca, Fe^{3+}, Mg and Na contents increase from the mafics to the ultramafics with increasing Mg# (Figure 58b,c,d,f,g,i). When Al$^{(t)}$, Ti, Ca and Na contents are examined in detail, for py of ultramafic rocks, each element displays a broad reverse pattern for each rock type. This may be due to lack or minor occurrence of plag in the ultramafics where Al$^{(t)}$ mainly partitioned into py and mica. In general, py is similar to mica in terms of Al$^{(t)}$ content, i.e. both minerals have lower Al$^{(t)}$ for mafic rocks than that for ultramafic rocks. However, in detail, this relationship varies within the minerals of ultramafic rocks. That means, Al$^{(t)}$ content decreases for py while it increases for mica through CPXnite WHMP, CPXnite and PHLtite. This can be explained by partitioning of Al$^{(t)}$ between py and mica
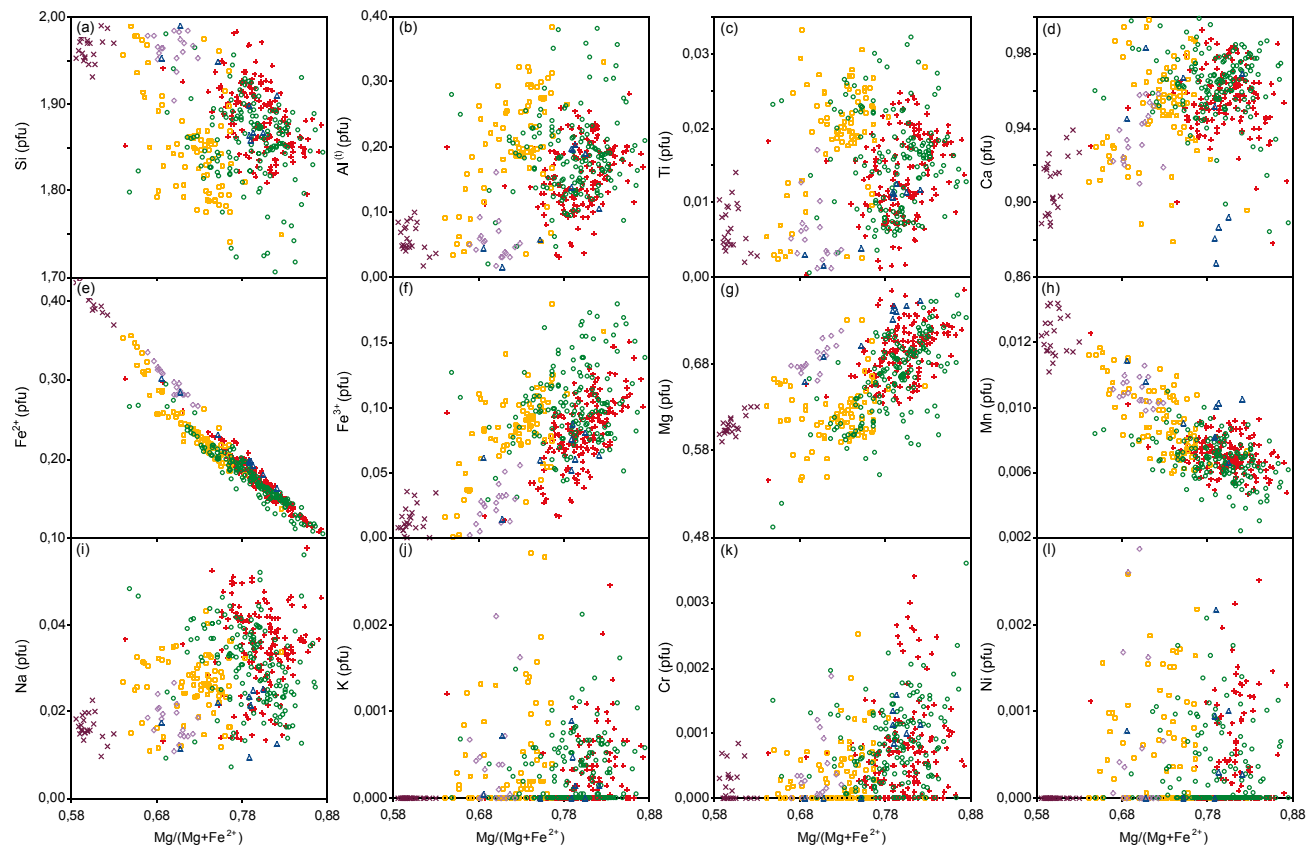
Figure 58. Variation diagrams for major and minor element compositions of py from ultramafic-mafic plutonic rocks (the symbols are as in Figure 28).

where plag is absent or less than 7-8 %. Mg content of py forms two trends, one of which is for py from the ultramafics and the other one for those of mafic rocks (Figure 58g). The compositional change in terms of Na content of py increasing through the mafics to the ultramafics is similar to that observed for mica. K, Cr and Ni contents are lowest for py of mafic rocks while they are higher for those of ultramafic rocks (Figure 58j,k,l). Na and K contents of py from the ultramafics, despite their low values (but higher than those of the mafics), may indicate that the melt system from which the rocks were formed, was affected by relatively alkaline compositions. Moreover, this may also indicate presence of Na in the system at the beginning of crystallization.

The exteremely rare py crystals from HBdite, found as relicts in amph crystals, show varying compositions.

Ti and $Al^{(t)}$ display a weak positive correlation with $Fe^{(t)}/(Fe^{(t)}+Mg)$ known as fractionation index (Figure 59). Absence of iron oxide minerals may be the reason of this positive relation according to (Marcelot et al., 1988), because oxide mineral crystallization causes negative correlation. Another possible reason for this weak positive correlation is chemical effect from outside to the system, i.e. metasomatism.

Py in all rock types shows high Ca# (Ca/(Ca+Mg)=0.54-0.71) and the relation of Ca# to Mg# define two trends (Figure 60). HBdite, LG and DIO define one of the two trends, and the other one is formed by PHLtite, CPXnite, CPXnite WHMP. This relation supports the broad relations of elements to Mg# (Figure 58) and may indicate genetic relations of the rocks. In conclusion, two major rock groups can be distinguished based on the mineral assemblages and major element composition of py. The first group is that of ultramafic rocks except for HBdite. Mafic rocks and HBdite define the second group.

4.3.2. Nomenclature and Substitution Mechanisms

Formula calculation and nomeclature for py were made according to the recommendations of the IMA (Morimoto, 1989). Morimoto (1989) proposed a general chemical formula as $M2M1T_2O_6$ in which both $M2$ and $M1$ represent
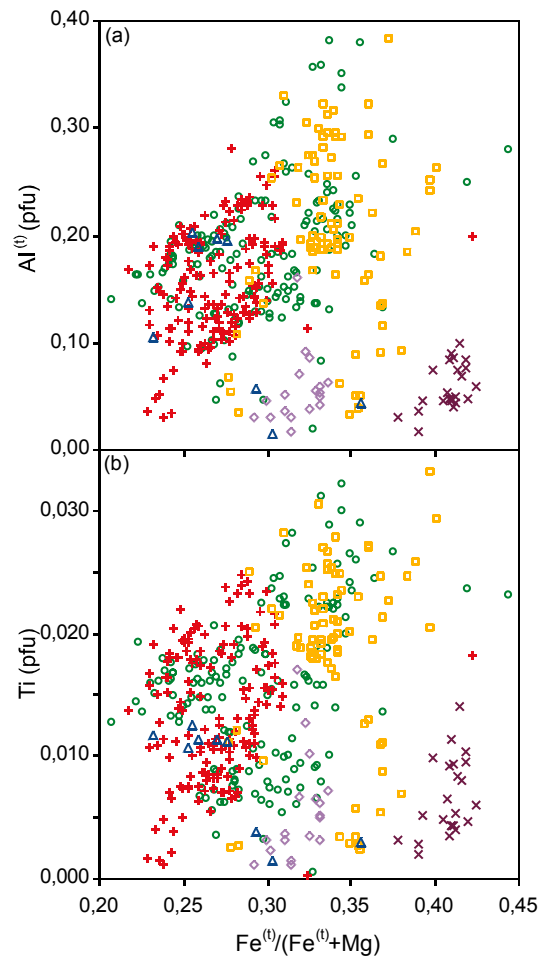
Figure 59. Covariation diagrams of $Al^{(t)}$ and Ti against $Fe^{(t)}/(Fe^{(t)}+Mg)$ (the symbols are as in Figure 28).

cations of the octahedral site (*M*2 for distorted coordinations and *M*1 for regular coordinations), and *T* is representative for cations of the tetrahedral site. For the studied py, the site allocations of the cations were done as recommended by Morimoto (1989); *T* is filled by Si, Al, then Fe^{3+} (sum to 2); *M*1 is filled by Al, Fe^{3+} (resting after that used in *T* site) and then Ti, Cr, Mg, Fe^{2+}, Mn (sum to 1); *M*2 is filled by Mg, Fe^{2+}, Mn (resting after that used in *M*1) and then Ca, Na (sum to 1).
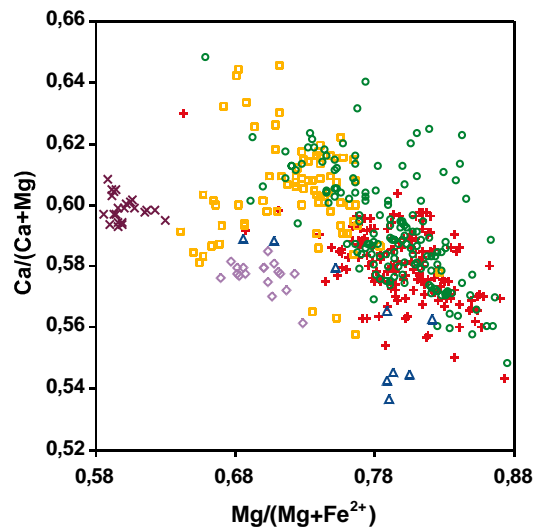
Figure 60. The relation Ca# to Mg# for py of ultramafic-mafic plutonic rocks (the symbols are as in Figure 28).

Chemical data show that py's from each rock type have similar compositions and belongs to the Ca-Mg-Fe py group ($Ca_2Si_2O_6$ (Wo) - $Mg_2Si_2O_6$ (En) - $Fe_2Si_2O_6$ (Fs)) as shown in Figure 61. All analyses plot in the di field of the ternary system Wo-En-Fs based on the calculations of Morimoto (1989) (Figure 62a) where most of the data display a Ca-oversaturated composition. The Ca-oversaturation is mainly observed in py from CPXnite, CPXnite WHMP and PHLtite. In the more evolved rocks such are HBdite, LG and DIO, py are not Ca-oversaturated and plot in the di field. They also differ from py of ultramafic rocks, showing lower Mg# as discussed above. This

might be explained taking Al and Fe^{2+} contents into consideration. The studied py are classified as ferroan aluminous di.

The plots of Wo-En-Fs % calculated after Lindsley (1983) result in a decrease of Wo content. Py compositions range from di to di'dic aug, better supporting the petrographical observations (Figure 62b). Therefore, cpx compositions defined after Lindsley (1983) are reliable and used in following sections. The compositional ranges for cpx type are $Wo_{44.1-51.9}En_{29.2-40.5}Fs_{11.2-23.1}$ based on calculations after Morimoto (1989) and $Wo_{33.5-48.8}En_{32.3-54.6}Fs_{7.70-23.5}$ based on the calculations after Lindsley (1983).
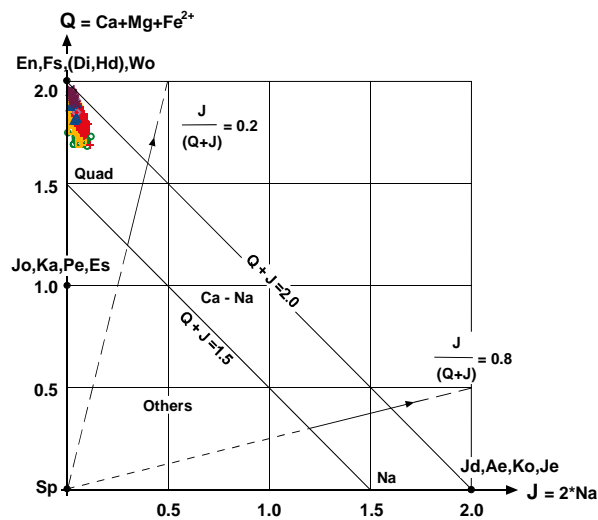
Figure 61. The place of py data on the Q-J diagram of Morimoto and Kitamura (1983) on which the positions of the 13 accepted end-members are indicated (the symbols are as in Figure 28).

Py, composed of variable amounts of Al_2O_3 (up to 8.66 wt%), shows the following substitution mechanisms: $(Fe^{2+})^{[6]} \Leftrightarrow Mg^{[6]}$, $2Al^{[6]} \Leftrightarrow 3Ca^{[6]}$ $(Ca+Mg+Fe^{2+}+Mn)^{[6]}+Si^{[4]} \Leftrightarrow Al^{[6]}+Al^{[4]}$ and $(Ca+Mg+Fe^{2+}+Mn)^{[6]}+2Si^{[4]} \Leftrightarrow Ti^{[6]}+Al^{[4]}$, and Ti/Al ratio between 1:5-1:20 (Figure 63). These features indicate that Al entered py structure as Ca-tschermaks molecule (cats). This is clear in the classification diagram proposed by Papike et al. (1974) based on Ti-Na-
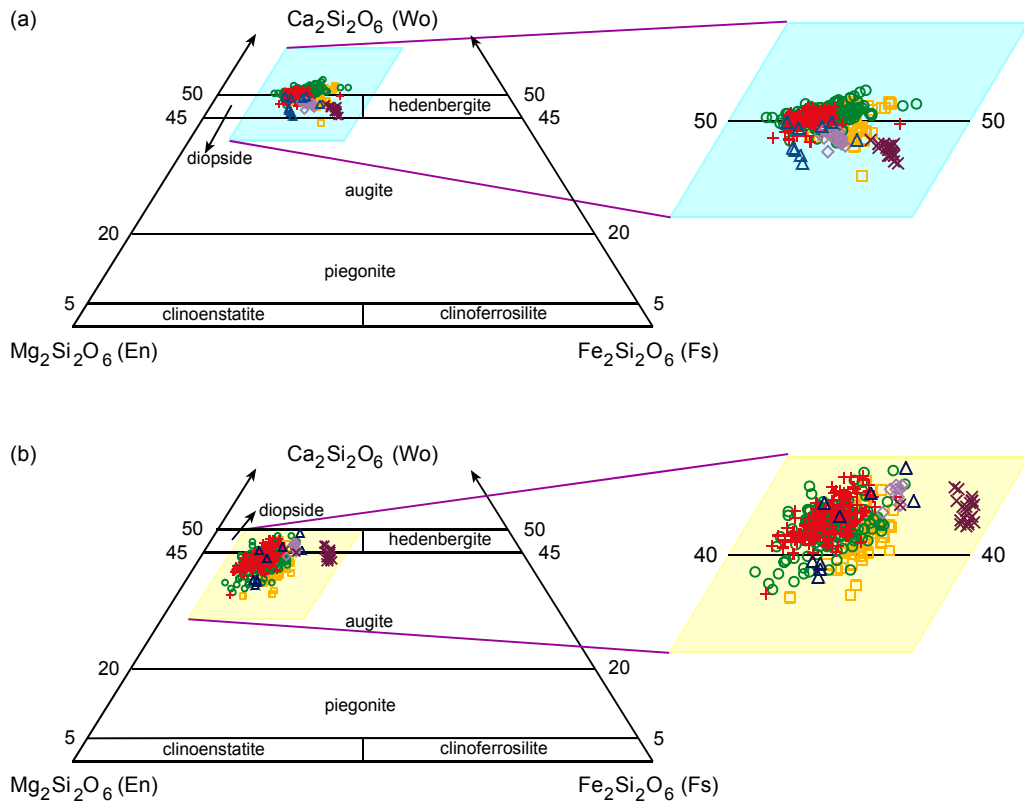
Figure 62. The plots of py on the Ca-Mg-Fe cpx classification diagram with accepted names after Morimoto (1989) where calculations of Wo, En, Fs values based on the formulae by Morimoto (1989) for (a), and the formulae by Lindsley (1983) for (b) (the symbols are as in Figure 28).
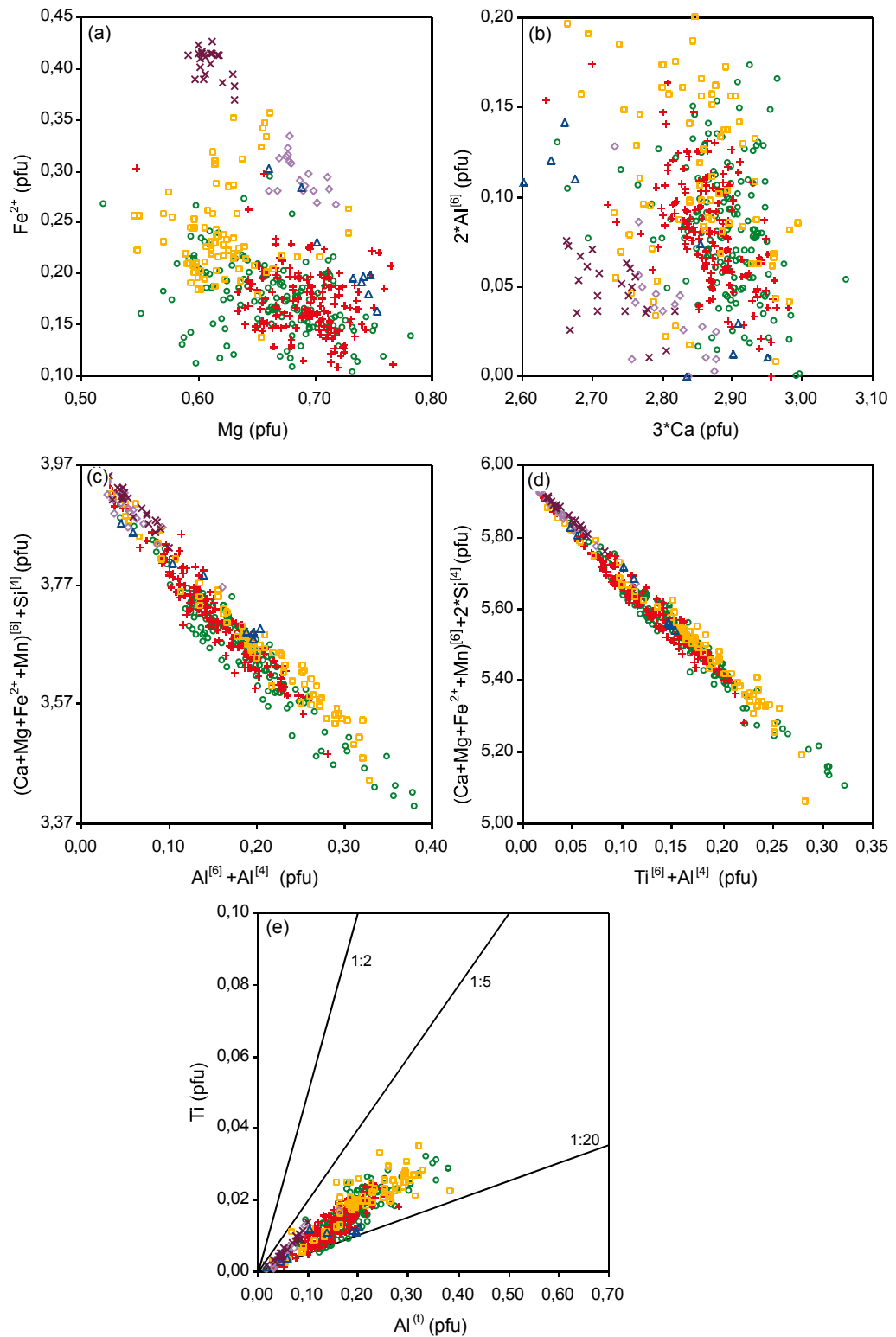
Figure 63. The substitution mechanisms and Ti-Al[(t)] ratio diagram displaying the presence of cats component in the studied py chemistry (the symbols are as in Figure 28).

Al$^{[4]}$ where all the data plot in the cats corner of the triangle (Figure 64). The substitution mechanisms, $(Fe^{2+})^{[6]} \Leftrightarrow Mg^{[6]}$ and $2Al^{[6]} \Leftrightarrow 3Ca^{[6]}$, display scattered relations with two trends; one of which in mafic rocks and the other one in ultramafic rocks (Figure 63a,b). On the other hand, the coupled substitutions given in Figure 63c,d correlate well. This indicates that coupled substitution mechanisms are the controlling factor for py of the Kurançalı rocks.

There is an extensive, well correlated variation between Si and Al$^{(t)}$ (Figure 65) that could result from (1) extensive re-equilibration (may be due to metasomatism), (2) high SiO_2 activity of parent magma, (3) sub-solidus re-equilibration (Hébert and Laurent, 1990).
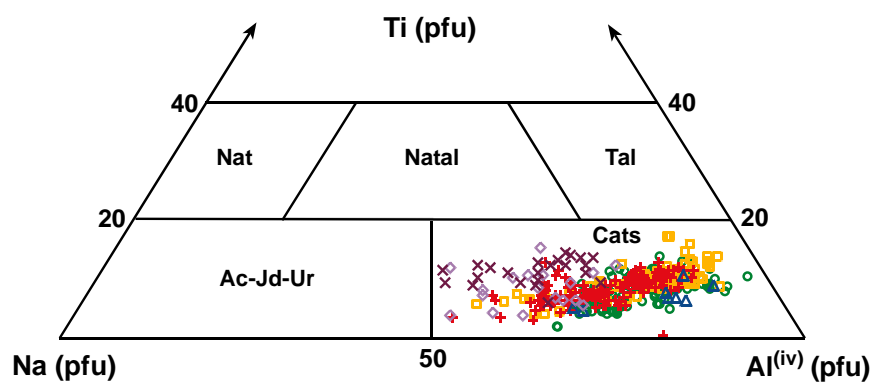
Figure 64. The place of the py data on the Ti-Na-Al$^{[4]}$ triangle diagram proposed by Papike et al. (1974) (the symbols are as in Figure 28).

4.3.3. Elemental Variations within a Zoned Crystal

The chemical data obtained along profiles from rim to core of optically zoned py crystals display of zoning (Figure 66). The zoned cpx crystals typically show rims enriched in Al$^{(t)}$, Ti, Fe$^{(t)}$, K and Ni (pfu), and depleted in Si, Mg, Mn and Cr (pfu) compared to cores. In detail, there is a complex pattern with four well-defined zones. The outermost zone (Zone 1) can be

characterized by an abrupt decrease in K, Cr, Ni and an abrupt increase in Ca and Mn, but there is no significant change in other elements. It is possible to mention about a steady increase for Si, Mg, Mn, and steady decrease for Al$^{(t)}$, Ti, Fe from rim to core. However, the profiles of K, Cr, Na, Ni are not steady. Ni and Cr decrease in Zone 2, but increase in Zone 3, while K and Na opposes them. Abrupt changes in K and Cr are very diagnostic in Zone 3. So zones 2 and 3 can not be represented as regular zones reflecting simlar compositions for all elements. In the innermost zone (Zone 4) displaying the core composition, Si, Ca, Mg, Mn and Cr are enriched relative to those in Zone 1, while Al, Ti, Fe, K, Na and Ni are depleted. In summary, the decreasing profiles of K and Ni from rim to core are not as regular as the profiles of Al$^{(t)}$, Ti, Fe$^{(t)}$. Moreover, the increasing profile for Si, Mg is regular than that for Mn and Cr. Ca content shows a strong zig-zag pattern from rim to core.
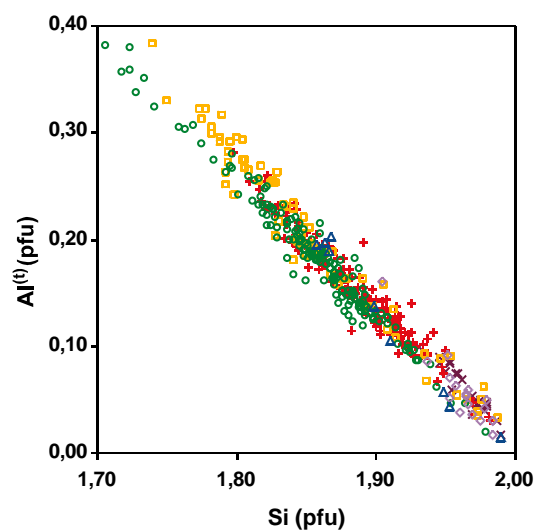
Figure 65. The plot showing extensive variation of Si and Al$^{(t)}$ (the symbols are as in Figure 28).

Al$_2$O$_3$ and TiO$_2$ contents of the zoned crystals highly vary from 3.20 to 8.64 (wt%) and 0.48 to 1.02 (wt%), respectively, from core to rim. Moreover, these elements display a wide range of composition in the rocks. Duda and
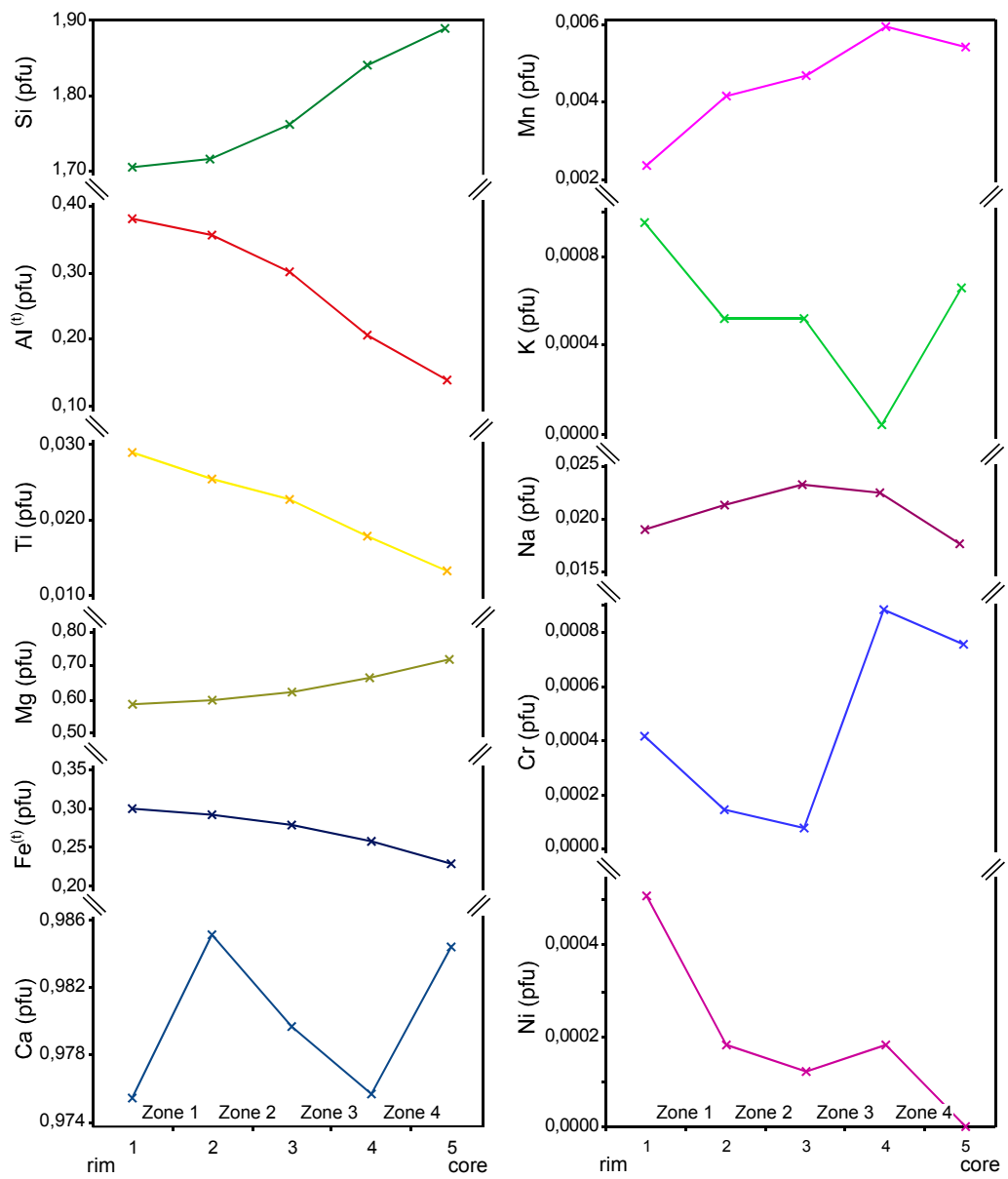
Figure 66. Elemental changes (cation pfu) along a profile of a zoned py crystal (the symbols are as in Figure 28).

Schminke (1978) showed that $Al_2O_3 > 4.5$ wt% and about 2 wt% TiO_2 are common for alkaline rocks, and therefore the enrichment in Al, Ti, Na and K contents from core to rim may be explained by an effect of later event, such as alkaline metasomatism.

The Mg-Fe zoning and zig-zag change of Ca content from rim to core of py crystal, is shown on a Wo-En-Fs diagram (Figure 67). The Wo-En-Fs values (after Lindsley, 1983) along a profile of zoned crystals display increasing Wo% values from rim to core as Mg content increases and Fe^{2+} decreases. The compositional change on the quadrilateral displays that change of Mg is not effective, and the main control is due to Fe^{2+} content and zig-zag change of Ca content. This shows enrichment in aug'tic composition from core to rim. The compositional change from di to aug (from core to rim) may result from alkaline metasomatism.
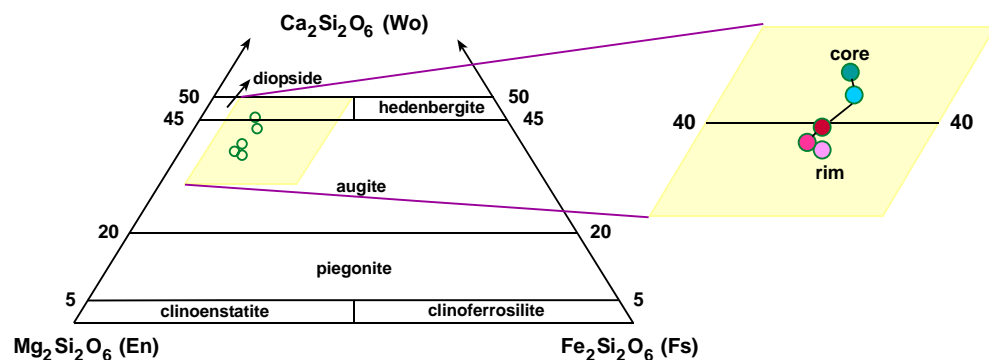
Figure 67. The compositional change along a profile of a zoned py crystal on the Ca-Mg-Fe cpx classification diagram where the calculations Wo, En, Fs values based on the formulae by Lindsley (1983) (the symbols are as in Figure 28).

4.3.4. Compositional Relation of Pyroxene to Host Rocks

The Mg#'s of cpx (0.59-0.88) decreasing moderately from CPXnite through PHLtite, CPXnite WHMP, HBdite, LG to DIO fit well to the host rock compositions (Figure 68). It is evident from Figure 68 that all plots deviate from

1:1 slope of the graph. That means, Mg# of py is slightly higher than that of its host rock, and composition of whole rock is slightly richer in iron. This leads to consider that, iron was most likely present as Fe^{3+} due to oxidizing conditions in the melt at the time of crystallization, and thus, the iron partitioned into the dark mica structure. Because $FeO^{(t)}$ contents of dark mica (the crystallizing phase following py in the rocks) are slightly higher than those of the host rocks as discussed in Section 4.2.5, and iron oxide phases are absent in the host rocks.
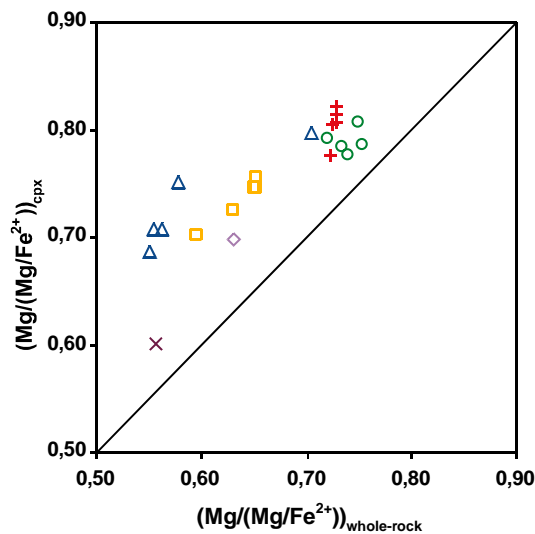
Figure 68. The variation Mg# of py against Mg# of host rock (the symbols are as in Figure 28).

4.3.5. Implications for Petrology and Tectonic Environment

Incorporation of Si, Al, Ti, Ca and Na into the cpx lattice depends on the degree of alkalinity of the parental magma of volcanic rocks (Le Bas, 1962; Leterrier et al., 1982). The proposed approaches may also provide evidences for the origin of the rocks from the Kurançalı area. The chemical data of py are plotted on covariation diagrams of SiO_2-Al_2O_3 (wt%) and Ti-Ca+Na (pfu) (Figure 69). Composition of the system from which py is formed display high
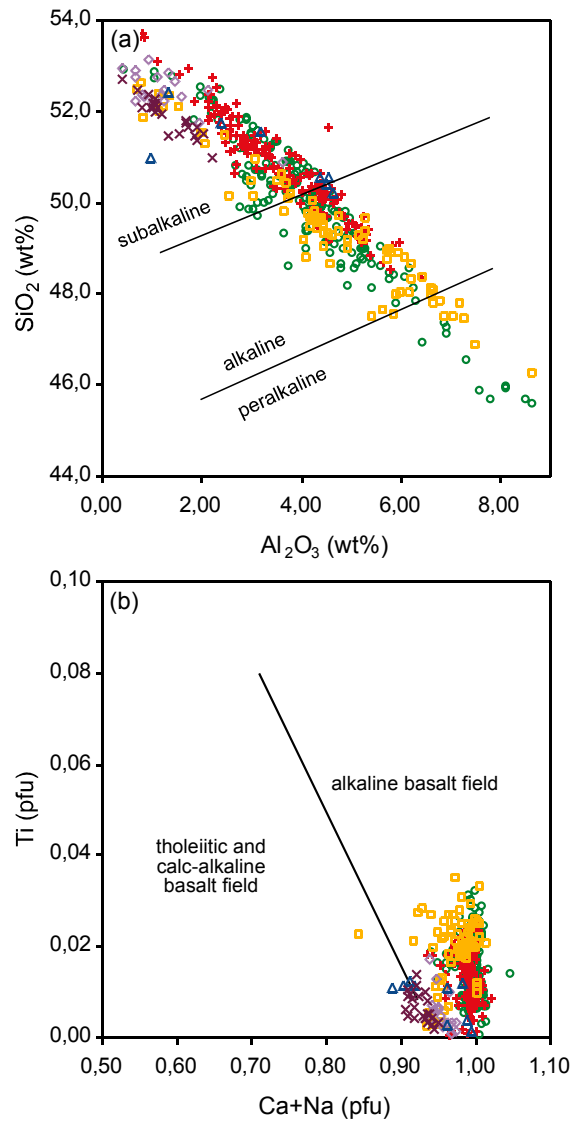
Figure 69. The place of the py data on the diagrams of; (a) SiO_2-Al_2O_3 (wt%) (Le Bas, 1962), and (b) Ti-Ca+Na (pfu) (Leterrier et al., 1982) (the symbols are as in Figure 28).

variations ranging from subalkaline to alkaline even few data plotting in peralkaline field (Figure 69a). Py from CPXnite and CPXnite WHMP display transitional character between subalkaline to alkaline composition. However the data of py mainly plot in the alkaline field on Ti-Ca+Na diagram; this is actually due to the Ca-enrichment (Figure 69b). Transitional character of py having a wide range of compositions may indicate a complex history for the rocks.

The tetrahedral site of py is almost completely filled by Si (1.71-1.99 pfu). Py consistently shows an excess of Al over that needed to complete the tetrahedral site. This is actually due to high Si content almost filling the tetrahedral site to 2.00. That means there is no deficiency in the tetrahedral site of py, therefore, py may not be originated from alkaline magma. Because the deficiency in the tetrahedral site is a characteristic feature of cpx from alkaline rocks (Conticelli, 1998 and references therein). On the other hand, there are some evidences of alkaline character that may be achieved by metasomatism. Therefore, the chemical data for py is compared with cpx from alkaline basalts, alkaline oceanic gabbros and HBdite's, and old oceanic crust metasomatized by alkaline magma (Figure 70). py with lower Mg# (0.58-0.71) and the lowest Al substitution for Si from LG and DIO falls not only within the range of gabbros from the Mid-Atlantic Ridge but also within the range of alkaline gabbro from the Canary Islands and metasomatized xenoliths belonging to the old oceanic crust (Figure 70). They are, however, slightly depleted in TiO_2 compared to those from gabbros in Mid-Atlantic Ridge while they plot in the field of cpx in metasomatized oceanic material affected by alkaline melt (Figure 71). Py from the ultramafics cover a relatively wide range in compositions (Mg#=0.64-0.88, 0.02-1.25 wt% TiO_2, 0.36-8.66 wt% Al_2O_3, 0.10-0.97 wt% Na_2O) and they are similar to cpx in metasomatized gabbroic xenoliths in alkaline basalts. They mainly plot within the field of the metasomatized xenoliths (Figure 70b) although some of the data from py of the ultramafics overlap with the field of Mid-Atlantic gabbro and alkaline volcanic rocks. Py from the ultramafics having relatively higher Al_2O_3 and TiO_2 contents also plot within the field of alkali metasomatized old oceanic crust (Figure 71b). Py from HBdite show a transitional character between mafic rocks and ultramafic rocks.

116
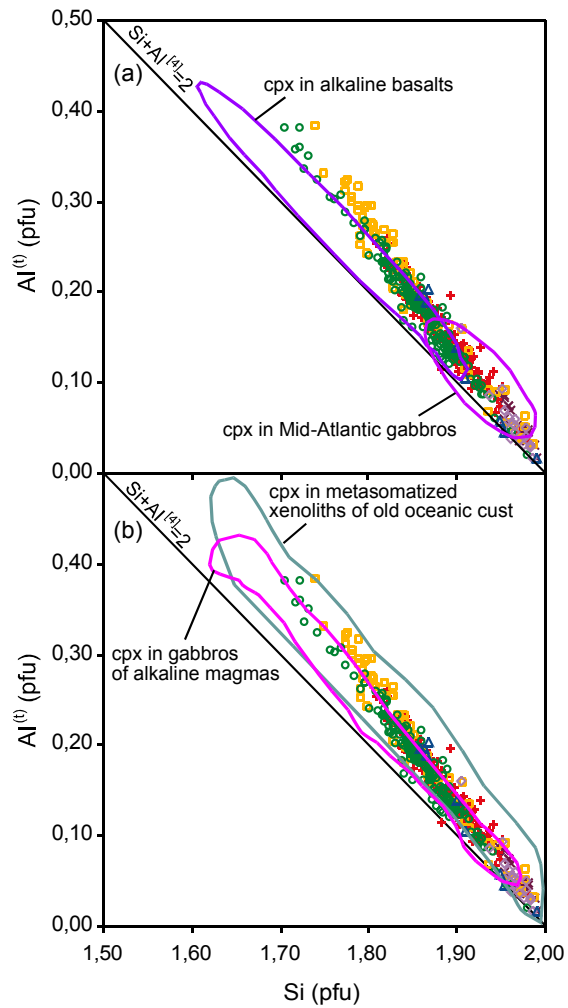
Figure 70. Al$^{(t)}$-Si (pfu) relations for the studied py and their comparison with cpx's (a) in gabbroic rocks from the Mid-Atlantic Ridge (Cannat et al., 1997; Gaggero and Cortesogno, 1997), in alkali basalts (Neumann et al., 1999), (b) in metasomatized xenoliths of old oceanic crust, and in alkaline gabbros and HBdites from the Canary Islands (Neumann et al., 2000) (the symbols are as in Figure 28).

117
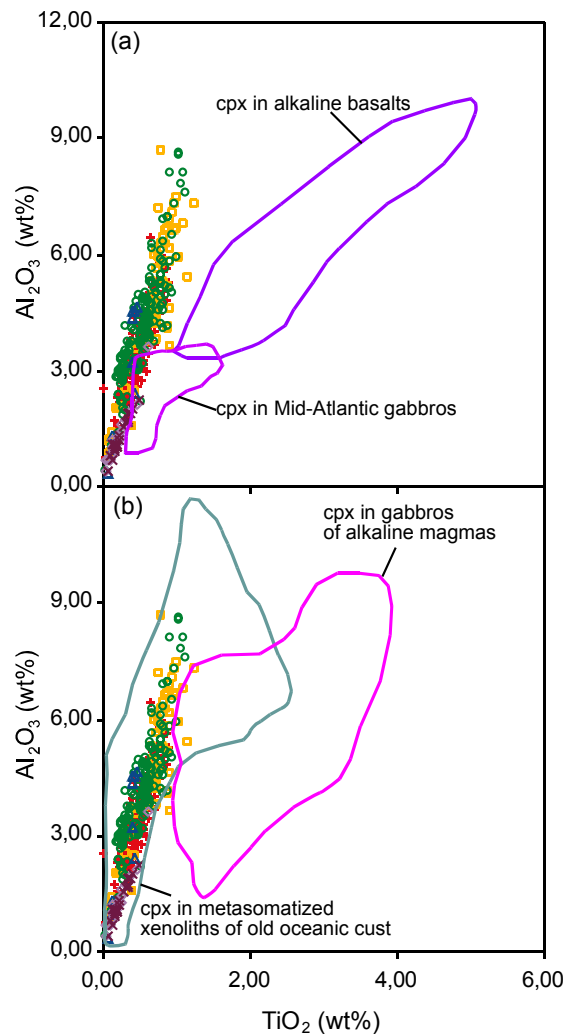
Figure 71. Al$_2$O$_3$-TiO$_2$ (wt%) relations for the studied py and their comparison with cpx's (a) in gabbroic rocks from the Mid-Atlantic Ridge (Cannat et al., 1997; Gaggero and Cortesogno, 1997), in alkali basalts (Neumann et al., 1999), (b) in metasomatized xenoliths of old oceanic crust, and in alkaline gabbros and HBdites from the Canary Islands (Neumann et al., 2000) (the symbols are as in Figure 28).

As a result, the comparison of py with those in alkaline rocks (both intrusive and extrusive) and with those in oceanic material metasomatized by alkaline melt reaction displays that py in ultramafic rocks shows chemical similarity to cpx in metasomatized rocks.

The covariation of Ti and $Al^{(t)}$ of py is also compared with that of cpx in lamproites and peridotitic xenoliths carried by lamproites in Italy (data from Conticelli, 1998) (Figure 72). There is a good correlation between Ti and $Al^{(t)}$ for the studied py, that is parallel to a trend for cpx of metasomatized peridotitic enclaves of subcontinental mantle. However, the enrichment in $Al^{(t)}$ of the studied py shows a wider range compared to cpx compositions from enclaves. This relation may be a clue of alkaline metasomatism. This may also be evidenced by large chemical variations that are found in zoned crystals where the rims of py crystals have higher Al_2O_3 content than the cores (given in Section 4.3.3). That means, extensive substitution of Al for Si in the tetrahedral site is present at rims that mainly plot in the field of metasomatized rock. The center of the zoned crystals, depleted in TiO_2 and Al_2O_3, are relatively MgO-rich.

The comparison of Ca# of the studied py and cpx from metasomatized subcontinental mantle beneath the Vitim volcanic field of East Siberia (data from Litasov et al., 2000) showed that py from the Kurançalı area generally shows higher Ca# than the others (Figure 73). From this comparison, it may be concluded that the origin of the studied rocks are not related to metasomatized subcontinental mantle although py shows similar characteristics to those from metasomatized mantle rocks. It may be assumed that the studied rocks from the Kurançalı area are related to suboceanic mantle affected by metasomatism. This idea can be supported by Al_2O_3 (wt%) contents of py that are, in general, less than 5.00 wt% in spite of few higher values up to 8.66 wt%. The studied py with Al_2O_3 wt%<5.00, in general, can be defined as Al-poor according to Litasov et al. (2000) who explained that Al-poor vein pyroxenite groups are characteristic for dunite-pyroxenite-gabbro intrusive bodies from ophiolites, where they are interpreted as shallow level mantle products of interaction between basaltic magma and depleted peridotite, i.e. mantle metasomatism.
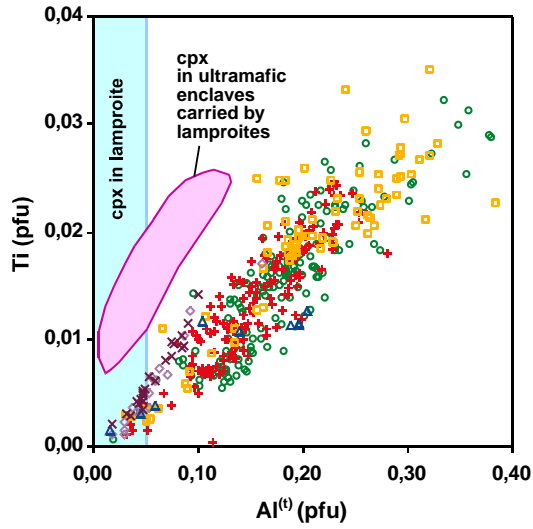
Figure 72. Covariation diagram of Ti and Al$^{(t)}$ of the studied py and their comparison with that of cpx in lamproites and metasomatized peridotitic xenoliths carried by lamproites (data from Conticelli, 1998) (the symbols are as in Figure 28).
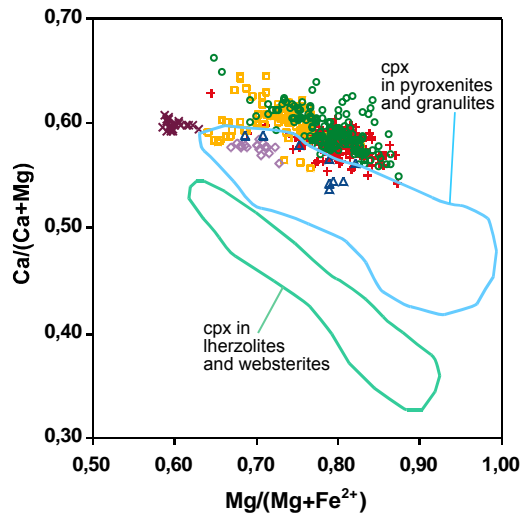
Figure 73. Comparison for Ca#-Mg# variation between cpx from the studied rocks and those from metasomatized subcontinental mantle beneath the Vitim volcanic field of East Siberia (data from Litasov et al., 2000) (the symbols are as in Figure 28).

There are evidences of mantle metasomatism but what kind of metasomatic event(s) is/are present is an important question. Comparison of py composition with cpx data from metasomatized xenoliths by different compositions such as adakitic, carbonatitic, basaltic melts or fluids may give a clue (Figure 74). Py data of the Kurançalı overlap well with the field of cpx from adakitic and alkaline metasomatized xenoliths. Some of the data for py from PHLtite, CPXnite shift into the field of cpx from carbonatite metasomatized xenoliths with traces of old basaltic metasomatism. This may be due to reaction of depleted peridotite with basaltic melt (e.g. Menzies et al., 1987) or H_2O-rich fluids (O'Reilly and Griffin, 1988). It may be inferred from mineral assemblages, i.e. presence of interstitial parg and phl, accessory minerals (rt and ap) and lack of glass (Gorring and Kay, 2000).

The partition of elements into cpx structure may also provide evidences for tectonic environment. The composition of py displays similarity to those from the island arc related gabbros (data from Burns, 1985), gabbros in Sarıkaraman Opholite (Yalınız and Göncüoğlu, 1999) and Mersin Ophiolite (Parlak et al., 1996) formed in intra-ocenic arc setting (Figure 75). The plot of Ti+Cr againts Ca shows close relation to arc environment rather than MOR environment in spite of much higher Ca content of the studied py (Figure 76a). The studied py plot in the overlapping field of calc-alkaline basalt (CAB) and island arc tholeiite (IAT) on the Ti-Al[(t)], but there are also points outside the fields, this relation may indicate a complex history of the rocks as mentioned above (Figure 76b). A resemblance to a calc-alkaline system is due to the di, aug (high Ca content) compositional character of the studied py. Such limited cpx compositions (di to Ca-rich aug) is not representative of a tholeiitic character but rather orogenic andesite suites (Arculus and Wills, 1980). Therefore we can exclude an IAT origin.

Py with high SiO_2, moderately high Mg# shows lower Ti/Al (<0.2) relatively to MORB, BABB and alkali basalts (e.g. Leterrier et al., 1982; Duncan and Green, 1987; Arculus et al., 1992; Lapierre et al., 1992; Conticelli, 1998; Conticelli et al., 1997). Moreover, covariation of $100*Al^{[4]}/(Al^{[4]}+Si)$ (percentage of the tetrahedral sites occupied by Al) and TiO_2 (wt%) for py approaches the arc related trend defined by Loucks (1990) (Figure 77). The Ti
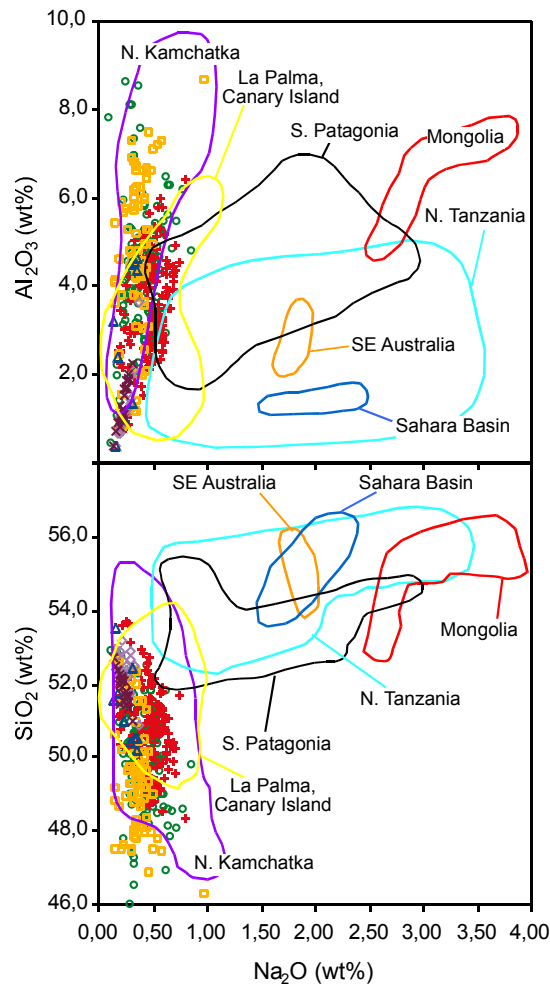
Figure 74. Plots of Al_2O_3 (a) and SiO_2 (b) against Na_2O (wt) for py from the hydrous ultramafic-mafic plutonic rocks and their comparison with cpx from adakite metasomatized xenoliths (from northern Kamchatka: Kepezhinzkas et al., 1995, 1996), carbonatite metasomatized xenoliths (from Tanzania: Rudnick et al., 1993; southern Australia: Yaxley et al., 1991; Sahara Basin: Dautria et al., 1992; Mongolia: Ionov et al., 1994), carbonatite metasomatized xenoliths with traces of old basaltic metasomatizm (from southern Patagonia: Gorring and Kay, 2000), and alkaline metasomatized (from La Palma, the Canary Islands, Neumann et al., 2000) (the symbols are as in Figure 28).

122
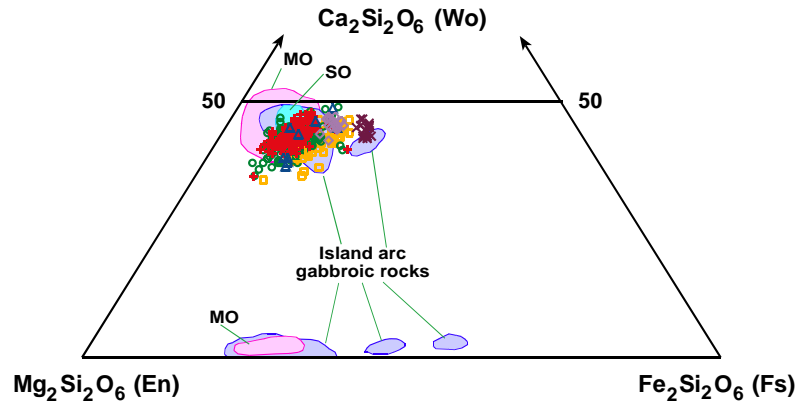
Figure 75. The comparison of the compositions of py from the Kurançalı rocks with those from well-defined island arc gabbros (fields from Burns, 1985) and those from island arc gabbros in Turkey (data for SO (Sarıkaraman Ophiolite) from Yalınız and Göncüoğlu (1999), and for MO (Mersin Ophiolite) from Parlak et al. (1996)) (the symbols are as in Figure 28).

contents of the studied py display a wide range from depleted to enriched values (Ti(pfu)*1000=0.37-35.93). This is not the usual case. Ti content of cpx reflects the degree of depletion of a mantle source and the Ti-activity of parent magma (Pearce and Norry, 1979). Very low Ti indicates that Ti is removed from cpx structure during one or several partial melting events. If the Ti content of cpx is lower than that of MOR cpx and increases slightly as differentiation of parent magma proceeds, it will indicate crystallization of cpx in Ti-poor magma (Pearce and Norry, 1979). The data for Ti content of the studied py is compared with those from MOR (Figure 78). Some of the data are comparable to those from MOR but lower values are also present as discussed in whole-rock data (in Section 5.5.1.). This may lead to consider that a depleted mantle source is affected by Ti-rich composition. Moreover, Cr content of py is much lower than that of cpx from MOR and low values of Cr for the studied py may again reflect a depleted mantle source. The covariation of Ti and Cr for py and their comparison with those in MOR and island arc environments (Figure 78) display a relation from plutonics in island arc environment rather than to plutonics from MOR (Figure 78).
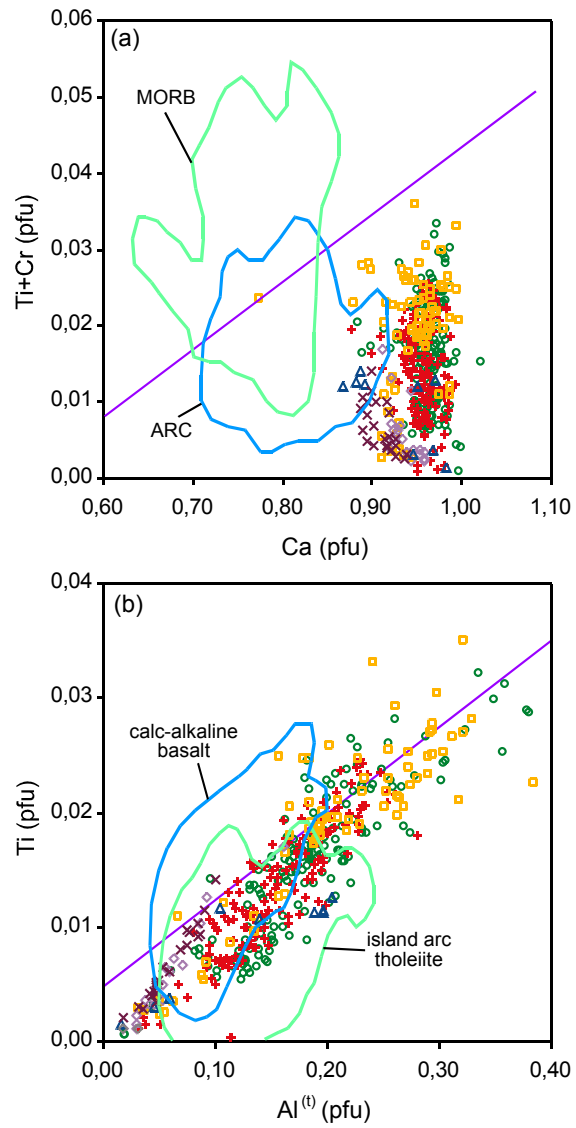
Figure 76. The place of the py data on the diagrams of; (a) Ti+Cr-Ca (pfu) and (b) Ti-Al$^{(t)}$ (pfu) (compositional fields from Leterrier et al., 1982) (the symbols are as in Figure 28).
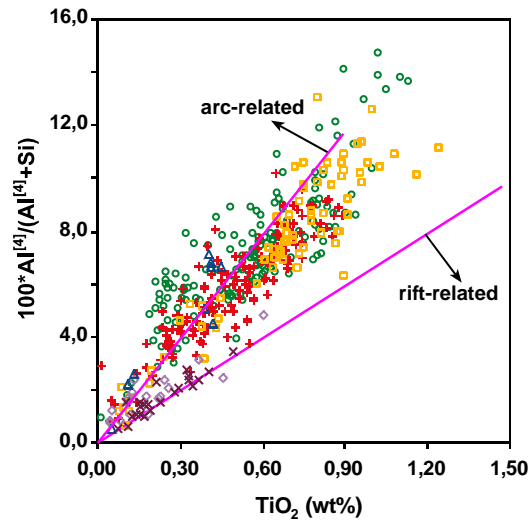
Figure 77. The relation of $100*Al^{[4]}/(Al^{[4]}+Si)$ (percentage Al occupied into the tetrahedral site) and TiO_2 (wt%) for py from the Kurançalı ultramafic-mafic rocks where the reference lines defining arc and rift-related gabbro are from Loucks (1990) (the symbols are as in Figure 28).
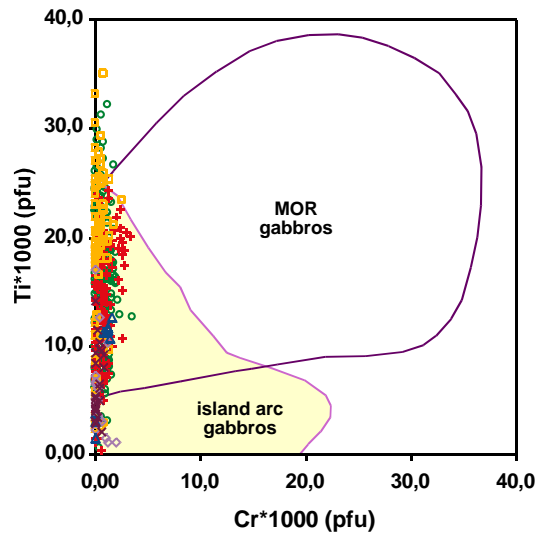
Figure 78. Covariation of Ti and Cr contents of the studied py and their comparison with cpx in gabbros from island arc and mid-ocean ridge (MOR) environments (island arc data from Troodos layered gabbro (Hébert and Laurent, 1990), layered gabbro of Wadi Haymiliah section of Semail ophiolite/Oman (Lachize et al., 1996), MOR data from compiled from Elthon et al. (1992)) (the symbols are as in Figure 28).

The covariation of maximum An (Ca/(Ca+Na)) content in plag and maximum Mg# of cpx are plotted for the rocks from the Kurançalı area in Figure 79. It is compared with tectonically well-defined gabbros. The data of the studied rocks plot within the field of arc gabbros despite few data outside of the field.

Based on the chemistry of py, the plutonic ultramafic-mafic rocks from the Kurançalı area seem to have originated in an island arc environment rather than MOR. This approach is also supported by comparison of the data with cpx compositions from ophiolitic rocks of different origins from various locations (Figure 80). However, Ti, Na, Al[(t)], Al[4] contents of py are higher than those from island arc related rocks. Enrichments in these elements may be due to a metasomatizing event affecting a depleted peridotitic mantle source.
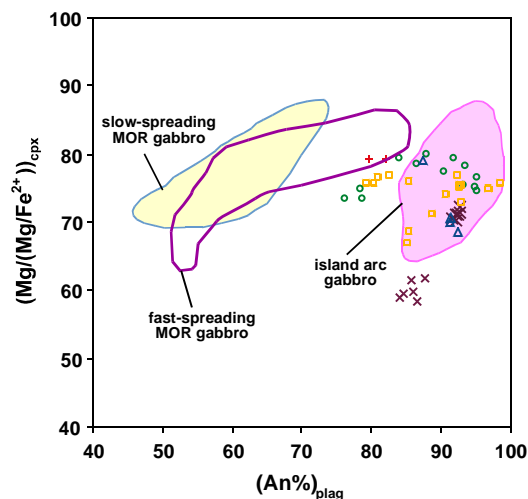
Figure 79. The covariation diagram of plag An content and cpx Mg#, and their comparison with gabbros from island arc, slow spreading MOR (fields from Burns, 1985) and fast spreading MOR (field from Coogan et al., 2002) (the symbols are as in Figure 28).
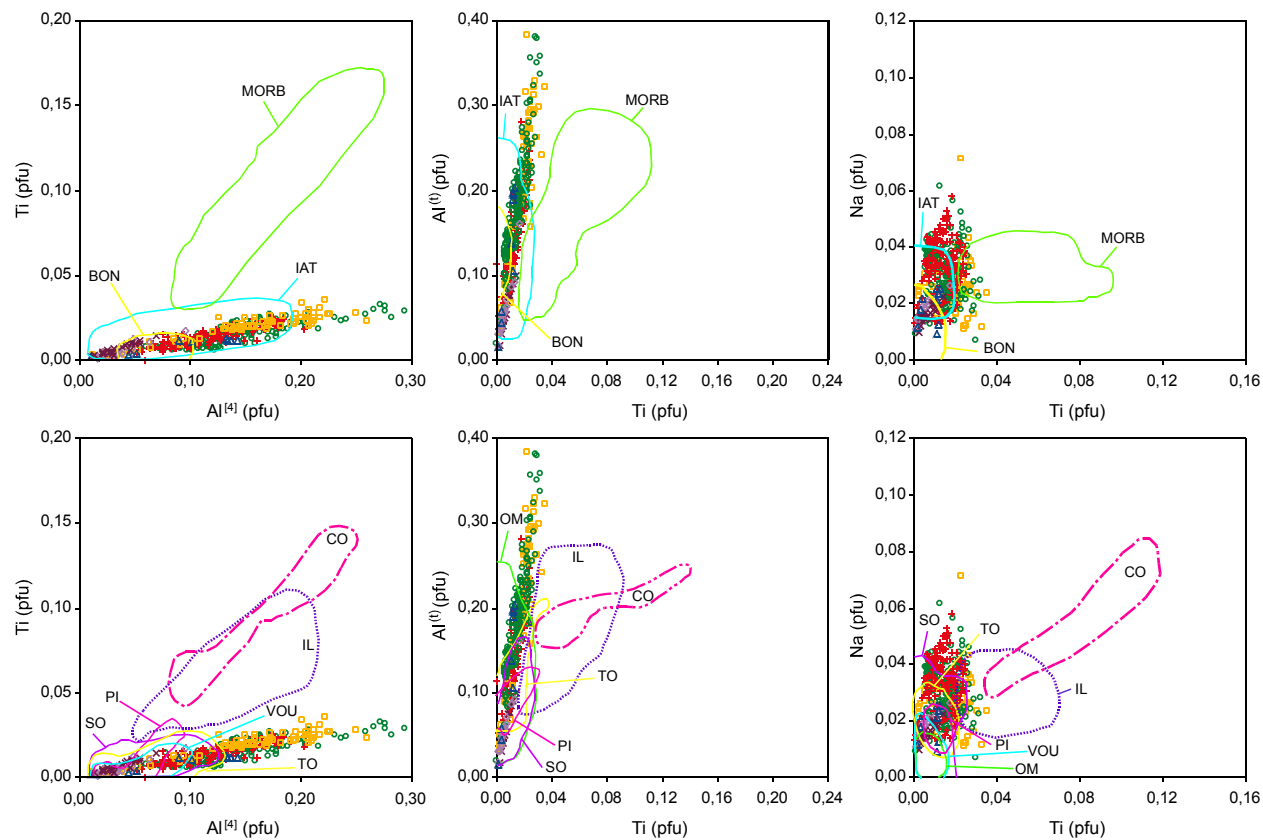
Figure 80. Covariation diagrams of the studied py and their comparisons with compositional fields of cpx from well-defined tectonic settings and well-known ophiolites (fields for tectonic settings (MORB: mid-ocean ridge basalt, BON: boninite, IAT: island arc tholeiite) and ophiolites (TO: Troodos, OM: Oman, VOU: Vourinos, CO: Corsica, IL: Interal Ligurian, PI: Pindos) from Beccaluva et al., 1989; and SO: Sarıkaraman Ophiolite from Yalınız and Göncüoğlu, 1999) (the symbols are as in Figure 28).

4.3.6. Geothermobarometry

There is no appropriate geothermobarometer for the present mineral assemblages. The following considerations shall help to estimate ranges that allow constraining and limiting pressure-temperature conditions.

Although no opx is present in the Kurançalı rocks, the two py-thermometer of Lindsley (1983), a graphical thermometer projected on Di- En-Fs-Hd quadrilateral, was used for py (di, au) to get minimum temperature since py is nearly pure (Wo+En+Fs > 98%) (Figure 81). Py data having Wo+En+Fs > 98%, Al_2O_3 > 8 wt% and enriched Ca content were eliminated considering the limitations given by Lindsley (1983). The qualitatively estimated temperature for the studied py ranges between 675 and 1150°C. However, the estimated values greater than 950°C resulted in meaningless outcomes in temperature dependent geobarometer of Nimis (1995, 1999), Nimis and Ulmer (1998), and only the range between 675 and 937°C with an average of 809±46°C in both ultramafic and mafic rocks gave meaningful pressure estimates as discussed below. However, the obtained range can be lower than the original temperature, due to uncertainties such as microscopically indefinable exsolution, incorrect calculation of Fe^{3+} and highly variable Al content. The obtained values represent minimum temperatures. According to Lindsley (1983) a single type of py, e.g cpx, gives a minimum temperature for the crystallization of a single py since at or below the temperature of saturation a second py would have formed.

Cpx geobarometry for magmatic rocks of a wide compositional range (Nimis, 1995, 1999; Nimis and Ulmer, 1998) was applied for py of the Kurançalı rocks. Py data with (Ca+Na) > 0.5 and Mg# > 0.7 have been used for pressure estimation as suggested by the authors. However, it requires an independent accurate temperature estimate and the temperature obtained by py-solvus geothermometry (Lindsley, 1983) gives only minimum values. Accepting them as minimum, they were used for pressure calculations using the CpxBar program by Nimis (with hydrous magma option) and a range of 5.83-16.45 kbar with an average of 11.38±1.72 kbar was obtained. These values will correspond to a maximum for the pressure estimate.

Underestimating temperature by 20°C causes an increase of 1 kbar for the calculated pressure.
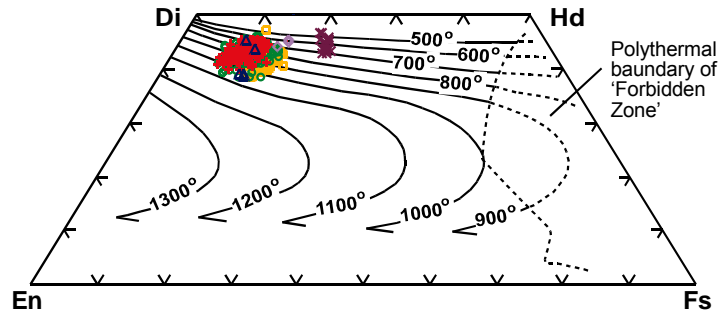
Figure 81. The comparison of the py data with isotherms prepared by Lindsley (1983) on the py quadrilateral to get qualitative temperature estimation at pressure of 5 kbar (the symbols are as in Figure 28).

A variety of mafic-ultramafic calc-alkaline rocks (ol-py-HBdites, cpx-hb-gabbros, hb-gabbros) from the Adamello batholith, having cpx and amph (parg) crystallizing earlier than plag, were interpreted to be polybaric with pressure and temperature ranges of 7-10 kbar at 1000-1050°C and 2-3 kbar at ~900°C (Nimis and Ulmer, 1998). The rocks from the Kurançalı area also include a high amount of pargasitic amph and even phl that crystallized before plag. Therefore, the approximations based on py chemisty for pressure and temperature seem to be useful with some limitations.

The covariation of Al[4] and Al[6] may also provide relative pressure estimates according to Aoki and Kushiro (1968) and Aoki and Shiba (1973) (Figure 82). The variation of Al[4] data against Al[6] for the studied py displays conditions of basalts with granulites and inclusions. They plot close to boundary to the field of igneous rocks and few of the data are in this field. Py with Al[6]/Al[4] < 1 (even < 0.5) suggests low pressure because Al favors to substitute into a tetrahedral site at relatively low pressures and high temperatures. Simonetti et al. (1996) also interpreted low Al[6] (<1 pfu) as an indicator of crystallization at shallow levels, i.e. at low pressure conditions.
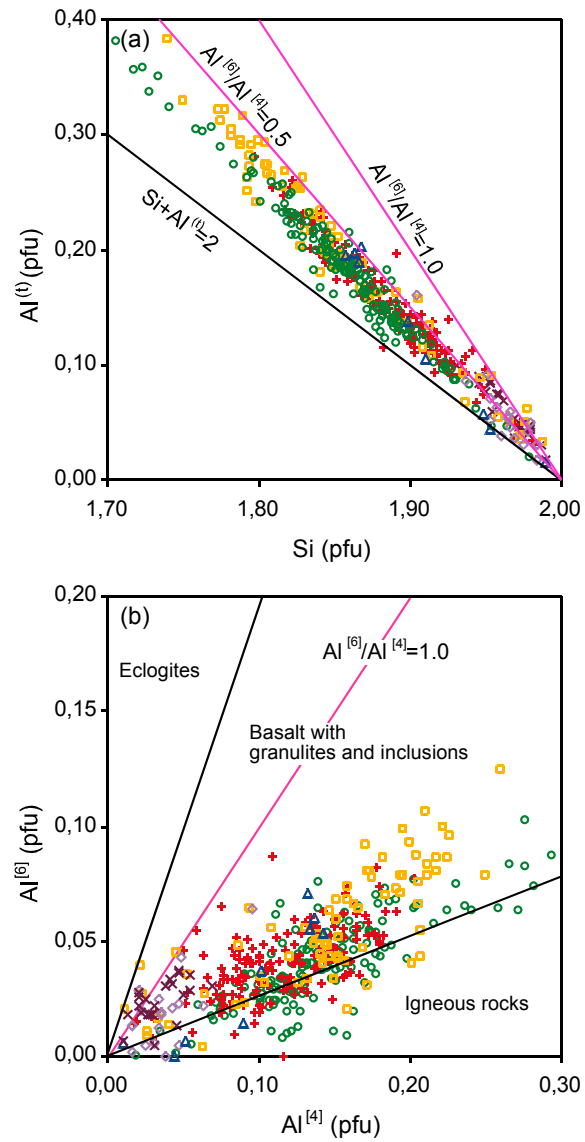
Figure 82. Covariation diagrams for Al$^{(t)}$-Si and Al$^{[6]}$-Al$^{[4]}$ for py of the Kurançalı rocks to estimate relative pressure based on the divisions after Aoki and Kushiro (1968), Aoki and Shiba (1973) (the symbols are as in Figure 28).

All py data display high-Ca cpx composition, even most of them are Ca-oversaturated based on the Morimoto's (1989) formulae for Wo-En-Fs % calculations. High-Ca cpx is defined to originate at shallow depths, i.e. low pressure by Litasov et al. (2000). The data for py are comparable to low pressure rocks with high Ca# from metasomatized subcontinental mantle material from East Siberia (data from Litasov et al., 2000). Despite the higher Ca#, the chemical data for the studied py showed that they have Mg# similar to those from the compared data. The comparison shows that few of the data plot in field of cpx from low pressure pyroxenites and granulites (<11 kbar) while most of the Ca# for the studied py, show higher values. This may suggest pressures even lower than 11 kbar for the formation of the rocks from the Kurançalı area (Figure 83).

The pressure-temperature estimates from py chemistry give just an approach for crystallization conditions rather than accurate values. This is actually due to absence of appropriate quantiative geothermometers. Moreover, cpx's that re-equilibrated after magmatic crystallization or melting during subsolidus processes are not suitable for geothermobarometric calculations.

4.4. Amphiboles

About 380 point analyses were performed on amph's of 19 specimens from all rock types except for amph free DIO. Measurements were taken on amph's with different textural characteristics including primary and late magmatic phases, and low grade metamorphic products.

4.4.1. Compositional Variations

The compositional ranges for primary and late magmatic phases are summarized below but the data of the alteration product amph are excluded in the ranges given.
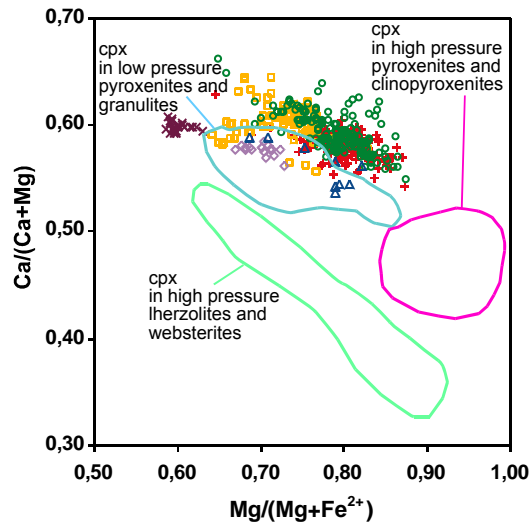
Figure 83. Pressure estimate for the studied py by comparing it with cpx whose formation pressure is well-defined (data from cpx in metasomatized subcontinental mantle beneath the Vitim volcanic field of East Siberia, Litasov et al. (2000) (the symbols are as in Figure 28).

The chemical data for magmatic amph, either primary or late, do not show significant compositional variation except for a single specimen of the fine-grained HBdite (Appendix D). The rocks having moderately high Mg# (0.47-0.76), in general, are divided into three groups based on slight variations; CPXnite, CPXnite WHMP and PHLtite are of group 1, HBdite is of group 2 and LG is of group 3. Amph's from group 1 are late magmatic phases (blebs, lamellae, rims on py crystals, interstitials between py crystals, and pseudomorph after py). Amph's from group 1 have compositional ranges between 38.27-41.60 (SiO_2 wt%), 12.93-16.31 (Al_2O_3 wt%), 0.96-2.61 (TiO_2 wt%), 13.17-19.69 ($FeO^{(t)}$ wt%), 7.76-11.93 (MgO wt%), 10.47-12.75 (CaO wt%), 1.27-2.88 (Na_2O wt%), 0.23-3.11 (K_2O wt%), 0.12-0.36 (MnO wt%). The Cr_2O_3 and NiO contents are very low, 0.00-0.12 and 0.00-0.08 wt%, respectively.

Primary amph from pegmatitic HBdite of group 2 shows similar Mg# values (0.48-0.63) with those of py. However, primary amph from fine-grained HBdite of group 2 has higher Mg# (0.72-0.76) from that in pegmatitic HBdites. As seen from the ranges for Mg#, the largest compositional difference between

fine- and coarse-grained HBdites are in MgO and FeO$^{(t)}$ (wt%) contents; FeO$^{(t)}$ (wt%) = 14.07-17.40 (for coarse-grained), 12.11-12.77 (for fine-grained), and MgO (wt%) = 8.02-11.42 (for coarse-grained), 12.58-13.08 (for fine-grained). Compositional ranges of other oxides are slightly wider than those in group 1 rocks. The compositional ranges are; 37.69-42.29 (SiO$_2$ wt%), 12.70-15.24 (Al$_2$O$_3$ wt%), 1.30-3.15 (TiO$_2$ wt%), 10.79-12.47 (CaO wt%), 1.53-2.42 (Na$_2$O wt%), 0.81-2.27 (K$_2$O wt%), 0.14-0.31 (MnO wt%). The Cr$_2$O$_3$ and NiO contents are very low, like those of amph in group 1 rocks.

Amph from LG of the last group have chemical compositions with narrower ranges but they are within the limits of those from the other rocks. The compositions of amph from LG are; 39.63-40.93 (SiO$_2$ wt%), 14.02-14.97 (Al$_2$O$_3$ wt%), 2.15-2.53 (TiO$_2$ wt%), 13.24-17.08 (FeO$^{(t)}$ wt%), 8.74-10.87 (MgO wt%), 11.89-12.10 (CaO wt%), 1.54-1.61 (Na$_2$O wt%), 1.64-1.94 (K$_2$O wt%), 0.21-0.25 (MnO wt%). The Cr$_2$O$_3$ and NiO contents are similar to those from the other rocks.

The studied amph's of both primary and late magmatic origins have high CaO, MgO and TiO$_2$ (>1.00 wt% except for one analyses) contents. TiO$_2$ saturation can be assumed on the base of Ti-phases, rt, ilm and sph.

The chemical changes are best inferred from covariation of elements (pfu) vs. Mg# (Figure 84). There is a compositional difference between amph in fine-grained HBdite and the rest of the rock types due to higher Mg# of amph in fine-grained HBdite. Si, Al$^{(t)}$, Mn, Ca contents of both high and low Mg# amph, in general, show compositional overlap (Figure 84a,b,c,h). Two groups of amph can be distinguished based on Ca content and this is slightly supported by Ti and Mg (Figure 84d,g,h). Some of the data from CPXnite, CPXnite WHMP, pegmatitic HBdite and all data from fine-grained HBdite show lower Ca content than the rest of the data. However, groups created by Ca content are not related to either texture, origin of amph or rock type. Mg content slightly supporting groups based on Ca, results in two parallel trends for Mg and Fe^{2+} contents that are very close to each other (Figure 84e,g). Amph's from CPXnite, CPXnite WHMP and HBdite are present in both trends. However, Fe^{3+} contents of amph's broadly correlate to Mg# (Figure 84f). Na
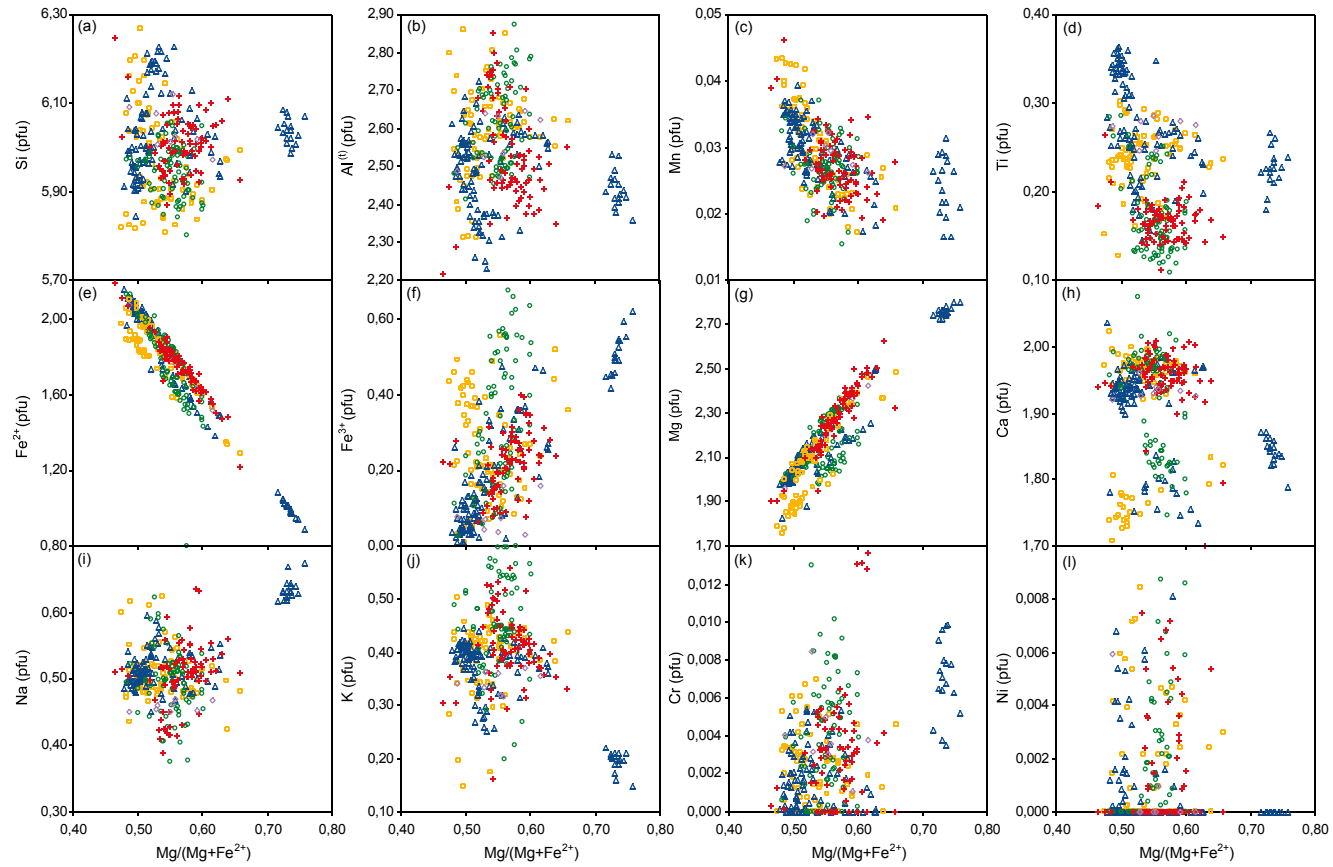
Figure 84. Covariation diagrams of major and minor element compositions for amph's of magmatic origin from ultramafic rocks and LG (the symbols are as in Figure 28).

134

contents of fined grained HBdite are relatively higher than those of other rocks (Figure 84i) while K contents of fine-grained HBdite are lower than those of others in a similar manner to Ca (Figure 84j). K contents of amph from CPXnite and PHLtite are relatively higher than those of other rocks. The most obvious difference among rock types is in their Ti contents (Figure 84d) that are lowest for patchy amph's of CPXnite and PHLtite and some of CPXnite WHMP. Pseudomorph amph crystals from CPXnite WHMP and also some of CPXnite display rather higher Ti contents overlapping the field of primary phases from pegmatitic HBdite. Cr and Ni contents display similar ranges for the all rock types. The elemental ranges for amph from LG, always overlap the field of others.

4.4.2. Nomenclature and Substitution Mechanisms

The formula for amph's was calculated on the basis of 23 oxygen assuming (OH^-, Cl^-, F^-) equal 2, since H_2O and halogen contents are uncertain from the measurements. The biggest uncertainty in formulation of amph is due to lack of H_2O data and measurement of iron as $FeO^{(t)}$. Moreover, amph's have no either fixed cation total or fixed cationic charge (due to variable OH content), and thus there is no simple method to calculate ferric and ferrous iron from $FeO^{(t)}$ and to prepare formula. The crystal-chemical constraints may provide limits on the possible range of Fe^{3+} and Fe^{2+} contents. Leake et al. (1978) (IMA) proposed that subtotals of cations might provide the most appropriate estimates for Fe^{3+} and Fe^{2+} depending on the type of amph such as calcic, sodic-calcic, sodic, and Mg-Fe-Mn-Li amph's. The stoichiometric value of any of these subtotals results in maximum or minimum estimate of Fe^{3+}. Since the studied amph's are of calcic type after the petrographic observations, the formulae were recalculated on the basis of 13eCNK subtotals (cation subtotal through Si, Al, Cr, Ti, Fe, Mg, Mn), and then Fe^{3+} contents were calculated using the method of Droop (1987) which resulted in the maximum values.

Assignments of cations and nomenclature of amph's were done according to the current IMA recommendations (Leake et al., 1997). The classification is based on the standard amph formula, $A\ B_2^{[6]}\ C_5^{[6]}\ T_8\ O_{22}\ (OH)_2$,

in which site allocations are suggested as following; T is filled by Si, Al, then Ti (sum to 8); C is filled by Al, Ti (resting after that used in T site) and then Cr, Fe^{3+}, Mn, Mg, Fe^{2+}, Mn (sum to 5); B is filled by Mg, Fe^{2+}, Mn (resting after that used in C) and then Ca, Na (sum to 2); A is filled by Na (resting after that used in C) and all K (sum to 1). According to the given site allocations, the range of the average structural formula for the primary and late phase magmatic amph of ultramafic and mafic rocks is following:

$$(()_{0.01-0.44}Na_{0.19-0.84}K_{0.00-0.60})^{[A]}(Ca_{1.69-2.08}Na_{0.00-0.31})^{[B]}(Mg_{1.76-2.63}Fe^{2+}_{1.22-2.19}Al_{0.36-0.87}$$
$$Fe^{3+}_{0.01-0.80}Ti_{0.11-0.36}Mn_{0.02-0.05}Cr_{0.00-0.01})^{[6]}(Si_{5.80-6.27}Al_{1.73-2.20})^{[4]}O_{22}(OH)_2$$
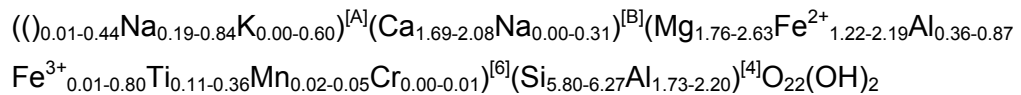
In the terminology of Leake et al. (1997), all the studied amphs of magmatic origin are members of calcic amph group, with Ca ranging from 1.69 to 2.08 and Na_B from 0.00 to 0.31 (pfu). A majority of them is parg and a few are ferro-parg excluding amph of the fine-grained HBdite (Figure 85a). The transitional compositions from parg to Fe-parg may result from either inaccurate Fe^{3+} and Fe^{2+} estimations from $FeO^{(t)}$ or high iron-oxidation at surface. Amph of fine-grained HBdite is of calcic type as well, but it is magnesio-hs in composition. Amph having low grade metamorphic origin is a member of calcic group, namely act (Figure 85b).

Amph compositions vary along several vectors, among which the parg'tic composition is a linear combination of end members namely ed and 0.5 ts (ed: $NaCa_2Mg_5(Si_7Al)O_{22}(OH)_2$ and ts: $()^{[A]}Ca_2Mg_3Al_2(Si_6Al_2)O_{22}(OH)_2)$. Moreover, the hs'tic composition is equivalents of hb and gl end members in which Fe^{3+} replaces $Al^{[6]}$ (hb is eqivalent of 0.5 ts, and gl: $()^{[A]}Na_2Mg_3Al_2Si_8O_{22}(OH)_2)$. The substitutions of Na, K in A-site, and $Al^{[6]}$, Fe^{3+}, Ti in the octahedral sites, which are compensated by substitution of Al for Si in the tetrahedral sites, is shown with a mechanism $Al^{[4]} \Leftrightarrow (Na+K)^{[A]}+(Al+Fe^{3+}+2Ti)^{[6]}$ by Robinson et al. (1971) (Figure 86a). The resulting good 1:1 relation indicates that the studied amph's are dominated by a combination of ed, parg, hb and hs substitutions, together with their titanian equivalents according to the interpretation of Blundy and Holland (1990). Moreover, the strength of the correlation confirms that the substitutions which accomodate Fe^{3+}, $Al^{[6]}$ or $Na^{[A]}$ via $Na^{[B]}$ (such as rb, gl, or
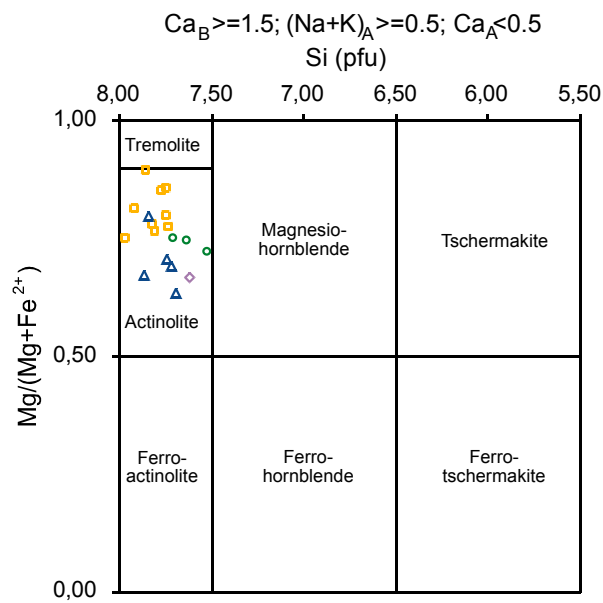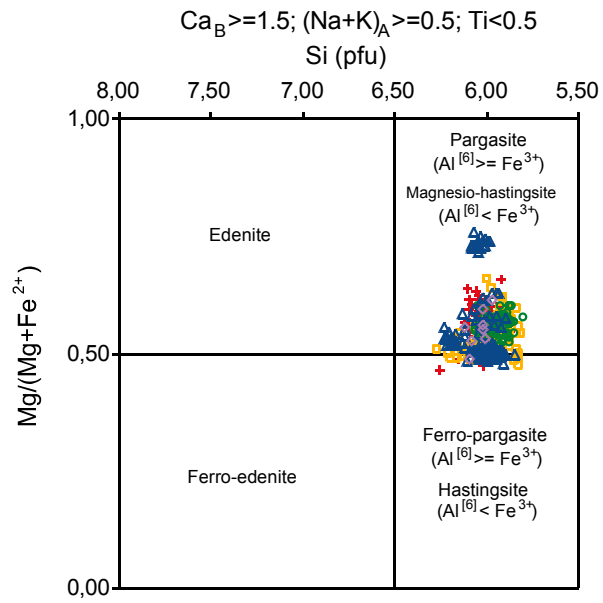
Figure 85. Plots of amph's on nomenclature diagram of calcic amph after Leake et al. (1997) (the symbols are as in Figure 28).
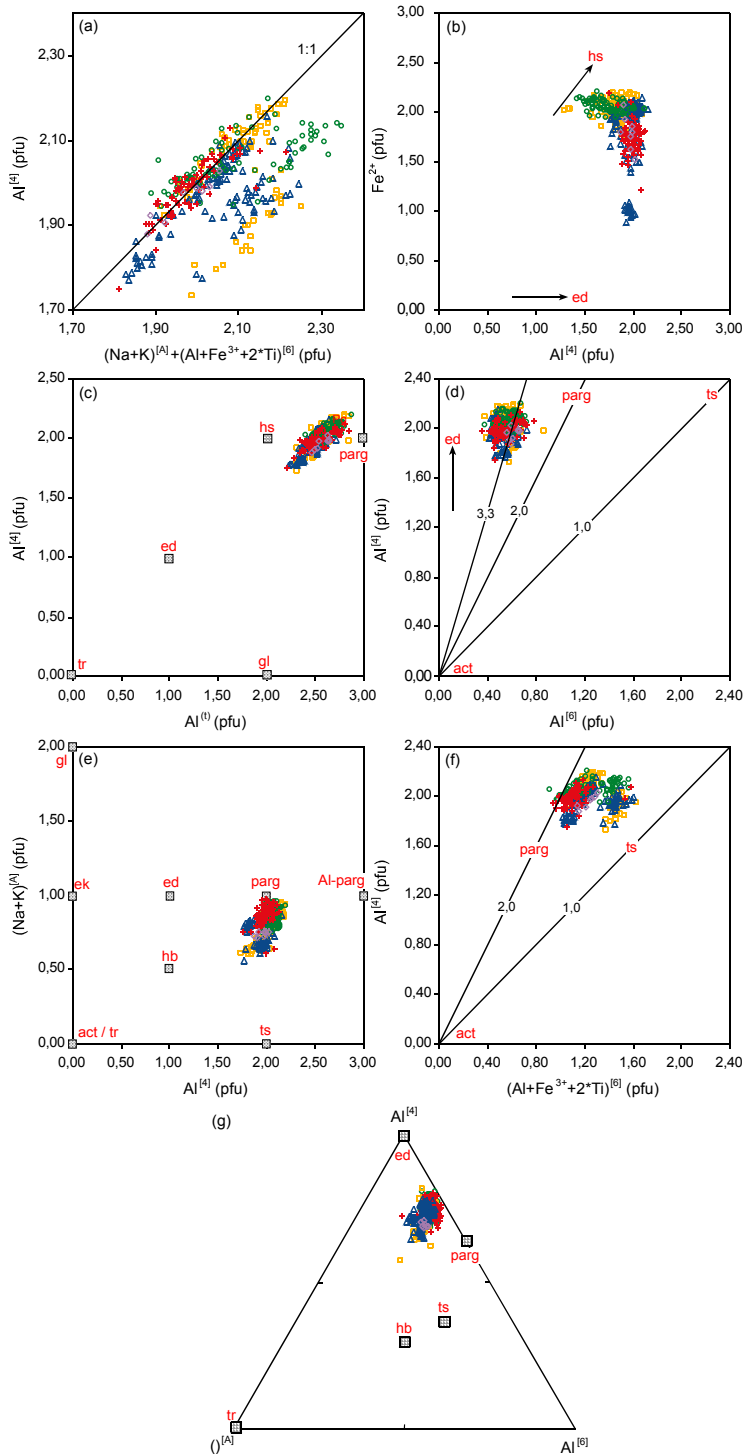
Figure 86. The plots of chemical data on several covariation diagrams and a triangular diagram showing relations of different amph components. The positions and trends of components are from Hammarstrom and Zen (1986) for (c), Fleet and Barnett (1978) for (d), Searle and Malpas (1982) for (e), Liogys and Jenkins (2000) for (f), and Blundy and Holland (1990) for (g) (the symbols are as in Figure 28).

138

rc) have no influence on the chemistry of these amph's (Blundy and Holland, 1990). The proposed substitutions are also clearly shown in various covariation diagrams and a triangular diagram (Figure 86b-g). The relation of Fe^{2+} substitution in the octahedral site to $Al^{[4]}$ substitution in the tetrahedral site display ed and hs'tic exchange compositions (Figure 86b). The plots of amph data on the $Al^{[4]}$-$Al^{(t)}$ covariation diagram lie in an area of hs-ed-parg triangle join (Figure 86c). The data just plot between ed and parg end members on the $Al^{[4]}$-$Al^{[6]}$ diagram showing the relations of ed, parg, ts and act compositions (Figure 86d). On covariation diagram of $(Na+K)^{[A]}$ and $Al^{[4]}$, amph data concentrate on parg side of parg-ts and/or parg-act/tr joins with slight inclination towards Al-parg (Figure 86e) which shows ts component of the studied amph's and inclination shows ed'tic substitution. The ts component of the parg'tic amph is also clearly observed from relation of $Al^{[4]}$ to $(Al+Fe^{2+}+2Ti)^{[6]}$ (Figure 86f). Compositional variation of amph's on $Al^{[4]}$-$()^{[A]}$-$Al^{[6]}$ triangular diagram is bounded by the ed-parg-hb-ts quadrilateral and the predominant variation is parallel to parg-ts join (Figure 86g).

The following substitution mechanisms, either simple or coupled, support the identified types for the studied amph's which are of magmatic origin; Fe^{2+} ⇔ Mg, Mn ⇔ Mg, $Si^{[4]}+Mg^{[6]}$ ⇔ $Al^{[4]}+Al^{[6]}$ (Al-ts), $2Si^{[4]}+Mg^{[6]}$ ⇔ $2Al^{[4]}+Ti^{[6]}$ (Ti-ts), $Si^{[4]}+Mg^{[6]}$ ⇔ $Al^{[4]}+(Fe^{3+})^{[6]}$ (Fe^{3+}-ts), $Si^{[4]}+()^{[A]}$ ⇔ $Al^{[4]}+(Na+K)^{[A]}$ (ed), $2Si^{[4]}+Mg^{[6]}+()^{[A]}$ ⇔ $2Al^{[4]}+Al^{[6]}+Na^{[A]}$ (parg) (Figure 87). Al-ts, Ti-ts, ed and parg substitutions are strong but Fe^{3+}-ts substitution is rather weak. ts-exchange is a feature of calc-alkaline magmas (Hollister et al., 1987).

4.4.3. Elemental Variations within Single Crystal

Measurements across an amph crystal in contact with cpx and plag from CPXnite WHMP display compositional variation (Figure 88). Si and Fe^{3+} contents decrease from rim coexisting with cpx to rim coexisting with plag. The decrease in Si content is regular while the decrease of Fe^{3+} is sudden from rim with cpx to core, and then it slightly decreases from core to rim with plag. Ca profile is just reverse of Fe^{3+} profile where Ca is low at rim with cpx and suddenly increases towards other rim with plag. Mg of amph shows slightly increasing pattern from rim with cpx to core and it show sudden decrease at
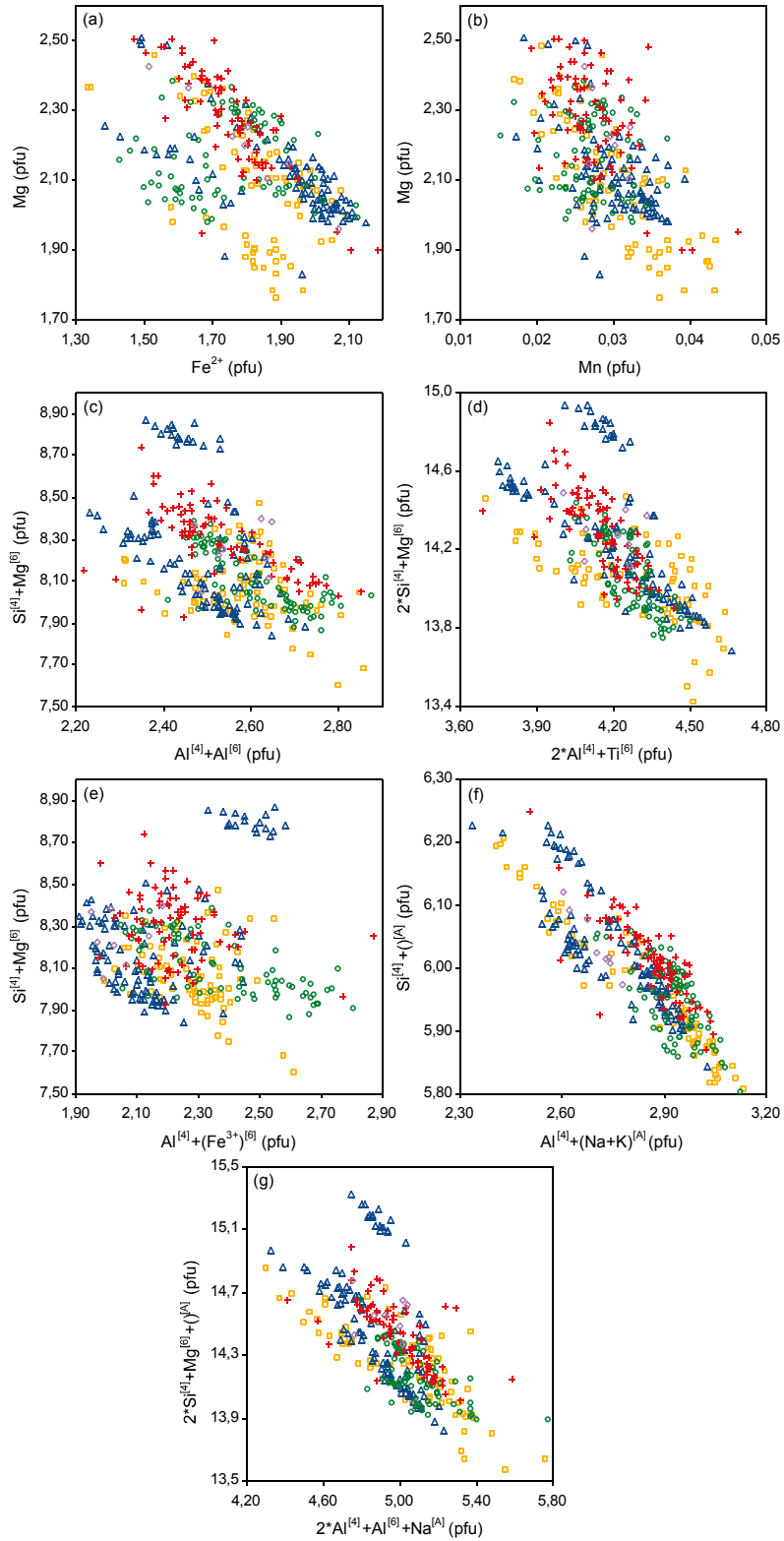
Figure 87. The substitution mechanisms defining ts, ed and parg components in the amph chemistry (the symbols are as in Figure 28).

140
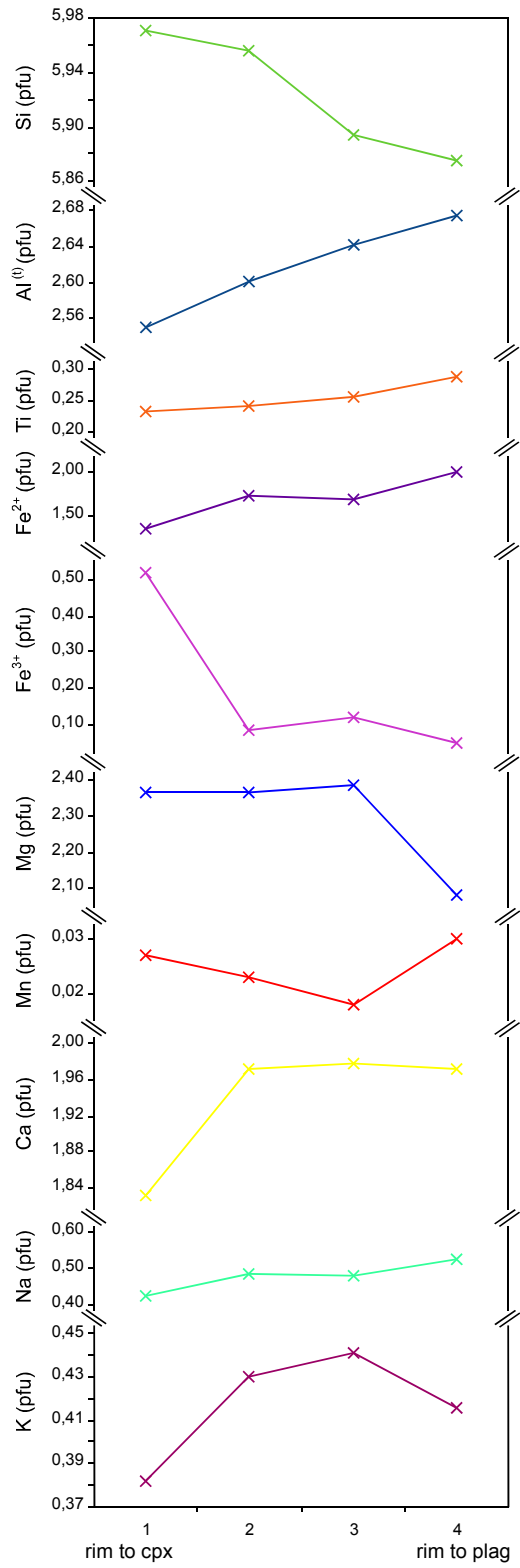
Figure 88. Chemical variation across an amph crystal in contact with plag at one side and cpx at other side.

rim with plag. The profile for Mn is reverse of that for Mg which can be explained by substitution of Mn for Mg. $Al^{(t)}$, Ti, Fe^{2+} and Na contents slightly increases from rim with cpx to rim with plag. K content of the crystal, which is lowest at rim with cpx, is high at core and then decreases again at rim with plagioclase.

4.4.4. Compositional Relation of Amphibole to Coexisting Clinopyroxene

Average Mg# values of amph's, either intersititial / bleb amph's or pseudomorphs after cpx / primary amph's, are compared with those of py in the same sample (Figure 89). A good correlation between the Mg# values of these two minerals is obvious. This may suggest buffering of the Mg/Fe of amph by the cumulate mineral, cpx (Coogan et al., 2001a).
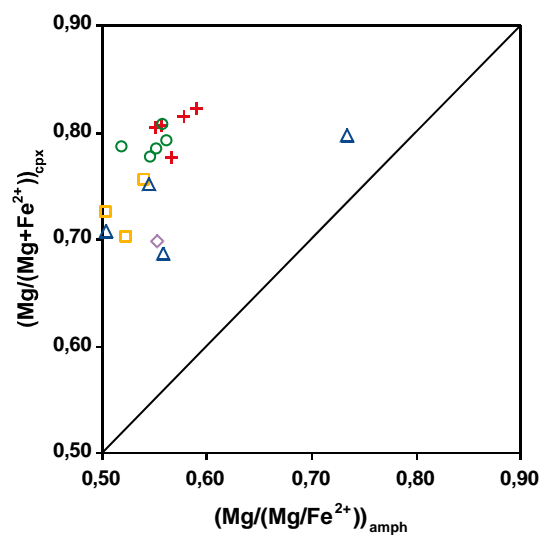
Figure 89. Comparison of the average Mg# values of cpx and amph in the same samples (the symbols are as in Figure 28).

4.4.5. Compositional Relation of Amphibole to Host Rocks

The change in $Fe^{(t)}\#$ of parg'tic amph's with increasing $Fe^{(t)}\#$ of host rock is limited or negligible where the biggest difference is of hs'tic amph of the fine-grained HBdite (Figure 90a). parg'tic amph found as blebs and interstitials from CPXnite and PHLtite deviates from 1:1 slope towards lower $Fe^{(t)}\#$ of host rocks and slightly lower $Fe^{(t)}\#$ of amph. However, pseudomorp of cpx and primary amph from CPXnite WHMP and HBdite, respectively, have slighly higher $Fe^{(t)}\#$ than bleb and intersititial amph's that are considered to be late phase amph's. Host rocks of these primary amph and pseudomorphs have much higher $Fe^{(t)}\#$ than the others. Similar to increasing $Fe^{(t)}\#$ of micas with incrasing $Fe^{(t)}\#$ of its host rock, $Fe^{(t)}\#$ values of amph's also increases with increasing $Fe^{(t)}\#$'s of their host rocks. But the increase for amph's is limited. Moreover, $Fe^{(t)}\#$ for amph's display slight to negligible decrease with increasing SiO_2 of host rocks (Figure 90b). The negligible change in $Fe^{(t)}\#$ of amph's with increasing $Fe^{(t)}\#$ and SiO_2 contents of host rocks may indicate absence of progressive magmatic oxidation or variation in oxidation state. This is also supported by positive correlation of $Fe^{2+}/(Fe^{2+}+Fe^{3+})$ values for amph and the host rocks (Figure 90c). Data scatter due to the uncertainity introduced by the calculation of Fe^{3+}.

4.4.6. Implications for Petrology

The chemical data for amph's having variable textural relations, either in forms of bleb, lamellae, intestitial or psedumorphs after cpx or fine-grained to pegmatitic primary crystals, show similar compositions. Amph's either primary or late phase in origin show extensive replacement of Si by $Al^{[4]}$ (Si = 5.80-6.27 pfu), and have relatively high $Al^{[6]}$ (0.36-0.87 pfu). The studied amph's, which are Si-depleted, have higher $Al^{[4]}$ contents than those of any amph in plutonic rocks from continental margins, island arcs, Troodos type intrusives, oceanic cumulates from MOR (Figure 91a). Amph's, having also high Na+K contents, are most comparable to those generated in an island arc environment from Lesser Antilles. Ti content amph's also supports the close similarity to amph's from Lesser Antilles (Figure 91b).
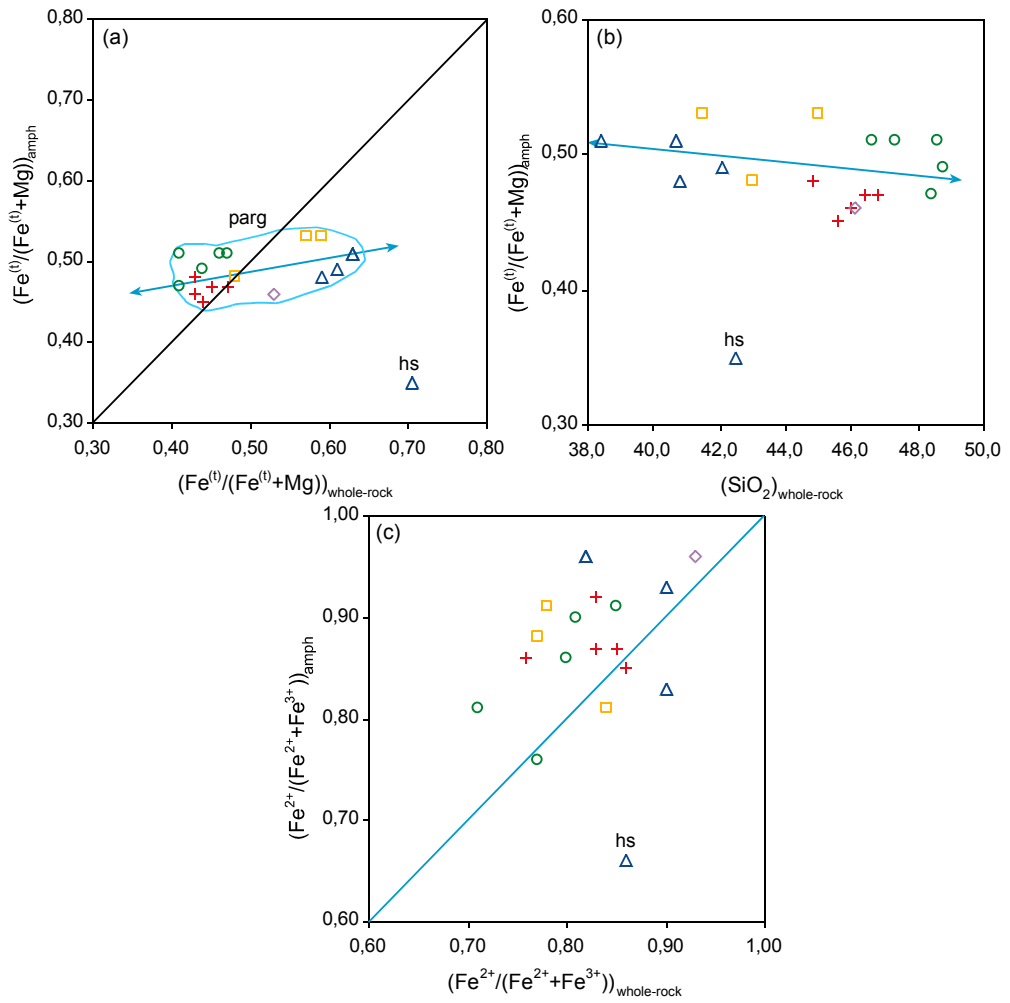
Figure 90. (a) Comparison of the average $Fe^{(t)}\#$ values of amph's and their host rocks, (b) the change in $Fe^{(t)}\#$ of amph's with changing SiO_2 (wt%) of host rocks, and (c) comparison of $Fe^{2+}/(Fe^{2+}+Fe^{3+})$ values of amph's with those of host rocks (the symbols are as in Figure 28).

144
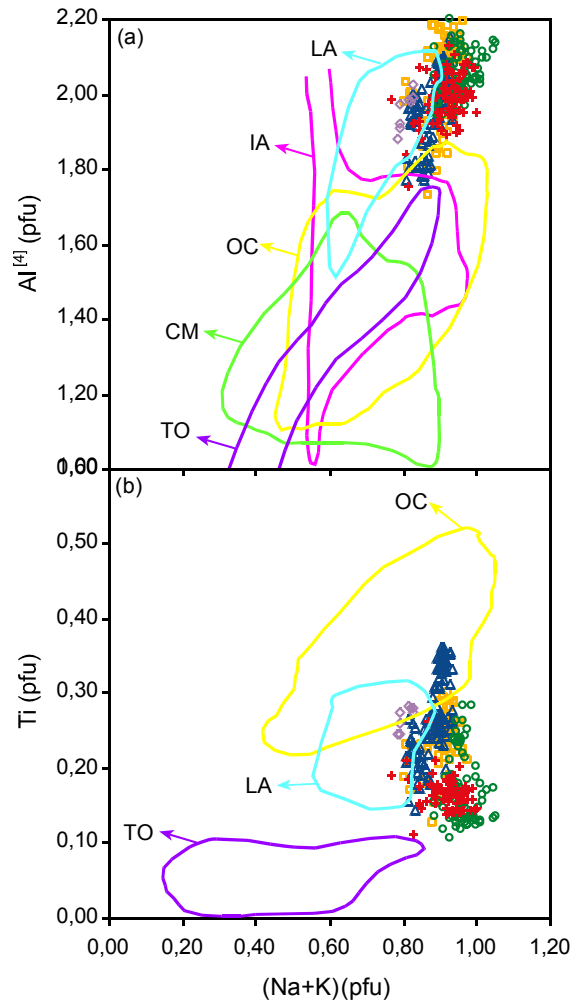
Figure 91. Al[4]-(Na+K) (pfu) (a), and Ti-(Na+K) (pfu) (b) relations for the studied amph's and their comparisons with amph's from Troodos ophiolites and oceanic cumulates (TO and OC, respectively: Hébert and Laurent, 1990), continental margins and island arcs (CM, IA, respectively: Jakes and White, 1972) and Lesser Antilles (LA: Arculus and Wills, 1980) (data compiled from Hébert and Laurent, 1990) (the symbols are as in Figure 28).

The Al[4] contents of amph's, which are quite higher than those found in gabbros of MOR, are similar to those from metasomatized oceanic gabbro xenoliths and alkaline gabbros from the Canary Islands (data from Neumann et al., 2000) (Figure 92a). Ti contents of amph's are lower than those from alkaline gabbros but they are within the range of alkaline metasomatized oceanic gabbro xenoliths. Thus the high Al[4] and intermediate Ti contents of amph's from ultramafic rocks may infer metasomatism. This idea is supported by high (Na+K) (Figure 91). As seen in Figure 92b, amph's are oversaturated in K_2O relative to those from the Canary Islands (either metasomatized gabbroic xenoliths or alkaline gabbros) and Mid-Atlantic Ridge. K_2O contents of the bleb and intersititial amph's from CPXnite and PHLtite are higher than those from pseudomorphic and primary amph's from CPXnite WHMP, LG and HBdite. This may suggest that amph's found as bleb and intersititial forms in py and mica and between cpx crystals, respectively, from CPXnite and PHLtite are late magmatic phases. In general, an effect of Al-Na-K enriched liquid on the system may be suggested as a metasomatizing event.

The chemical data for amph's are also compared with those from alkaline rocks (lamproite, kimberlite and melilitite) (Figure 93). Even though they are enriched in Al, Na, K, Ti relative to other rocks, their compositions are absolutely different from amph's of the alkaline rocks having much higher Ti, Na, Na/K and lower Fe contents.

Intersititial amph's and amph blebs, having similar major element compositions to pseudomorphs after cpx and primary crystals, display slightly lower TiO_2 and slightly higher Al_2O_3 contents (Figure 94). All amph types have lower SiO_2 and higher Al_2O_3 than interstitial amph's and amph blebs in gabbros from Mid-Atlantic Ridge which are defined to be magmatic amph formed during metasomatism by an evolved hydrous silicate melt (data from Coogan et al., 2001a).

The data for amph's are also compared with amph's in equilibrium with magma compositions ranging from hydrous low Mg - high Al basalt to rhyolite (Figure 95). This comparison may give an idea about what kind of magma composition is in equilibrium with the studied amph's. All amph data have
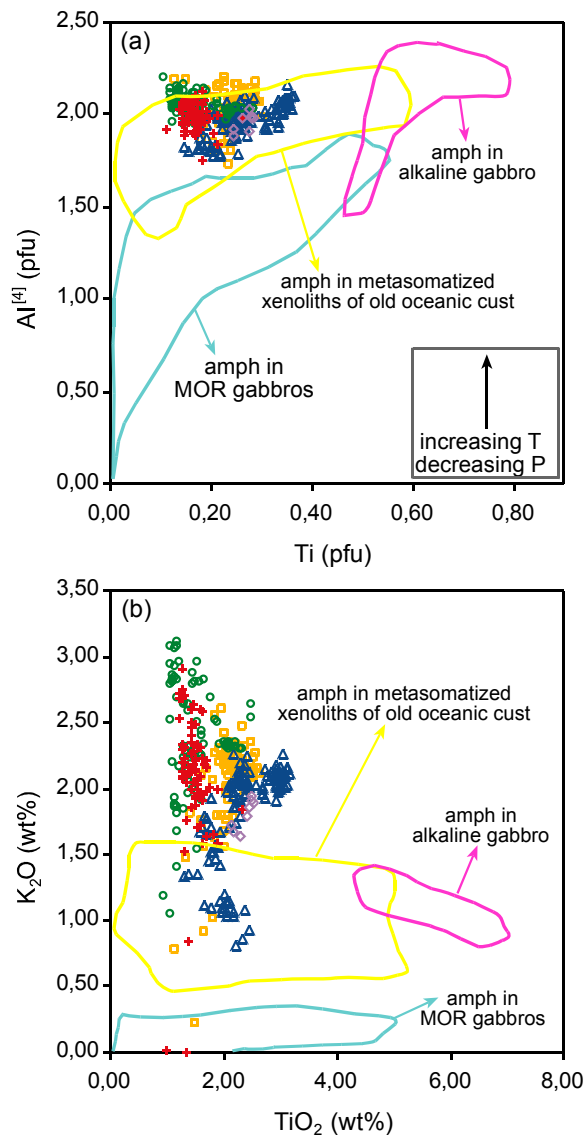
Figure 92. Al[4]-Ti (pfu) (a), and K$_2$O-TiO$_2$ (wt%) (b) relations for the studied amph's and their comparisons with amph's in metasomatized old oceanic crustal xenoliths and alkaline gabbro from the Canary Islands (Neumann et al., 2000), and in gabbroic rocks from the Mid-Atlantic Ridge (Cannat et al., 1997; Gaggero and Cortesogno, 1997) (the symbols are as in Figure 28).
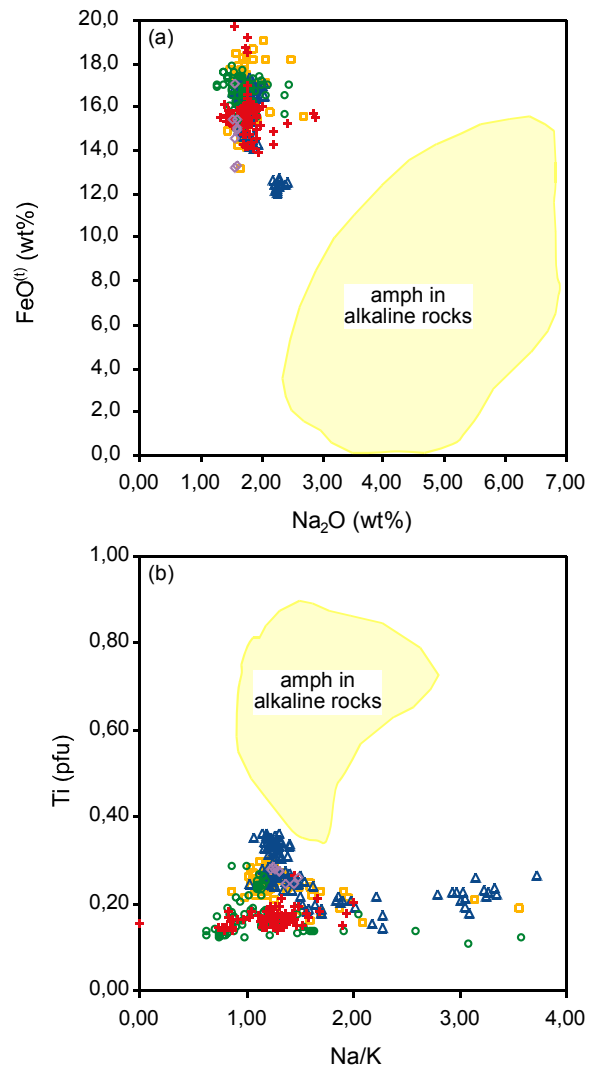
Figure 93. (a) FeO$^{(t)}$-Na$_2$O (wt%) covariation, and (b) Ti-Na/K covariation for the amph's and their comparisons with those from alkaline rocks (lamproite, kimberlite and melilitite) (data from Mitchell and Bergman, 1991) (symbol are as in Figure 28).
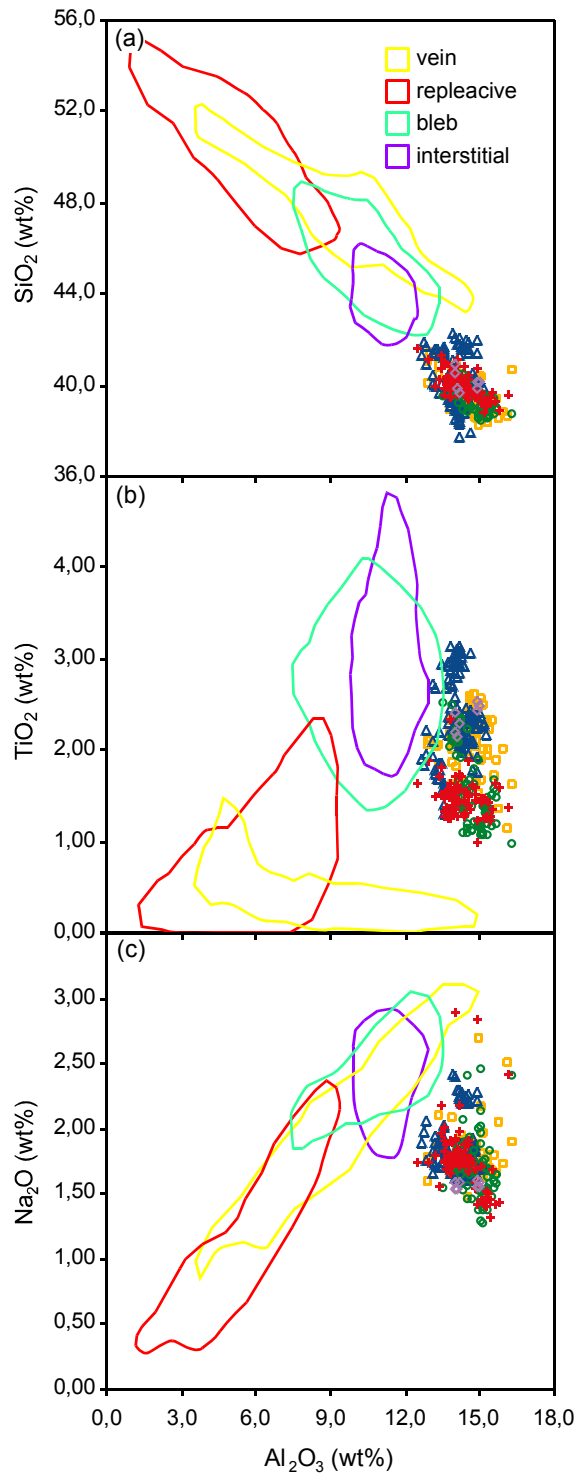
Figure 94. Major element covariation plots of the studied amph's and their comparisons with amph's from metasomatized crystal mush by an evolved hydrous silicate melt from Mid-Atlantic Ridge (data from Coogan et al., 2001) (the symbols are as in Figure 28).
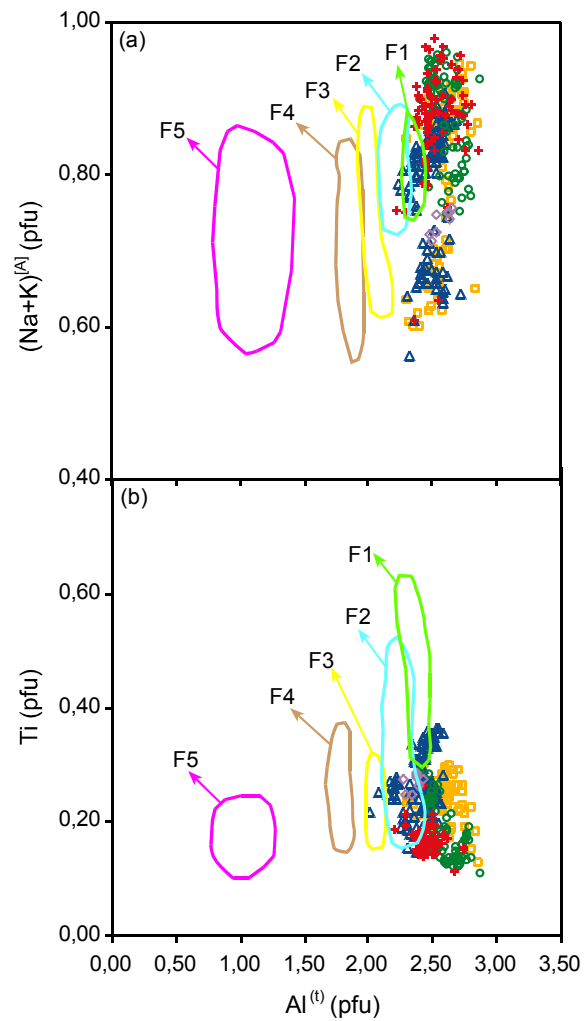
Figure 95. Covariations of (Na+K)[A] (a) and Ti (b) against Al(t) for all amph's except for low grade metamorphic amph's and their comparisons with melts from felsic to mafic in composition. Fields representing the melt compositions, from either volcanic rocks or experimental studies at low to moderate pressure (2-5 kbars), were compiled from Gillis and Meyer (2001) where F1: hydrous low Mg - high Al basalt, basaltic andesite; F2: andesite; F3: dacite; F4: rhyodacite; F5: rhyolite (the symbols are as in Figure 28).

150

higher Al(t) than any of amph's from different magma compositions. Oversaturation in Al(t) content may be inferred from low SiO_2 activity. Their compositions seem to be more appropriate of amph's in equilibrium with hydrous basalts / basaltic andesite, and andesite (fields F1 and F2, respectively in Figure 95) in terms of Al(t) content. In spite of their high Al(t) content, they also show similarity to amph's from felsic melts in terms of Ti content and wide range of Na+K in A site (fields F3 and F4 in Figure 95). From these compositional comparisons, it is supposed that history of the Kurançalı system is complex and it is affected by more than one compositional event.

4.4.7. Geothermobarometry

The total Al content of amph is a function of both temperature and pressure (Spear, 1981; Hammarstrom and Zen, 1986; Blundy and Holland; 1990; Holland and Blundy, 1994; Anderson and Smith, 1995). The studies (Johnson and Rutherford, 1989; Schmidt, 1992; Ague and Brandon, 1996) strongly suggest that pressure sensitive change in amph Al content is due to ts substitution, i.e. the higher pressure, the higher the Al content in amph structure. Moreover, increase of temperature promote ed substitution enriching amph in Al[6] but not in Al[4] (Holland and Blundy, 1994; Anderson and Smith, 1995).

Quantitative pressure estimate from Al in amph is not possible due to inappropriate mineral assemblages. Thus, qualitative estimate was carried out using covariation of Al[4] and Al[6] (pfu) values of the studied amph's (Figure 96) because Al[6] in amph structure increase with increasing pressure (Fleet and Barnett, 1978). Fleet and Barnett (1978) proposed that Al[4]/Al[6]=2.0 ratio approximates the 5 kbar boundary of Raase (1974). All the chemical data displaying Al[4]/Al[6] ≅ 3.3 may infer pressure of crystallization less than 5 kbars.

Many of the substitutions are controlled by equilibrium with other phases in the assemblage, and some of these may be sufficiently temperature and/or pressure sensitive to be of practical use in thermobarometry. Amph bearing assemblages are suitable for application of amph-plag thermometers of Holland and Blundy (1994) that was expressed as an appropriate method for

calculating amph formation temperatures in oceanic gabbros by Manning et al. (2000) and Coogan et al. (2001a).
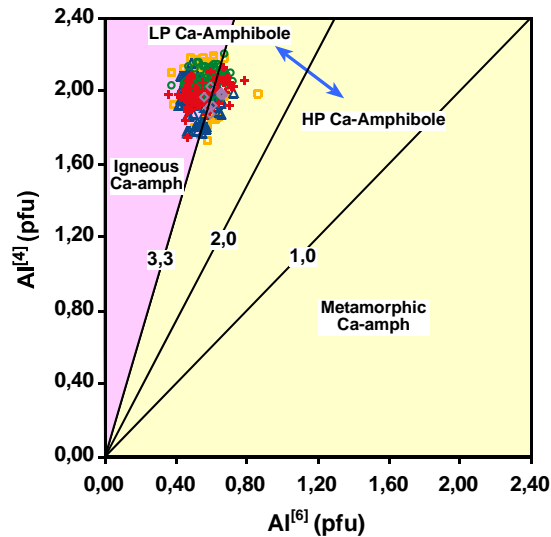
Figure 96. Covariation of Al[4] and Al[6] contents (pfu) in the structure of amph's. The Al[4]/Al[6] ratios and field divisions are from Fleet and Barnett (1978) (the symbols are as in Figure 28).

The ed-rc thermometer of Holland and Blundy (1994) was used to calculate equilibration temperatures from amph-plag pairs which is based on Al[4] content of amph and coexisting plag in both silica saturated and undersaturated rocks. This thermometer works efficiently only when the plag in assemblage has An_{10-90} and amph contains Si in the range 6.0-7.7 pfu, $X^{[B]}_{Na}>0.03$ and Al[6]<1.8. The thermometer, being thought to be useful for a temperature range of 500-900°C (±40°C) is pressure dependent (Holland and Blundy, 1994). Since pressure calculation is not available for the rock assemblage, temperature was separately calculated at pressures of 0, 5, 10 and 15 kbar. The temperatures for each type of amph's in the studied rocks are quite consistent at applied pressures that are 828±55°C at P=0 kbar, 865±66°C at P=5 kbar, 911±70°C at P=10 kbar, and 956±75°C at P=15 kbar. Whatever pressure is assumed, amph-plag equilibration temperature is higher

than 825°C that may indicate magmatic or metasomatic origin of amph's rather than hydrothermal origin.

Pressure independent temperature calculations, which were made using the formulae of Colombi (1989), result in temperatures of 844±49°C. The obtained average temperature, based on Ti content (increasing with raising temperature), is intermediate between the average temperatures obtained at pressures of 0 and 5 kbars using the thermometer of Holland and Blundy (1994).

Pressure-temperature (P-T) conditions of the magmatic amph crystallization were also estimated using semi-quantitative geothermobarometer of Ernst and Liu (1998) that is based on isopleths of Al_2O_3 (P-T dependent) and TiO_2 (T-dependent) (wt%) (Figure 97). Semi-quantitatively estimated temperature range (~750-925°C) for amph is consistent with that obtained by the other methods. Moreover, this is consistent with Ernst and Liu (1998)'s interpretation indicating that parg'tic amph forms at 800-950°C. However, estimated pressure range (~8,5-18 kbar) is higher than that estimated by other methods. The overestimation for pressure of amph crystallization is most probably due to exsolution of TiO_2 from amph to form Ti-phases as rt and sph during slow cooling (Ernst and Liu, 1998) because rt, ilm and sph are the most common accessory minerals in the studied rocks.

An empirical amph-cpx thermometer calibrated by Perchuk et al. (1985), was also applied for the mineral pairs in the studied rocks. The thermometer, based on the Fe/Mg exchange between these two minerals, just correlates the Mg# values of cpx and coexisting amph. Because of uncertainties in determination of Fe^{2+} and Fe^{3+}, the thermometer is not very exact. Nevertheless, it was used to crosscheck the results of amph-plag thermometry. The plots for the Mg# values of the studied mineral assemblages on the graphical thermometer (Figure 98) give temperatures in the range of ~750-980°C. Actually most of the data give less than 930°C, only two of the data from PHLtite give high temperature about 980°C that is probably due to

high Mg content of mica dominant in the rock. Except for 980°C, the obtained temperature is consistent with those obtained by other applied methods.

The calculated average temperature approximate (summarized in Table 2) experimentally determined amph liquidus temperatures in hydrous basaltic systems at low pressure (~900°C; Spear, 1981; Spulber and Rutherford, 1983). The temperature range, in general, is wide, i.e. difference between the lowest and the highest values is about 250°C. This may reflect a hypersolidus history of the rocks.
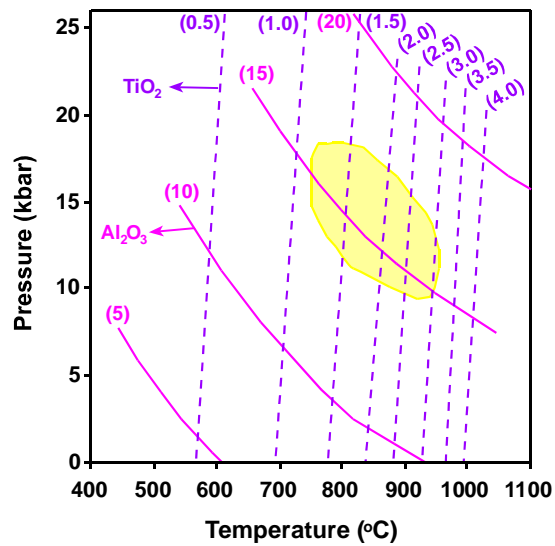
Figure 97. The place for the average compositions of amph's for each sample on semiquantitative geothermobarometer of Ernst and Liu (1998) based on Al_2O_3-TiO_2 isopleths.
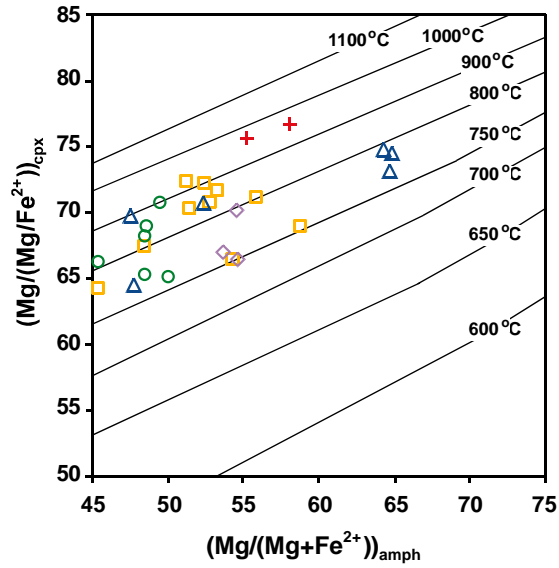
Figure 98. The plots for the cpx-amph pairs from the studied rocks on graphical cpx-amph thermometer of Perchuk et al. (1985) (the symbols are as in Figure 28).

Table 2. Summary of the estimated pressure and temperature.

	Pressure (P kbar)	Temperature (T°C)
Fleet and Barnett (1978) Raase (1974)	P < 5	-
Perchuk et al. (1985)	-	~750-980
Holland and Blundy (1994)	for P=0 P=5 P=10 P=15	828±55 865±66 911±70 956±75
Ernst and Liu (1998)	-	~750-925
Colombi (1989)	-	844±49

4.5. Plagioclase

Micro-chemical analyses were performed for 404 points on plag, which is the only felsic mineral in the studied rocks (Appendix E). The measurements were taken considering both mineral assemblages and their textural relations on 20 representative specimens of ultramafic rocks with variable amounts of plag (less than 3 % in CPXnite and PHLtite to 10-40% in leucocratic parts of HBdite).

4.5.1. Compositional Variations

Chemical compositions of the plag either post-cumulus in origin or from amph-plag veins were examined in detail. The plag crystals display a wide range of compositions, unrelated to differences in texture or coexisting minerals. The plag of all rock types have similar compositional ranges; 43.54-58.45 (SiO_2 wt%), 25.76-35.31 (Al_2O_3 wt%), 8.27-20.21 (CaO wt%), 0.16-6.17 (Na_2O wt%), 0.00-8.09 (K_2O wt%). In addition to the major oxides BaO (0.00-0.29 wt%), MnO (0.00-0.09 wt%), MgO (0.00-0.87 wt%), $Fe_2O_3^{(t)}$ (0.01-0.82 wt%) are present in negligible amounts.

The elemental relations for plag are best represented by cations pfu against Si (pfu) (Figure 99). Si content reversely controls Al and Ca contents where there seems to be two parallel trends. Ca with lower values than the main trend compensates Al deviating from the main trend (Figure 99a,b). Actually, there is no textural control for the present trends. Variation of Na against Si opposes those for Al and Ca (Figure 99c). In spite of its low values, K content displays weak positive correlation with Si (Figure 99d). Especially, the plag crystals from PHLtite have relatively high K content and this may be explained by abundance of dark mica rich in K.

4.5.2. Nomenclature and Substitution Mechanisms

The formula for the studied plag was calculated on the basis of five cations since the feldspar structure is composed of a three-dimensional framework of tetrahedra that encloses large, irregularly coordinated sites. The cations are allocated to sites as following; tetrahedral site is filled by Si, Al
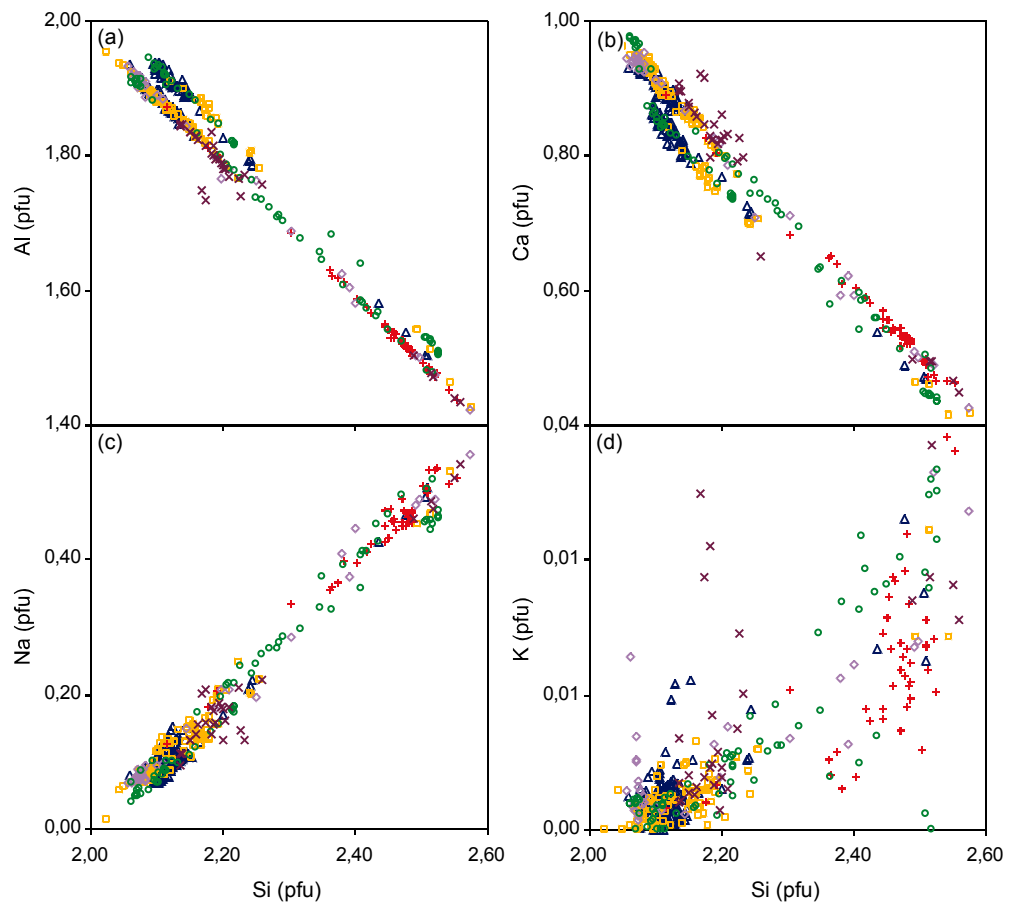
Figure 99. Variation diagrams of elements against Si (pfu) (the symbols are as in Figure 28).

(sum to 4); large cation site is filled by Na, Ca, K and Ba (sum to 1). Types of plag were determined using the relations among the important end members: $NaAlSi_3O_8$ (ab), $CaAl_2Si_2O_8$ (an) and $KAlSi_3O_8$ (K-feld). The an, ab and K-feld contents for the studied plag crystals were calculated from $100*Ca/(Ca+Na+K)$, $100*Na/(Ca+Na+K)$, $100*K/(Ca+Na+K)$, respectively. The calculated end-member values are plotted on K-feld - ab - an ternary diagram (Figure 100). As seen from Figure 100, both the post-cumulus and those from amph veins show negligible amounts of K-feld content with highly varying amounts of an-ab contents, $K-feld_{0.0-0.59}-ab_{1.42-59.39}-an_{40.61-98.58}$. The chemical data for the plag show high abundance in by'tic and an'tic compositions with an content greater than 70%, even though labr and and'tic plag also are present. The wide range of the plag composition is not related to the rock type, plag's from all rocks display silimar ranges. Moreover, there is no textural control on wide range plag composition.

Changes in plag composition is not only related to substitution of Na and Ca in the large sites but also related to substitution of Al and Si in the tetrahedral framework. Therefore, a coupled, charge-balanced substitution Ca+Al $\Leftrightarrow$ Na+Si control the solid solution between ab and an (Figure 101).

4.5.3. Elemental Variations within Zoned Crystals

Only few optically zoned plag crystals were detected among numerous specimens and chemical measurements were taken across rim to core of them. The change in an % of the zoned crystals are given in Figure 102. Neither regular change in an % along a profile nor consistency among profiles from different crystals is present. The non-systematic chemical variations may result from chemical re-equilibration due to interactions between feld and/or melt and alkali-rich vapor phase as proposed by Van Kooten (1980).

4.5.4. Petrologic Implications

Variation of $Fe_2O_3^{(t)}$ against an % content is an important petrologic indicator; (a) negative relation indicates magmatic differentiation from a closed system, (b) positive relation may infer an open system representing interaction
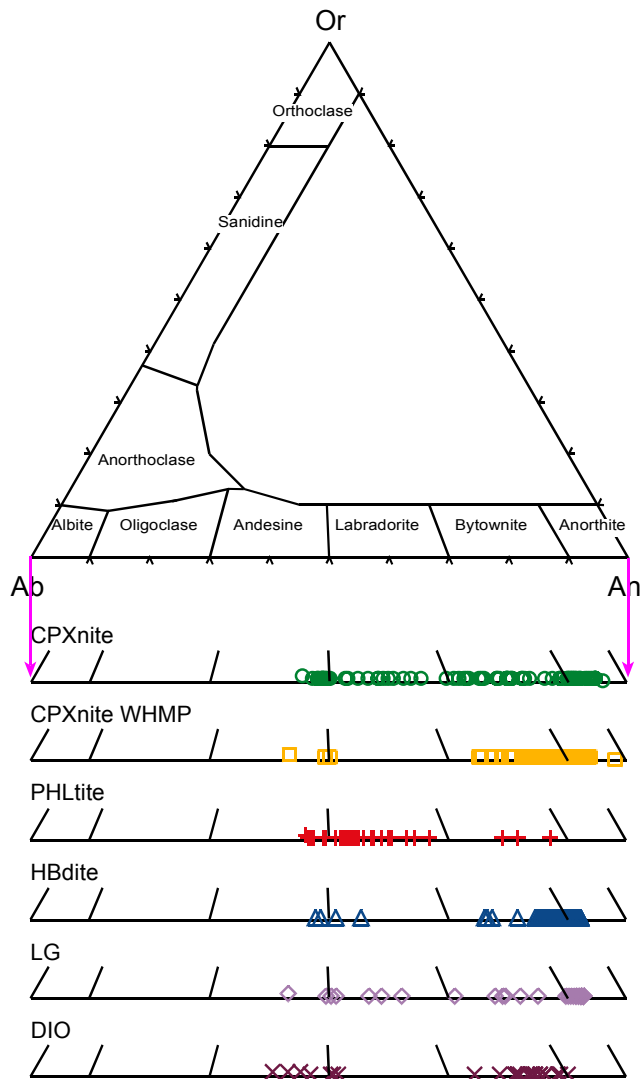
Figure 100. The plots for the studied plag's on feld ternary diagram (the symbols are as in Figure 28).

of acidic and basic end-member magmatic compositions if the relation becomes weaker and weaker as an% increases (Tegner, 1997). $Fe_2O_3^{(t)}$ contents of the plag do not change either positively or negatively with increasing an% (Figure 103a). Few scattered $Fe_2O_3^{(t)}$ data are due to surface oxidation. As seen in Figure 103a, in spite of a wide range of an %, $Fe_2O_3^{(t)}$ contents of the studied plag are almost constant for all of ultramafic rocks. This may suppose strong hybridization in mantle source and strong re-equilibration.
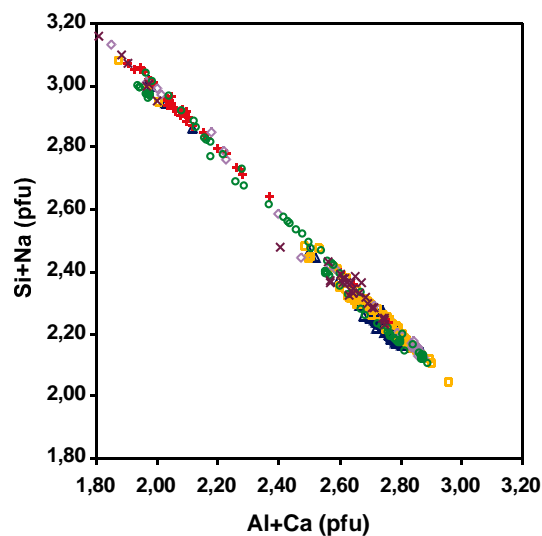
Figure 101. Coupled substitution mechanism controlling the plag chemistry (the symbols are as in Figure 28).

Although K_2O content of plag is very low, it increases with decreasing an % content and this reverse relation becomes stronger at lower an % (Figure 103b). This relation can be controlled by either composition of the sytems or temperature of crystallization (Hattori and Sato, 1996). The stronger reverse relation at lower an % is mainly observed in plag crystals from PHLtite. plag's with lower an % (<70) from other rocks also show strong reverse relation. This can be due to the high amounts of mica in PHLtite. On the other hand, the plag data from mica dominated DIO display both low and high K contents at variable an % contents. Therefore, a reverse relation can not be explained by

mica abundance in PHLtite. Moreover, a reverse relation is also observed for plag's from other rocks. Thus, the reverse relation at lower an% can be due to a thermal disequilibrium. This idea is supported by wide range of an % (40.61-98.58). High an % indicates high Ca/Na ratio of liquid from which plag is crystallized. A latter liquid rich in Na may necessiate plag to re-equilibriate. Considering these discussions as well as the properties of the mafic minerals, it may be assumed that there was a strong physicochemical disequilibrium in the system representing metasomatism of mantle source of these hydrous ultramafic-mafic plutonic rocks.
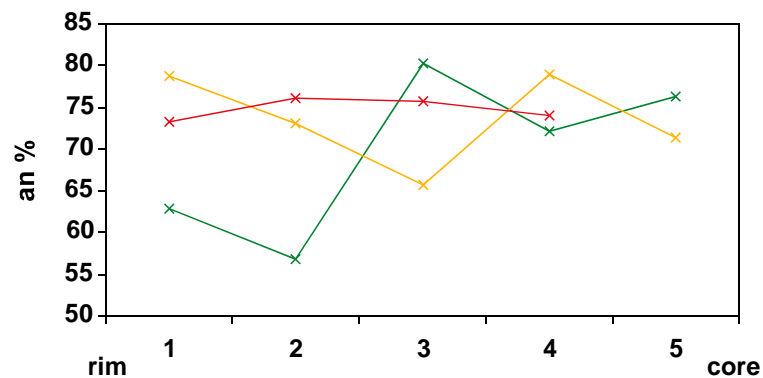
Figure 102. Variation of an % across rim to center of the zoned plag crystals.

Plag should derive from a liquid with high CaO/NaO ratio and/or crystallized under high P_{H2O} and oxygen fugacity close to NNO and HM buffers (Conrad et al., 1983). Although an content of plag is highly variable, the values greater than 80% are dominant. The high an % of plag supports the idea of a water saturated system (Helz, 1973). Moreover, the high an-plag coexisting with high Mg# cpx represents occurrence in an arc environment (e.g. Arculus and Wills, 1980; Burns, 1985; Beard, 1986) (Section 4.3.5).
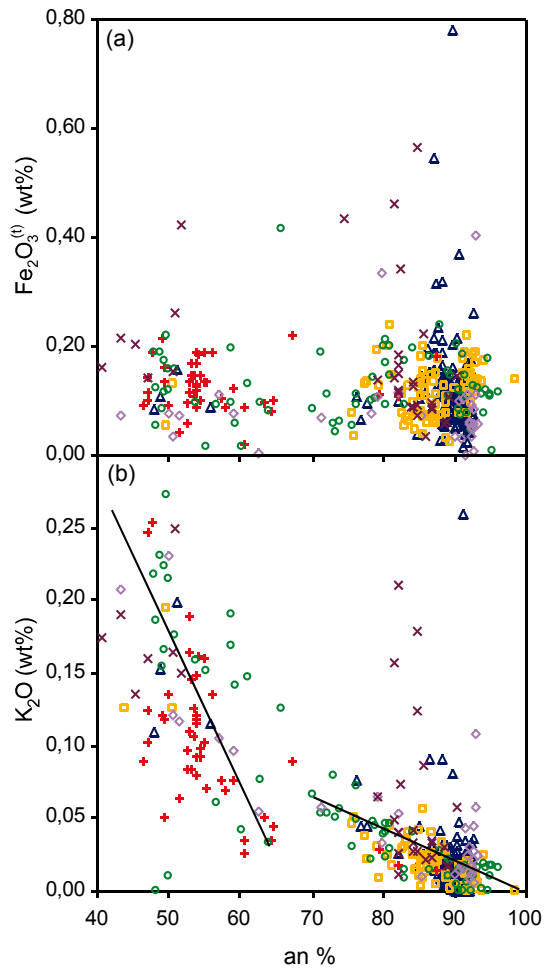
Figure 103. Covariations $Fe_2O_3^{(t)}$ and K_2O (wt%) against an% for the studied plag (the symbols are as in Figure 28).

4.6. Quenched Magmatic Enclave

Three small quenched magmatic enclaves were petrographically identified in one HBdite specimen (sample no: KK-34) that was chemically analyzed. The analyses were performed on both glassy matrix and crystals varying in size (e.g. 3 to 200 μm). All the crystals are of parg'tic amph composition. Moreover, the glass has exactly the same composition as the crystals, i.e. parg'tic composition with Si undesrsaturated and Al-oversaturated content. Moreover, the compositions of both the glass and amph crystals are within the compositional range of amph of the host rock, HBdite. There is no compositional difference.

4.7. Accessory Minerals

Chemical analyses were also carried out on accessory minerals such are Ti-phases (i.e. sph, rt, ilm), ap and pyr but most of the analyses are problematic except for those on sph due to small crystal sizes. Unfortunately, rt could not be analysed because of its very tiny needle crystals in amph and py. Measurements on rt always gave the composition of the host minerals in which rt is included. Moreover, numerous analyses performed on ilm and pyr did not give useful data because of their small crystal sizes and so contamination from coexisting minerals. Just few ilm crystals gave relatively good results with some degree of contamination from SiO_2, CaO, K_2O of coexisting minerals. The oxide ranges for the ilm are; 44.70-52.38 wt% for TiO_2, 27.56-42.71 wt% for $FeO^{(t)}$, 1.08-5.43 wt% for MnO,

Analyses on the sph crystals, the most common accessory mineral either as post-cumulus or exsolution in cpx, gave the following range of compositions; 30.33-31.10 wt% SiO_2, 30.22-37.16 wt% TiO_2, 24.35-29.34 wt% CaO and 1.77-2.98 wt% Al_2O_3. Total oxide values ranges from 88.28 to 99.71 wt% and low values may arise from unmeasured elements that can be found at elevated concentrations in sph such as Nb, Zr, Hf, Ta (e.g. Gill, 1981), Ba, V (e.g. Mitchel and Meyer, 1989).

Ap, another mineral accessorily present in the studied rock, is composed of 39.74-43.82 wt% P_2O_5 and 48.71-55.50 wt% CaO.

4.8. Low Grade Metamorphism and Surface Alteration Products

Petrographic studies showed that act, chl, pump, ep are rarely present as low grade metamorphic phases in addition to surface alteration products cc, verm and ser. They were also chemically defined. The low grade metamorphic amph is act (Figure 85b) with compositional ranges of 52.39-59.96 wt% SiO_2, 0.58-3.86 wt% Al_2O_3, 0.01-0.21 wt% TiO_2, 11.24-16.21 wt% $FeO^{(t)}$, 12.80-19.00 wt% MgO, 0.17-0.37 wt% MnO, 10.66-12.28 wt% CaO, 0.04-0.38 wt% Na_2O, 0.00-0.33 wt% Cr_2O_3 and 0.00-0.05 wt% NiO.

Ep is rarely observed and mainly has SiO_2, Al_2O_3, CaO and $Fe_2O_3^{(t)}$, 39.5-42.27, 27.87-30.60, 13.32-24.39 and 1.86-4.15 wt%, respectively. Rarely found pump has 35.37-36.29 wt% SiO_2, 20.38-20.85 wt% Al_2O_3, 14.54-14.97 wt% $Fe_2O_3^{(t)}$, 19.99-20.99 wt% CaO, and 0.03 wt% K_2O.

Chl and verm display close similarity in compositional ranges: 26.38-33.71 wt% SiO_2, 11.57-20.37 wt% Al_2O_3, 8.51-17.74 wt% MgO, 14.44-26.13 wt% $FeO^{(t)}$, 0.04-4.14 wt% CaO, 0.05-3.05 wt% TiO_2, 0.16-0.34 wt% MnO, 0.06-6.61 wt% K_2O and 0.01-0.20 wt% Na_2O. But K_2O of verm is higher than that of chl. The occurrence of verm was proven by x-ray diffractometry, and associated differential thermal and thermogravimetric method (Toksoy, 1998; Toksoy-Köksal et al., 1999, 2000, 2001b).

Carb crystals are rarely observed as filling the interstices between the major minerals, and in plag crystals. The chemical analyses on carb resulted in pure cc composition.

Pressure and temperature calculations from the low grade metamorphic minerals can not be applied since there is no appropriate assemblage.

CHAPTER 5

WHOLE-ROCK CHEMISTRY
AND PETROGENETIC IMPLICATIONS

5.1. Introduction

Major, trace and rare earth element (REE) geochemistry have been studied for fifty-two whole-rock samples (50 ultramafic, 1 layered gabbro and 1 diorite) of the hydrous mineral rich ultramafic-mafic rocks from the Kurançalı area (see Appendix F). Large ion lithophile element (LILE) (e.g. Ba, Th, U) and high field strength element (HFSE) (e.g. Nb, Ta, Zr, Hf, Ti, Y) ratios combined with rare earth element (REE) abundances, and major-minor element concentrations have been widely used to identify the geochemical character and original tectonic environment.

5.2. Effect of Alteration on Whole-Rock Composition

Petrographical and mineralogical studies showed that low grade metamorphism and surface alteration products are present in limited amounts. Since both alteration and metamorphism may cause serious problems in petrogenetic interpretations of ophiolitic rocks (e.g. Humphris and Thompson, 1978; Coish et al., 1982; Meffre et al., 1996; Bédard, 1999), the degree of alteration for the studied rocks was petrographically and chemically controlled before evaluating the chemical data.

The studies in literature show that alteration typically results in loss or gain of most of alkali earth elements and LILE such as Cs, Rb, Sr, Ba, Pb and U. Some minor and trace elements (e.g. Ti, Zr, Hf, Y, Th, Nb, Ta P, Ni, Cr, Al,

and REE) are relatively immobile under conditions of low grade hydrothermal metamorphism (e.g. Campbell et al., 1984), except for conditions of high water/rock ratios and carbonate alteration (Humphris, 1984).

To identify the degree of alteration, the elements tending to be mobile were plotted against an immobile element, here Ti (Figure 104). Most of the elements show good correlation with Ti except for few that scatter. However, the scattering elements are strongly related to the chemistry of the major minerals rather than to alteration. The samples enriched in plag and mica show a scatter in the plots. This is well-visible in Figure 105 where Sr is plotted against CaO. Covariation of Rb and Ba with K_2O show similar results because Sr is compatible with plag while Rb and Ba are compatible with mica. A large degree of mobilization would disturb good covariations. Similarly, plag bearing samples with lower MgO content display relatively scattered plots. The smooth REE and multi-element variation patterns (given in Section 5.6.) also suggest that their concentrations have not been modified by alteration. It is concluded that alteration is unlikely to have modified the compositions of the studied rocks.

5.3. Compositional Variations

Modal mineralogy controls the chemistry of the cumulate ultramafic and mafic rocks, therefore wide ranges of compositions are present: 38.40-48.80 (wt% SiO_2), 6.14-26.7 (wt% Al_2O_3), 10.45-22.5 (wt% CaO), 0.34-2.97 (wt% TiO_2), 0.25-3.52 (wt% Fe_2O_3), 3.23-13.17 (wt% FeO), 3.08-12.87 (wt% MgO), 0.17-4.21 (wt% K_2O), 0.46-1.83 (wt% Na_2O), 0.07-0.50 (wt% MnO), 0.02-0.90 (wt% P_2O_5), 0.01-0.1 (wt% Cr_2O_3). The whole-rock compositions reflect relative proportions of the minerals, especially amph and cpx (Figure 106). The major elements have quite continuous covariations with SiO_2 (wt%) increasing from HBdite to CPXnite. SiO_2 concentrations of PHLtite, LG and DIO are intermediate between HBdite and CPXnite. CPXnite WHMP, containing all minerals in varying amounts, displays the widest range of SiO_2 concentrations overlapping all rock types. The scatters for Al_2O_3 and MgO are due to plag enrichment in CPXnite WHMP (Figure 106b,d). CaO content increases as SiO_2 increases; this unusual case is completely controlled by modes of cpx and
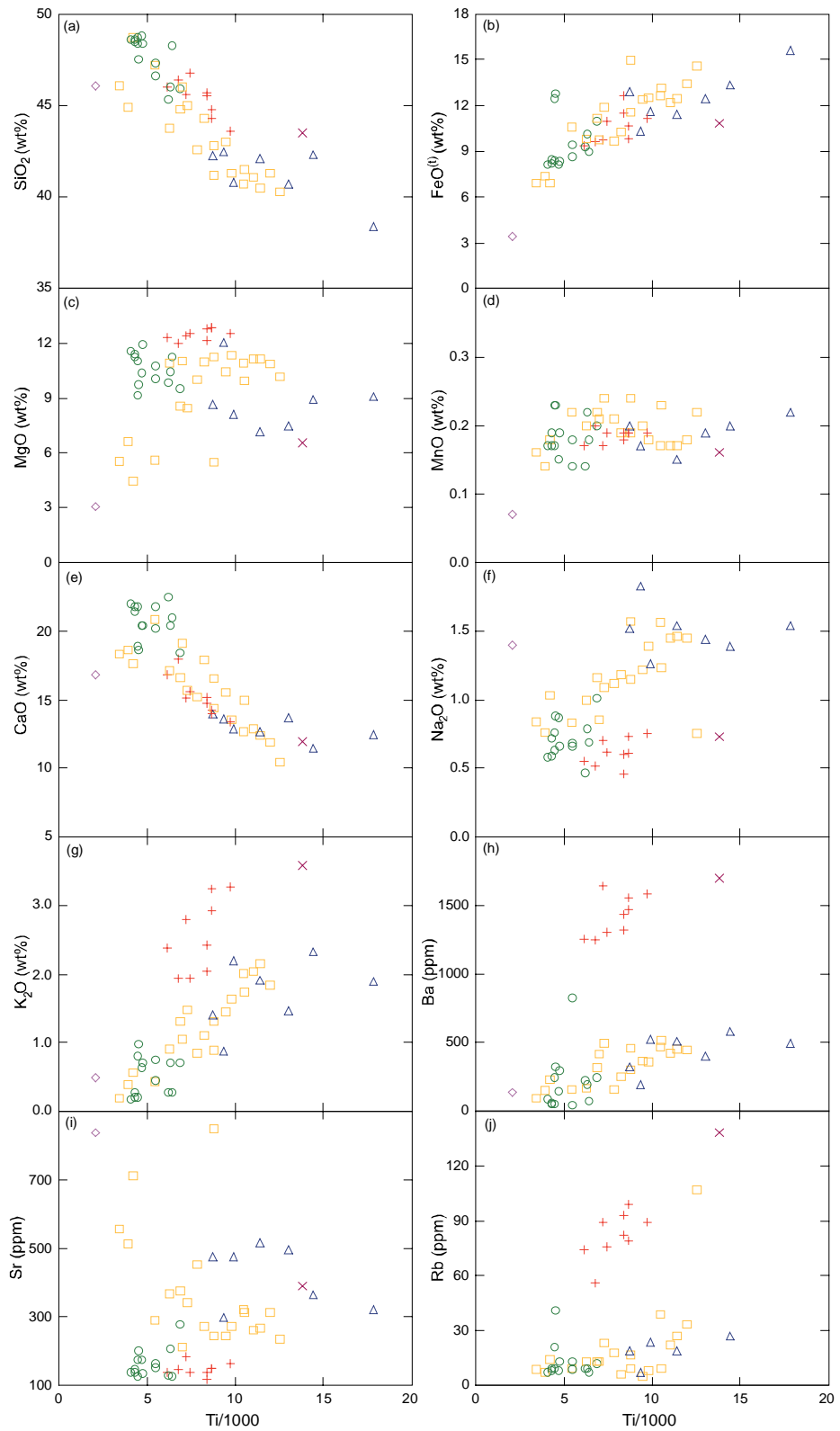
Figure 104. Chemical control on alteration whether it affects the whole-rock composition or not (the symbols are as in Figure 28).
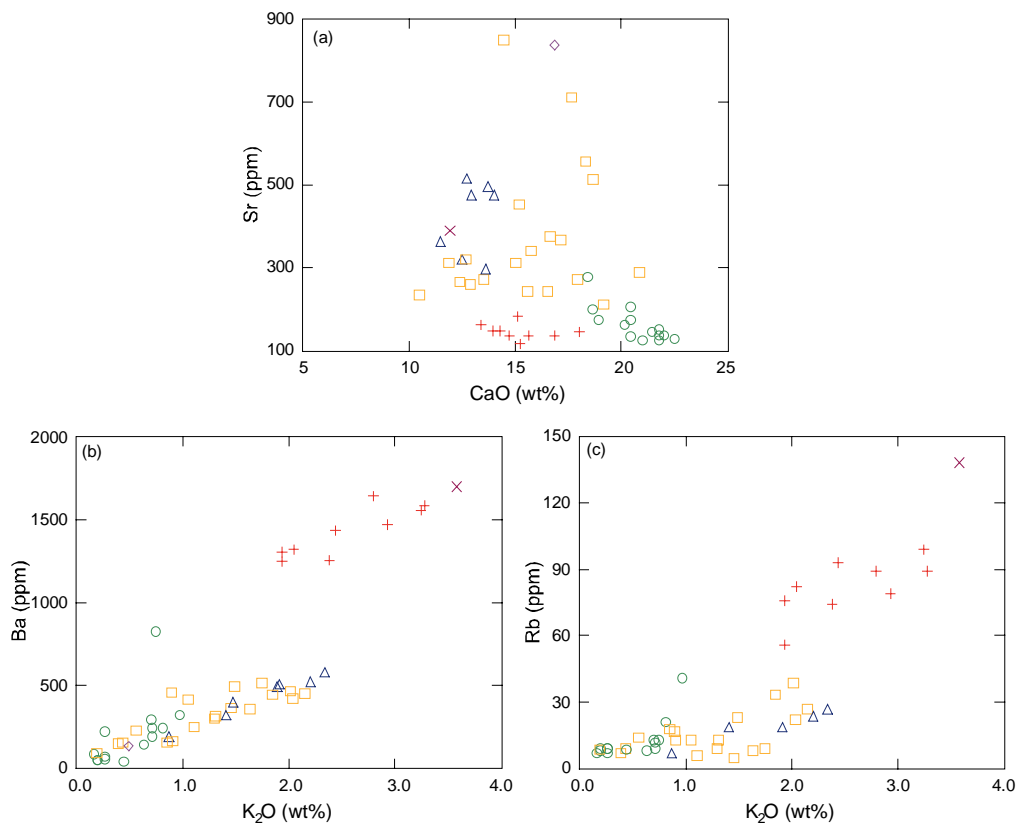
Figure 105. Covariation diagrams for Sr-CaO, Ba-K$_2$O and Rb-K$_2$O to show mineralogical control for the scattered plots Figure 104 (the symbols are as in Figure 28).
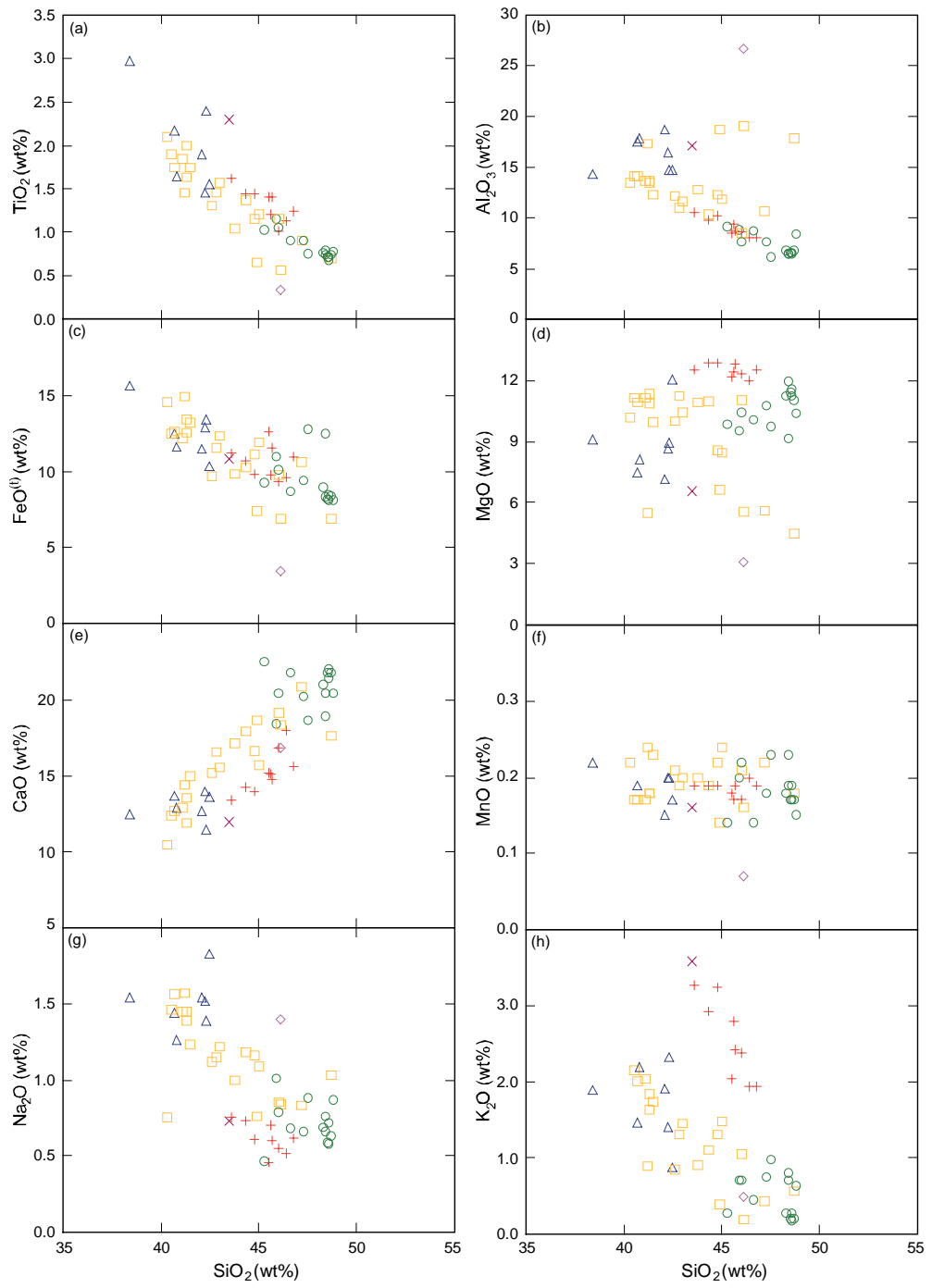
Figure 106. Major element systematic against SiO_2 (wt%) for ultramafic-mafic rocks from the Kurançalı area (the symbols are as in Figure 28).

amph, i.e. CaO and SiO_2 contents are highest for cpx while they are lowest for amph (Figure 106e). TiO_2, $FeO^{(t)}$, Na_2O and K_2O decreases with increasing SiO_2 from HBdite to CPXnite, the rest of the rocks are intermediate between them (Figure 106a,c,g,h). This relation is controlled again by element contents of amph with highest TiO_2, $FeO^{(t)}$, Na_2O and lowest SiO_2, while cpx has lowest TiO_2, $FeO^{(t)}$, Na_2O and highest SiO_2.

The rocks are characterized by moderately high Mg# (0.44-0.75). The highest Mg# values (0.62-0.75) are from CPXnite and PHLtite (Figure 107). However, the lowest Mg# is from CPXnite WHMP due to its plag content, i.e. the higher the plag content, the lower the Mg#. Al_2O_3 and CaO contents are highly variable against the slightly changing Mg#'s (Figure 107b,d). Al_2O_3 decreases and CaO increases with increasing Mg#. These variations are due to highly varying modal ratios of plag/cpx and amph/cpx. Na_2O, K_2O (wt%) and Sr (ppm) contents recognizably increase as the Mg# values decrease (Figure 107g,h,k). This is a common feature of calc-alkaline plutons (Beard, 1986; Lachize et al., 1996). K_2O and Ba contents for mica dominant PHLtite are higher than those for other rocks (Figure 107h,i). Because of the lower Mg# and higher TiO_2 content of amph (Section 4.4), and a higher modal amount of Ti-phases in HBdite, TiO_2 correlates negative with decreasing Mg# (Figure 107c). Rb content reaching highest values in DIO and PHLtite, is nearly constant for most of the rocks (Figure 107j). Y, Nb and V contents decrease with increasing Mg# from HBdite to CPXnite (Figure 107l,n,p). The scattered data for Y, Nb and V are due to plag enrichment in CPXnite WHMP. The highest scatter of Zr is observed in CPXnite (Figure 107m). No modal compositional control on Th that shows quite scattered plots (Figure 107o) was identified.

The high enrichment of TiO_2, $FeO^{(t)}$, Nb, Y, V observed in HBdite is due to the minerals of the rocks (amph, ilm, rt) having high distribution coefficients for those elements, middle REE and TiO_2 (e.g. Pearce and Parkinson, 1993; Teklay et al., 2002; Coogan et al., 2001b). This may rule out the addition of an alkaline component to increase the incompatible elements of the source (McPherson et al., 1996). Moreover, the unusual behaviour of SiO_2 (i.e.
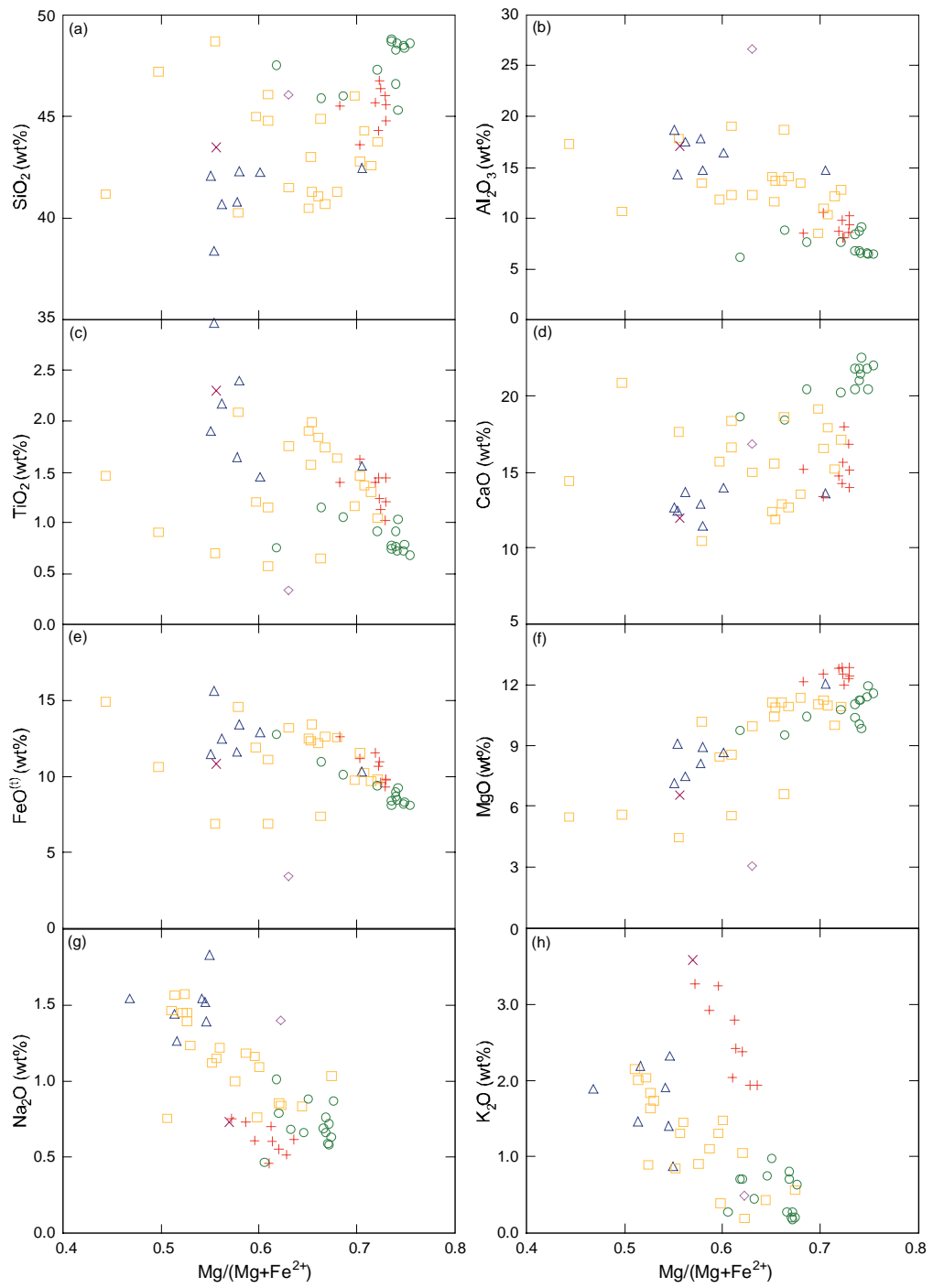
Figure 107. Major and trace element systematic against Mg# for ultramafic-mafic rocks from the Kurançalı area (the symbols are as in Figure 28).

171
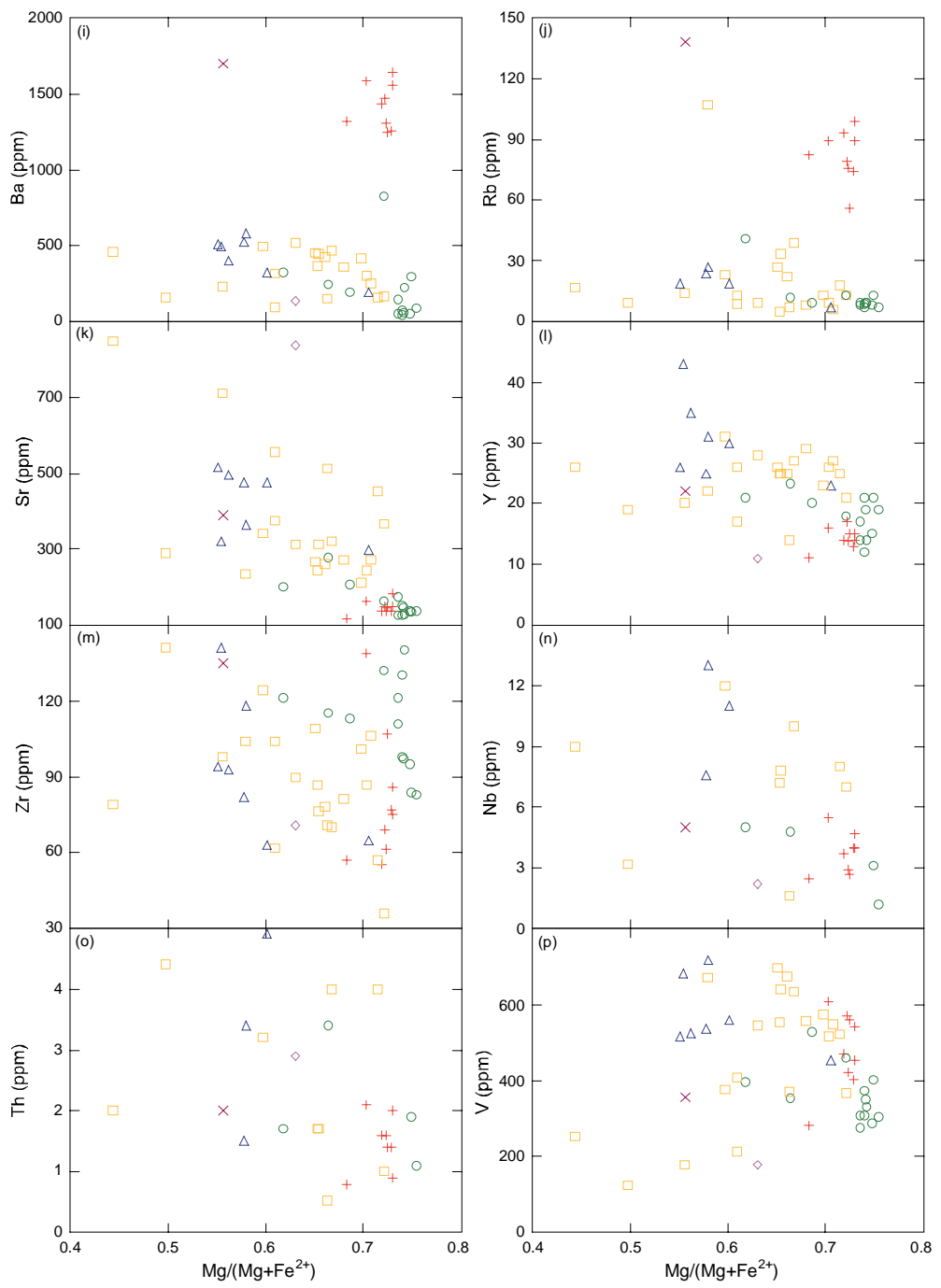
Figure 107 (continued).

decreasing with decreasing Mg# from CPXnite to HBdite) can be explained by alkaline magma metasomatism.

5.4. Chemical Classification

The Kurançalı rocks with variable alkali contents (0.74-4.96 wt%) show a transitional character from alkaline to subalkaline on the $Na_2O+K_2O-SiO_2$ diagram (Irvine and Baragar, 1971), while all these rocks plot in subalkaline field in a Na_2O-SiO_2 diagram (Middlemost, 1975) (Figure 108a,b). The transition to an alkaline character is largely caused by variable K_2O contents (Figure 108c). Subalkaline character of the studied rocks is also confirmed by a trace element based classification ($Zr/TiO_2*0.0001-Nb/Y$; Winchester and Floyd, 1977) (Figure 109). Ultramafic rocks seem to be tholeiitic while LG and DIO follow calc-alkaline trend on AFM ($Na_2O+K_2O-FeO^{(t)}-MgO$) diagram (Irvine and Baragar, 1971) (Figure 110). This might be caused by K-metasomatism.

The samples from CPXnite and LG, and few from CPXnite WHMP, PHLtite plot in CAB field on Ti/1000-Zr, Ti/100-Zr-Y*3 and Ti/100-Zr-Sr/2 diagrams (after Pearce and Cann, 1973) (Figure 111). However, the HBdite, PHLtite, CPXnite WHMP and DIO samples with abundant hydrous minerals display scattered plots. CPXnite, lack of hydrous phases and plotting in calc-alkaline basalt (CAB) field, might be a representative of primary composition. That means, as the amount of hydrous phases increases, the compositional disequilibrium also increases, and therefore the samples of CPXnite WHMP, HBdite, PHLtite and DIO show scattered plots. The samples of HBdite plot in island arc basalt (IAB) field in a Ti/100-Zr-Sr/2 diagram (Figure 111c).

The rocks with moderately high Mg#'s plot in the low-Mg basalt field of Wood (1978)'s classification (Figure 112). The low-Mg rocks show increasing SiO_2 contents at nearly constant $FeO^{(t)}/MgO$ ratios ranging between 0.70-1.12, expect for two samples (Figure 113). Increasing SiO_2 content at nearly constant $FeO^{(t)}/MgO$ ratios is typical of cumulates, formed during calc-alkaline differentiation (Miyashiro, 1974; Beard, 1986; Lachize et al., 1996). However, the studied rocks have quite lower SiO_2 contents except for CPXnite than the calc-alkaline rocks to which they are compared (Figure 113). The samples of
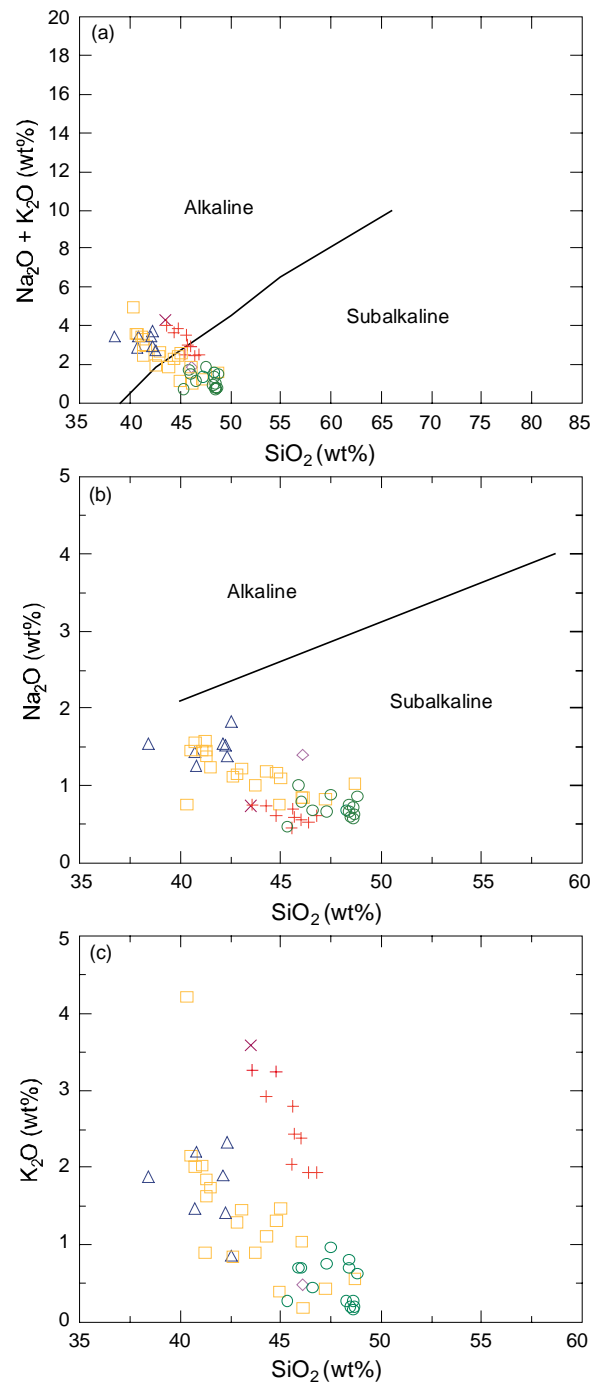
Figure 108. Plots for the rocks to determine their characteristics as alkaline or subalkaline based on alkali and SiO$_2$ contents; division lines after (a) Irvine and Baragar (1971) and (b) Middlemost (1975) (the symbols are as in Figure 28).

CPXnite plot in the field of calc-alkaline plutonic rocks occurring in marginal oceanic basin settings above subducting slabs of oceanic crust. Rocks with calc-alkaline character reported in literature (e.g. from Aleutian arc (Kay et al., 1982), Wadi Haymiliyah section of Semail Ophiolite, Oman (Lachize et al., 1996) show enrichment in SiO_2 as differentiation proceeds. However, the studied rocks, considered to be calc-alkaline, contain less SiO_2 than CPXnite (with almost pure cpx) as they become more evolved and more hydrous (high amounts of amph, mica and plag). This is due to the control of modal composition on whole-rock chemistry. This reverse relation of SiO_2 may indicate a complex, possibly open system rather than a simple closed system. The presence of quenched magmatic enclaves in SiO_2 undersaturated HBdite also supports the complexity in whole-rock composition, because quenched magmatic enclaves display totally hydrous, SiO_2-depleted compositions for both glassy matrix and parg'tic amph (Section 4.6.).
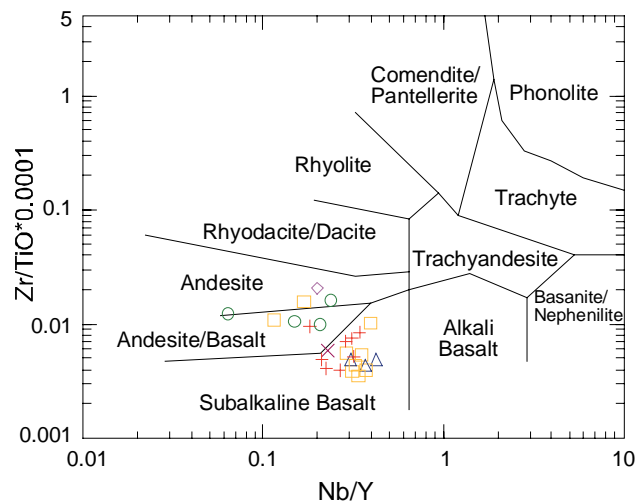
Figure 109. $Zr/TiO_2*0.0001$-Nb/Y geochemical discrimination diagram (after Winchester and Floyd, 1977) showing subalkaline character of the rocks (the symbols are as in Figure 28).
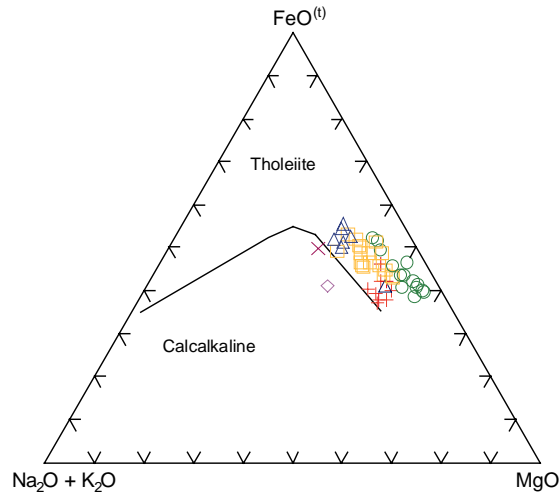
Figure 110. Plots for the rocks to determine their characteristics as tholeiitic or calc-alkaline on Na_2O+K_2O-$FeO^{(t)}$-MgO diagram; division line after Irvine and Baragar (1971) (the symbols are as in Figure 28).

5.5. Implications for Tectonic Setting

Minor and trace element diagrams were used to discriminate possible tectonic setting in which the studied hydrous plutonic rocks are formed. From the plots on a V-Ti/1000 diagram (Shervais, 1982) an arc environment for the formation of ultramafic-mafic rocks is inferred (Figure 114a). However, few samples having higher Ti content plot in the ocean floor basalt (OFB) field. Most of the samples plot in the IAB field on a Cr-Y diagram and only few samples, rich in amph from CPXnite WHMP and HBdite show transition to the mid-ocean ridge basalt (MORB) field (after Pearce, 1980; Pearce et al., 1984) (Figure 114b). The samples also plot in IAB field on the Ti/Cr-Ni diagram after Beccaluva et al. (1979) (Figure 114c). Nb/Th ratios, recording the development of negative Nb and Y anomalies in multi-variant patterns (Figure 115), show a typical arc-like signature (fields after Jenner et al., 1991) (Figure 114d). The limited data with Hf/Th<3 from CPXnite, CPXnite WHMP and PHLtite all plot in the calc-alkaline volcanic arc field on Hf/3-Th-Ta and Hf/3-Th-Nb/16 diagrams (Wood, 1980) (Figure 114e,f). The covariation of Na and Rb contents also display a volcanic arc basalt (VAB) character according to the divisions by Pearce (1982) (Figure 114g). But few samples from CPXnite WHMP and

176
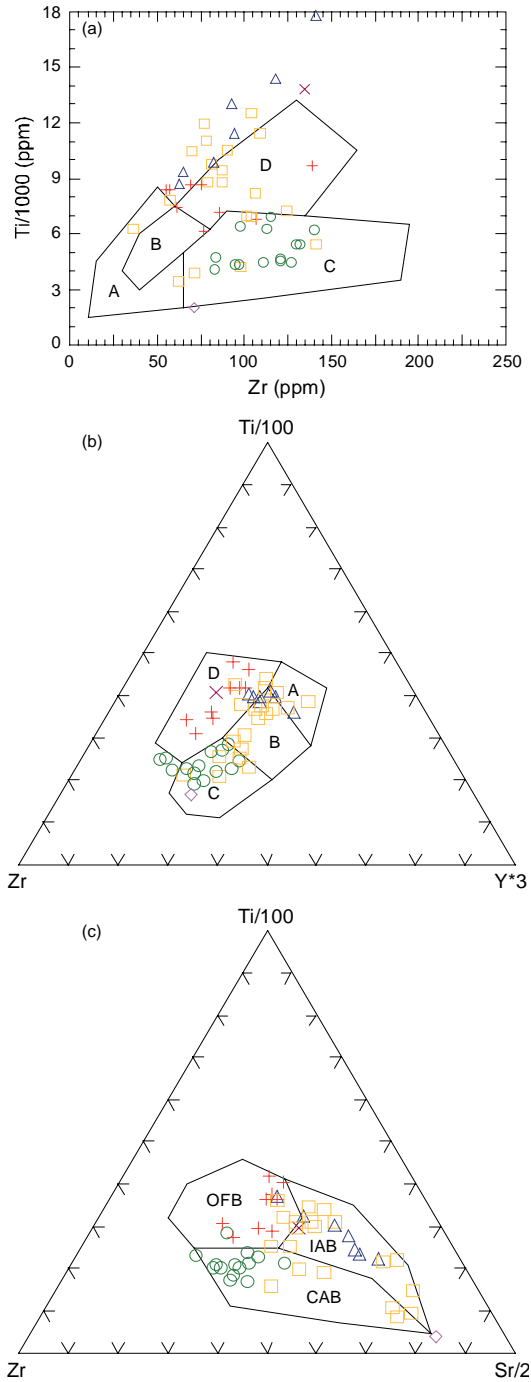
Figure 111. The plots for the studied rocks on geochemical discrimination diagrams after Pearce and Cann (1973); (a) Ti/1000-Zr diagram (where A,B: LKT; A,C: CAB; B,D: OFB), (b) Ti/100-Zr-Y*3 diagram (where A,B: LKT; C: CAB; D: OFB), (c) Ti/100-Zr-Sr/2 diagram (LKT: low potassium tholeiite, CAB: calc-alkaline basalt, OFB: ocean floor basalt, IAB: island arc basalt) (the symbols are as in Figure 28).

HBdite plot in within plate basalt (WPB) field because of a high partition of Nb into amph. Despite few scattered data, the trace and minor element contents strongly support an island arc tectonic setting.

Mg# values of the studied ultramafic rocks are lower than the ultramafics from the arc environments (Beard, 1986). They plot in the area of arc related mafic cumulates rather than in the field of arc related ultramafic cumulates on an AFM diagram (after Beard, 1986) (Figure 114h). This is largely due to lower MgO contents and absence of ol and opx in these rocks.

The studied ultramafic-mafic plutonic rocks rich in hydrous minerals show a calc-alkaline character and display arc affinity.
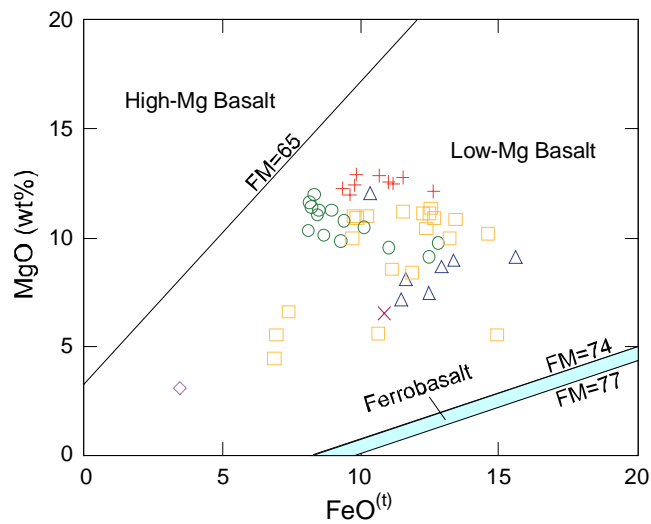
Figure 112. Plots of the rocks on MgO-FeO$^{(t)}$ (wt%) classification of Wood (1978) showing their low-Mg character (the symbols are as in Figure 28).
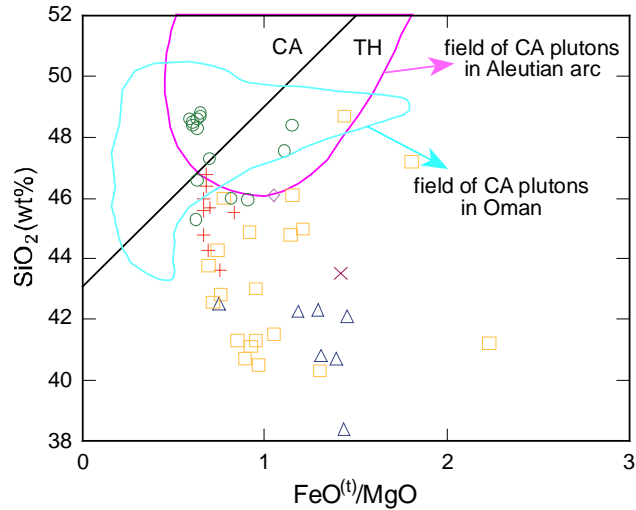
Figure 113. Covariation of SiO$_2$ and FeO$^{(t)}$/MgO for whole-rock compositions of the studied rocks and their comparison with calc-alkaline (CA) and tholeiitic (TH) rocks. CA-TH division line is from Miyashiro (1974), areas of CA plutonic rocks from Aeolian arc (Kay et al., 1982), Wadi Haymiliyah section of Semail Ophiolite, Oman (Lachize et al., 1996) (the symbols are as in Figure 28).

5.6. Spider and Rare Earth Element Patterns

Multi-element trace and rare earth element (REE) patterns are examined by normalizing the data to N-MORB values from Sun and McDonough (1989). The patterns of both multi-element variations and REE, almost parallel for ultramafic and mafic rocks, exhibit a steep slope.

5.6.1. Spider Diagrams

All of the studied rocks are characterized by a strong enrichment of LILE (e.g. Rb, Ba, Th and U) and depletion in HFSE. Although all samples are depleted in HFSE compared to LILE, some samples show slight enrichment in HFSE relative to N-MORB (Figure 115).

Although all of the rocks have similar patterns, there are slight differences due to the control of modal mineralogy. CPXnite WHMP having varying amounts of amph and phl shows a wide range of enrichment levels. All rocks showing strong positive Ba, Rb and K anomalies, differ in the degree of

179
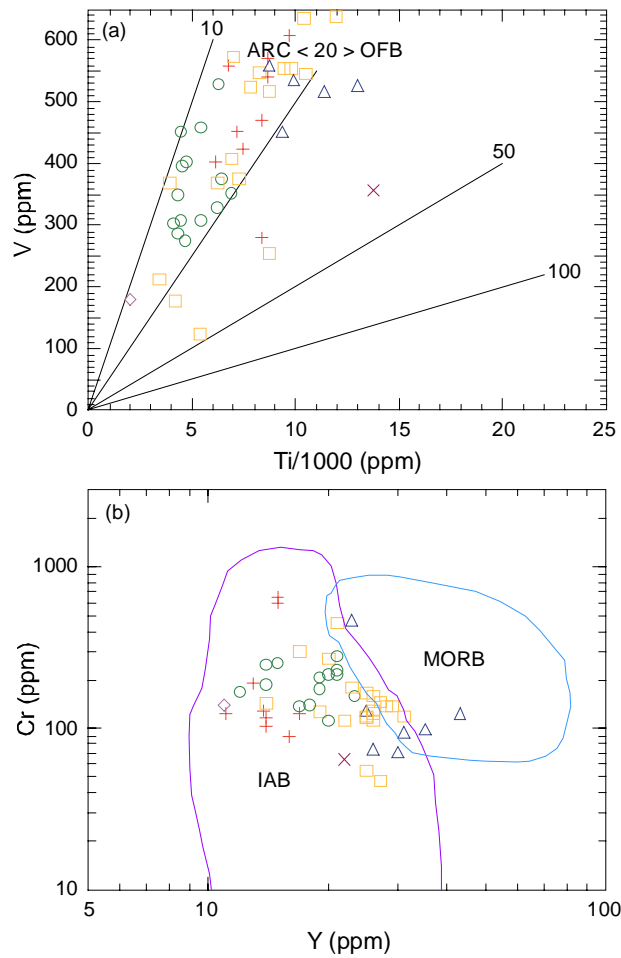
Figure 114. The plots on tectonic environment discrimination diagrams; (a) V-Ti/1000 diagram (after Shervais, 1982), (b) Cr-Y diagram (after Pearce, 1980; Pearce et al., 1984), (c) Ti/Cr-Ni diagram (after Beccaluva et al., 1979), (d) Nb/Th-Y diagram (after Jenner et al., 1991), (e,f) Hf/3-Th-Ta and Hf/3-Th-Nb/16 diagrams (A: N-MORB, B: E-MORB, WPB, D: VAB (D1: CA (Hf/Th<3); D2: TH (Hf/Th>3) (after Wood, 1980), (g) Na-Rb diagram (after Pearce, 1982), (h) Na$_2$O+K$_2$O-FeO$^{(t)}$-MgO diagram (after Beard, 1986) (OFB: ocean floor basalt, IAB: island arc basalt, MORB: mid-ocean ridge basalt, VAB: volcanic arc basalt, WPB: within plate basalt, CA: calc-alkaline, TH: tholeiitic) (the symbols are as in Figure 28).

Figure 114 (continued).

(f)

Hf/3

A

D1

B

D2

C

Th

Nb/16

(g)

Nb (ppm)

WPB

VAB

Rb (ppm)

FeO$^{(t)}$

(h)

Arc related non-cumulate
gabbro and diorite field

Arc related mafic
cumulate field

Arc related ultramafic
cumulate field

Na$_2$O + K$_2$O

MgO
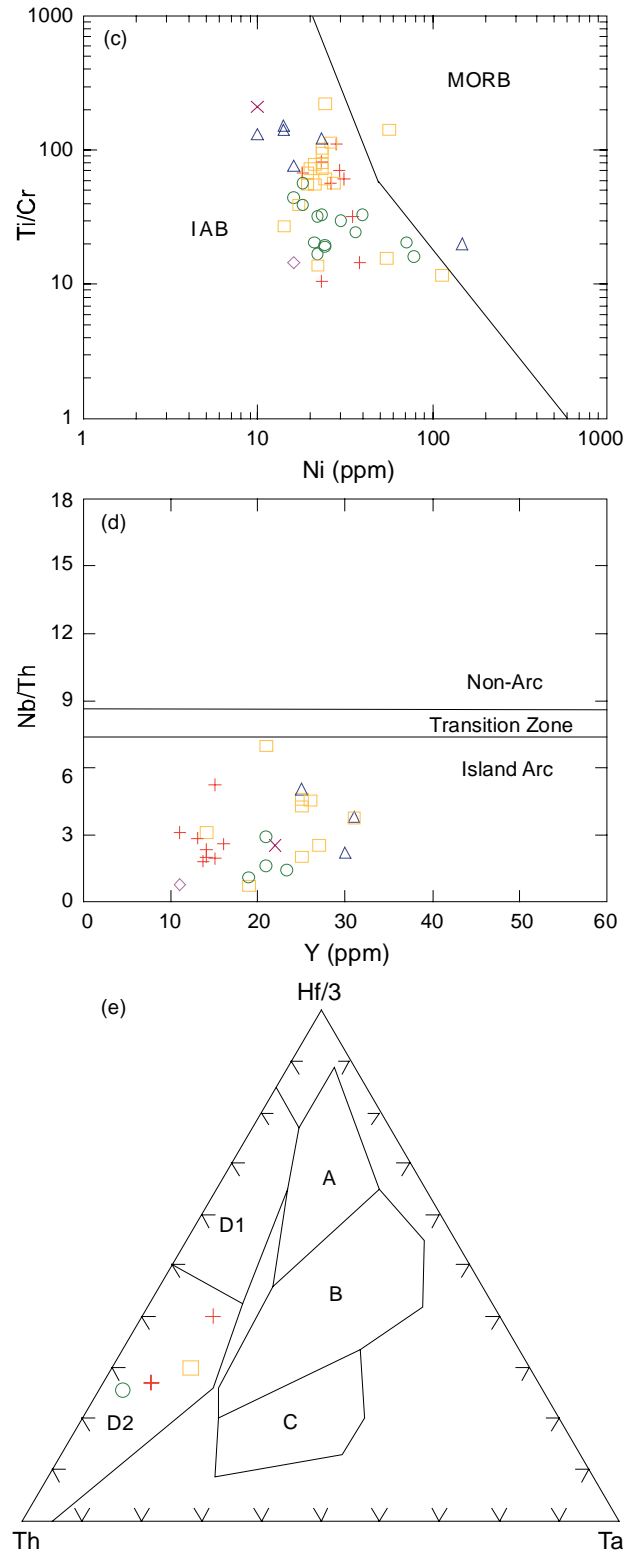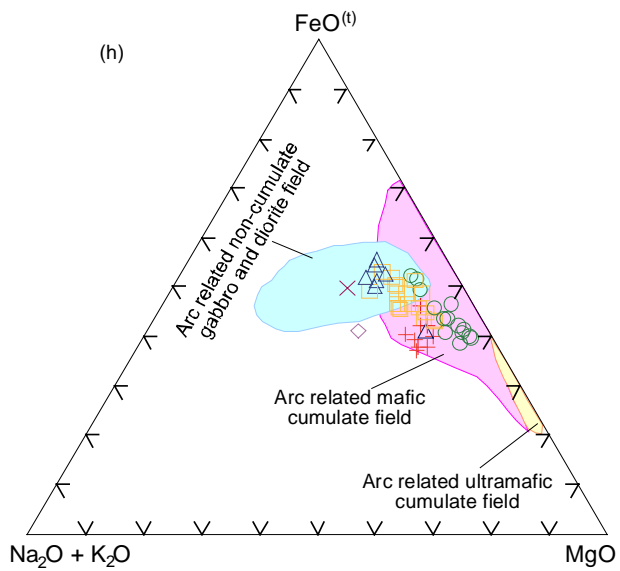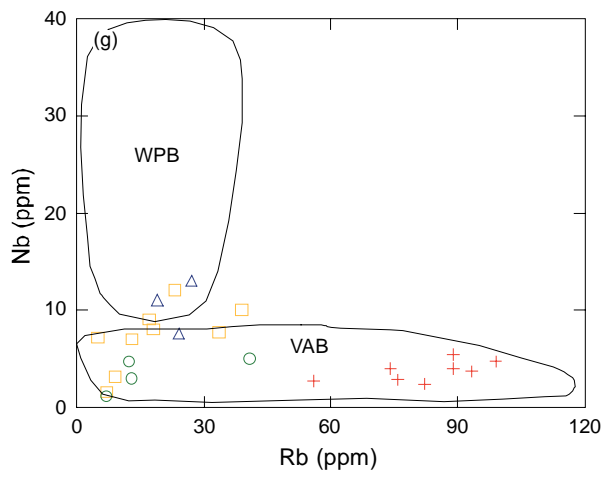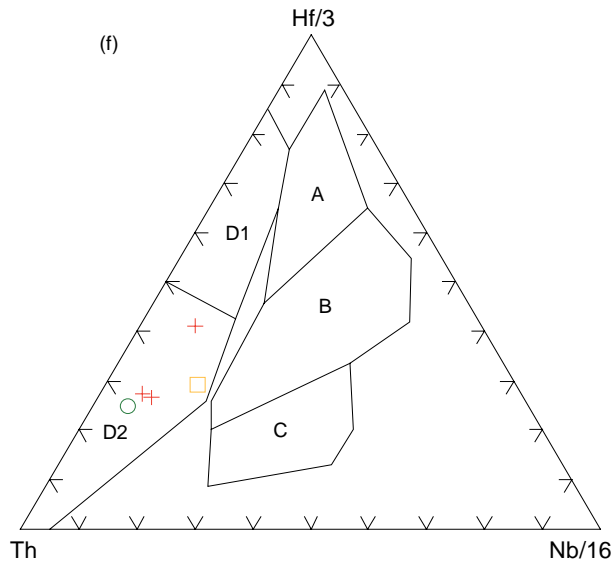
Figure 114 (continued).
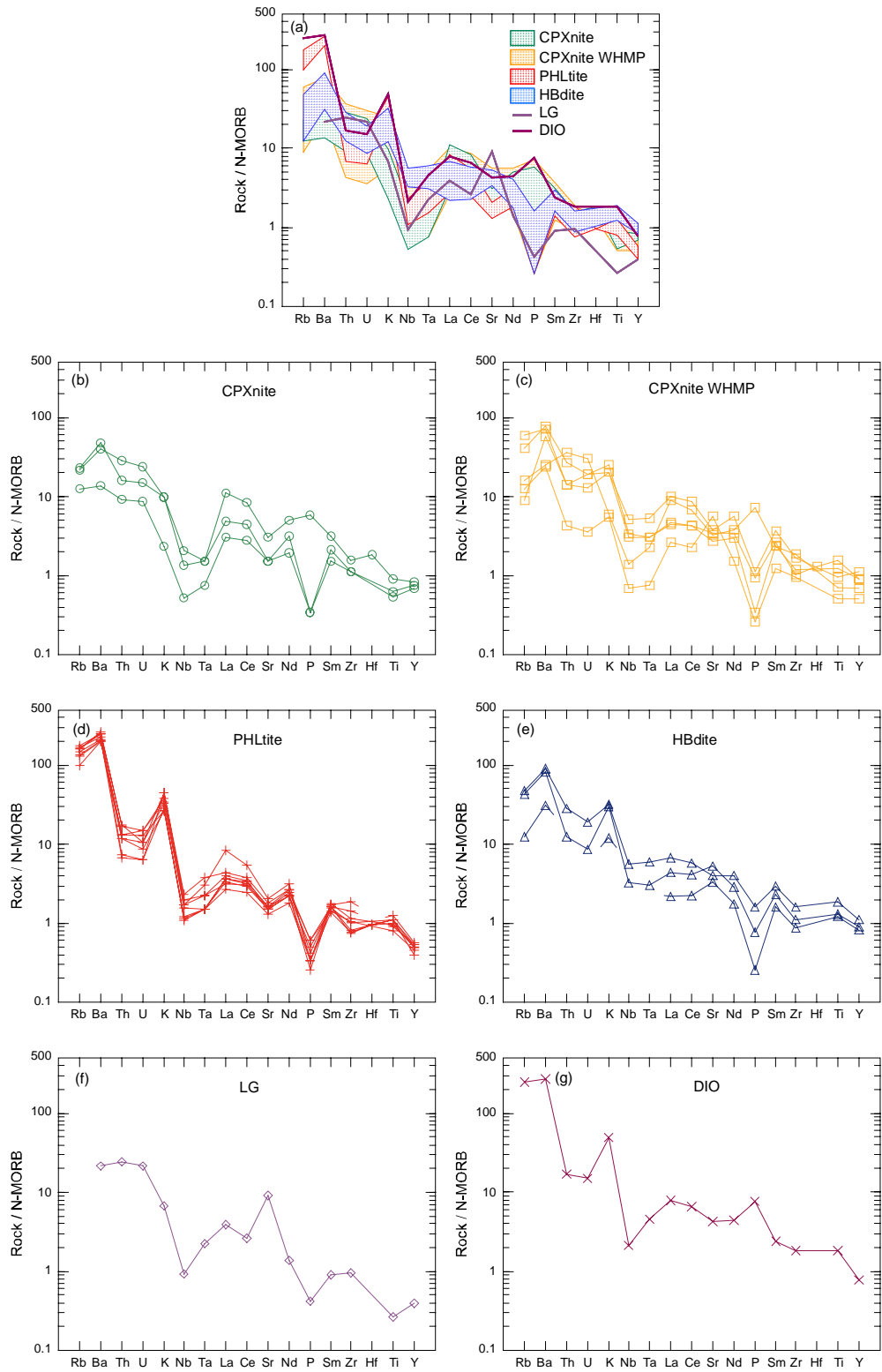
Figure 115. N-MORB normalized trace elements patterns for ultramafic-mafic rocks from the Kurançalı area (normalization data from Sun and McDonough, 1989).

183

enrichment. The PHLtite and DIO samples have the highest concentrations in Ba, Rb and K. This difference should result from higher partition of these elements into mica dominant in PHLtite and DIO. HBdite samples also show enrichment in K while CPXnite has the lowest K contents. Even though all rocks have positive Th anomalies, CPXnite shows stronger anomalies than the other rocks. Th of PHLtite and DIO is lower than that of HBdite. U enrichment levels are almost similar in all rock types but U values of PHLtite, DIO are slightly lower than those of the others. All rock types, especially CPXnite WHMP (rich in plag) and LG, are enriched in Sr content. The positive or negative Sr anomalies reflect plag accumulation or removal in the rocks.

The multi-element variation patterns are characterized by negative Nb and Ta anomalies. In spite of their negative anomalies, Nb and Ta for these rocks are enriched compared to N-MORB. The highest enrichment is shown by HBdite with slight to negligible negative Nb and Ta anomalies. The strongest negative Nb and Ta anomalies are found in CPXnite, PHLtite, LG and DIO. CPXnite has also negative Nb and Ta anomalies. Few samples from CPXnite, CPXnite WHMP and LG show Nb values lower than N-MORB.

Ti concentration, a petrologically important element, is variable from depleted to slightly enriched rocks depending on the abundance of hydrous minerals. LG display the strongest negative Ti anomaly. CPXnite samples have negative to negligible anomalies. However, samples from HBdite, PHLtite and DIO have positive anomalies and are enriched relative to N-MORB. CPXnite WHMP with varying amounts of hydrous phases show both depleted and enriched values relative to N-MORB.

Zr contents show both enriched and depleted patterns relative to N-MORB. Zr in PHLtite is relatively depleted while HBdite samples show depleted to enriched values. CPXnite samples showing positive anomalies are enriched relative to N-MORB. LG has no anomaly while DIO displays enrichment relative to N-MORB. CPXnite WHMP samples have also highly variable Zr contents similar to Ti, Nb, P.

The P anomalies are also highly variable. The samples from CPXnite except for one, PHLtite and HBdite display strong negative P anomalies.

CPXnite WHMP displays both strong negative and positive P anomalies. The DIO sample and one CPXnite sample display strong positive anomaly for P. The large variation may be due to rare sporadic occurrence of ap domains in the rocks.

As discussed above, the marked differences are observed in Th, Nb, P, Zr and Ti contents, which are characteristically important for the interpretation of the source rock and tectonic environment. The presence and abundance of hydrous minerals strongly affect the anomalies.

The multi-element patterns of the rocks, normalized to N-MORB values of Pearce (1982), are compared with those from well-known tectonic settings such as BABB (East Scotia Sea, Mariana Trough, Lau and North Fiji basins, Bransfield Strait; data from Saunders and Tarney, 1991), OIB and MORB (average values from Sun and McDonough, 1989) (Figure 116). Spider patterns of the studied rocks show enrichment for almost all elements relative to MORB (Sun and McDonough, 1989) and differ from MORB (Figure 116a). The rocks have different patterns than those of BABB in having higher K, Ba, Th and negative trough of Nb-Ta (Figure 116b). The rocks also show higher Ce, P and Sm than those of BABB. The studied rocks mainly differ from OIB in having negative Nb-Ta anomalies, despite their relative enrichment than those of MORB (Figure 116c). PHLtite and DIO show higher Ba and Rb concentrations than OIB. Moreover, the rocks contain lower Zr and Hf concentrations than those of OIB. P concentrations of rocks showing both negative and positive anomalies depending irregularly enrichment of ap in the rocks, show similarities to OIB by there positive anomalies. Sm, Ti, Y and Yb concentrations reach levels of those from OIB although most of the samples show lower values than OIB. Even though, the studied rocks show enrichment and depletion values comparable with OIB, they show characteristic LFSE content of CAB with depletions in Nb-Ta comparable with OIB. Such variations in high LFSE/HFSE ratios and negative anomalies of Nb, Ta and Ti are typical of all island-arc, calc-alkaline rocks. For example, especially the very distinctive Ba enrichment is a peculiar feature of ultramafic xenoliths containing also phl as in extreme cases from the Philippine arc (Maury et al., 1992).
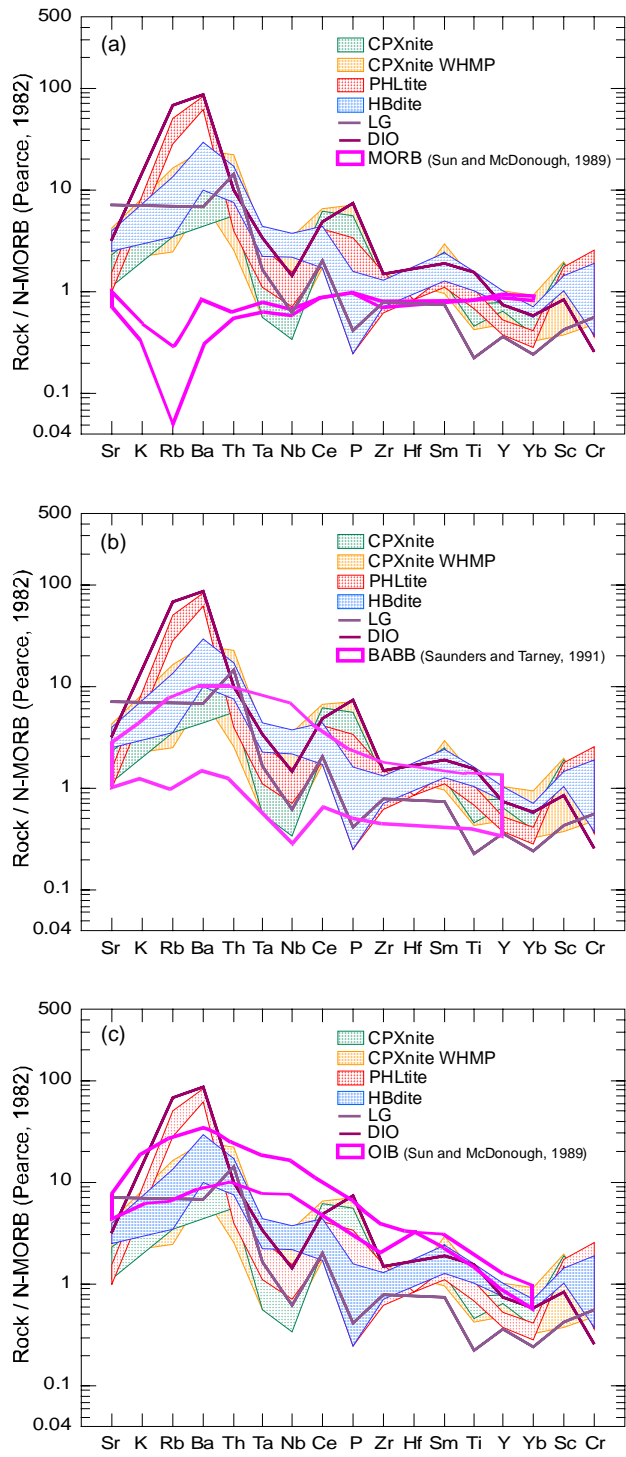
Figure 116. N-MORB-normalized trace element patterns after Pearce (1982) for the studied rocks and their comparisons with well-known tectonic settings. Data taken from OIB and MORB averages from Sun and McDonough (1989), BABB from Saunders and Tarney (1991).

HFSE, having negative anomalies relative to adjacent elements, are also fractionated from each other such that Nb/Ta ratio ranges between 7.3 and 24 (with an average of 14.9), and Zr/Hf ranges between 17.7-29.3 (with an average of 31.1) (data for Zr and Hf are available only from 5 samples from the rocks). Ti and Eu contents of the rocks, which vary from depleted to enriched relative to N-MORB, display a wide range of Ti/Eu ratio (1853-12164) with an average of 6969 while the ratio for N-MORB is 7451. Moreover, Ca/Al and Na/Al ratios are highly variable (0.63-3.38 with an average of 1.67, and 0.04-0.14 with an average of 0.09, respectively).

5.6.1.1. Comparison with High-K Calc-alkaline and Alkaline Basalts

Incompatible trace element patterns of each rock type, normalized to N-MORB values from Pearce (1982), are separately compared with rocks having high-K calc-alkaline (from New Hebrides: Gordon, 1977) and alkaline (from Grenada, Lesser Antilles: Pearce et al., 1984) characters (Figure 117).

CPXnite show lower Sr, K, Rb, Ba contents than both high-K calc-alkaline and alkaline rocks (Figure 117a,b). Nb and Ta contents of CPXnite are comparable with those of high-K calc-alkaline rocks while Zr and Hf values are comparable with those of alkaline ones. Ce, P, Ti, Y, Yb enrichment levels range between high-K calc-alkaline and alkaline rocks. CPXnite is enriched in Sc and Cr contents relative to high-K calc-alkaline rocks.

The CPXnite WHMP samples having variable amounts of hydrous phases and plag, display compositions ranging between those of high-K calc-alkaline to alkaline basaltic rocks (Figure 117c,d).

The PHLtite samples, dominated by phl, are strongly enriched in K, Rb, Ba relative to high-K calc-alkaline and alkaline basalts (Figure 117e,f). Th contents are almost the same as in high-K calc-alkaline basalts. Nb and Ta contents are higher than in high-K calc-alkaline rocks but lower than the alkaline ones. P content of PHLtite is highly variable, ranging from depleted to enriched, and the maximum value of P is very close to that of high-K calc-alkaline rocks. Zr, Hf and Ti values are similar to those of high-K calc-alkaline
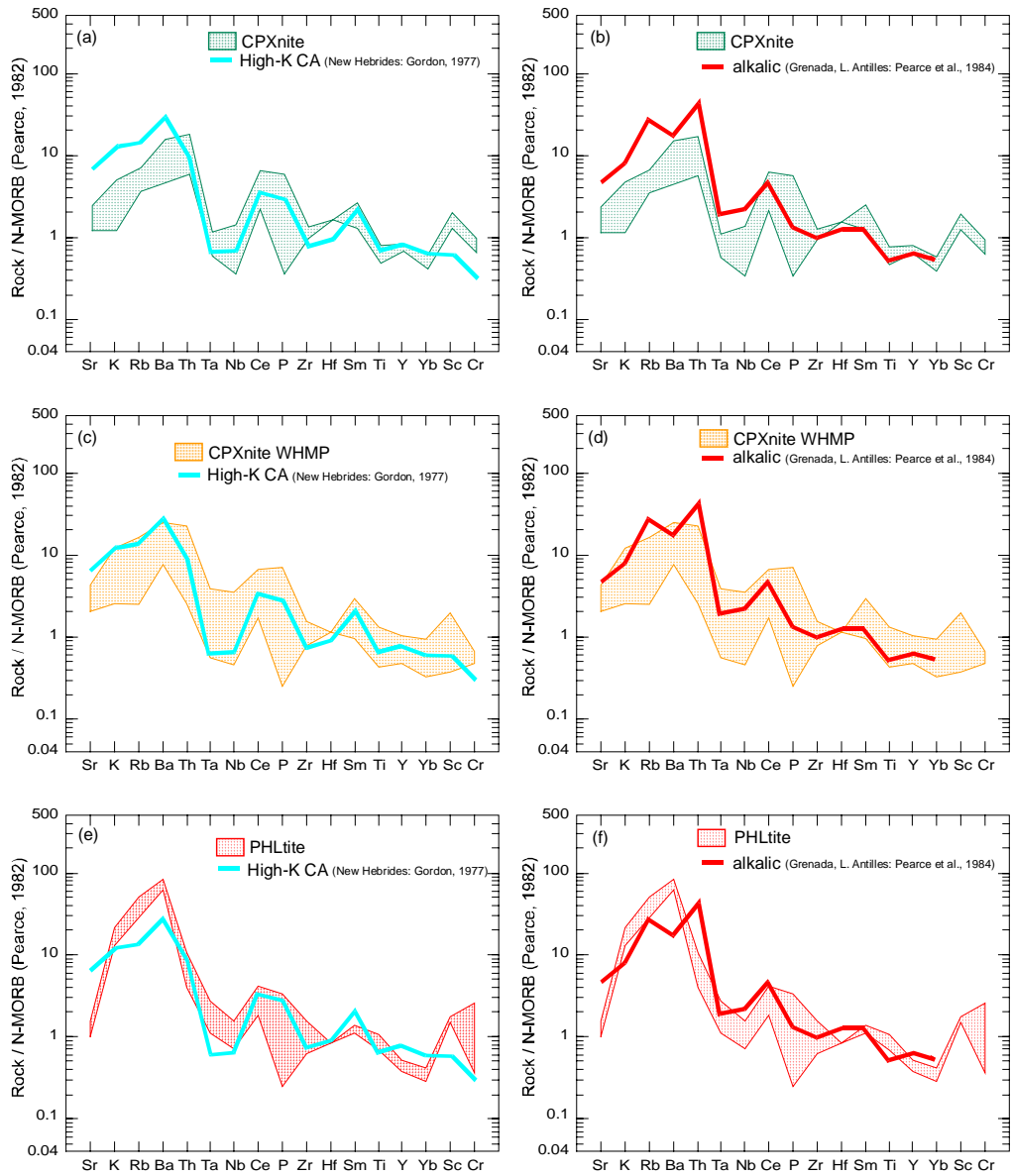
Figure 117. N-MORB-normalized trace element patterns after Pearce (1982) for the studied rocks and their comparisons with high-K calc-alkaline (high-K CA) (from New Hebrides: Gordon, 1977) and alkaline basaltic rocks (from Grenada, Lesser Antilles: Pearce et al., 1984).
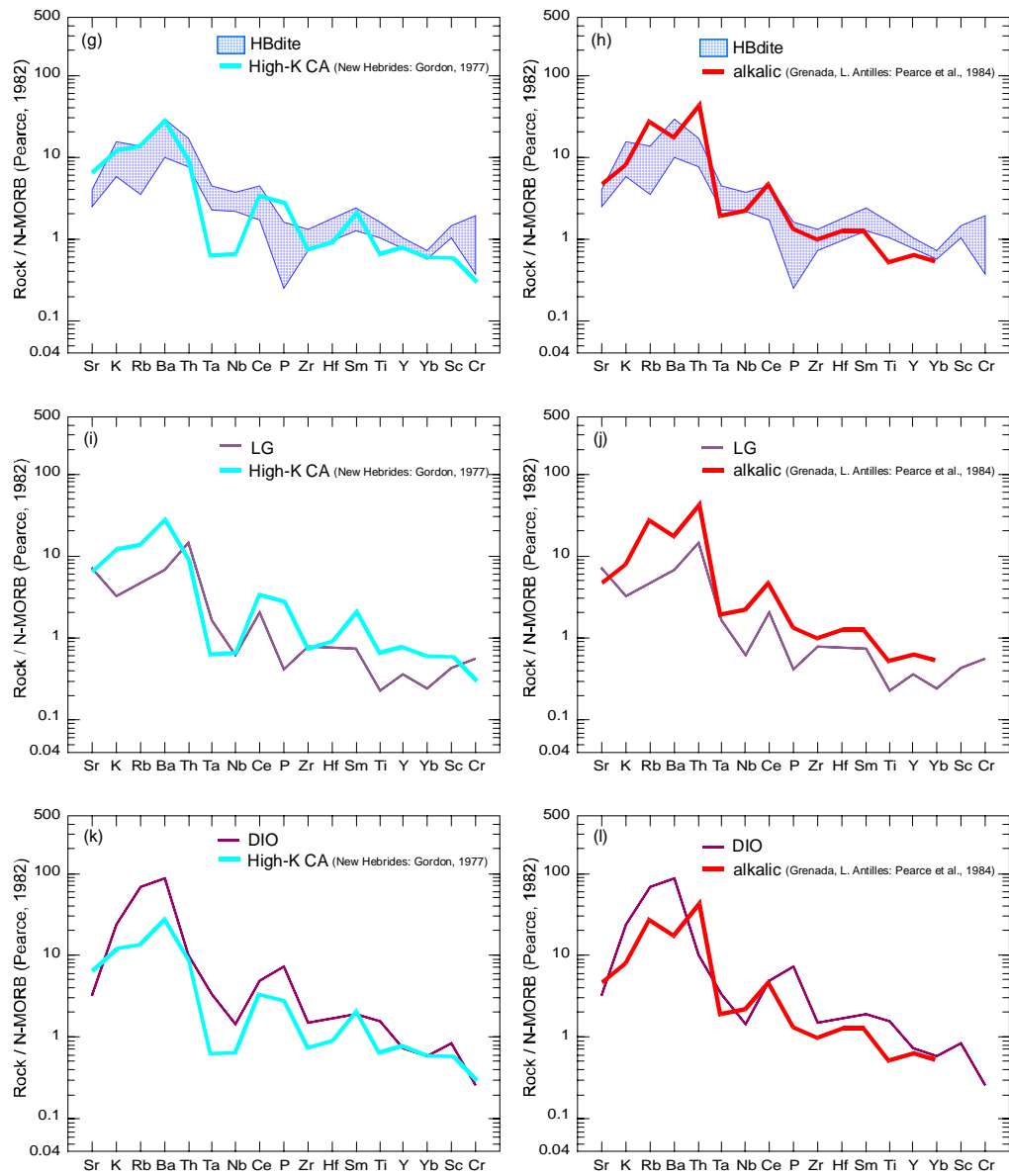
Figure 117 (continued).

rocks. PHLtite samples are enriched Cr and Sc relative calc-alkaline basaltic rock.

The HBdite samples have Nb, Ta, Zr, Hf contents similar to alkaline basalt while the rest of the elements are most similar to those of high-K calc-alkaline rocks (Figure 117g,h). HBdite is enriched in Sc and Cr relative to high-K calc-alkaline rocks.

Similar to ultramafic rocks, the LG sample shows a transitional character between high-K calc-alkaline and alkaline rocks (Figure 117i,j). Nb, Ta values are similar to those of calc-alkaline one while Ti content is lower than those of high-K calc-alkaline and alkaline ones. Unlike ultramafic rocks, Cr and Sc contents of DIO are comparable to those of high-K calc-alkaline rock.

The last rock type, DIO, dominated by Fe-enriched phl and plag, has a pattern quite similar to that of PHLtite. Nb and Ta contents are similar to those of alkaline basalt (Figure 117l). P concentration is higher than high-K calc-alkaline and alkaline rocks (Figure 117k). Cr and Sc values are similar to high-K calc-alkaline ones.

In summary, the studied rocks mainly show a high-K calc-alkaline character with some transitional features to an alkaline character. Especially, the samples with abundant hydrous minerals are similar to alkaline basaltic rock in terms of Nb, Ta, Zr, Hf and Ti contents.

5.6.2. Rare Earth Element Diagrams

The N-MORB normalized REE patterns are characterized by significant enrichment in light REE (LREE) relative to heavy REE (HREE) and N-MORB (Figure 118). HREE are depleted compared to N-MORB. Thus, the patterns are characterized by a steep slope. The high abundances of amph and py may explain enriched LREE pattern relative to N-MORB because these minerals are the major host of middle- and heavy-REE.
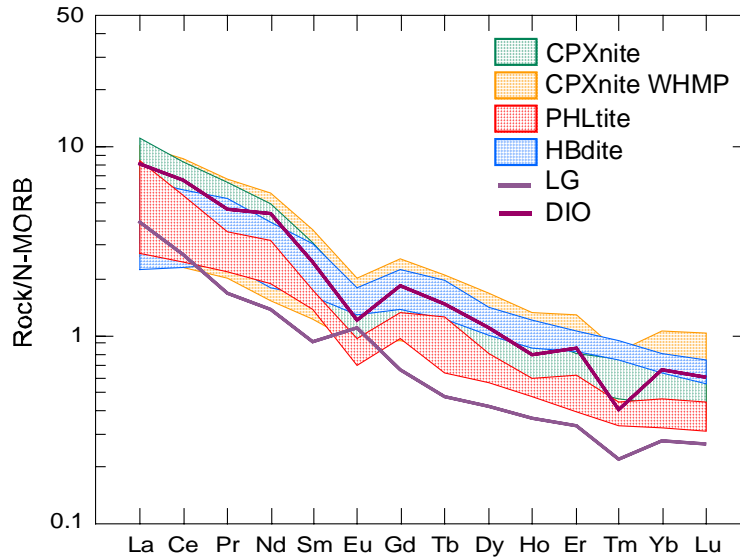
Figure 118. N-MORB-normalized REE patterns for the studied rocks (normalization data from Sun and McDonough, 1989).

N-MORB normalized $(La/Yb)_n$ and $(Sm/Nd)_n$ ratios for ultramafic-mafic rocks are 7.41-21.35 and 0.56-0.73, respectively. This variability is highly controlled by modes of the constituents in the rocks. CPXnite WHMP having variable amounts of hydrous minerals and plag has a wide range of REE values overlapping all of the rocks. LG shows the lowest enrichment in LREE and the highest depletion in HREE.

Even though CPXnite WHMP, HBdite and DIO samples have variable amounts of plag, all the rock types except for LG show pronounced negative Eu anomalies, contrarily LG shows a strong positive Eu anomaly.

The parallel patterns from multi-element and REE variations for all types of the studied ultramafic-mafic rocks suggest that they are possibly petrogenetically related. The rocks are highly enriched in LILE with troughs at Nb-Ta and Ti. The rocks which are also enriched in LREE, show high LREE/HREE and $(La/Yb)_n$ ratios. In the light of trace element data, the rocks show compositions similar to high-K calc-alkaline series with some transitional features to alkaline rocks. These features are typical of subduction related magmas (e.g. Pearce, 1983) because enrichment in LREE, and in particular

elements, such as Rb, Ba, U, and Sr, K, is consistent with refertilization from a subducting-slab-derived fluid. The trace element enrichment in CPXnite (e.g. low Sm/Nd=0.25), showing parallel patterns to those of hydrous mineral enriched rocks, may reflect enrichment also in cpx because CPXnite is dominated by cpx. If this is the case, the trace element enrichment in cpx, and presence of phl and parg in the rocks are consistent with a metasomatic agent that was hydrous in nature (Menzies, 1983; Brandon and Draper, 1996). Moreover, the occurrence of calc-alkaline plutonics may reflect mature arc (Miyashiro, 1974).

CHAPTER 6

DISCUSSION ON THE GENESES
OF THE KURANÇALI ROCKS

6.1. General Features

The ultramafic-mafic plutonic rocks from the Kurançalı area, found as an allochthonous isolated body on a metamorphic ophiolitic mélange, are mainly composed of cpx, phl, parg and high Ca-plag in varying modes and crystal sizes from fine-grained to pegmatitic. The order of crystallization for the minerals of the studied cumulate rocks is cpx → phl → parg → plag. They have accessory Ti-saturated phases (sph, rt, ilm), pyr and ap. Both, rocks and their constituent minerals display unusual chemical compositions.

The LILE–LREE enriched rocks from the Kurançalı area, which are ol and opx free, are characterized by moderately high Mg# (0.44-0.75) and low contents of compatible elements (Cr=47-651 ppm and Ni=16-38 ppm) compared to primary basaltic melts (Wilson, 1989). These features may be representative for several magmatic processes such as fractional crystallization, crustal contamination, removal of an ol-rich fraction early in the evolution of the magma in the source area, a low degree of partial melting, mantle metasomatism, or a combination of these processes (Alirezaei and Cameron, 2002). The relatively low Mg/Fe ratios and the low Cr and Ni contents in the rocks might be attributed to an early fractionation of ol in the source area, or a low degree of partial melting from a depleted mantle source. The absence of major Mg-rich cumulates, such as peridotites, argues against fractional crystallization as the main cause of the enrichment in LILE-LREE. Mg is a compatible element that fractionates into the early-phase minerals,

whereas Fe concentrates in the residual melt, during crystallization of mafic magmas. HFSE behave incompatibly during crystallization of mafic magmas, concentrating in the last, Fe-rich fractions. However, enrichment of LILE and LREE relative to HREE and HFSE suggest that a depleted mantle was metasomatized by LILE–LREE bearing fluids/melts. The high LILE/HFSE ratios may be attributed to the introduction of LILE from a subducting oceanic crust (e.g. Pearce, 1983; Hawkesworth et al., 1994).

6.2. Mineralogical Constraints

Phl, characterized by a gradational change in composition from ultramafic to mafic rocks, has higher MgO and Al_2O_3 but lower $FeO^{(t)}$ and TiO_2 concentrations in PHLtite and CPXnite than that in the mafic rocks. Depletion of TiO_2 content in phl from ultramafic rocks should be caused by Ti-rich phases (rt, ilm and sph). Substitution mechanisms and chemistry of phl point out a typical calc-alkaline character to the host rocks with transitional features to alkaline compositions. However, the studied phl is not deficient in tetrahedral cations as that in metasomatized mantle xenoliths carried by kimberlites and related rocks (Dawson and Smith, 1977).

Phl displays remarkably low $Fe^{2+}/(Fe^{2+}+Mg)$ ($Fe^{2+}\#$) ratios of 0.25-0.51. According to Rowins et al. (1991), dark mica compositional trends with low $Fe^{2+}\#$ are unmistakably magmatic, although the minor development of hydrous replacement indicates a limited extent of late- to post-magmatic fluid alteration. Despite their magmatic origin based on Rowins et al. (1991)'s definition, the studied phl having positive correlation between $Al^{(t)}$ and Mg do not show a magmatic fractionation trend defined by Hecht (1994) with a negative relation of Mg and $Al^{(t)}$. This relation may indicate metasomatism in source. Moreover, $Al^{(t)}$ content, which is quite high, is comparable to that of phl in alkaline rocks and peridotitic xenoliths (both suboceanic and subcontinental) metasomatized by alkaline rocks. Ti and $Fe^{(t)}$ contents are also similar to those of metasomatic phl. However, Mg# values of phl in the studied rocks, in agreement with compositions of other mafic minerals and of whole-rock samples, are lower than those in metasomatic rocks in literature. Published Mg# values range from 0.64 to 0.92 for phl's in xenoliths carried by alkaline

lavas (Ionov and Hofmann, 1995) and between 0.93 and 0.95 in phl from the peridotite at Finero (Zanetti et al., 1999) which were metasomatized by subducting slab components. In the Lherz complex occurrences affected by multiple metasomatic episodes show Mg# between 0.86-0.91 (Woodland et al., 1996; Zanetti et al., 1996) and a range of 0.89-0.95 for phl's from South African gr-phl-peridotite xenoliths in kimberlites was published by Erlank et al. (1987).

Phl of the studied rocks, having relatively high Fe^{2+}, Fe^{3+}, $Al^{[6]}$, Ti contents, differ from those originated in continental arc-related magmas (Feldstein et al., 1996) while they show similarities to those generated in OIB related oceanic environments (Fitton et al., 1991). Despite some similarities to phl in OIB-type rocks, the studied ones have higher OH- and Al-contents, and lower Si concentrations. In addition, phl of the studied rocks are enriched in Ba compared to phl from mantle derived alkaline rocks. This may infer a derivation from a subducting slab and addition to an overlying mantle wedge peridotite. Phl crystallizing just after cpx in the studied rocks might have taken most of Ba into their structure because Ba easily enters mica structures during the earliest stages of crystallization (Shaw and Penzack, 1996). These compositional features and the calc-alkaline character, which is slightly transitional to alkaline, may infer a process of alkaline metasomatism in an intra-oceanic arc environment.

Cpx (di, di-aug) composition, displaying intra-crystal and inter-sample variations, covers a wide range (Mg#=0.64-0.88, 0.02-1.25 wt% TiO_2, 0.36-8.66 wt% Al_2O_3, 0.10-0.97 wt% Na_2O). Chemistry of cpx infers a calc-alkaline rather than a tholeiitic character as discussed in Section 4.3.5. Comparison between cpx of the studied rocks and cpx from oceanic rocks of different tectonic settings infer an island arc environment rather than MOR. cpx from the Kurançalı rocks show higher Ti, Na, $Al^{(t)}$, $Al^{[4]}$ contents than those from island arc related rocks. High Si content, almost filling the tetrahedral site, characterizes cpx of the studied rocks. Various plots revealing the control of the degree of alkalinity in substitutions of Si, Al, Ti, Ca and Na on the cpx lattice (Le Bas, 1962; Leterrier et al., 1982) display a transitional character between subalkaline to alkaline (discussed in Section 4.3.5.). In spite of a

transitional character to an alkaline composition, the tetrahedral site is almost filled by Si and there is no deficiency, as observed in cpx crystallized from alkaline magmas (Conticelli, 1998 and references therein). A transitional character of cpx with a wide range of compositions may indicate a complex history for the rocks. The studied cpx with high Ca, $Al^{(t)}$ and relative high Ti contents show some transitional features comparable to those of cpx's from metasomatized mafic-ultramafic xenoliths in alkaline melts. Therefore, the cpx's may infer crystallization from a system metasomatized by an alkaline melt rather than formation from alkaline melt itself. The zoned cpx crystals show Al-Ti-Na-K-poor and Si-rich cores, overgrown by Al-Ti-Na-K-rich, relatively Si-poor rims similar to cpx from alkaline metasomatized gabbros and alkaline cumulate xenoliths from La Palma (Neumann et al., 2000). Relatively high Na content and a weak fractionation trend (defined by relation of Ti and $Al^{(t)}$ to $Fe^{(t)}/(Fe^{(t)}+Mg)$) also support metasomatism. The chemistry of cpx indicates interaction between a magma and a depleted peridotite, i.e. mantle metasomatism (Litasov et al., 2000).

Cpx of the studied rocks are similar to cpx from adakitic and alkaline metasomatized xenoliths (discussed in Section 4.3.5.). They show a transitional character to cpx in carbonatite metasomatized xenoliths with traces of old basaltic metasomatism. This may be inferred from interstitial parg and phl, accessory minerals (rt and ap) and lack of glass (Gorring and Kay, 2000) and may result from reactions of a depleted peridotite with basaltic melts (e.g. Menzies et al., 1987) or H_2O-rich fluids (O'Reilly and Griffin, 1988).

Textural (intercumulus phase enclosing cpx, and primary pegmatitic grains) and compositional (rich in Ti and alkalis) characteristics of parg infer primary crystallization, similar to those reported in amph-gabbros, e.g. Tonsina, Alaska (Burns, 1985; DeBari and Coleman, 1989), as well as in lower crustal xenoliths from mature island arcs, (e.g. the Aleutian arc, DeBari et al., 1987). Parg from the Kurançalı area differs from those in plutonic rocks from continental margins, tholeiitic island arcs, Troodos type intrusives, cumulates from MOR by extensive substitution of $Al^{[4]}$ for Si, and higher K_2O-contents as discussed in Section 4.4.6. High $Al^{[4]}$ content of parg, is similar to that from metasomatized oceanic gabbro xenoliths and alkaline cumulates from the

Canary Islands (data from Neumann et al., 2000). Thus, this gives a strong support for crystallization from an alkaline magma. K_2O content of parg is higher than those from MOR while Na_2O, TiO_2 contents are quite lower than those from alkaline metasomatized and alkaline cumulate rocks of La Palma. Their Na/K ratios are comparable to those from the La Palma rocks. parg closely matches those in transitional adakites in the island arc environment from the Lesser Antilles in terms of Na+K and Ti contents although it shows similarities to those of La Palma. These observations may propose a system metasomatized by alkaline magma rather than alkaline magma itself in an arc environment.

Comparison of parg in the studied rocks with amph's from hydrous low Mg - high Al basalt to rhyolite showed that its composition relies closest to that in equilibrium with hydrous basalts / basaltic andesite, and andesite in terms of $Al^{(t)}$ content (discussed in Section 4.4.6.). However, Na+K in A site and Ti content of parg is similar to that from felsic melts. These compositional comparisons support the idea that the history of the system is complex and it is affected by more than one compositional event.

Parg having high-Ti values (0.96-2.61 wt%) may have a further importance for the assumption of primary phl. Johnson et al. (1996) assumed that high Ti-amph (0.82-3.66 wt%) generally, have high K_2O suggesting a transition to K-rich environment where phl might occur with amph. High-Ti (>1.5 wt%) in amph is also characteristic of interaction between magma and peridotite resulting in formation of hydrous upper mantle (Johnson et al., 1996). This can be explained by hybridization of magmas above subducting oceanic crust.

Plag mainly characterized by high an content (>70 %) display a wide range of composition (an %= 40.61-98.58) with negligible K-feld content for all rock types. A wide range of an % may infer a later re-equilibration due to introduction of Na into the system. The plag crystals in HBdite, found both as material between parg crystals and small euhedral crystals enclosed in parg, display identical compositions. This compositional similarity may indicate that

small euhedral crystals of plag enclosed in pegmatitic parg might be due to filter pressing.

The presence of ap in the studied rocks may infer CO_2 in the system from which cpx, parg, phl and Ti-rich accessory phases (rt, ilm, sph) crystallized. Pyr, accessorily present in the rocks, may indicate that S is an important element of the metasomatic fluid to produce pyr from decomposed oxides (Haggerty, 1991).

The presence of primary magmatic parg and phl (Green, 1982), and the late crystallization of high-Ca plag (Burnham, 1979; Allan and Carmichael, 1984) requires introduction of significant amounts of water into the source. They favor high water pressure and oxygen fugacities during the formation of the Kurançalı ultramafic-mafic rocks. High oxygen fugacity is also evidenced by phl composition displaying NNO to HM buffer conditions. This is not characteristic for peridotites from MOR or BAB (Pearce et al., 2000). Therefore, the studied rocks are expected to have formed in marginal basin settings above subducting slabs of oceanic crust. That means, the parental magma should be compatible with a process of hydrous partial melting of a mantle source affected by previous metasomatic events. In addition to the observed mineral assemblages, whole-rock trace element enrichment pattern for CPXnite dominated in cpx (as will be discussed below) infers metasomatism at high oxygen fugacities (Menzies, 1983; Brandon and Draper, 1996).

Because there is no appropriate geothermobarometer for the mineral assemblages of the rocks, various geothermobarometer estimations were applied for the allochthonous ultramafic-mafic plutonic rocks just to constrain pressure-temperature conditions. The pressure-temperature estimates with various limitations giving just an approximation for crystallization conditions rather than accurate values are summarized as following: Phl follows a low-pressure trend (5-15kbar±4kbar and 1090-1160°C) on qualitative geobarometer after Righter and Carmichael (1996). Temperature based cpx geobarometry calculations (Nimis, 1995, 1999; Nimis and Ulmer, 1998) give 5.83-16.45 kbar (11.38±1.72 kbar) using the qualitatively estimated

temperature values (675-937°C with an 809±46°C after Lindsley, 1983). Al[4]-Al[6] relation in cpx providing an opportunity of qualitative estimation for pressure suggests low pressure (after Aoki and Kushiro, 1968; Aoki and Shiba, 1973). cpx with high Ca# is defined to originate at low pressure (<11 kbar) based on the Litasov et al. (2000)'s approach.

Qualitative pressure estimation based on Al[4]-Al[6] relation in amph after Fleet and Barnett (1978) and Raase (1974) suggests pressure of crystallization less than 5 kbar. Temperature calculations based on pressure dependent ed-rich thermometer of Holland and Blundy (1994) gives 828±55°C at P=0 kbar, 865±66°C at P=5 kbar, 911±70°C at P=10 kbar, and 956±75°C at P=15 kbar. Temperature was separately calculated at pressures of 0, 5, 10 and 15 kbar. Whatever pressure is assumed, amph-plag equilibration temperature is higher than 825°C. Moreover, pressure independent temperature calculations (Colombi, 1989) result in 844±49°C that is intermediate between the average temperatures obtained at pressures of 0 and 5 kbars using the thermometer of Holland and Blundy (1994). Qualitative geothermometer based on amph-cpx assemblage (Perchuk et al., 1985) results in a temperature range of ~750-980°C. Semi-quantitative geothermobarometer of Ernst and Liu (1998) giving a range of ~750-925°C supports the previous results. Moreover, this is consistent with Ernst and Liu (1998)'s interpretation indicating that parg'tic amph forms at 800-950°C. However, estimated pressure range (~8,5-18 kbar) is higher than that estimated by other methods using amph, but relatively consistent with those obtained from phl and cpx. Intense substitution of Al[4] for Si in the tetrahedral position of parg may indicates crystallization at high temperature and low pressure as proposed by Adam and Green (1994).

6.3. Geochemical Constraints

The rocks except for CPXnite show quite scattered plots on geochemical and tectonic discrimination diagrams due to their hydrous mineral contents. However, all samples of the studied ultramafic-mafic rocks display parallel N-MORB trace-element and REE patterns. All patterns, characterized by strong

enrichment in LREE and LILE relative to HREE and HFSE, show strong positive anomalies for Rb, Ba, K, Th, Sr, negative trough for Nb-Ta, strong depletion in P with few exceptions, and relatively depleted to negligible Zr, Hf, Ti anomalies. The rocks showing transitional features of high-K calc-alkaline and alkaline melts may infer subduction-related or crustal-derived melts. The troughs observed at Nb-Ta and Ti for the rocks, however, strongly favor subduction related magmas (e.g. Pearce, 1983). Because the negative Nb anomaly is a characteristic feature in arc environments, and has been explained in terms of retention of this element within amph, rt, sph during dehydration and/or partial melting of the subducting plate (Pearce and Peate, 1995; Pearce, 1996; Noll et al., 1996) or their low solubility in transporting fluids (e.g. Noll et al., 1996). Moreover, enrichment in LFSE and/or LILE elements is now widely attributed to metasomatism of a sub-arc magma source due to transfer of melt or fluid from the subducting oceanic crust (e.g. Noll et al., 1996). The multi-element variation patterns are similar to those from intra-oceanic island arc basalts (e.g. Pearce et al., 1984, 1994; Teklay et al., 2002).

In addition to normalized multi-element and REE patterns of the ultramafic-mafic rocks, elemental ratios and ratio-ratio diagrams give indications about the genesis (i.e. subduction related enrichment vs. crustal contamination).

The rocks display higher Sr/Nd (5.91-83.7) (few lower values are present due to high enrichment of Nd, as well), U/Nb (0.05-0.45), Th/Yb (0.47-3.49), and lower Ce/Pb (0.32-8.90), Nb/La (0.15-0.76) and Ti/Eu ratios (1853-12164, highly variable with quite low ratios) than those of average N-MORB (Sr/Nd=12.33, U/Nb=0.02, Th/Yb=0.04, Ce/Pb=25.0, Nb/La=0.93, and Ti/Eu=7451; Sun and McDonough, 1989). The rocks with high Sr/Nd, U/Nb, Th/Yb, and low Ce/Pb, Nb/La, Ti/Eu ratios show strong volcanic-arc signatures. In addition to these ratios, LREE enrichments such as $(Sm/Nd)_{N-MORB}$=0.55-0.90 (for N-MORB =0.36), are characteristic for volcanic-arc rocks which may reflect either an addition of slab-derived fluids to the mantle wedge melting region (Perfit et al., 1980; Pearce, 1983) or the melting of slightly

enriched mantle wedge source with the presence of a HFSE-bearing residual phase (Morris and Hart, 1983; Sun and McDonough, 1989).

Moreover, the samples plot in subduction related fields on ratio-ratio diagrams (Figure 119a,b,c). Most of the data plot in an area where continental margin arc/alkaline oceanic arc fields overlap while few plot in oceanic arc field on the Th/Yb - Ta/Yb diagram of Pearce (1983) (Figure 119a). The elemental ratios, Nb/Y, Nb/Zr, pled against a Nb-enriched source such as continental lithospheric mantle (CLM) (Figure 119b, c). CLM origin is also done away with by Ta/Yb, La/Ta, Ce/Pb ratios (Figure 119a,b). The covariation of Th/Ta and La/Ta suggest a mixing process between a mantle and a Th-La enriched end-member (Figure 119d). The high ratios of Ba/La (7.1-197), Sr/Ce (4.12-41.9), Ba/Rb (4.94-72.8) may support fluid metasomatism of mantle wedge due to subducting oceanic slab (e.g. Serri, 1990).

Ce/Nb and Th/Nb ratios are compared with average continental crust composition and various basaltic rocks such as ocean ridge basalt (N-type and E-type MORB), island arc basalt (IAB), back-arc basalt (BAB) and intra-plate basalt (OIB) (compiled from Saunders and Tarney, 1991). The high ratios of calc-alkaline rocks display a transitional character between those of IAB and BABB (Figure 120a). This transition should arise from relatively high Nb content in hydrous mineral bearing- and enriched-rocks. The samples are plotted in the Ce/Nb-Ce diagram after Abouchami et al. (1990) (Figure 120b). In this diagram, the samples with significantly high Ce/Nb ratios mostly plot in IAB field. However, some of the samples plot outside of the field because of their considerably higher Ce concentrations than OIB rocks. The ultramafic-mafic rocks with high Ce/Nb and Th/Nb ratios display features of arc magmatism relatively enriched in OIB-like composition.

Even though, trace element characteristics of the rocks suggest an arc setting, the rocks show a relative enrichment in Nb, Ta, Ti, and Zr with respect to average N-MORB (Sun and McDonough, 1989). What type of source can be responsible for the enrichment of these elements, i.e. a subduction component or an OIB-like silicate melt? The rocks with higher Nb/Yb (0.92-5.42), Zr/Yb (31.0-99.3) and Ti/Yb (2267-8653) ratios than average N-MORB (Nb/Yb=0.76,
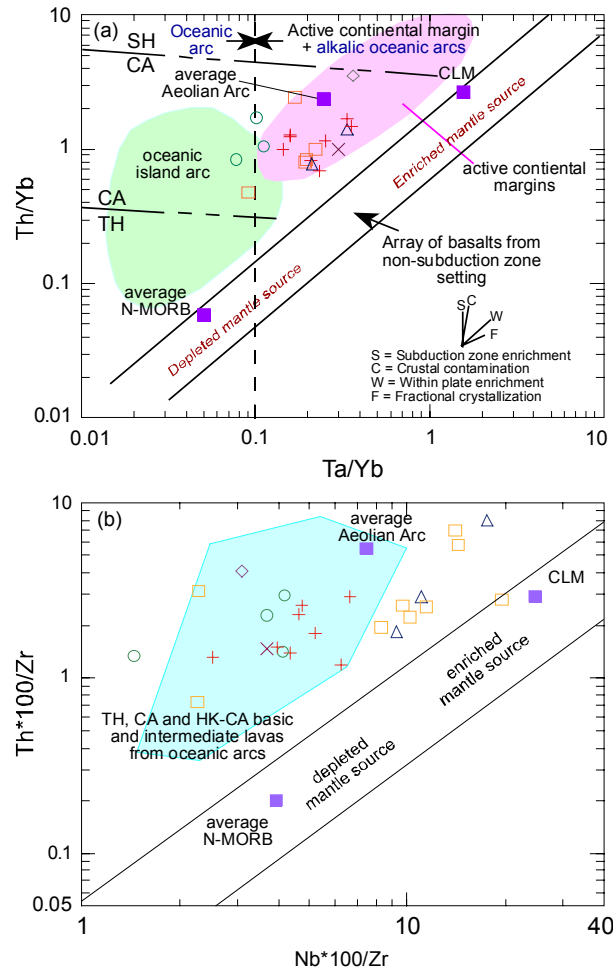
Figure 119. Covariations of incompatible element ratios and their comparisons with average N-MORB (compiled from Rottura et al., 1998), Aeolian arc volcanics (Francalanci et al., 1993), oceanic island arc (OIB) (Karsten et al., 1996), continental lithospheric mantle (CLM) (McDonough, 1990). (a) Th/Yb-Ta/Yb (after Pearce, 1983), (b) Th*100/Zr-Nb*100/Zr (after Serri, 1990), (c) Ba/La-Ce/Pb (after Haas et al., 1996; Rottura et al., 1998), (d) Th/Ta-La/Ta (SH: shoshonite, CA: calc-alkaline, HK-CA: high-K calc-alkaline, TH: tholeiite) (the symbols are as in Figure 28).
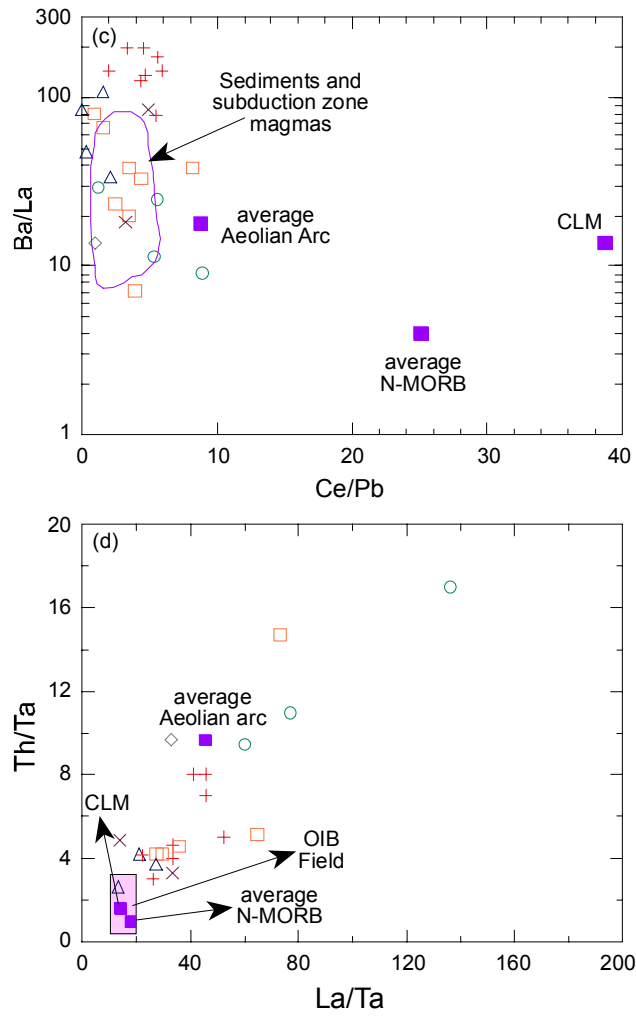
Figure 119 (continued).
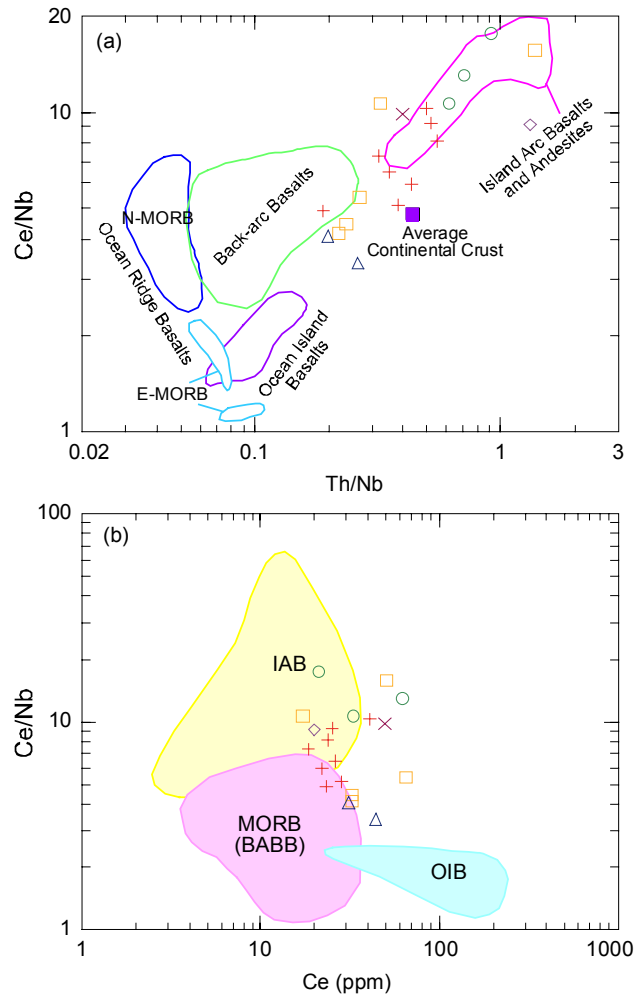
Figure 120. (a) Covariation of Ce/Nb - Th/Nb ratios and for the samples and their comparison with average contiental crust composition and basaltic composition from various tectonic settings (data sources from Saunders and Tarney, 1991), (b) Variation of Ce/Nb ratio against Ce for the samples and comparison of the data with the MORB, IAB and OIB fields compiled from Abouchami et al. (1990) (the symbols are as in Figure 28).

Zr/Yb=24.3 and Ti/Yb=2492) indicate a contribution from an incompatible element-enriched melt as observed in OIB-type mantle sources. For example, covariation of Zr/Nb and Nb/Yb ratio plots for the samples display that they are mainly aligned along the MORB-OIB array after Pearce and Peate (1995) (Figure 121). This variation indicates that Zr, Ti, and Nb are from OIB-like composition rather than subduction component.
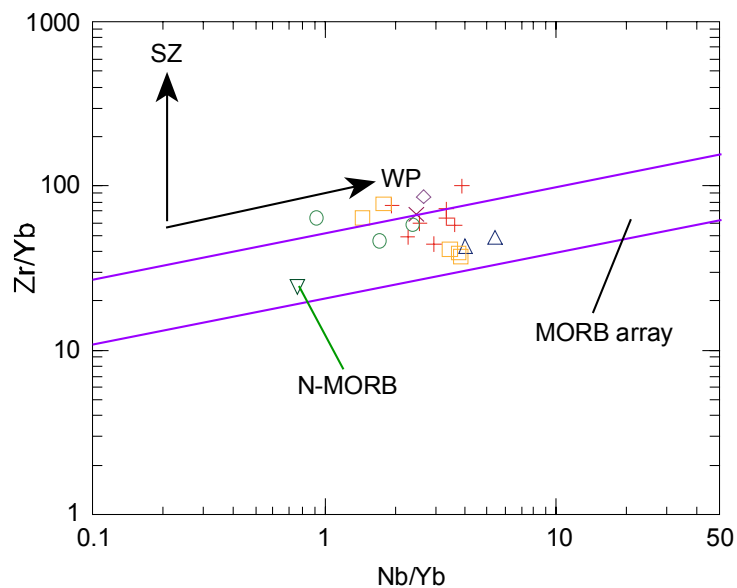
Figure 121. Covariation of Zr/Yb - Nb/Yb ratios for the studied rocks MORB, WP (within plate) and SZ (subduction zone) arrays after Pearce and Peate (1995), average N-MORB from Sun and McDonough (1989) (the symbols are as in Figure 28).

(Sm/Nd)$_n$ ratios (0.56-0.73; chondrite normalization values from Sun and McDonough, 1989) are within the limits of depleted peridotites in an arc environment of a SSZ ((Sm/Nd)$_n$=0.08-1.16; Wang et al., 2001, 2002). However, the (La/Yb)$_n$ ratios (7.41-21.35) are much higher than those of depleted mantle peridotites ((La/Yb)$_n$=4.88-6.59, Wang et al., 2001, 2002) and many gabbros with arc affinity (e.g. Wang et al., 2001, 2002). REE elemental ratios indicate either an initially depleted mantle source that is enriched in LREE by external REE derived from a subducting slab (e.g. Zanetti et al.,

1999; Tribuzio et al., 1999, 2000), or a mantle source that is enriched by an OIB-component before subduction (Teklay et al., 2002).

Arc-generated magmas can tap a multitude of reservoirs including slab-derived fluids, variably depleted and metasomatized mantle wedge, and oceanic crust and sediments from the subducting slab. Melting of mantle wedge peridotite is triggered by aqueous fluids, which originate from prograde dehydration of a subducting slab. Composition of typical arc melts can therefore be quantified by slab dehydration, hydration of the overlying mantle wedge, melting of mantle wedge peridotite, and fractional crystallization/crustal assimilation (e.g. Ayers, 1998). However, melt derived from a subducting slab may also modify the composition of an overlaying mantle wedge. Direct melting of a slab is possible; (1) if the subducting slab is exceptionally young and relatively hot (Defant and Drummond 1990), or (2) if an older and colder slab displays a flat subduction mechanism (Gutscher et al., 2000), or (3) if the edge of a torn old oceanic slab is exposed to mantle flow, it results in slab ablation, heating, and eventually melting lithosphere (Yogodzinski et al., 2001). Magmas thought to represent melts from subducting slabs (wet melting of gr-amphibolite or basaltic eclogite, experimentally shown by Green (1982), Rapp et al. (1991), Sen and Dunn (1994) are collectively known as adakitic melts (Defant and Drummond, 1990) which are typically andesitic to dacitic in composition and characterized by strongly fractionated REE patterns.

The coexistence of melts from the slab itself and from the SSZ mantle wedge is expected because prograde dehydration from relatively hot slabs triggers melting of the mantle wedge peridotite and they can create hybrid melts in which the typical adakite geochemical fingerprint is obscured (Kamber et al., 2002). It is generally argued that interaction of adakite with peridotite do not greatly disturb its original incompatible element ratios (e.g. Zanetti et al., 1999; Kamber et al., 2002). However, the incompatible element content could be seriously affected if the melts include both crust and sediment of an oceanic slab. Even a relatively small melt contribution from metasediments can effectively mimic typical island arc incompatible element geochemistry even though the melt is derived from the slab because this sediment material inherits the chemical signature of continental crust (Kamber et al., 2002).

Yogodzinski et al. (1994) termed the rocks having compositional character overlapping between adakites and typical arc basalts as transitional adakites referring hybrid melts. The rocks from the Aeolian arc are a good example of transitional adakites with their high-Al low-Mg basalt composition (Francalani et al., 1993; Yogodzinski et al., 1994).

The studied plutonic rocks, showing typical N-MORB-normalized patterns of subduction-related magmas, are well comparable with high-Al basalts from the Aeolian arc (Francalanci et al., 1993) (Figure 122) (The comparison of this plutonic rocks with extrusive rocks is done according to Yumul (2002) who proposed that the intrusives of arc system may correspond to extrusives). PHLtite and DIO are more enriched in K, Ba, Rb due to the selective enrichment of the elements (Figure 122c,f). The studied rocks, having different degrees of enrichment in Nb and Ta relative to N-MORB despite their negative trough relative to adjacent elements, show slight depletion or enrichment relative to Aeolian arc basalts. This difference should be the result of selective enrichment of Nb and Ta in amph.

The unusual enrichment in REE of the studied rocks is also similar to that of the island arc basalts from the Aeolian arc (Francalanci et al., 1993), Lesser Antilles Island (Thirlwall and Graham 1984), Agardagh Tes-Chem Ophiolite, Central Asia (Pfänder et al., 2002), Kudi ophiolites, China (Wang et al., 2001, 2002). REE profiles with about 22 to 125 times chondrite LREE concentrations, about 4 to 20 times chondrite HREE abundances are similar to those of calc-alkaline island arc basaltic rocks from the Aeolian arc (Francalanci et al., 1993), and the Lesser Antilles Islands (Thirlwall and Graham, 1984) (Figure 123). The studied rocks differ only in their Eu anomalies, i.e. strong positive anomaly for LG, negative anomaly for the rest of the rocks.

The adakitic affinity of the studied plutonic rocks can be examined by ratio-element and ratio-ratio plots (Figure 124). Because the best distinction between arc magmas from the SSZ mantle wedge and those formed by direct melting of subducted crust (i.e. adakites) is possible with element ratios that are mobile during slab dehydration and refertilizes depleted mantle wedge
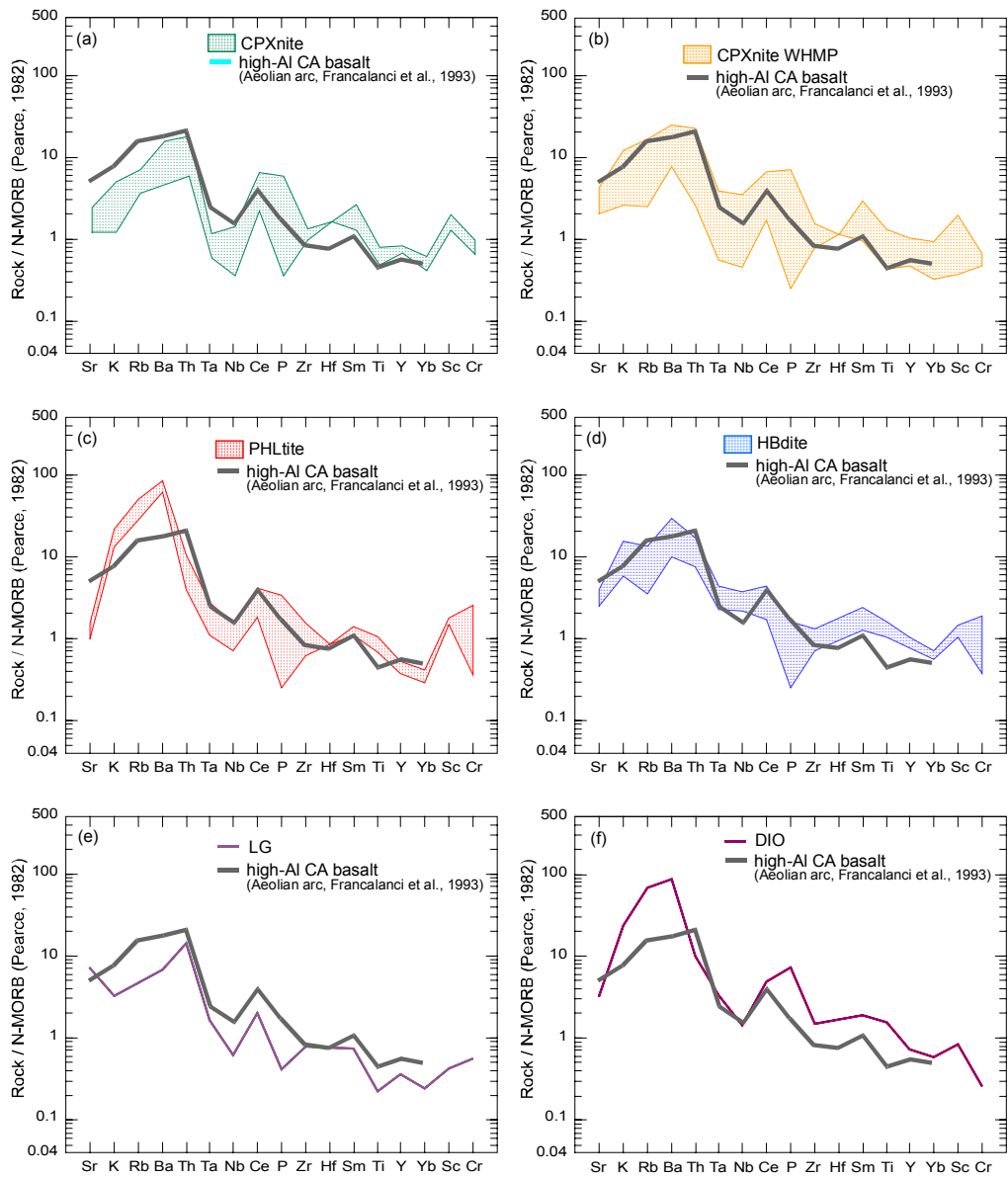
Figure 122. The comparison of N-MORB-normalized trace element patterns after Pearce (1982) with high-Al calc-alkaline basalt from Aeolian arc (Francalanci et al., 1993).

(Defant and Drummond, 1990; Kamber et al., 2002). The Kurançalı rocks, plot in the island arc field with some transitional features to adakite field due to lower Y values (Figure 124a,b). On the other hand, the studied rocks with their high La/Yb ratios plot in adakite field (Figure 124c). The rocks have highly variable Pb/Nd (0.16-0.76) (with an average of 0.39; two anomalous values excluded, 2 (LG sample) and 4.57 (HBdite sample)) and Nb/Ta ratios (7.3-24) (with an average of 14.3). Despite variable values, average of Pb/Nd and Nb/Ta ratios for the rocks are intermediate between those of adakite (Pb/Nd=0.33, Nb/Ta=15.7) and typical arc rocks (Pb/Nd=0.5, Nb/Ta=12.9). Both average ratios are quite different than those for an average continental crust (Pb/Nd=0.50-0.63, Nb/Ta=10) and modern MORB (Nb/Ta=16.7). The average values used for comparison are complied from Kamber et al. (2002).

Figure 123. Comparison of chondrite-normalized REE from calc-alkaline island-arc basaltic rocks from Aeolian arc (pink solid line, Francalanci et al., 1993), and the Lesser Antilles Islands (blue shaded area, Thirlwall and Graham, 1984) (the symbols are as in Figure 28).
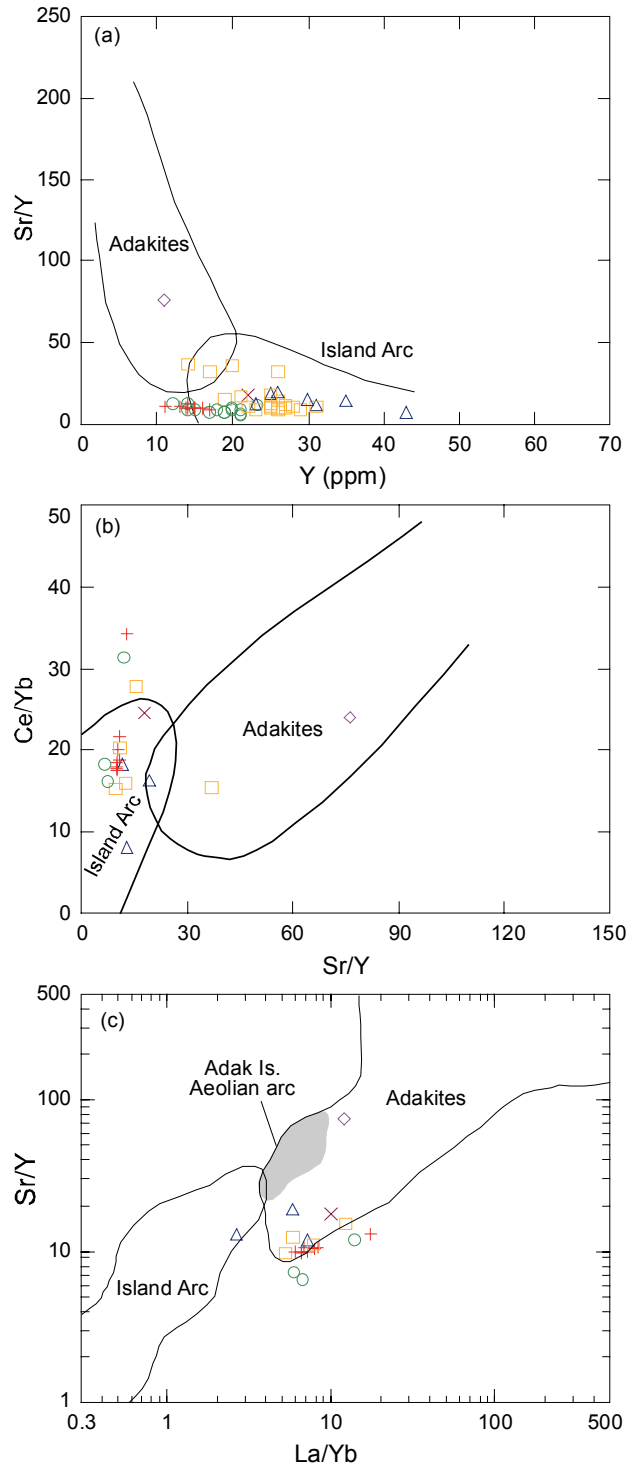
Figure 124. The plots of the studied rocks on (a) Sr/Y-Y, (b) Ce/Yb-Sr/Y and (c) Sr/Y-La/Yb rocks discriminating typical island arc and adakite melts. Fields for adakite and island arc for (a) and (b) from Defant and Drummond (1990) and for (c) compiled from Kamber et al. (2002) (the symbols are as in Figure 28).

The lowest Pb/Nd ratios and the high La/Yb ratios (i.e. those with the strongest adakitic affinity) and the high Pb/Nd values approaching that of typical arc basalts infer that adakitic melts are hybridized with ordinary wedge-derived melts (Kamber et al., 2002) or contaminated by peridotite (Yogodzinski et al., 1995). Moreover, the high variation and quite high values (especially for Pb/Nd) infer a contribution of metasediment into a subducting crustal melt (Kamber et al., 2002). So it can be argued that the studied rocks represent hybrid magmas derived from melting of eclogitic subducted oceanic crust, a subducted sediment component and a SSZ component. The samples with quite high Nb/Ta may indicate enriched mantle wedge.

Major and minor element concentrations of the Kurançalı rocks, which are similar to high-Al basalt with adakitic affinity in terms of trace elements and REE, are compared. Even though the studied rocks are highly variable in composition, all rock types have lower SiO_2 content than high-Al basalts. CPXnite with the highest SiO_2 contents have considerably higher CaO, MgO, Mg#, lower FeO, Na_2O, K_2O concentrations than high-Al basalts (Table 3). Moreover, silica-undersaturated rocks, HBdite and CPXnite WHMP, do not show any relations to high-Al basalts in terms of major and minor elements.

Although the studied rocks are comparable with high-Al basalts in terms of trace and rare earth elements, their major and minor elements are uncomparable. The rocks may be infered as products resulting from interaction of a mantle wedge peridotite and melt derived from a subducting slab. Although trace element content of the slab melt (crust and/or sediment) is not modified highly from interaction, major element composition seem to be modified. The reaction between a slab melt and a subarc mantle results in metasomatism of the subarc mantle that is evident from peridotite mantle nodules (Sajona et al., 2000). Experimental studies also displayed that small amounts of adakitic melt (i.e. peridotite:adakitic melt ratio=1:1) are entirely consumed in reaction with the host peridotite to form metasomatized zones (Sekine and Wyllie, 1983; Carroll and Wyllie, 1989; Sen and Dunn, 1995; Rapp et al., 1999).

Table 3. Comparison of the studied rocks with average high-Al basalts from Aeolian arc (compiled from Brophy and Marsh, 1986) for major, minor elements, and Cr, Ni.

	average high-Al basalt	compositional range for the studied rocks
SiO_2	49.84	38.40-48.80
TiO_2	0.92	0.34-2.97
Al_2O_3	18.98	6.14-19.00 (26.7 for LG)
Fe_2O_3	-	0.25-3.52
FeO	9.79	3.23-13.17
MnO	0.19	0.07-0.50
MgO	5.77	3.08-12.87
CaO	10.69	10.45-22.5
Na2O	3.36	0.46-1.83
K_2O	0.99	0.17-4.21
P_2O_5	0.22	0.02-0.90
Mg#	51	0.44-0.75
Cr	11	47-651
Ni	13	16-38

The studied ultramafic-mafic rocks with a calc-alkaline chemistry inferring an arc magmatism show a wide range in whole-rock chemistry. The degree of silica undersaturation, for the rocks characterized by low MgO (3.08-12.87 wt%) (Mg#=0.44-0.75), increases from CPXnite to HBdite, and HBdite with high $FeO^{(t)}/MgO$. Therefore their calc-alkaline character can not be explained simply by closed system fractional crystallization. Moreover, LREE-enrichment in the rocks with high Ti parg'tic amph may not be achieved by closed system crystallization and implies that an external REE source is required, such as a highly evolved, interstitial melt (Tribuzio et al., 1999) or magmatic H_2O-CO_2 vapours (Tribuzio et al., 2000).

The overall enrichment of incompatible elements, clear in N-MORB normalized multi-element and REE patterns, and ratio-ratio plots, proposes metasomatic enrichment of an initially depleted/enriched peridotite in an

oceanic-arc environment. The overall patterns of metasomatic enrichment may be contolled by; (a) modal mineralogy, (b) composition of metasomatic fluid(s) (e.g. H_2O- or CO_2-rich fluids; basaltic, adakitic, and carbonatitic melts), (c) mechanism; open system exchange (e.g. high melt/rock ratios) or closed system addition (e.g. bulk mixing).

Petrographical, mineralogical and geochemical studies indicate that the studied rocks have metasomatic signs comparable with those from alkaline, adakitic and basaltic melts, and carbonatite components.

The rocks showing strong fractionation between LILE and HFSE have high Rb/Sr ratio (0.01-0.70) and Th/U ratio (5.11-29.0). These high ratios might be related to the release of hydrous fluids from sediments of subducting slab (Tatsumi, 1989; Arculus, 1994; Tatsumi and Kogiso, 1997). The reaction between such a fluid (or melt) and mantle peridotite can produce an ol-poor hybrid phl-pyroxenite (Wyllie and Sekine, 1982).

HFSE are potential markers of metasomatic effects in island arc magma sources (Green, 1995). They are not carried in appreciable amounts by hydrous fluids released from the dehydration of a subducting oceanic slab (Tatsumi and Kogiso, 1997; Ayers, 1998). However, adakites contain appreciable amounts of HFSE (Drummond et al., 1996) even they display negative anomalies with respect to LILE. Highly variable Nb/Ta ratios (7.3-24) of the studied rock show both significantly lower and higher values than that of N-MORB (17.7, Sun and McDonough, 1989). The low Nb/Ta values can be explained by precipitation of phl and/or amph from a carbonatite melt (e.g. Ionov and Hoffman, 1995). This is due to high K_d^{amph} for Ta than for Nb in equilibrium with carbonatitic liquids (Green et al., 1992). On the other hand, quite high Nb/Ta values (up to 33) of high-K calc-alkaline rocks from Sunda arc indicate hydrous fluid metasomatized arc mantle (mantle reacted with adakitic melts) (Stolz et al., 1996; Münker, 1998). High Nb/Ta ratio is caused by metasomatic slab melt agent as a consequence of rt (Jenner et al., 1994). The hydrous fluid inclusions from metasomatized mantle peridotite xenoliths carried by adakitic melts infer both slab derived fluids and slab derived adakitic melts

caused by metasomatism on a subarc peridotite (Batan Island, Maury et al., 1998; Sajona et al., 2000).

The higher Ca/Al and Zr/Hf and lower Ti/Eu, Nb/Ta ratios of the rocks than those of N-MORB can be interpreted as the result of carbonatite metasomatism (e.g. Yaxley et al., 1991; Dautria et al., 1992; Rudnick et al., 1993; Gorring and Kay, 2000). However, the rock samples having similar or lower values for Zr/Hf, Ca/Al, and similar or higher values for Ti/Eu than N-MORB indicate a Fe-Ti rich basaltic melt metasomatic component (e.g. Menzies et al., 1987). The assemblage of amph, phl, rt, ilm mineralogy also favor Fe-Ti-K-rich basaltic metasomatism that is often found in xenoliths from continental basalts (Menzies et al., 1987; Kempton, 1987), but the studied rocks have a specific HFSE-enrichment similar to those from volcanic fields in the Baikal Rift region (Ionov and Hofmann, 1995; Ionov et al., 1997, Litasov et al., 2000).

Moreover, Fe-Ti oxides, ap, zrc and sph are always found in adakitic melts (Prouteau et al., 2000), and thus adakite metasomatized mantle rocks may also contain these minerals. Moreover, mantle wedge interactions with adakitic melt liquids results in crystallization of metasomatic parg and phl (Sekine and Wyllie, 1982; Sen and Dunn, 1995). Ionov and Hoffman (1995) reported that parg and phl, which crystallized from interaction of a depleted mantle and a supercritical silicic fluid derived from a subducted slab, show significantly high Zr/Hf (11-90 for parg, 19-54 for phl) and Nb/Ta (16-83 for parg, 27-55 for phl).

Therefore, the studied rock having wide ranges of elemental ratios, and high amounts of high-Ti parg-phl±rt±ilm±sph infer signs of more than one metasomatic event.

Rapp et al. (1991) experimentally showed that H_2O-undersatured, silica-rich melts derived from eclogite-facies subducted plate may contain some CO_2. Zanetti et al. (1999) supposed that these melts infiltrate the overlying harzburgitic mantle that is heated during decompression because of the higher temperature of rocks in contact with the subducted slab. Since the viscosity of the melt decreases at decompression, it favors infiltration of large mantle

volumes. If the rock/melt ratio is high, the melts will reach a temperature close to that of the peridotite. Zanetti et al. (1999) proposed two possible mechanisms depending on temperature; (1) if the temperature is lower than that required for inducing initial melting in the resulting hydrous peridotite system, melt would react with the peridotite during percolation and increase the amount of opx and forming new reaction phases with direct evidence of the slab-derived melt (from glass inclusions) (Godard et al., 1995). (2) If the resulting temperature is higher than that of incipient melting in a hydrous peridotite system (possible in supra-subduction mantle wedge (Davies and Stevenson, 1992; Kelemen et al., 1993), the infiltrated melt equilibrates with the peridotite (Zanetti et al., 1999). In this case, ol dissolves and the melt volume increases. It is well known that infiltrating alkaline melts dissolve opx at lithospheric mantle depth as well (Fabriès et al., 1989; Zinngrebe and Foley, 1995). Melt extraction is inhibited and crystallization conditions approach equilibrium until the melt percolation paths are clogged by the crystallizing phases. Initially anhydrous phases such as cpx will crystallize depending of temperature during cooling. This increases P_{H2O} of the residual melt, which would intersect the phl and amph stability fields. Crystallization of hydrous phases results in an increase of CO_2/H_2O value in the last residual melt, which reacts with previous phases to form di, ap and even carb's, and/or induces the separation of an immiscible CO_2-rich melt.

Zanetti et al. (1999) proposed that pyroxenites are not products of a mafic melt intruded into the peridotite but they represent melt-dominated regions in the former crystal mush causing variations in the mode of the minerals but not in their major compositions. Lower MgO/FeO ratio of the bulk system may be imposed by the low peridotite/melt ratio.

By significant cpx crystallization, residual melt may become slightly enriched in Fe and, later on, progressively enriched in incompatible and volatile elements. The rocks from the Kurançalı area seem to have undergone such a mechanism. The ap-bearing zones are due to increase in CO_2/H_2O ratio of the residue as amph and phl crystallization increases (Zanetti et al., 1999) and the P enriched patterns of the studied samples may represent randomly distributed ap-bearing regions and thus the areas of the last residual

melt crystallization. Zanetti et al. (1999) also calculated equilibrium melts having calc-alkaline affinity of andesitic-dacitic systems with geochemical signatures closer to those of slab-derived melts ((La/Yb)n down to 40 and strong depletions in Nb, Zr and Ti relative to the neighbouring REE), and the results are comparable with the trace element patterns of slab-derived melts (Rapp et al., 1991). Zanetti et al. (1999) also proposed a model in which amph is formed under closed-system conditions during crystallization of trapped, interstitial melt which was completely consumed by crystallization of hydrous minerals and overgrowth on previously crystallized minerals. If this were the case, then amph composition by itself should closely approach the geochemical signatures of the REE-enriched and Nb-, Ti-depleted melt, as observed. Zanetti et al. (1999) suggested that during the late stages of evolution the melt became CO_2-oversaturated after H_2O used by crystallization of amph and phl. Zanetti et al. (1999) interpreted that carbonatitite like metasomatism does not necessarily imply mantle-derived carbonatite components, but may result also from the evolution of a silicate liquid containing some CO_2, whatever its origin. This type of mechanism may explain evidences of carbonatite-like metasomatism in the studied rocks.

This model requires melting of a subducted slab under eclogite facies conditions that is possible under conditions of hot oceanic crust subduction and/or of high geothermal gradients (Poli and Schmidt, 1995 and references therein), and a resulting melt should include H_2O and CO_2 (evidenced from fluid inclusions and brines in eclogite-facies rocks; Philippot, 1993; Andersen et al., 1993; Philippot and Scambelluri, 1995). This mechanism seems to be appropriate to producing the rocks from Kurançalı.

Contrarily to the above mechanism, discussing metasomatism due to a subducting slab derived fluid/melt, Nb/Yb, Ti/Yb, Zr/Yb ratios, which are higher than those of N-MORB, suggest that relative enrichment of these elements is not caused by subducting slab fluid/melt (as discussed above, e.g. Figure 121). According to these ratios, the enrichment in HFSE is favorably caused by an OIB-like melt. At this point, it is important to clarify whether the enrichment by OIB-type melt was caused before or after subduction. Actually, such an incompatible element-enriched mantle source is only observed in modern

active continental margin rocks (Teklay et al., 2002). However, the elemental ratios such as Nb/Y, Nb/Zr, Ta/Yb, La/Ta, Ce/Pb rule out the absence of CLM content (as discussed above), and so continental margin setting. Therefore, subduction-taking place beneath a trace element enriched mantle (by OIB-type melt) should be considered in an intra-oceanic subduction zone. Freezing of mantle plume-derived melts (White, 1995; fossil plume model of Stein and Hofmann, 1992) may cause incompatible element enrichment in the oceanic mantle lithosphere. Pre-enrichment of the mantle wedge source prior to subduction was previously suggested for the Neoproterozoic calc-alkaline arc magmas from the northern and the southern Arabian-Nubian Shield (Stein and Goldstein, 1996; Teklay et al., 2002, respectively).

Alternatively, OIB-like alkaline melt may derive from asthenoshperic mantle during roll-back mechanism as subduction continues. This melt may cause enrichment of a previously depleted mantle wedge peridotite that was enriched by subduction derived hydrous fluid/melt. If this is the case, silica-undersaturated melts interact with hydrous peridotite (melting degree lower) and result in highly enriched hydrous melts. Teklay et al. (2002) suggested that a thermal anomaly in the upper mantle caused by a plume head may result in the production of large amounts of juvenile calc-alkaline magmatic rocks over a short period of time.

Another alternative to explain the geochemical data is that mantle was not as depleted as present-day mantle. However, chondrite normalized $(Sm/Nd)_n$ ratios of the Kurançalı rocks are similar to those of depleted peridotites from SSZ (Wang et al., 2001, 2002).

In addition to a possible adakitic type metasomatic event with a carbonatitite component discussed above,s the cpx-parg-phl dominated plutonic rocks from Kurançalı, may indicate an alkaline metasomatic component. That is evidenced from both mineral chemistry and geochemical data (the multi-element and REE patterns enriched in K, Rb, Ba (LILE), Sr and LREE with respect to HREE and creating smoothly decreasing profiles from LREE to HREE (chondrite normalized values $(La/Yb)_n$=7.41-21.35)). Various studies showed that alkaline metasomatism is responsible for the

crystallization of cpx, parg and phl. It was also relatively depleted in Nb (negative anomaly).

TiO_2/Al_2O_3 ratios and MgO contents of the rocks are comparable with oceanic gabbros metasomatized by alkaline magma from the Canary Islands (Neumann et al., 2000) (Figure 125). Therefore, multi-element and REE patterns of the studied rocks with minerals having tendency to alkaline compositions, are compared with strongly alkaline metasomatized gabbros and hornblendite cumulates of alkaline melt (OIB-type) from La Palma, the Canary Islands (Neumann et al., 2000) (Figures 126, 127). Although N-MORB-normalized trace-element patterns of the studied rocks show some similarities to the rocks from La Palma, they differ in detail (Figure 126a,b). The studied rocks differ from alkaline metasomatized rocks in terms of their negative Nb-Ta trough, strong positive K anomaly, relative enrichment in Rb, Ba, Th, U, relative depletion in La, Ce. The rocks are strongly depleted in P similar to metasomatized rocks except for three samples (Figure 126a). The rocks are more enriched in Rb and Ba than the alkaline hornblendite cumulate rocks from La Palma (Figure 126b). Th, U enrichment levels are similar. The Kurançalı rocks and La Palma alkaline cumulates differ in Nb, Ta and Ti. Even though most of the studied rocks show slight enrichment in Nb, Ta relative to N-MORB, they are characterized by negative trough relatively to adjacent element U and K. Highly variable Nb-Ta and Ti values, especially for the hydrous mineral rich rocks, approximates to those of alkaline cumulates from La Palma. Although the rocks from both Kurançalı and La Palma show parallel trends for La, Ce, Sr, Nd, Sm, Zr and Hf, the Kurançalı rocks are relatively depleted with respect to La Palma alkaline cumulate rock.

The chondrite-normalized REE patterns of the Kurançalı rocks show subparallel-parallel patterns to those of alkaline metasomatized gabbroic rocks and alkaline cumulate rocks from La Palma (Figure 127a,b). The rocks from La Palma, both alkaline metasomatized and alkaline cumulate rocks, are slightly enriched in LREE relative to the studied rocks. The most significant difference of the Kurançalı rocks from the La Palma rocks is for Eu, i.e. recognizable negative Eu anomaly of the ultramafics and DIO, and positive anomaly of LG.

The trace-element characteristics of the studied rocks may result from alkaline metasomatism of previously hydrated and LILE-enriched mantle wedge material, which is initially depleted, in an arc environment. This might have led to crystallization of amph, phl and cpx at the expense of opx, resulting in selective enrichment in Rb, Ba, K and other elements compatible with these phases, as well as, general enrichment in incompatible elements with relative depletions in Nb, Ta, P, Ti. Together with mineral assemblage, the geochemical features of the rocks except for their Eu anomalies and slightly enriched HFSE, are consistent with those of melts derived from an eclogite-facies slab. Eclogite-derived melts would have high $(La/Yb)_n$ ratios (because of the presence of garnet in the residue; Rapp et al., 1991), would be enriched in LILE and Sr and would have no Eu anomaly (because of the absence of plag), and would be relatively depleted in Ti and Nb (because of the presence of rt and/or sph phases in the residue; Kelemen et al., 1993).
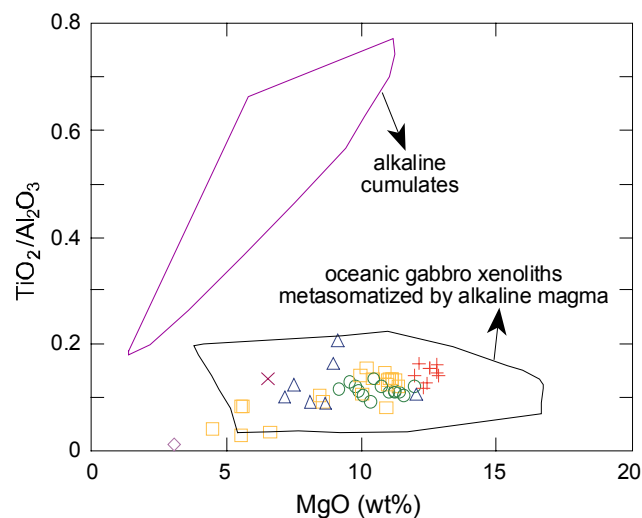
Figure 125. Whole rock TiO_2/Al_2O_3-MgO relations for the studied rocks and their comparison with gabbroic cumulates of alkaline magma and oceanic gabbros metasomatized by alkaline magma from the Canary Islands (data from Neumann et al., 2000) (the symbols are as in Figure 28).
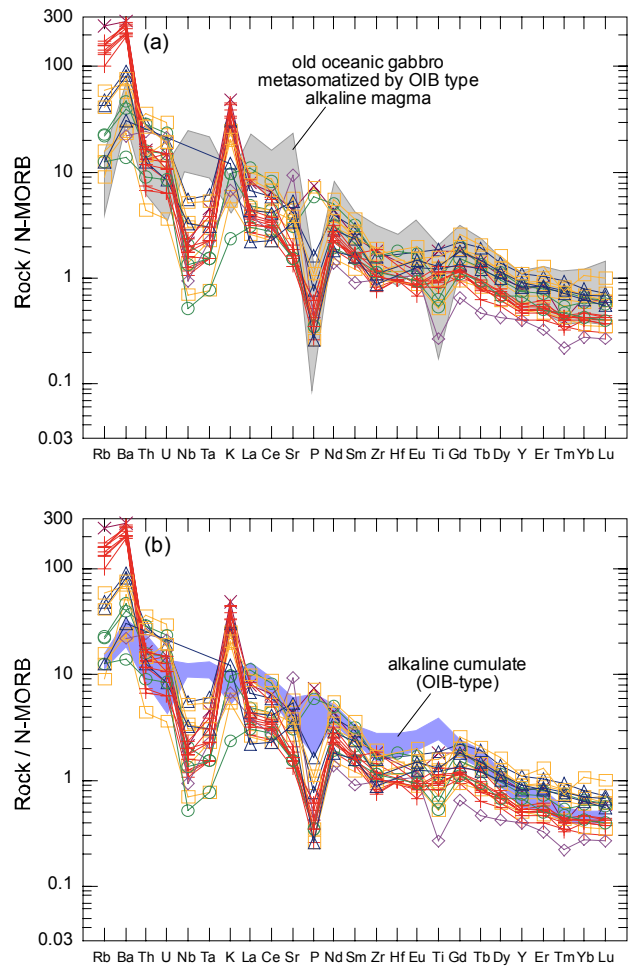
Figure 126. Comparison of N-MORB multi-element patterns of the studied rocks with (a) xenoliths of old oceanic crust metasomatized by OIB-type alkaline magma,and (b) xenoliths of hornblendite cumulates of OIB-type alkaline magma from La Palma, the Canary Islands (data from Neumann et al., 2000) (the symbols are as in Figure 28).
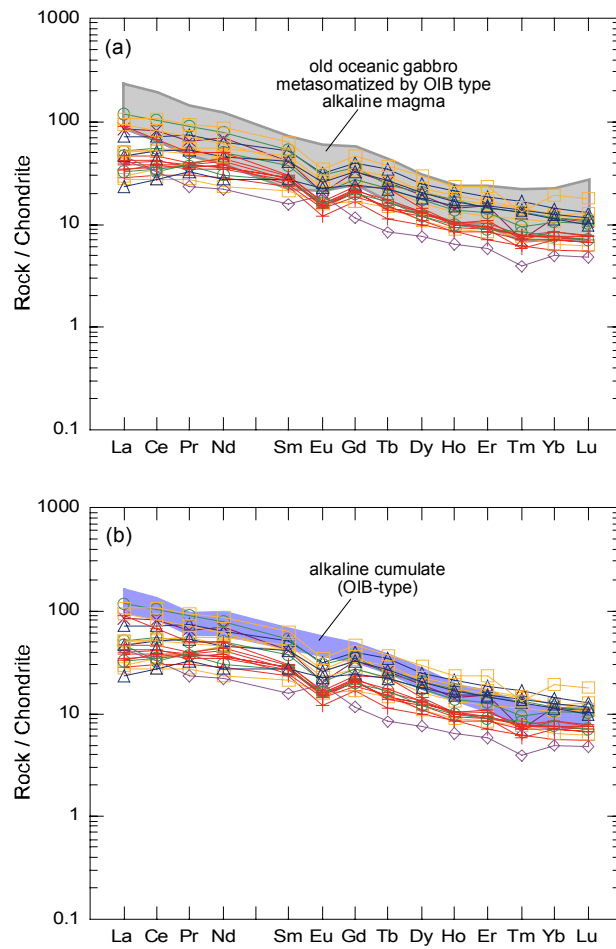
Figure 127. Comparison of chondrite-normalized REE patterns of the studied rocks with (a) xenoliths of old oceanic crust metasomatized by OIB-type alkaline magma, and (b) xenoliths of hornblendite cumulates of OIB-type alkaline magma from La Palma, the Canary Islands (data from Neumann et al., 2000) (the symbols are as in Figure 28).

Therefore, an OIB-like melt metasomatized mantle source with an additional selective enrichment of LILE induced by slab-derived fluids may also be suggested for the Kurançalı rocks. The crystallization order of the minerals for the studied cumulate rocks, which can not be the result of simple fractional crystallization, may also support alkaline metasomatism. Hybrid magma produced by partially molten hydrous mantle wedge material and alkaline melt may be responsible for the formation of hydrous silica undersaturated aluminous rocks.

6.4. Correlation with other Mafic-Ultramafic Bodies in the CACC

In any case, all evidences may explain that the ultramafic-mafic plutonic rocks from Kurançalı, rich in hydrous minerals (parg and phl), are derived from hybridization above subducted oceanic crust. All considerations, strongly favoring a subduction related setting, are against any other source or process (e.g. within continental plate alkaline magmatism, continental rift zone or continental basaltic magmatism). Nonetheless, phl and amph can be stabilized in the subduction environment at depths >110 km (Sudo and Tatsumi, 1990; Thompson, 1992; Davies, 1994). Isotopic studies by Brandon et al. (1999) on Simeoe mantle xenoliths showed that the hybridized hanging wall mantle may act for tens of million years as a reservoir for slab-derived material. That means, a subduction-derived fluid component could be preserved in areas of regional convergence, and then recycled by a later episode of magmatism related to rifting in back-arcs, both in an oceanic and a continental crust. Even though, mineralogical and geochemical evidences suggest intra-oceanic arc environment rather than continental arc setting for the Kurançalı hydrous plutonic rocks.

This is further supported by the regional geological constraints, discussed in detail by Göncüoğlu et al. (1992), geochemical evidences from other locations in Central Anatolia, described in various studies (e.g. Yalınız et al., 1996, 1999, 2000; Yalınız and Göncüoğlu; 1998; Floyd et al., 2000), and overall mineralogical - geochemical constraints reject a continental arc origin.

In addition, the ultramafic-mafic rocks were also compared with gabbroic outcrops that have been interpreted as "continental arc assemblages" within the CACC continental crust (Yılmaz-Şahin and Boztuğ, 1997; Kadıoğlu et al., 1998), and average values of upper and lower continental crust values (data from Taylor and McLennan, 1985) (Figure 128). The rocks are enriched in K, Ba, Sm, Y, Yb, Sc, Cr and depleted in Nb, Ta, Zr, Hf relative to upper continental crust. Moreover, the rocks are strongly enriched in LILE, relatively enriched in Nb, Ta, Zr, Hf, Sc, Cr but depleted in Yb relative to lower continental crust. Even though there is no complete data set for the gabbroic rocks interpreted as continental arc-related intrusive rocks in CACC continental crust, they show a higher degree of depletion than the Kurançalı rocks. This comparison and ratio-ratio plots discussed above show that there is no relation between the Kurançalı rocks and continental arc gabbroic rocks.
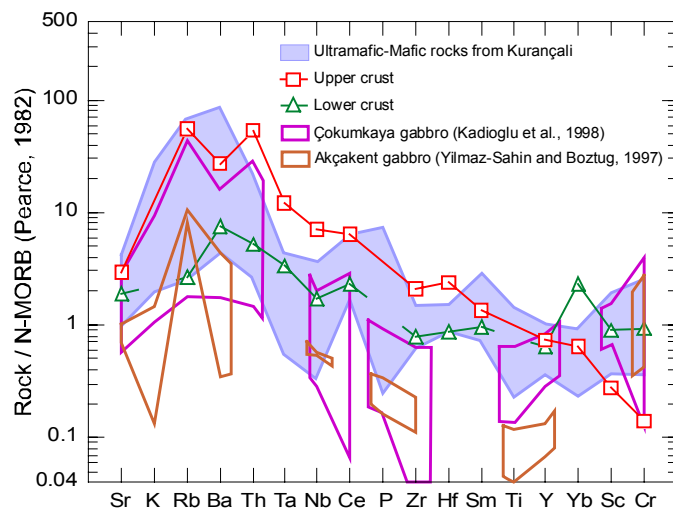
Figure 128. N-MORB normalized multi-element variation diagrams comparing the studied rocks with gabbros of intrusive assemblages within CACC continental crust (Yılmaz-Şahin and Boztuğ, 1997; Kadıoğlu et al., 1998), and average values of upper and lower continental crust values (data from Taylor and McLennan, 1985) (N-MORB normalization values from Pearce, 1982).

The Kurançalı rocks, characterized by calc-alkaline affinity with some transitional features of alkaline affinity (as interpreted in Chapter 5), are strongly affected by a distinct subduction component. As interpreted previously, the rocks also display some features of OIB, as well as CAB. Even though, the rock have similarities to OIB, they are certainly CAB in character due to their relative depletion in Nb-Ta-Zr-Hf, and Ti-P (for most of the samples). These geochemical features are characteristics of island arc calc-alkaline rocks (Pearce et al., 1994). The studied rocks having a calc-alkaline character are possibly in association with an eruptive setting of IAB as evidenced from various discrimination diagrams, ratio-ratio plots and comparisons of multi-element patterns with those possible eruptive settings (MORB, BABB, OIB) as interpreted in Chapter 5 and discussed above.

Geochemical comparison of the Kurançalı rocks with other mafic-ultramafic bodies in Central Anatolia is given in Figures 129, 130. The rocks are compared with a group of rocks comprising samples from gabbros, dykes, and volcanic section of the stratiform and remnant ophiolitic bodies of the CAO (Figure 129a). The samples used for comparison are from Sarıkaraman, Çiçekdağ and structurally isolated outcrops having ophiolitic affinities (Yalınız et al., 1996, 2000; Floyd et al., 2000). They show typical features of SSZ ophiolites and are comparable with other SSZ-type ophiolites from the Neotethyan zone (e.g. Pindos, Troodos, Oman; Yalınız et al., 1996). The isolated pillow lavas of CAO, having subduction related signatures with MORB-like components, show characteristics of BABB while dikes and metagabbros are akin to IAB (Floyd et al., 2000). In Figure 129b, the OIB rocks used for comparison with the studied rocks are representative alkalic basalts in the Ankara Mélange (Floyd, 1993; Floyd et al., 2000). In Figure 129c, the tholeiitic metabasites from both metamorphosed ophiolitic mélange in the CACC basement and in the Ankara Mélange display MORB-like features (Floyd et al., 2000). BABB and alkalic basalts of OIB from central Anatolia are comparable with those from the western Pacific (Woodhead et al., 1993) and the OIB of St. Helena (Floyd, 1993; Floyd et al., 2000), respectively.

It is obvious in Figure 129 that the rocks from Kurançalı, are quite different from the better-studied groups of the CAO and the Ankara Mélange.
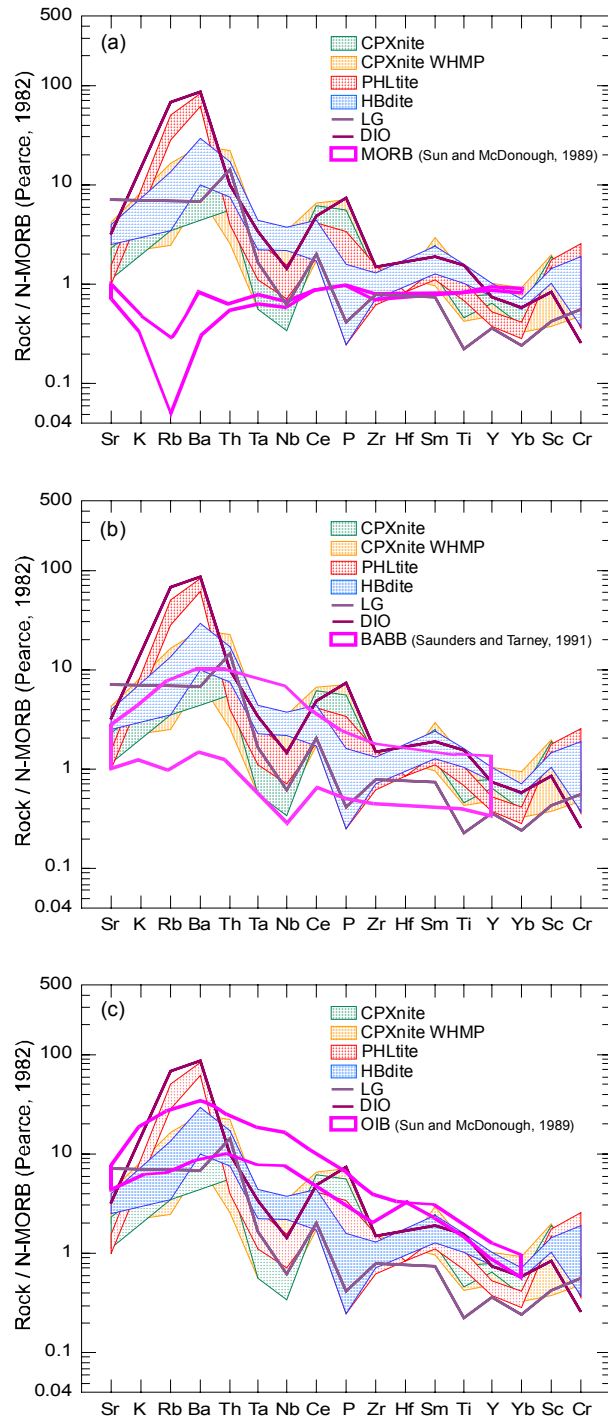
Figure 129. N-MORB normalized multi-element variation diagrams comparing the studied rocks with (a) stratiform and remnant ophiolitic fragments from the Central Anatolian Ophiolites (CAO), (b) alkaline ocean island basalts (OIB) in Ankara Mélange and Central Anatolian Crystalline Complex (CACC), (c) metabasites having MORB character in Ankara Mélange and CACC basement (data compiled from Floyd et al., 2000) (N-MORB normalization values from Sun and McDonough, 1989).

They are highly enriched in all elements including LILE, incompatible LFSE, and especially HFSE relative to the units of the CAO (e.g. Sarıkaraman, Çiçekdağ ophiolites and isolated ophiolitic remnants) (Figure 129a). The Kurançalı rocks are also different from the OIB-type rocks of the Ankara Mélange either by their enrichment in Ba, K, Cs (also Rb in PHLtite and DIO) or relative depletion in HFSE (high in Nb, Ta, relative in Zr, Hf, La, Nd, Ti) (Figure 129b). P content of the Kurançalı varies from enriched to highly depleted, relative to that of OIB. Lastly, they are also quite different from the MORB-type rocks of both CACC basement and Ankara Mélange (Figure 129c).

The gabbroic rocks with IAB, and IAB-BABB features from CAO (e.g. Sarıkaraman and Çiçekdağ ophiolites from Yalınız et al., 1996, 2000a) display flat patterns, however, the studied rocks highly enriched in REE (Figure 130).
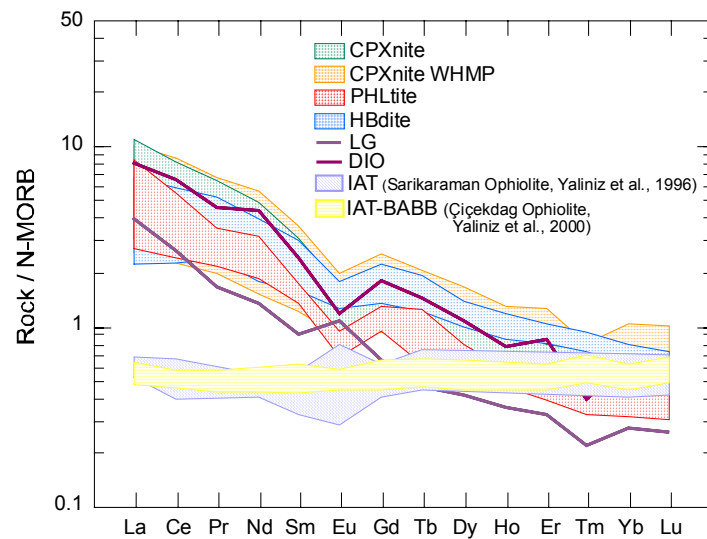
Figure 130. REE patterns comparing the studied rocks with IAT-type units in Sarıkaraman Ophiolite (Yalınız et al., 1996) and IAT-BABB-type units in Çiçekdağ Ophiolite (Yalınız et al., 2000) (N-MORB normalization values from Sun and McDonough, 1989).

Variation of V/Ti ratios against Zr of the Kurançalı rocks are compared with tectonically well-defined rocks from both ophiolitic units from CAO and Ankara Mélange metabasites (compiled from Floyd et al., 2000), and other locations (IAB and BABB from Woodhead et al. (1993); N-MORB from Floyd and Castillo (1992); alkaline-OIB of St. Helana from Chaffrey et al. (1989)) (Figure 131). The Kurançalı rocks mainly plot into the IAB field, however, the samples with hydrous minerals (i.e. relatively enriched in Ti) plot in MORB and BABB fields. The rocks plotting in the IAB field overly the field of CAO while those plotting into MORB-BABB fields are in overlapping field of CAO and OIB-type basalts of the Ankara Mélange. Even if some Kurançalı rocks plot in the MORB-BABB fields, they show no relation to these rocks as discussed above. This transition might be due to an unusual relative enrichment of the rocks in HFSE (e.g. Ti, Zr, Nb, Ta) caused by either strong metasomatism of depleted peridotite by subduction derived fluids/melts and so hybridization in mantle wedge, or metasomatism by both OIB-like melt and subduction derived fluids/melts of depleted mantle wedge peridotite. The second option is also preferred because of higher Nb/Yb, Ti/Yb, Zr/Yb ratios than those of N-MORB suggesting that relative enrichment of these elements is not caused by subducting slab fluid/melt (as discussed above, e.g. Figure 121).

The compositional differences between the Kurançalı rocks and the compared ophiolitic units of the CAO may result from different upper mantle compositions (from which the original primary magmas were generated) or different degrees of partial melting of the same upper mantle (assuming a homogeneous composition over a relatively large area), or different degrees of influence on mantle wedge source from subducting slab component (fluid/melt from oceanic crust and/or sediment).

6.5. Overall Evaluation

In summary, present mineralogical and whole-rock geochemical data suggest that the hydrous ultramafic-mafic plutonic rocks were generated in a SSZ environment. They display features of IAB-type oceanic crust and are extremely enriched LILE and HFSE (relative to MORB) reflecting alkaline

metasomatism in the source region. The geochemical features are of typical modern island arc basements (Pearce et al., 1994).
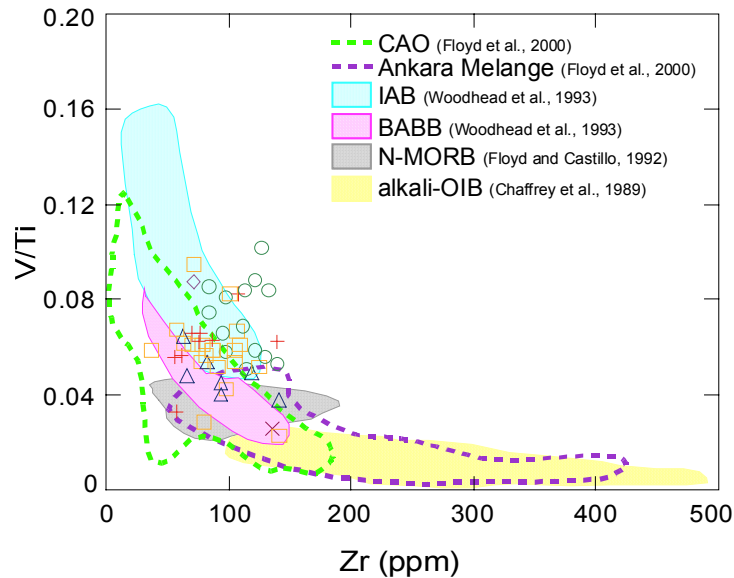
Figure 131. V/Ti-Zr diagram comparing data for the studied rocks with fields of stratiform and remnant ophiolitic fragments from Central Anatolian Crystalline Complex (CACC), metabasites from Ankara Mélange and CACC (data compiled from Floyd et al., 2000), island arc basalts (IAB) and back-arc basin basalts (BABB) from Woodhead et al. (1993), mid-ocean ridge basalts (N-MORB) from Floyd and Castillo (1992), alkaline ocean island basalts (OIB) from St. Helena from Chaffrey et al. (1989) (the symbols are as in Figure 28).

Although, mineralogical and geochemical data, and regional geological constraints strongly favor an intra-oceanic arc setting for the formation of the studied rocks, there are confusing points as discussed above. Therefore, radiogenic and stable isotopic studies are necessary to clarify the source region composition, whether there are contributions from slab components or from OIB components. The source of the fluids must be characterized as well.

The relative enrichment of HFSE elements for the rocks is identified as due to OIB-like melt interaction from the element ratio-ratio plots. Ratio-ratio plots may not represent the real situation. The best indication will come from

Sr, Nd Pb isotope data, which can give the most adequate result either for relative enrichment in HFSE, and REE caused by subduction derived melt or a plume related melt (e.g. Hofmann, 1997).

If a subduction-derived fluid/melt is proposed as the source of metasomatism in a depleted mantle wedge, what kind of material from the subducted slab was included in the fluid/melt and in which amount. It is difficult to distinguish the role of sediment modifiying the subarc mantle beacuse sediment contribution, in form of either hydrous fluids from sediment dehydration or silicate melt could also cause strong trace element enrichment (e.g. Tatsumi, 1989). Fluids from dehydrating sediments carry significant amounts of LILE and LREE (including Sr, La), but not Y and HREE into an overlaying mantle wedge (e.g. Tatsumi, 1989; Tatsumi amd Kogiso, 1997). In contrast, melting experiments on pelagic sediments by Nicholls et al. (1994) display gr as a residual phase which may further buffer Y and Yb in the mixed melts of oceanic crust and sediment. The compositional contribution of a slab sediment (either dehydration or melt) may cause relative enrichments and depletions in trace element composition of a mantle wedge. This contibution is quite similar to that from crustal slab melts. Isotope data (e.g. Re-Os, Sm-Nd, Sr, and U-Th-Pb) may provide data to clarify whether there is a contibution from a sediment or not, because contribution from a subducted sediment easily masks the isotope composition of a subducting crustal melt (having MORB isotope composition) (e.g. Hartmann and Wedepohl, 1993; Keppler, 1996; Shimoda et al., 1998; Brandon et al., 1999; Sajona et al., 2000).

For the formation of the Kurançalı rocks with their unusual composition, there may be more than one metasomatic event or a multi-stage metasomatic model that may explain the system as proposed by Brandon et al. (1999) in the light of isotopic data. In the first stage, subduction derived fluids or melts with similar Pb isotopic compositions as the slab component are transferred into the overlying hanging wall mantle and react with it, i.e. hybridization after Wyllie and Sekine (1982). This hybridized mantle is allowed to evolve with high U/Pb and Th/Pb ratios to the present-day to generate higher radiogenic Pb isotopic compositions. In the second stage, the hybridized hanging wall mantle is remobilized as melt or fluid. In the third stage, this fluid or melt migrates

upward through the mantle wedge and acts as a metasomatic agent that subsequently interacts with the overlying mantle lithosphere.

It is important to identify the source of fluid from which these hydrous rocks result, but this is often difficult. Possible sources may involve devolatilization of rocks within the oceanic crust or subducting slab, outgassing of the mantle, and deep circulating of surface fluid. Seawater trapped as pore-water in the subducting oceanic crust and sediments can be transported down by subduction. The H_2O-rich fluid then degasses from the slab and flows into the overlying mantle wedge, where it may locally cause melting of the host rock generating hydrous melts. Source fluid can be investigated with O, H, B isotope data. Hydrogen isotope composition of amph and phl may be indicative on the origin of fluids (e.g. Hartmann and Wedepohl, 1993).

CHAPTER 7

CONCLUSIONS

The ultramafic-mafic plutonic rocks from the Kurançalı area (Kaman-Kırşehir), an example of numerous isolated units of the CAO, are found within a tectonic sliver thrusted on a metamorphic ophiolitic mélange of the CAM of the CACC. The felsic dykes of the Late Cretaceous CAG intrude both plutonic rocks and underlying units. The observed field relations of the rocks units are characteristic for the CAO units in the CACC.

The ultramafic-mafic plutonic rocks from Kurançalı (the Kurançalı rocks) are characterized by unusual enrichment in hydrous mineral contents, dark mica and amph. The rocks are also composed of py, plag as major phases but they lack ol and opx. They are highly variable in modes and crystal sizes from fine-grained to pegmatitic (up to 20 cm for amph, 2-2.5 cm for dark mica). Based on the modes of minerals, the rocks are divided into six types; clinopyroxenite (CPXnite), clinopyroxenite with hydrous minerals and plag (CPXnite WHMP), phlogopitite (PHLtite), hornblendite (HBdite), layered gabbro (LG) and diorite (DIO).

Petrographical study showed that all rock types are composed cpx (di, di-aug), dark mica (phl), amph (parg) and plag crystallizing in the order of cpx → phl → parg → plag in varying amounts. They are characterized by ortho- and adcumulate textures where plag is the intercumulus phase. The rocks are not influenced intensely by low grade metamorphism and surface alteration. They have rarely metamorphic phases (act, chl, pump, ep) and alteration minerals (verm, ser, cc). The rocks have accessorily Ti-saturated phases (sph, rt, ilm), pyr and ap.

Detailed electron microprobe analyses were carried out for the constituents of the Kurançalı rocks. It was observed that there is a compositional variation for each mineral not only between several samples but also within a single sample.

Dark mica is phl in composition and has remarkably low ($Fe^{2+}\#$) ratios of 0.25-0.51 inferring magmatic origin. It shows a compositional change from ultramafic to mafic rocks, i.e. higher MgO and Al_2O_3 but lower $FeO^{(t)}$ and TiO_2 contents in micas of PHLtite and CPXnite. Phl has unusual positive correlation between $Al^{(t)}$ and Mg and so does not have magmatic fractionation trend. Phl shows similarities to those generated in OIB related oceanic environments due to its relatively high Fe^{2+}, Fe^{3+}, $Al^{[6]}$, Ti contents but differs from them due to its higher Ba-, OH- and $Al^{[4]}$-contents, and lower Si. Phl, not deficient in tetrahedral cations, has substitution mechanisms and chemistry that allocate a typical calc-alkaline character to the host rocks with transitional features to alkaline compositions.

The first crystallizing phase cpx having di and di-aug compositions displays a wide compositional range (Mg#=0.64-0.88, 0.02-1.25 wt% TiO_2, 0.36-8.66 wt% Al_2O_3, 0.10-0.97 wt% Na_2O) not only intra-crystal but inter-sample. High Si content, almost filling the tetrahedral site, characterizes cpx of the studied rocks. Chemistry of cpx, which is not tetrahedral deficit, infers a calc-alkaline character with transitional features to alkaline due to its high Ca, Ti, Na, $Al^{(t)}$, $Al^{[4]}$ contents similar to alkaline metasomatized cpx's. The zoned cpx crystals show Al-Ti-Na-K-poor and Si-rich cores, overgrown by Al-Ti-Na-K-rich, relatively Si-poor rims. Moreover, relatively high Na content and a weak fractionation trend (defined by relation of Ti and $Al^{(t)}$ to $Fe^{(t)}/(Fe^{(t)}+Mg)$) infers metasomatism. cpx of the Kurançalı rocks shows similarities to cpx from adakitic and alkaline metasomatized xenoliths.

Both of primary and late phase magmatic amph's from all rock types except for fine-grained HBdite display parg'tic composition while amph of fine-grained HBdite is hs in composition. They are rich in Ti and alkalis and characterized by extensive substitution of $Al^{[4]}$ for Si similar to that from metasomatized oceanic gabbro xenoliths and alkaline oceanic cumulates.

Their Na/K ratios are comparable to those of oceanic alkaline metasomatized gabbros. They are also comparable to those in transitional adakites in terms of Na+K and Ti contents, as well similarities to those from metasomatized rocks. Al$^{(t)}$ content of parg display similarity to that in hydrous low Mg - high Al basalt / basaltic andesite, and andesite while (Na+K)$_A$ and Ti contents are is similar to that from felsic melts. parg having high-Ti values (0.96-2.61 wt%) strongly favor primary origin of phl and interaction between magma and peridotite resulting in formation of hydrous upper mantle above subducting oceanic crust.

Intercumulus phase plag displaying a wide range of composition (an %= 40.61-98.58) is mainly characterized by high an content (>70 %). A wide range of an % may infer generation of two melts which are Na-rich and Ca-rich melts.

The mineral assemblage, both major and accessory phases, seems to represent the metasomatic enrichment resulting in the pervasive presence of phl and parg with Ti-rich accessory phases (rt, ilm, sph), and rarely sporadic occurrence of small ap domains. The presence of ap in the studied the rocks may infer CO_2 in the system.

Pressure-temperature estimates from various methods with several limitations gave just an approximation since there is no appropriate geothermobarometer for the mineral assemblages. In general, the estimates resulted in wide range of pressure values 5-15kbar $\pm$ 4kbar and temperature values 825-980°C.

The mineral assemblage, primary magmatic parg and phl, and intercumulus high-Ca plag, necessitates significant amounts of water into the source, high water pressure and oxygen fugacities (NNO to HM buffer conditions). These conditions strongly suggest marginal basin settings above subducting oceanic slab and a parental magma compatible with a process of hydrous partial melting of a mantle source affected by previous metasomatic events.

Whole-rock geochemical data showed that the cumulate ultramafic-mafic rocks are characterized by moderately high Mg# (0.44-0.75) and low contents of compatible elements (Cr=47-651 ppm and Ni=16-38 ppm). CPXnite

samples suggest calc-alkaline affinity occurring in an arc environment based on chemical and tectonic discrimination diagrams while hydrous mineral bearing and enriched rocks display scattered plots. Despite the scattered plots on discrimination diagrams, all rocks display parallel patterns on multi-element and REE diagrams indicating their petrological relations to each other.

Spider diagram profiles for all of the Kurançalı rocks are characterized by enrichment of LILE and LREE relative to HREE and HFSE. They show strong positive anomalies for Rb, Ba, K, Th, Sr, negative trough for Nb-Ta, strong depletion in P with few exceptions, and relatively depleted to negligible Zr, Hf, Ti anomalies. Despite depletion in Nb and Ta relative to LILE, these elements show enrichment relatively to N-MORB. Comparison of multi-element patterns with those of well-defined rocks from different settings strongly favors high-K calc-alkaline features transitional to alkaline character and generation in an intra-oceanic island arc setting.

Elemental ratios such as higher Sr/Nd, Sr/Ce, Ba/La, Ba/Rb, U/Nb, Th/Yb, Ce/Nb and lower Ce/Pb, Nb/La and Ti/Eu ratios than those of average N-MORB show strong arc signatures and fluid metasomatism of mantle wedge due to subducting oceanic slab. Moreover, Sm/Nd ratios are within ranges of depleted mantle peridotites while La/Yb ratios are higher than N-MORB values. However, the rocks show some transitional features to OIB-type mantle sources with higher Nb/Yb, Zr/Yb and Ti/Yb ratios than average N-MORB. Elemental ratios indicate either an initially depleted mantle source that is enriched in LREE by external REE derived from a subducting slab or a mantle source that is enriched by an OIB-component before or after subduction.

Two models are proposed for the Kurançalı rocks having unusual mineral contents and chemical propoperties of both minerals and whole-rocks. Model 1: Petrographical, mineralogical and geochemical studies indicate that the studied rocks have metasomatic signs comparable with those from alkaline, adakitic and basaltic melts, and carbonatite components. Multi-element variation and REE patterns for the Kurançalı rocks are well comparable with high-Al basalts from the Aeolian arc. La/Yb ratios of the

Kurançalı rocks are similar to those of adakitic melts. Moreover, Pb/Nd and Nb/Ta ratios of the rocks range between those of adakites and typical arc rocks. Highly variable Nb/Ta ratios (significantly lower and higher values than that of N-MORB) and rare sporadic enrichment of ap domains display influence of carbonatite component (resulting in low Nb/Ta) and of adakitic melts (resulting in high Nb/Ta) on source mantle rock. Higher Ca/Al and Zr/Hf and lower Ti/Eu, Nb/Ta ratios of the rocks than those of N-MORB infer signs of carbonatite metasomatism while lower values for Zr/Hf, Ca/Al, and similar or higher values for Ti/Eu than N-MORB indicate a Fe-Ti rich basaltic melt metasomatic component. The studied rock having wide ranges of elemental ratios, and high amounts of high-Ti parg-phl±rt±ilm±sph infer that hydrous adakitic melts having CO_2 component are hybridized with mantle wedge source.

Model 2: Alkali element enrichments of the minerals, and TiO_2/Al_2O_3 ratios and MgO contents of whole-rocks comparable to metasomatized rocks by OIB-type alkaline melt, and higher elemental Nb/Yb, Ti/Yb, Zr/Yb and La/Yb ratios of the rocks than those of N-MORB favor metasomatism by OIB-like alkaline melt. Metasomatism by OIB-like component is possible before or after subduction. OIB-like alkaline melt derived during roll-back mechanism may cause enrichment of a previously hydrated and LILE-enriched mantle wedge component, which is initially depleted. This may result in juvenile calc-alkaline magmatic rocks over a short period of time.

In any case, both models strongly favor mantle wedge metasomatism above subducted slab resulting in selective enrichment of LILE induced by slab-derived fluids. Hybrid magma produced by partially molten hydrous mantle wedge material and OIB-type alkaline melt or adakite melt are responsible for the formation of hydrous silica undersaturated aluminous rocks.

Although, present mineralogical and geochemical data, and regional geological constraints strongly favor mantle metasomatism in an intra-oceanic arc setting, isotope data and trace element data for the constituent minerals may provide further input on the proposed metasomatizing components.

Comparisons of the Kurançalı rocks with other mafic-ultramafic units in the CACC having fore-arc and back-arc affinities and generated in SSZ environment show that they are different both in mineral content, mineral chemistry and geochemical compositions. The Kurançalı rocks are assumed to be derived from basement of an intra-oceanic island arc formed during closure of İzmir-Ankara-Erzincan branch of Neotethyan Ocean, and emplaced on the CACC.

REFERENCES

Abbate, E., Bortolotti, V., and Paserini, P., 1976. Major structural events related to ophiolites of the Tethyan Belt. Ofioliti, 1, 5-32.

Abdel-Fattah, M.A., 1994. Nature of biotites from alkaline, calc-alkaline, and peraluminous magmas. Journal of Petrology, 35(2), 525-541.

Abdel-Fattah, M.A., 1996. Discussion on the comment on nature of biotites in alkaline, calc-alkaline, and peraluminous magmas. Journal of Petrology, 37(5), 1031-1035.

Abouchami, W., Boher, M., Michard, A., and Albare`de, F., 1990. A major 2.1 Ga event of mafic magmatism in West Africa: an early stage of crustal accretion. Journal of Geophysical Research, 95, 17605-17629.

Abrecht, J.A., and Hewitt, D.A., 1988. Experimental evidence on the substitution of Ti in biotite. American Mineralogist, 73, 1275-1284.

Adam, J., and Green, T.H., 1994. The effects of pressure and temperature on the partitioning of Ti, Sr and REE between amphibole, clinopyroxene and basanitic melts. Chemical Geology, 117, 219-233.

Ague, J.J., and Brandon, M.T., 1996. Regional tilt of the Mount Stuart batholith, Washington, determined using aluminum-in-hornblende barometry: Implications for northward translation of Baja British Columbia. Geological Society of America Bulletin, 108(4), 471-488.

Alirezaei, S., and Cameron, E.M., 2002. Mass balance during gabbro-amphibolite transition, Bamble Sector, Norway: implications for petrogenesis and tectonic setting of the gabbros. Lithos, 60, 21–45.

Allan, J.F., and Carmichael, I.S.E., 1984. Lamprophyric lavas in the Colima graben, SW Mexico. Contributions to Mineralogy and Petrology, 88, 203–216.

Andersen, T., Austrheim, H., Burke, E.A.J., and Elvevold, S., 1993. N_2 and CO_2 in deep crustal fluids: evidence from the Caledonides of Norway. Chemical Geology, 108, 113-132.

Anderson, J.L., and Smith, D.R., 1995. The effects of temperature and oxygen fugacity on the Al-in-hornblende barometer. American Mineralogist, 80, 549–559.

Aoki, K., and Kushiro, I., 1968. Some clinopyroxenes from ultramafic inclusions in Dreiser Weiher, Eifel. Contributions to Mineralogy and Petrology, 21, 743-749.

Aoki, K., and Shiba, I., 1973. Pyroxene from lherzolite inclusions of Itinome-gata, Japan. Lithos, 6, 41-51.

Arculus, R.J., 1994. Aspects of magma genesis in arcs. Lithos, 33, 189-208.

Arculus, R.J., and Wills, K.J.A., 1980. The petrology of plutonic blocks and inclusions from the Lesser Antilles island arc. Journal of Petrology, 21, 743-799.

Arculus, R.J., Pearce, J.A., Murton, B.J., and Van der Laan, S.R., 1992. Igneous stratigraphy and major-element geochemistry of Holes, 786A and 786B. Proceedings of the Ocean Drilling Program, Scientific Results, 125, 143-169.

Ashchepkov, I.V., Litasov, Yu.D., and Dobretsov, N.L., 1994. Pyroxenites and composite garnet peridotite xenoliths from picrite-basalt, Vitim Plateau Transbaikal: implication for thermobarometry and mantle reconstruction. Proc. 5th Int. Kimb. Conf., Rio de Janeiro, Brazil, 1A, 455-466.

Ataman, G., 1972. The preliminary study on the radiometric age of Cefalık Dağı that is one of the granitic-granidioritic bodies in the SW of Ankara. Journal of Hacettepe Nature and Applied Sciences, 2, 44-49 (in Turkish).

Aydın, N.S., Göncüoğlu, M.C., and Erler, A., 1998. Latest Cretaceous magmatism in the Central Anatolian Crystalline Complex: review of field, petrographic and geochemical features. Turkish Journal of Earth Sciences, 7, 259-268.

Ayers, J., 1998. Trace element modelling of aqueous fluid-peridotite interaction in the mantle wedge of subduction zones. Contributions to Mineralogy and Petrology, 132, 390-404.

Bachinski, S.W., and Simpson, E.L., 1984. Ti-phlogopites of the Shaw's Cove Minette: A comparison with micas of the other lamprophyres, potassic rocks, kimberlites, and mantle xenoliths. American Mineralogist, 69, 41-56.

Bailey, D.K., 1985. Fluids, melts, flowage and styles of eruption in alkaline-ultra-alkaline magmatism. Trans. Geol. Society of South Africa, 88, 449-457.

Beard, A.D., Downes, H., Vetrin, V., Kempton, P.D., and Maluski, H., 1996. Petrogenesis of Devonian lamprophyre and carbonatite minor intrusions, Kandalaksha Gulf (Kola Peninsula, Russia). Lithos, 39, 93-109.

Beard, A.D., Downes, H., Hegner, E., Sablukov, S.M., Vetrin, V.R., and Balogh, K., 1998. Mineralogy and geochemistry of Devonian ultramafic minor intrusions of the southern Kola Peninsula, Russia: implications for the petrogenesis of kimberlites and melilitites. Contributions to Mineralogy and Petrology, 130, 288-303.

Beard, J.S., 1986. Characteristic mineralogy of arc-related cumulate gabbros: implications for the tectonic setting of gabbroic plutons and for andesite genesis. Geology, 14, 848-851.

Beccaluva, L., Ohnenstetter, D., and Ohnenstetter, M., 1979. eochemical discrimination between ocean-floor and island arc tholeiites-application to some ophiolites. Canadian Journal of Earth Sciences, 16, 1874-1882.

Beccaluva, L., Maccciotta, G., Piccardo, G.B., and Zeda, O., 1989. Clinopyroxene composition of ophiolite basalts as petrogenetic indicator. Chemical Geology, 77, 165-182.

Bédard, J.H., 1999. Petrogenesis of boninites from the Betts Cove ophiolite, Newfoundland, Canada: identification of subducted source components. Journal of Petrology, 40, 1853-1889.

Bingöl, E., 1989. 1/2.000.000 scaled geological map of Turkey. Publication of the General Directorate for Mineral Research and Exploration, Ankara.

Bisdom, E.R.A., Stoops, G., Delvigne, J., Curmi, P., and Altemuller, H.J., 1982. Micromorphology of weathering biotite and its secondary products. Pedologie, 32, p. 225-252.

Blundy, J.D., and Holland, T.J.B., 1990. Calcic amphibole equilibria and a new amphibole-plagioclase geothermometer. Contributions to Mineralogy and Petrology, 104, 208-224.

Bodinier, J.-L., Dupuy, C., and Dostal, J. 1988. Geochemistry and petrogenesis of eastern Pyrenean peridotites. Geochimica et Cosmochimica Acta, 52, 2893-2907.

Brandon, A.D., and Draper, D.S., 1996. Constraints on the origin of the oxidation state of mantle overlying subduction zones: an example from Simcoe, Washington, USA. Geochimica et Cosmochimica Acta, 60, 1739-1749.

Brandon, A.D., Becker, H., Carlson, R.W., and Steven, B.S., 1999. Isotopic constraints on time scales and mechanisms of slab material transport in the mantle wedge: evidence from the Simcoe mantle xenoliths, Washington, USA. Chemical Geology, 160, 387-407.

Brophy, J.G., and Marsh, B.D., 1986. On the origin of high-Al arc basalt and the mechanics of melt extraction. Journal of Petrology, 27(4), 763-789.

Burnham, C.W., 1979. The importance of volatile constituents. In: Yoder, H.S. (ed.), The Evolution of the Igneous Rocks. Fiftieth Anniversary Perspectives, 439-482.

Burns, L.E., 1985. The Border Ranges ultramafic and mafic complex, south-central Alaska: Cumulate fractionates of island arc volcanics. Canadian Journal of Earth Sciences, 22, 1020-1038.

Campbell, I.H., Lesher, C.M., Coad, P., Franklin, J.M., Gorton, M.P., and Thurston, P.C., 1984. Rare earth element mobility in alteration pipes below massive sulfide deposits. Chemical Geology, 45, 181–202.

Cannat, M., Chatin, F., Whitechurch, H., and Ceuleneer, G., 1997. Gabbroic rocks trapped in the upper mantle at the Mid-Atlantic Ridge. In: Karson, J.A., Cannat, M., Miller, D.J., and Elton, D. (eds.), Proceedings of the Ocean Drilling Program, Scientific Results, 153, 243-264.

Carmichael, I.S.E., 1991. The redox state of basic and silicic magmas: a reflection of their source regions? Contributions to Mineralogy and Petrology, 106, 129-141.

Carroll, M.J., and Wyllie, P.J., 1989. Experimental phase relations in the system tonalite-peridotite-H2O at 15 kbar, implications for assimlation and differentiation processes near the crust-mantle boundary. Journal of Petrology, 30, 1351-1382.

Chaffrey, D.J., Cliff, R.A., and Wilson, B.M., 1989. Characterization of the St. Helena magma source. In: Saunders, A.D., and Norry, M.J. (eds.), Magmatism in ocean basins. Geological Society of London, Special Publication, 42, 257-276.

Chalot-Prat, F., and Boullier, A.M., 1997. Metasomatism in the sub-continental mantle beneath the Eastern Carpathians Romania: new evidence from trace element geochemistry. Contributions to Mineralogy and Petrology, 129, 284-307.

Coish, R.A., Hickey, R., and Frey, F.A., 1982. Rare earth element geochemistry of the Betts Cove ophiolite, Newfoundland: complexities in ophiolite formation. Geochimica et Cosmochimica Acta, 46, 2117-2134.

Colombi, A., 1989. Métamorphisme et géochemie des roches mafiques des Alpes ouest-centrales (géoprofil Viéege-Domodossola-Locarno). Mémoires de Géologie (Lausanne), 4, 1-216.

Coltorti, M., Beccaluva, L., Bonadiman, C., Salvini, L., and Siena, F., 2000. Glasses in mantle xenoliths as geochemical indicators of metasomatic agents. Earth and Planetary Science Letters, 183, 303-320.

Conrad, W.K., Kay, S.M, and Kay, R.W., 1983. Magma mixing in Aleutian arc: Evidence from cognate inclusions and composite xenoliths. Journal of Volcanology and Geothermal Research, 18, 279-295.

Conticelli, S., 1998. The effect of crustal contamination on ultrapotassic magmas with lamproitic affinity: mineralogical, geochemical and isotope data from the Torre Alfina lavas and xenoliths, Central Italy. Chemical Geology, 149, 51-81.

Conticelli, S., Francalanci, L., Manetti, P., Cioni, R., and Sbrana, A., 1997. Petrology and geochemistry of the ultrapotassic rocks from the Sabatini Volcanic Disrict, central Italy: the role of the evolutionary processes in the genesis of varibaly enriched alkaline magmas. Journal of Volcanology and Geothermal Research, 75, 107-136.

Coogan, L.A., Thompson, G., and MacLeod, C.J., 2002. A textural and geochemical investigation of high level gabbros from the Oman ophiolite: implications for the role of the axial magma chamber at fast-spreading ridges. Lithos, 63, 67– 82.

Coogan, L.A., Wilson, R.N., Gillis, K.M., and MacLeod, C.J., 2001a. Near-solidus evolution of oceanic gabbros: Insights from amphibole geochemistry. Geochimica et Cosmochimica Acta, 65(23), 4339–4357.

Coogan, L.A., MacLeod, C.J., Dick, H.J.B., Edwards, S.J., Kvassnes, A., Natland, J.H., Robinson, P.T., Thompson, G., and O'Hara, M.J., 2001b. Whole-rock geochemistry of gabbros from the Southwest Indian Ridge: constraints on geochemical fractionations between the upper and lower oceanic crust and magma chamber processes at very slow-spreading ridges. Chemical Geology, 178, 1-22.

Costa, F., Dungan, M.A., and Singer, B.S., 2001. Magmatic Na-rich phlogopite in a suite of gabbroic crustal xenoliths from Volcán San Pedro, Chilean Andes: Evidence for a solvus relation between phlogopite and aspidolite. American Mineralogist, 86, 29–3.

Criss, R.E., and Taylor, H.P., 1986. Meteoric-hydrothermal systems. In: Stable Isotopes, Valley, J.W., Taylor, H.P., and O'Neil, J.R. (eds.), Mineralogical Society of America, Reviews in Mineralogy, Washington DC, 16, 373–424.

Cullers, R.L., Dorais, M.J., Berendsen, P., and Chaudhuri, S., 1996. Mineralogy and petrology of Cretaceous subsurface lamproite sills, southeastern Kansas, USA. Lithos, 38, 185-206.

Czamanske, G.K., Ishihara, S., and Atkin, S.A., 1981. Chemistry of rock-forming minerals of the Cretaceous-Paleocene Batholith in Southwestern Japan and Implications for magma genesis. Journal of Geophysical Research, 86(B1), 10431-10469.

Dalton, J.A., and Presnall, D.C., 1998. The continuum of primary carbonatitic-kimberlitic melt compositions in equilibrium with lherzolite: data from the system $CaO-MgO-Al_2O_3-SiO_2-CO_2$ at 6 Gpa. Journal of Petrology, 39, 1953-1964.

Dautria, J.M., Dupuy, C., Takheist, D., and Dostal, J., 1992. Carbonate metasomatism in the lithospheric mantle: peridotitic xenoliths from a melititic district of the Sahara basin. Contributions to Mineralogy and Petrology, 111, 37-52.

Davies, J.H., 1994. Lateral water transport across a dynamic mantle wedge: a model for subduction zone magmatism. In: Ryan, M.P. (ed.), Magmatic Systems, Academic Press, 197-221.

Davies, J.H., and Stevenson, D.J., 1992. Physical model of source region of subduction zone volcanics. Journal of Geophysical Research, 97, 2037-2070.

Dawson, J.B., and Smith, J.W., 1977. The MARID (mica-amphibole-rutile-ilmenite-diopside) suite of xenoliths in kimberlite. Geochimica et Cosmochimica Acta, 41, 309–323.

DeBari, S.M., and Coleman, R.G., 1989. Examination of the deep levels of an island arc: evidence from the Tonsina ultramafic-mafic assemblage, Tonsina, Alaska. Journal of Geophysical Research, 94, 4373-4391.

DeBari, S.M., Kay, S.M., and Kay, R.W., 1987. Ultramafic xenoliths from Adagdak Volcano, Adak, Aleutian Islands, Alaska: deformed igneous cumulates from the Moho of an island arc. Journal of Geology, 95, 329-341.

Deer, W.A., Howie, R.A., and Zussman, J., 1980. An Introduction to the Rock Forming Minerals. 1st Edition (20th Impression), Longman, London, 528 p.

Deer, W.A., Howie, R.A., and Zussman, J., 1992. An Introduction to the Rock Forming Minerals. 2nd Edition, Longman, London, 632 p.

Defant, M.J., and Drummond, M.S., 1990. Derivation of some modern arc magmas by melting of young subducted lithosphere. Nature, 347, 662-665.

Draper, D.S., and Green, T.H., 1997. P-T phase relations of silicic, alkaline, aluminous mantle-xenolith glasses under anhydrous and C-O-H fluid saturated conditions. Journal of Petrology, 38, 1187-1224.

Droop, G.T.R., 1987. A general equation for estimating Fe^{3+} concentrations in ferromagnesian silicates and oxides from microprobe analysis, using stoichiometric criteria. Mineralogical Magazine, 51, 431-437.

Drummond, M.S., and Defant, M.J., and Kepezhinskas, P.K., 1996. Petrogenesis of slab-derived trondhjemite–tonalite–dacite/adakite magmas. Transactions of the Royal Society of Edinburgh: Earth Sciences, 87, 205–215.

Duda, A., and Schminke, H.-U., 1978. Quaternary basanites, melilite nephelinites and tephrites from the Laacher See area (Germany). Neues Jahrbuch für Mineralogie Abhandlungen, 132, 1-33.

Duncan, R.A., and Green, D.H., 1987. The genesis of refractory melts in the formation of oceanic crust. Contributions to Mineralogy and Petrology, 96, 326-342.

Düzgören-Aydın, N.S., Malpas, J., Göncüoğlu, M.C., and Erler, A., 2001. A review of the nature of magmatism in Central Anatolia during the Mesozoic post-collisional period. International Geological Review, 43, 695-710.

Dymek, R.F., 1983. Titanium, aluminum and interlayer cation substitutions in biotite from high-grade gneisses, West Greenland. American Mineralogist, 68, 880-899.

Edgar, A.D., Green, D.H., and Hibberson, W.O., 1976. Experimental petrology of a highly potassic magma. Journal of Petrology, 17, 339-356.

Elthon, D., Steward, M., and Ross, D.K., 1992. Compositional trends of minerals of minerals in oceanic cumulates. Journal of Geophysical Research, 97, 15189-15199.

Erdoğan, B., Akay, E., and Uğur, M.Ş., 1996. Geology of the Yozgat Region and Evolution of the Collisional Çankırı Basin. International Geology Review, 38(9), 788-806.

Erkan, Y., and Ataman, G., 1981. An investigation on metamorphism age of Central Anatolian Massif by K-Ar method. Journal of Earth Sciences Hacettepe University, 8, 27-31 (in Turkish).

Erlank, A.J., Waters, F.G., Hawkesworth, C.J., Haggerty, S.E., Rickard, R.S., and Menzies, M., 1987. Evidence for mantle metasomatism in peridotite nodules from the Kimberley pipes, South Africa. In: Menzies, M., Hawkesworth, C.J. (eds.), Mantle Metasomatism, Academic Press, London, 221-312.

Ernst, W.G., and Liu, J., 1998. Experimental phase-equilibrium study of Al- and Ti-contents of calcic amphibole in MORB: A semiquantitative barometer. American Mineralogist, 83, 952-969,

Ertan, I.E., and Leeman, W.P., 1996. Metasomatism of Cascades sub-arc mantle: evidence from a rare phlogopite orthopyroxenite xenolith. Geology, 24, 451-454.

Esperança, S., and Holloway, J.R., 1987. On the origin of some mica lamprophyres: experimental evidence from a mafic minette. Contributions to Mineralogy and Petrology, 95, 207-216.

Fabriès, J., Bodinier, J.L., Dupuy, C., Lorand, G.P., and Benkerrou, C., 1989. Evidence for modal metasomatism in the orogenic spinel lherzolite body from Caussou (Northeastern Pyrenees, France). Journal of Petrolgoy, 30, 199-228.

Feldstein, S.N., Lange, R.A., Vennemann, T., and O'Neil, J.R., 1996. Ferric-Ferrous ratios, H_2O contents and D/H ratios of phlogopite and biotite from lavas of different tectonic regimes. Contributions to Mineralogy and Petrology, 126 (1/2), 51-66.

Fitton, J.G., James, D., and Leeman,W.P., 1991. Basic magmatism associated with Late Cenozoic extension in the western United States: Compositional variations in space and time. Journal of Geophysical Research, 96, 13693–13711.

Fleet, M.E., and Barnett, R.L., 1978. $Al^{[4]}/Al^{[6]}$ partitioning in calciferous amphiboles from the mine, Sudbury, Ontario. Canadian Mineralogist, 16, 527-532.

Floyd, P.A., 1993. Geochemical discrimination and petrogenesis of alkalic basalt sequences in part of the Ankara melange central Turkey. Journal of Geological Society, London, 150, 541-550.

Floyd, P.A., and Castillo, P.R., 1992. Geochemistry and petrogenesis of Jurassic ocean crust basalts, ODP Leg 129, Site 801. In: Larson, R., Launcelot et al. (eds.), Proceedings of the Ocean Drilling Program, Scientific Results, College Station, Texas, 361-388.

Floyd, P.A., Yalınız, M.K., and Göncüoğlu, M.C., 1998. Geochemistry and petrogenesis of intrusive and extrusive ophiolitic plagiogranites, Central Anatolian Crystalline Complex, Turkey. Lithos, 42, 225-241.

Floyd, P.A., Göncüoğlu, M.C., Winchester, J.A., and Yalınız, M.K., 2000. Geochemical character and tectonic environment of Neotethyan ophiolitic fragments and metabasites in the Central Anatolian Crystalline Complex, Turkey. In: Bozkurt, E., Winchester, J.A., and Piper, J.D.A. (eds.), Tectonics and Magmatism in Turkey and the Surrounding Area. Geological Society of London, Special Publication, 173, 183-202.

Foster, M.D., 1960. Interpretation of the composition of trioctahedral micas. U.S. Geological Survey, Professional Paper, 354-B, 11-49.

Francalanci, L., Taylor, S.R., McCulloch, M.T., and Woodhead, J.D., 1993. Geochemical and isotopic variations in the calc-alkaline rocks of Aeolian arc, southern Tyrrhenian Sea, Italy: constraints on magma genesis. Contributions to Mineralogy and Petrology, 113, 300–313.

Fyfe, W., and McBirney, A.R., 1975. Subduction and the structure of andesite volcanic belts. Journal of American Science, 275A, 285-297.

Gaggero, L., and Cortesogno, L., 1997. Data report: metamorphic mineralogy of Leg 153 gabbros. In: Karson, J.A., Cannat, M., Miller, D.J., and Elton, D. (eds.), Proceedings of the Ocean Drilling Program, Scientific Results, 153, 531-546.

Gill, J.B.. 1981. Orogenic Andesites and Plate Tectonics. Springer-Verlag, Berlin, Heidelberg, New York, 390 p.

Gill, J.B., Morris, J.D., and Johnson, R.W., 1993. Timescale for producing the geochemical signature of island arc magmas: U-Th-Po and Be-B systematics in recent Papua New Guine lavas. Geochimica et Cosmochimica Acta, 57, 4269-4283.

Gillis, K.M., and Meyer, P.S., 2001. Metasomatism of oceanic gabbros by late stage melts and hydrothermal fluids: Evidence from the rare earth element compositions of amphiboles. Geochemistry, Geophysics, Geosystems, 2, paper number 2000GC000087.

Godard, M., Bodinier, J.L., and Vasseur, G., 1995. Effects of mineralogical reactions on trace element redistributions in mantle rocks during percolation processes: a chromatographic approach. Earth Planetary Science Letters, 123, 449-461.

Göncüoğlu, M.C., 1977. Geologie des Westlichen Nigde Massivs. University of Bonn, Ph.D. Thesis, 167 p. (unpublished).

Göncüoğlu, M.C., 1981. Niğde Masifinin jeolojisi. İç Anadolu'nun Jeolojisi Simpozyumu. Türkiye Jeoloji Kurumu Bülteni, 16-19.

Göncüoğlu, M.C., 1986. Geochronological data from the southern part (Niğde Area) of the Central Anatolian Massif. Bulletin of Mineral Research Exploration Institute, Turkey, 105/106, 83-96.

Göncüoğlu, M.C., and Türeli, K., 1993. Petrology and geodynamic interpretation of plagiogranites from Central Anatolian ophiolites (Aksaray-Türkiye). Doğa - Türk Yerbilimleri Dergisi, 2, 195-203.

Göncüoğlu, M.C., and Türeli, T.K., 1994. Alpine collision-type granitoids in the western Central Anatolian Crystalline Complex, Journal of Kocaeli University, 1, 39-46.

Göncüoğlu, M.C., Dirik, K., and Kozlu, H., 1996-1997. Pre-Alpine and Alpine terranes in Turkey: Explanatory notes to the terrane map of Tukey. Annetes Geologiques des Pays Helléniques, 37, 515-536.

Göncüoglu, M.C., Köksal, S., and Floyd, P.A., 1997. Post-collisional A-type magmatism in the Central Anatolian Crystalline Complex: petrology of the İdiş Dağı intrusives (Avanos, Turkey). Turkish Journal of Earth Sciences, 6, 65-76.

Göncüoğlu, M.C., Yalınız, M.K., Özgül, L., and Toksoy, F., 1998. Orta Anadolu Ofiyolitlerinin Petrojenezi: İzmir-Ankara-Erzincan Okyanus kolunun evrimine bir yaklaşım. Scientific and Technical Research Council of Turkey Report, 61 p. (in Turkish).

Göncüoğlu, M.C., Toprak, G.M.V., Kuşçu, İ., Erler, A., and Olgun, E., 1991. Geology of the western part of the Central Anatolian Massif: part II southern part. Unpublished Report No: 2909, Turkish Petroleum Company (in Turkish).

Göncüoğlu, M.C., Erler, A., Toprak, V., Yalınız, K., Olgun, E., and Rojay, B., 1992. Geology of the western part of the Central Anatolian Massif: part II central part: Unpublished Report No: 3155, Turkish Petroleum Company (in Turkish).

Göncüoğlu, M.C., Erler, A., Toprak, V., Olgun, E., Yalınız, K., Kuşçu, İ., Köksal, S., and Dirik, K., 1993. Geology of the central part of the Central Anatolian Massif: part III geological evolution of the Tertiary Basin of the Central Kızılırmak. Unpublished Report No: 3313, Turkish Petroleum Company (in Turkish).

Gorring, M.L., and Kay, S.M., 2000. Carbonanite metasomatized peridotite xenoliths from southern Patagonia: implications for lithospheric processes and Neogene plateau magmatism. Contributions to Mineralogy and Petrology, 140, 55-72.

Görür, N., Oktay, F.Y., Seymen, I., and Şengör, A.M.C., 1984. Paleotectonic evolution of Tuz Gölü Basin complex, central Turkey. In: Dixon, J.E., and Robertson, A.H.F. (eds.), The Geological Evolution of the Eastern Mediterranean. Geological Society of London, Special Publication, 17, 81-96.

Green, T.H., 1982. Anatexis of mafic crust and high pressure crystallization of andesite. In: Thorpe, R.S. (ed.), Andesites: Orogenic Andesites and Related Rocks. Wiley, New York, 465-488.

Green, T.H., 1995. Significance of Na/Ta as an indicator of geochemical processes in the crust-mantle system. Chemical Geology, 120, 347-359..

Green, T.H., Adams, J., and Sie, S.H., 1992. Trace element partitioning between silicate minerals and carbonatite at 25 kbar and application to mantle metasomatism. Mineralogy and Petrlogoy, 46, 179-184.

Guidotti, C.V., 1984. Micas in metamorphic rocks. In: Micas, Bailey, S.W. (ed.), Mineralogical Society of America, Reviews in Mineralogy, 13, 357-467.

Güleç, N., and Kadıoğlu, Y.K., 1998. Relative involment of mantle and crustal components in Agaçören granitoid, (central Anatolia-Tukey): estimates from trace and Sr-isotope data. Chemie der Erde, 58, 23-37.

Guo, J., and Green, T.H.,1990. Experimental study of Ba partitioning between phlogopite and silicate liquid at upper mantle pressure and temperature. Lithos, 24, 83-95.

Gutscher., M.A., Maury, R., Eissen, J.P., and Bourdon, E., 2000. Can slab melting be caused by flat subduction? Geology, 28, 535-538.

Haas, K.M., Devey, C.W., and Mertz, D.F., 1996. Geochemistry of lavas from Mohns Ridge, Norwegian–Greenland Sea: implications for melting conditions and magma sources near Jan Mayen. Contributions to Mineralogy Petrology, 123, 223–237.

Haggerty, S.E., 1991. Oxide textures - a mini atlas. In: Lindsley, D.H. (ed.), Oxide Minerals: Petrologic and Magnetic Significance, Mineralogical Society of America, Reviews in Mineralogy, 25, 129-219.

Hammarstrom, J.M., and Zen, E-an, 1986. Aluminum in hornblende: An empirical igneous geobarometer. American Mineralogist, 71, 1297–1313.

Hartmann, G., and Wedepohl, K.H., 1993. The composition of peridotite tectonites from the Ivrea Complex, northern Italy: residues from melt extraction. Geochimica et Cosmochimica Acta, 57, 1761-1782.

Hattori, K., and Sato, H., 1996. Magma evolution recorded in plagioclase composition in 1991 Pinatubo Eruption Products. American Mineralogist, 81, 982-994.

Hawkesworth, C.J., and Norry, M.J., 1983. Continental Basalts and Mantle Xenoliths. Shiva Publications, Nantwich, U.K., 378 p.

Hawkesworth, C.J., Erlank, A.J., Kempton, P.D., and Waters, F.G., 1990. Mantle metasomatism: isotope and trace element trends in xenoliths from Kimberley, South Afrşca. Chemical Geology, 85, 19-34.

Hawkesworth, C.J., Gallagher, K., Hergt, J.M., and McDermott, F., 1994. Destructive plate margin magmatism: geochemistry and melt generation. Lithos, 33, 169-188.

Hébert, R., and Laurent, R., 1990. Mineral chemistry of the plutonic section of the Troodos ophiolite: new constraints for genesis of arc related ophiolites. In: Malpas, J., Moores, E., Panayiotou, A., and Xenophontos, C. (eds.), Ophiolites-Oceanic Crustal Analogues. Proceeding of Troodos Ophiolite Symposium, 1987, Geological Survey Department, Cyprus, Nicosia, 149-163.

Hecht, L., 1994. The chemical composition of biotite as an indicator of magmatic fractionation and metasomatism in Sn-specialized granites of the Fichtelgebirge (NW Bohemian Massif, Germany). In: Seltmann, R., Kämpf, H., and Möller, P. (eds), Metallogeny of Collisional Orogens, Czech Geolical Survey, Prague, 295-300.

Helz, R.T., 1973. Phase relations of basalts in their melting range at P_{H2O}=5 kb as a function of oxyen fugacity. Part I. Mafic phases. Journal of Petrology, 14, 249-302.

Hewitt, D.A., and Abrecht, J., 1986. Limitations on the interpretation of biotite substitutions from chemical analyses of natural samples. American Mineralogist, 60, 854-862.

Hirschmann, M.M., and Stolper, E.M., 1996. A possible role for garnet pyroxenite in the origin of the garnet signature in MORB. Contributions to Mineralogy and Petrology, 124, 185-208.

Hofmann, A.W., 1997. Mantle geochemistry: the message from oceanic volcanism. Nature, 385, 219-229.

Holland T.J.B., and Powell, R., 1990. An enlarged and updated internally consistent thermodynamic dataset with uncertainties and correlations: the system K_2O-Na_2O-CaO-MgO-FeO-Fe_2O_3-Al_2O_3-TiO_2-SiO_2-C-H_2-O_2. Journal of Metamorphic Geology, 8, 89-124.

Holland, T., and Blundy, J., 1994. Non-ideal interactions in calcic amphiboles and their bearing on amphibole-plagioclase thermometry. Contributions to Mineralogy and Petrology, 116, 433-447.

Hollister, L.S., Grissom, G.C., Peters, E.K., Stowell, H.H., and Sisson, V.B., 1987. Confirmation of the empirical correlation of Al in hornblende with pressure of solidification of calc-alkaline plutons. American Mineralogist, 72, 231–239.

Humphris, S.E., 1984. The mobility of the rare earth elements in the crust. In: Henderson, P. (ed.), Rare Earth Element Geochemistry, Elsevier, Amsterdam, 317–342.

Humphris, S.E., and Thompson, G., 1978. Hydrothermal metamorphism of oceanic basalts by seawater. Geochimica et Cosmochimica Acta, 42, 107-125.

Hunter, R.H., and McKenzie, D., 1989. The equilibrium geometry of carbonate melts in rocks of mantle composition, Earth Planetary Science Letters, 92, 347-356.

Ionov, D.A., 1998. Trace element composition of mantle-derived carbonates and coexisting phases in peridotite xenoliths from alkali basalts. Journal of Petrology, 39, 1931-1941.

Ionov, D.A., and Hofman, A.W., 1995. Nb-Ta rich mantle amphiboles and micas: implications for subduction related metasomatic trace element fractionations. Earth and Planetary Science Letters, 131, 341-356.

Ionov, D.A., Griffin, W.L., and O'Reilly, S.Y., 1997. Volatile-bearing minerals and lithosphere trace elements in the upper mantle. Chemical Geology, 141, 153–184.

Ionov, D.A., Hoffman, A.W., and Shimizu, N., 1994. Metasomatism-induced melting in mantle xenoliths from Mongolia. Journal of Petrology, 35, 753-785.

Ionov, D.A., Ashchepkov, I.V., Stosch, H.-G., Witt-Eickschen, G., and Seck, H.A., 1993. Garnet peridotite xenolith from the Vitim volcanic field, Baikal region: the nature of the garnet-spinel peridotite transition zone in the continental mantle. Journal of Petrology, 34, 1141-1175.

Irvine, T.N., and Baragar, W.R.A., 1971. A guide to the geochemical classification of the common volcanic rocks. Canadian Journal of Earth sciences, 8, 523-548.

Jakes, P., and White, A.J.R., 1972. Major and trace element abundances in volcanic rocks of orogenic areas. Geological Society of American Bulletin, 83, 29-40.

Jenner, G.A., Dunning, G.R., Malpas, J., Brown, M., and Brace, T., 1991. Bay of Islands and Little Port complexes, revisited: age, geochemical and isotopic evidence confirm suprasubduction-zone origin. Canadian Journal of Earth Sciences, 28, 1635–1652.

Jenner, G.A., Foley, S.F., Jackson, S.E., Green, T.H., Fryer, B.J., and Longerich, H.P., 1994. Determination of partition coefficients for trace elements in high pressure-temperature experimental run products by laser ablation microprobe-inductively coupled plasma-mass spectrometry (LAM-ICP-MS). Geochimica et Cosmochimica Acta, 58, 5099-5103.

Jiang, Y.-H., Jiang, S.-Y., Ling, H.-F., Zhou, X.-R., Rui, X.-J., and Yang, W.-Z., 2002. Petrology and geochemistry of shoshonitic plutons from the western Kunlun orogenic belt, Xinjiang, northwestern China: implications for granitoid geneses. Lithos, 63, 165– 187.

Johnson, M.C., and Rutherford, M.J., 1989. Experimental calibration of the aluminum-in-hornblende geobarometer with application to Long Valley caldera (California) volcanic rocks. Geology, 17, 837–841.

Johnson, K.E., Davis, A.M., and Brynzia, L.T., 1996. Constructing styles of hydrous metasomatism in the upper mantle: An ion microprobe investigation. Geochimica et Cosmochimica Acta, 60, 1367-1385.

Kadıoğlu, Y.K., 1996. Genesis of Ağaçören Intrusive Suite and Its Enclaves (central Anatolia): Constraints from Geological, Petrographic, Geophysical and Geochemical Data. Ph.D. Thesis in Geological Engineering, Middle East Technical University, Ankara, 242 p. (unpublished).

Kadıoğlu, Y.K., and Güleç, N., 1996. Mafic microgranular enclaves and interaction between felsic and mafic magmas in the Ağaçören intrusive suite: Evidence from petrographic features and mineral chemistry. International Mineralogical review, 38, 854-867.

Kadıoğlu, Y.K., Ateş, A., and Güleç, N., 1998. Structural interpretation of gabbroic rocks in Ağaçören Granitoid, central Turkey: field observations and aeromagnetic data. Geological Magazine, 135(2), 245-254.

Kamber, B.S., Ewart, A., Collerson, K.D., Bruce, M.C., and McDonald., G.D., 2002. Fluid-mobile trace element constraints on the role of slab melting and implications for Archaean crustal growth models. Contributions to Mineralogy and Petrology, 144, 38-56.

Karsten, J.L., Klein, E.M., and Sherman, S.B., 1996. Subduction zone geochemical characteristics in ocean ridge basalts from the southern Chile Ridge: implications of modern ridge subduction systems for the Archean. Lithos, 37, 143–161.

Kay, S., Kay, R.W., and Citron, G.P., 1982. Tectonic controls on Aleutian tholeiitic and calc-alkaline magmatism. Journal of Geophysical Research, 87, 4051-4072.

Kelemen, P.B., Shimizu, N., and Dunn, T., 1993. Relative depletion of niobium in some arc magmas and continental crust: partitioning of K, Nb, La, Ce during melt/rock reaction in the upper mantle. Earth and Planetary Science Letters, 120, 111-134.

Kempton, P.D., 1987. Mineralogic and geochemical evidence for differing sytle of metasomatism in spinel lherzolite xenoliths: Enriched mantle source regions of basalts? In: Menzies, M.A., and Hawkesworth, C.J. (eds)., Mantle Metasomatism, Academic Press, London, 45-89.

Kepezhinzkas, P.K., Defant, M.J., and Drummond, M.S., 1995. Na metasomatism in the island arc mantle by slab melt-peridotite interaction: evidence from mantle xenoliths in the North Kamchatka arc. Journal of Petrology, 36, 1250-1267.

Kepezhinzkas, P.K., Defant, M.J., and Drummond, M.S., 1996. Progressive enrichment of island arc mantle by melt-peridotite interaction inferred from Kamchatka xenoliths. Geochimica et Cosmochimica Acta, 60 1217-1229.

Keppler, H., 1996. Constraints from partitioning experiments on the composition of subduction fluids. Nature, 380, 237-240.

Kjarsgaard, B.A., and Hamilton, D.L., 1989. The genesis of carbonattites by immiscibility. In: Bell, K. (ed.), Carbonatite, Unwin Hyman, London, 388-404.

Klein, C., and Hurlbut, C.S.Jr., 1985. Manual of Mineralogy. New York, John Wiley and Sons, 596 p.

Koçak, K., and Leake, B.E., 1994. The petrology of the Ortaköy district and its ophiolite at the western edge of the Middle Anatolian Massif, Turkey. Journal of African Earth Sciences, 18(2), 163-174.

Köksal, S., Romer, R.L., Göncüoğlu, M.C., and, Toksoy-Köksal, F., 2003. Timing of the Transition from Post-Collisional to A-Type Granitic Magmatism: Titanite U-Pb Ages From the Alpine Central Anatolian Granitoids, Turkey. International Journal of Earth Sciences (in review).

Kushiro, I., 1972. Effects of water on composition of magmas formed at high pressures. Journal of Petrology, 13, 311-334.

Lachize, M., Lorand, J.P., and Juteau, T., 1996. Calc-alkaline differentiation trend in the plutonic sequence of the Wadi Haymiliyah section, Haylayn massif, Semail ophiolite, Oman. Lithos, 38. 207-232.

Lapierre, H., Taylor, R.N., Rouer, O. and Chaisemartin, H., 1992. Mineral chemistry of forearc volcanics rocks from the Izu-Bonin arc, Holes 792E and 793B. Proceedings of the Ocean Drilling Program, Scientific Results, 126, 431-447.

Larsen, L.M., and Rex, D.C., 1992. A review of the 2500 Ma span of alkaline-ultramafic, potassic and carbonatitic magmatism in West Greenland. Lithos, 28, 367-402.

Le Bas, M.J., 1962. The role of alumina in igneous clinopyroxenes with relatio to their parentage. American Journal of Science, 260, 267-288.

Leake, B.E., 1978. Nomenclature of amphiboles. American Mineralogist, 63, 1023-1052.

Leake, B.E., Woolley, A.R., Arps, C.E.S., Birch, W.D., Gilbert, M.C., Grice, J.D., Hawthorne, F.C., Kato, A., Kisch, H.J., Krivovichev, V.G., Linthout, K., Larid, J., Mandarino, J.A., Maresch, W.V., Nickel, E.H., Rock, N.M.S., Schmacher, J.C., Smith, D.C., Stephenson, N.C.N., Ungaretti, L., Whittaker, E.J.W., and Youzhi, G., 1997. Nomenclature of amphiboles: report of the subcommittee on amphiboles of the International Mineralogical Association, Commission on New Minerals and Mineral Names. American Mineralogist, 82, 1019–1037.

Leterrier, J., Maurry, R.c., Thonon, P., Girard, D., and Marchal, M., 1982. Clinopyroxene composition as a method of identification of the magmatic affinites of paleo-volcanic series. Earth and Planetary Science Letters, 59, 139-154.

Lindsley, D.H., 1983. Pyroxene thermometry. American Mineralogist, 68, 477-493.

Liogys, V.A., and Jenkins, D.M., 2000. Hornblende geothermometry of amphibolite layers of the Popple Hill gneiss, north-west Adirondack Lowlands, New York, USA. Journal of Metamorphic Geology, 18, 513-530.

Litasov, K.D., Foley, S.F., and Litasov, Y.D., 2000. Magmatic modification and metasomatism of the subcontinental mantle beneath the Vitim volcanic field East Siberia : evidence from trace element data on pyroxenite and peridotite xenoliths from Miocene picrobasalt. Lithos, 54, 83–114.

Livermore, R.A., and Smith, A.G., 1984. Some boundary conditions for the evolution of the Mediterranean region. In: Stanley, D.J., and Wezel, F.C. (eds.), Geological Evolution of the Mediterranean Basin. Springer, 83-110.

Lloyd, F.E., and Bailey, D.K., 1975. Light element metasomatism of the continental mantle: the evidence and the consequences. Phys. Chem. Earth, 9, 389-416.

Loucks, R.R., 1990. Discrimination of ophiolitic from nonophiolitic ultramafic-mafic allochthons in orogenic belts by the Al/Ti ratio in clinopyroxene. Geology, 18, 346–349.

Maaloe, S., and Wyllie, P.J., 1979. The join grossularite-pyrope at 30 kb, and its petrological significance. American Journal of Science, 279, 288-301.

Manning, C.E., MacLeod, C.J., and Weston, P.E., 2000. Lower crustal cracking front at fast-spreading ridges: Evidence from the East Pacific Rise and Oman ophiolite. In: Ophiolites and Oceanic Crust: New Insights From Field Studies and the Ocean Drilling Program, Dilek, Y., Moores, E., Elthon, D., and Nicolas, A. (eds.), Geological Society of America, Boulder, CO, 261–272.

Marcelot, G., Bardinzeff, J.M., Maury, R.C., and Rançon, J.P., 1988. Chemical trends of early formed clinopyroxene phenocrysts from some alkaline and orogenic basic lavas. Bulletin of Geological Society of France, 8, 851-859.

Maury, R.C., Defant, M.J., and Joron, J.L., 1992. Metasomatism of the subarc mantle inferred from trace elements in Philippine xenoliths. Nature, 360, 661-663.

Maury, R.C., Defant, M.J., Bellon, H., Jacques, M., Joron, J.-L., McDermott, F., and Vidal, P., 1998. Temporal and geochemical trends in northern Luzon arc lavas (Philippines): Implications on metasomatic processes in the island arc mantle. Bulletin de la Société Géologique de France, 169, 69-80.

McDonough, W.F., 1990. Constraints on the composition of the continental lithospheric mantle. Earth and Planetary Science Letters, 101, 1–18.

McPherson, E., Thirlwall, M.F., Parkinson, I.J., Menzies, M.A., Bodinier, J.L., Woodland, A., and Bussod, G., 1996. Geochemistry of metasomatism adjacent to amphibole-bearing veins in the Lherz peridotite massif. Chemical Geology, 134, 135-157.

Meffre, S., Aitchison, J.C., and Crawford, A.J., 1996. Geochemical evolution and tectonic significance of boninites and tholeiites from the Koh ophiolite, New Caledonia. Tectonics, 15, 67-83.

Menzies, M., 1983. Mantle ultramafic xenoliths in alkaline magmas: evidence for mantle heterogeneity modified by magmatic activity. In: Hawkesworth, C.J., Norry, M.J. (eds.), Continental Basalts and Mantle Xenoliths. Shiva Publishing, Cheshire, 92-110.

Menzies, M.A., Rodgers, N., Tindle, A., and Hawkesworth, C.J., 1987. Metasomatic and enrichment processes in lithospheric peridotites, and effect of asthenosphere-lithosphere interaction. In: Menzies, M., and Hawkesworth, C.J. (eds.), Mantle Metasomatism, Academic Press, London, 313-361.

Middlemost, E.A.K., 1975. The basalt clan. Earth Science Review, 11, 337-364.

Mitchel, R.H., and Meyer, H.O.A., 1989. Niobian K-Ba-V titanites from micaceous kimberlite. Star Mine. Orange Free State. South Africa. Mineralogical Magazine. 53. 451-456.

Mitchell, R.H., and Bergman, S., 1991. Petrology Lamproites. Plenum, New York, 447 p.

Miyashiro, A., 1974. Volcanic rock series in arcs and active continental margins. American Journal of Science, 274, 321-355.

Morbidelli, L., Gomes, C.B., Beccaluva, L., Brotzu, P., Conte, A.M., Ruberti, E., and Traversa, G., 1995. Mineralogical, petrological and geochemical aspects of alkaline and alkaline-carbonatite association from Brazil. Earth Science Review, 39, 135-168.

Morimoto, N., 1989. Nomenclature of pyroxenes. Canadian Mineralogist, 27, 143-156.

Morimoto, N., and Kitamura, M. (1983). Q-J diagram for classification of pyroxenes. Journal of Japanese Association, Mineralogy, Petrology and Economic Geology, 78, p. 141 (in Japanese).

Morris, J.D., and Hart, S.R., 1983. Isotopic and incompatible trace element constraints on the genesis of island arc volcanics from Cold Bay and Amak Island, Aleutians, and implications for mantle structure. Geochimica et Cosmochimica Acta, 47, 2015–2030.

Münker, C., 1998. Nb-Ta fractionation in a Cambrian arc/back arc system, New Zeland: source constraints and apllication of refined ICP-MS techniques. Chemical Geology, 144, 23-45.

Mysen, B.O., and Boettcher, A.L., 1975a. Melting of hydrous mantle: I. Phase relations of natural peridotite at high pressures and temperatures with controlled activities of water, carbon dioxide and hydrogen. Journal of Petrology, 16, 520-548.

Mysen, B.O., and Boettcher, A.L., 1975b. Melting of hydrous mantle: II. Geochemistry of crystals and liquids formed by anatexis of mantle peridotite at high pressures and temperatures as a function of controlled activities of water, carbon dioxide and hydrogen. Journal of Petrology, 16, 549-592.

Neumann, E.-R., Sorensen, V.B., Simonsen, S.L., and Johnsen, K., 2000. Gabbroic xenoliths from La Palma, Tenerife and Lanzarote, Canary Islands: evidence for reactions between mafic alkaline Canary Islands melts and old oceanic crust. Journal of Volcanology and Geothermal Research, 103, 313-342.

Neumann, E.-R., Wulff-Pedersen, E., Simonsen, S.L., Pearson, N.J., Martí, J., and Mitjavila, J., 1999. Evidence for fractional crystallization of periodically refilled magma chambers in Tenerife, Canary Islands. Journal of Petrology, 40, 1089-1123.

Nicholls, G.T., Wyliie, P.J., and Stern, C.R., 1994. Subduction zone melting of pelagic seiments constrained by melting experiments. Nature, 371, 785-788.

Nicholls, I.A., and Ringwood, A.E., 1973. Effect of water on olivine stability in tholeiites and production of silica saturated magmas in island arc environment. Journal of Geology, 81, 285-300.

Nicolas, A., and Jackson, E.D., 1972. Repartitions en deux provinces des peridotites des chaines alpines longenat la Mediterranee, implications geotechniques. Swiss Bulletin of Mineralogy and Petrology, 52, 479-495.

Nimis, P., 1995. A clinopyroxene geobarometer for basaltic systems based on crystal-structure modeling. Contributions to Mineralogy and Petrology, 121, 115-125.

Nimis, P., 1999. Clinopyroxene geobarometry of magmatic rocks. Part 2. Structural geobarometers for basic to acid, tholeiitic and mildly alkaline magmatic systems. Contributions to Mineralogy and Petrology, 135, 62-74.

Nimis, P., and Ulmer, P., 1998. Clinopyroxene geobarometry of magmatic rocks. 1. An expanded structural geobarometer for anhydrous and hydrous, basic and ultrabasic systems. Contributions to Mineralogy and Petrology, 133, 314-327.

Nockolds, S.R., 1947. The relation between chemical composition and paragenesis in the biotite micas of igneous rocks. American Journal of Science, 245(5), 401-420.

Noll, P.D., Newsom, H., Leeman, W.P., and Ryan, I.G., 1996. The role of hydrothermal fluids in the production of subduction zone magmas: evidence from siderophile and chalcophile trace elements and boron. Geochimica et Cosmochimica Acta, 60, 587-611.

O'Reilly, S.Y., and Griffin, W.L., 1988. Mantle metasomatism beneath western Victoria, Australia, I. Metasomatic processes in Cr-diopside lherzolites. Geochimica et Cosmochimica Acta, 52, 433-447.

Özcan, A., Erkan, E., Keskin, A., Keskin E., Oral, A., Özer, S., Sümengen, M, and Tekeli, O., 1980. Kuzey Anadolu Fayı Kırşehir Masifi arasının temel jeolojisi. MTA Report No: 6722, Ankara (unpublished).

Papike, J.J., Cameron, K.L., and Baldwin, K., 1974. Amphiboles and pyroxenes: characterization of other than quadrilateral components and estimates of ferric iron from microprobe data. Geological Society of America, 6, 1053-1054.

Parlak, O., Delaloye, M., and Bingöl, E., 1996. Mineral chemistry of ultramafic and mafic cumulates an indicator of the arc-related origin of Mersin Ophiolite (Southern Turkey). Geologische Rundschau, 85, 647-661.

Parlak, O., 2000. Geochemistry and Significance of mafic dyke swarms in the Pozantı-Karsantı Ophiolite (Southern Turkey). Turkish Journal of Earth Sciences, 24, 29-28.

Parlak, O., Delaloye, M., and Bingöl, E., 2002. The supra-subduction zone Pozantı–Karsantı ophiolite, southern Turkey: evidence for high-pressure crystal fractionation of ultramafic cumulates. Lithos, 65, 205-224.

Parsons, I., Mason, R.A., Becker, S.M., and Finch, A.A., 1991. Biotite equilibra and fluid circulation in the Klukken Intrusion. Journal of Petrology, 32, 1299-1333.

Patino Douce, A.E., 1993. Titanium substitution in biotite: an emprical model with applications thermometry, O_2 and H_2O barometries, and consequences for biotite stability. Chemical Geology, 108, 133-162.

Patino Douce, A.E., and Johnston, A.D., 1991. Phase equilibria and melt productivity in the pelitic system: Implications for the origin of peraluminous granitoids and aluminous granulites. Contributions to Mineralogy and Petrology, 107, 202-218.

Patino Douce, A.E., Johnston, A.D., and Rice, J.M., 1993. Octahedral excess mixing properties in biotite: a working model with applications to geobarometry and geothermometry. American Mineralogist, 78, 113-131.

Pearce, J.A., 1980. Geochemical evidence for the genesis and eruptive settings of lavas from Tethyan ophiolites. In: Panayiotou, A. (ed.), Ophiolites. Geological Survey Department, Cyprus, 261–272.

Pearce, J.A., 1982. Trace element characteristics of lavas from destructive plate boundaries. In: Thorpe, R.S. (ed.), Andesites: Orogenic Andesites and Related Rocks, Jon Wiley and Sons, New York, 525-548.

Pearce, J.A., 1983. The role of sub-continental lithospere in magma genesis at destructive plate margins. In: Hawkesworth, C.J., Norry, M.J. (eds.), Continental Basalts and Mantle Xenoliths, Shiva, Nantwhich, 230–249.

Pearce, J.A., 1996. A user's guide to basalt discrimination diagrams. In: Wyman, D.A. (ed.), Trace Element Geochemistry of Volcanic Rocks: Applications for Massive Sulphide Exploration. Geological Association of Canada, Short Course Notes, 12, 79–113.

Pearce, J.A., and Cann, J.R., 1973. Tectonic setting of basic volcanic rocks determined using trace element analyses. Earth and Planetary Science Letters, 19, 290–300.

Pearce, J.A., and Norry, M.J., 1979. Petrogenetic implications of Ti, Zr, Y and Nb variations in volcanic rocks. Contributions to Mineralogy and Petrology, 69, 33-47.

Pearce, J.A., and Parkinson, I.J., 1993. Trace element models for mantle melting. Application to volcanic arc petrogenesis. In: Prichard, H.M., Alabaster, T., Harris, N.B.W., and Neary, C.R. (eds.), Magmatic Processes and Plate Tectonics. Geological Society of London, Special Publication, 76, 373-403.

Pearce, J.A., and Peate, D.W., 1995. Tectonic implications of composition of volcanic arc magmas. Annual Review of Earth Planetary Science, 23, 251-285.

Pearce, J.A., Lippard, S.J., and Roberts, S., 1984. Characteristics and tectonic significance of supra-subduction zone ophiolites. In: Kokelaar, B.P., Howells, M.F. (eds.), Marginal Basin Geology. Geological Society of London, Special Publication, 16, 77-94.

Pearce, J.A., Barker, P.F., Edwards, S.J., Parkinson, I.J., and Leat, P.T., 2000. Geochemistry and tectonic significance of peridotites from the South Sandwich arc-basin system, South Atlantic. Contributions to Mineralogy and Petrology, 139(1), 36-53.

Pearce, J.A., Ernewein, M., Bloomer, S.H., Parson, L.M., Murton, B.J., and Johnson, L.E., 1994. Geochemistry of Lau Basin volcanic rocks: influence of ridge segmentation and arc proximity. In: Smelle, J.L. (ed.), Volcanism Associated with Extension of Consuming Plate Margins. Geological Society of London, Special Publication, 53-75.

Perchuk, L.L., Aranovich, L.Y., Podlesskii, K.K., Lavrant'eva I.V., Gerasimov, V.Y., Fed'kin, V.V., Kitsul, V.I., Karsakov, L.P., and Berdnikov, N.V., 1985. Precambrian granulites of the Aldan Shield, eastern Siberia, USSR. Journal of Metamorphic Geology, 3, 265-310.

Pereira, L.C.J., Waerenborgh, J.C., Figueiredo, M.O., Prudencio, M.I., Gouveia, M.A., Silva, T.P., Morgado, I., and Lopez, A., 1993. A comparative study of biotite weathering from two different granitic rocks. Chemical Geology, 107, 301-306.

Perfit, M.R., Gust, D.A., Bence, A.E., Arculus, R.J., and Taylor, S.R., 1980. Chemical characteristics of island arc basalts. Implications for mantle sources.Chemical Geology, 30, 227-236.

Pfänder, H.A., Jochum, K.P., Kozakov, I., Kröner, A., and Todt, W., 2002. Coupled evolution of back-arc and island arc-like mafic crust in the late-Neoproterozoic Agardagh Tes-Chem ophiolite, Central Asia: evidence from trace element and Sr–Nd–Pb isotope data. Contributions to Mineralogy and Petrology, 143, 154-174.

Philippot, P., 1993. Fluid-melt-rock interaction in mafic eclogites and coesite-bearing metasediments: constraints on volatile recycling during subduction. Chemical Geology, 108, 93-112.

Philippot, P., and Scambelluri, M., 1995. The composition and behaviour of fluids in high-pressure rocks from Alps: a review. In: Lombardo, B. (ed.), Studies of Metamorphic Rocks and Minerals of the western Alps, vol Ugo Pognante,Torino, Boll Museo Reg Sci Nat, 13, 76-102.

Poli, S., and Schmidt, M.W., 1995. H_2O transport and release in subduction zones: experimental constraints on basaltic and andesitic systems. Journal of Geophysical Research, 100, 22299-22314.

Prouteau, G., Maury, R.C., Sajona, F.G., Cotton, J., and Joron, J.L., 2000. Behaviour of niobium, tantalum and other high field strength elements in adakites and related lavas from the Philippines. The Island Arc, 9(4), 487-498.

Raase, P., 1974. Al and Ti contents of hornblende, indicators of pressure and temperature of regional metamorphism. Contribution to Mineralogy and Petrology, 45, 231-236.

Rapp, R.P., Watson, E.B., and Miller, C.F., 1991. Partial melting of amphibolite/eclogite and the origin of Archean trondhjemites and tonalites. Precambrian Research, 51, 1-25.

Rapp, R.P., Shimizu, N., Norman, M.D., and Applegate, G.S., 1999. Reaction between slab melts and peridotite in the mantle wedge: experimental constraints at 38 Gpa. Chemical Geology, 160, 335-356.

Ricou, L.E., 1971. Le croissant ophioliquitie périarabe: une ceinture de nappes mises en palace au Crétacé supérieur. Review of Geographical, Physical and Geological Dynamics, 13, 327-349.

Rieder, M., Cavazzini, G., D'Yakonov, Y.s., Frank-Kamenetskii, V.A., Gottardi, G., Guggenheim, S., Koval, P.V., Müller, G., Neiva, A.M.R., Radoslovich, E.W., Robert, J.-L., Sassi, F.P., Takeda, H., Weiss, Z., and Wones, D.R., 1998. Nomenclature of the micas. Canadian Mineralogist, 36, 905-912.

Righter, K., and Carmichael, I.S.E., 1996. Phase equilibria of phlogopite lamprophyres from western Mexico: biotite-liquid equilibria and P-T estimates for biotite-bearing igneous rocks. Contributions to Mineralogy and Petrology, 123, 1–21.

Robert, J.-L., 1976a. Phlogopite solid solutions in $K_2O-MgO-Al_2O_3-SiO_2-H_2O$. Chemical Geology, 17, 195-212.

Robert, J.-L., 1976b. Titanium solubility in synthetic phlogopite solid solution. Chemical Geology, 17, 213-227.

Robertson, A.H.F., 2002. Overview of the genesis and emplacement of Mesozoic ophiolites in the Eastern Mediterranean Tethyan region. Lithos, 65, 1-67.

Robertson, A.H.F., and Dixon, J.E., 1984. Introduction: aspects of the geological evolution of the Eastern Mediterranean. In: Dixon, J.E., Robertson, A.H.F. (eds.), The Geological Evolution of the Eastern Mediterranean. Geological Society of London, Special Publication, 17, 1-74.

Robinson, P., Ross, M., and Jaffe, H.W., 1971. Composition of the anthophyllite-gedrite series, comparison of gedrite-hornblede, and the anthophyllite-gedrite solvus. American Mineralogist, 56, 1005-1041.

Rocci, G., Ohnenstetter, D., and Ohnenstetter, M., 1975. La dualite des ophiolites tethysiennes. Petrologie, 1, 172-174.

Rottura, A., Bargossi, G.M., Caggianelli, A., Del Moro, A., Visona, D., and Tranne, C.A., 1998. Origin and significance of the Permian high-K calc-alkaline magmatism in the central-eastern Southern Alps, Italy. Lithos, 45, 329–348.

Rowins, S.M., Lalonde, A.E., and Cameron, E.M., 1991. Magmatic oxidation in the syenitic Murdock Creek intrusion, Kirkland Lake, Ontario: evidence from the ferromagnesian silicates. Geological Journal, 99, 395-414.

263

Rudnick, R.L., McDonough, W.F., and Chappel, B.W., 1993. Carbonatite metasomatism in the northern Tanzanian mantle: petrographical and geochemical characteristics. Earth and Planetary Science Letters, 114, 463-475.

Rutherford, M.J., 1973. The phase relations of aluminous iron biotites in the system $KalSi_3O_8$-KAlSiO4-Al_2O_3-Fe-O-H. Journal of Petrology, 14(1), 159-180.

Sajona, F.G., Maury, R.C., Prouteau, G., Cotton, J., Schiano, P., Bellon, H., and Fontaine, L., 2000. Slab melt as metasomatic agent in island arc magma mantle sources, Negros and Batan (Philippines). The Island Arc, 9(4), 472-486.

Saunders, A., and Tarney, J., 1991. Back-arc basins. In: Floyd, P.A. (ed.), Oceanic Basalts, Blackie, London, 219-263.

Schiano, P., Clocciatti, R., Shimizu, N., Maury, R.C., Jochum, K.-P., and Hofmann, A.W., 1995. Hydrous, silica-rich melts in the sub-arc mantle and their relationship with erupted lavas. Nature, 377, 595-600.

Schmidt, M.W., 1992. Amphibole composition in tonalite as a function of pressure: An experimental calibration of the Al-in-hornblende barometer. Contributions to Mineralogy and Petrology, 110, 304–310.

Schumacher, J.C., 1991. Empirical ferric iron corrections: necessity, assumptions, and effects on selected geothermobarometers. Mineralogical Magazine, 55, 3-18.

Searle, M.P., and Malpas, J., 1982. Petrochemistry and origin of sub-ophiolitic metamorphic and related rocks in the Oman Mountains. Journal of Geological Society of London, 139, 236-248.

Seifert, W., Kampf, H., and Wasternack, J., 2000. Compositional variation in apatite, phlogopite and other accessory minerals of the ultramafic Delitzsch complex, Germany: implication for cooling history of carbonatites. Lithos, 53, 81-100.

Sekine, T., and Wyllie, P.J., 1982. Phase relationships in the system $KAlSiO_4$ - Mg_2SiO_4 - SiO_2 - H_2O as a model for hybridisation between hydrous siliceous melts and peridotite. Contributions to Mineralogy and Petrology, 79, 368-374.

Sekine, T., and Wyllie, P.J., 1983. Experimental simulation of mantle hybridization in sunduction zones. Journal of Geology, 91, 511-528.

Sen, C., and Dunn, T., 1994. Dehydration melting of a basaltic composition amphibolite at 1.5 and 2 Gpa: implications for the origin of adakites. Contributions to Mineralogy and Petrology, 117, 394-409.

Sen, C., and Dunn, T., 1995. Experimental modal metasomatism of a spinel lherzolite and the production of amphibole-bearing peridotite. Contributions to Mineralogy and Petrology, 119, 422-432.

Serri, G., 1990. Neogene-Quaternary magmatism of the Tyrrhenian region: characterization of the magma sources and geodynamic implications. Memorie Società Geologica Italiana, 41, 219–242.

Seymen, İ., 1984. Kırşehir Masifi metamorfitllerinin jeoloji evrimi. Ketin Simpozyumu, Türkiye Jeoloji Kurumu Publication, 133-148.

Shau, Y.-H., Yang, H.-Y., and Peacor, D.R., 1991. On oriented titanite and rutile inclusions in sagenitic biotite. American Mineralogist, 76, 1205-1217.

Shaw, C.S.J., and Penczak, R.S., 1996. Barium- and titanium-rich biotite and phlogopite from the western and eastern gabbro, Coldwell Alkaline Complex, northwestern Ontario. Canadian Mineralogist, 34, 967-975.

Shervais, J.W., 1982. Ti–V plots and the petrogenesis of modern and ophiolitic lavas. Earth and Planetary Science Letters, 59, 101–118.

Shimoda, G., Tatsumi, Y., Nohda, S., Ishizaka, K., and Jahn, B.M., 1998. Setouchi high-Mg andesites revisited: geochemical evidence for melting of subducting sediments. Earth and Planetary Science Letters, 36, 359-362.

Simonetti, A., Shore, M., and Bell, K., 1996. Diopside phenocrysts from nephenilite lavas, Napak volcano, eastern Uganda: evidence for magma mixing. Canadian Mineralogist, 34(2), 223-234.

Spear, F.S., 1981. An experimental study of hornblende stability and compositional variability in amphibolite. American Journal of Science, 281, 697-734.

Speer, J.A., 1984. Micas in igneous rocks. In: Micas, Bailey, S.W. (ed.), Mineralogical Society of America, Reviews in Mineralogy, Washington DC, 13, 299–356.

Spulber, S.D., and Rutherford, M.J., 1983. The origin of rhyolite and plagiogranite in oceanic crust: An experimental study. Journal of Petrology, 24, 1-25.

Stein, M., and Goldstein, S.L., 1996. From mantle head to continental lithosphere in the Arabian– Nubian Shield. Nature, 382, 773– 778.

Stein, M., and Hofmann, A.W., 1992. Fossil plumes beneath the Arabian lithosphere? Earth Planetary Science Letters, 114, 193– 209.

Stolz, A.J., Jochum, KP., Spettel, B., and Hofmann, A.W., 1996. Fluid- and melt-related enrichment in the subarc mantle: evidence from Nb/Ta varaitions in island arc basalts. Geology, 24, 587-590.

Sudo, A., and Tatsumi, Y., 1990. Phlogopite and K-amphibole in the upper mantle: implication for magma genesis in subduction zones. Geophysical Research Letter, 17, 29-32.

Sun, S.S., and McDonough, W.F., 1989. Chemical and isotopic systematics of ocean basalts: implication for mantle composition and processes. In: Saunders, A.D., Norry, M.J. (eds.), Magmatism in Ocean Basins, Geological Society of London, Special Publication, 42, 313-345.

Şengör, A.M.C., and Yılmaz, Y., 1981. Tethyan evolution of Turkey: a plate tectonic approach. Tectonophysics, 75, 81-241.

Tatsumi, T., 1989. Migration of fluid phases and genesis of basalt magmas in subduction zones. Journal of Geophysical Research, 94, 4697-4707.

Tatsumi, Y., and Kogiso, T., 1997. Trace element transport during dehydration processes in the subducted oceanic crust: 2. origin of chemical and physical characteristics in arc magmatism. Earth and Planetary Science Letters, 148, 207-221.

Taylor, H.P.Jr, 1977. Water-rock interaction and the origin of H_2O in granitic batholiths. Journal of Geological Society, London, 133, 509–588.

Taylor, S.R., and McLennan, S.M., 1985. The Continental Crust: its Composition and Evolution, Blackwell Scientific, Oxford, 312 p.

Tegner, C., 1997. Iron in plagioclase as a monitor of the Skeargaard Intrusion. Contributions to Mineralogy and Petrology, 128, 45-51.

Teklay, M., Kröner, A., and Mezger, K., 2002. Enrichment from plume interaction in the generation of Neoproterozoic arc rocks in northern Eritrea: implications for crustal accretion in the southern Arabian–Nubian Shield. Chemical Geology, 184, 167–184.

Thirlwall M.F., and Graham, A.M., 1984. Evolution of high-Ca, high-Sr C-series basalts from Grenada, Lesser Antilles: the effects of intra-crustal contamination. Journal of Geological Society, London, 141, 427-445.

Thompson, A.B., 1992. Water in the Earth's upper mantle. Nature, 358, 295-302.

Tiepolo, M., Tribuzio, R., and Vannucci, R., 1997. Mg- and Fe-gabbroids from Northern Apennine ophiolites parental liquids and igneous differentiation processes. Ofioliti, 22, 57-69.

Toksoy, F., 1998. Petrography and Mineralogy of the Vermiculitized Phlogopitic Metagabbro from the Kurançalı Area (Kırşehir-Central Anatolia). M.Sc. Thesis in Geological Engineering, Middle East Technical University, Ankara, 175 p. (unpublished).

Toksoy, F., and Göncüoğlu, M.C., 1998. Phlogopitic Metagabbro within Central Anatolian Ophiolites, Kurançalı (Kırşehir) Area, Turkey. 3rd International Turkish Geology Symposium, August 31 - September 4, 1998, Middle East Technical University, Ankara-Turkey, Abstracts, p. 175.

Toksoy, F., and Öner, A., 1997. Vermiculitization Process. In: Proceedings of 13th National Electron Microscopy Congress with International Participitation, Middle East Technical University, Ankara-Turkey, September 1-4, 1997, 761-768.

Toksoy-Köksal, F., Göncüoğlu, M.C., and Yalınız, M.K., 2001a. Petrology of the Kurançalı Phlogopitic Metagabbro: An island arc-type ophiolitic sliver in the Central Anatolian Crystalline Complex, Turkey. International Geological Review, 43(7), 624-639.

Toksoy-Köksal, F., Göncüoğlu, M.C., and Yalınız, M.K., 2002. Petrology of the Kurancali phlogopitic Metagabbro: an Island Arc-Type Ophiolitic sliver in the Central Anatolian Crystalline Complex. Ofioliti, 27(1), p. 75.

Toksoy-Köksal, F., Türkmenoğlu, A.G., and Göncüoğlu, M.C., 2001b. Vermiculitization of phlogopite in metagabbro, central Turkey. Clays and Clay Minerals, 49(1), 81-91.

Toksoy-Köksal, F., Türkmenoğlu, A., and Göncüoğlu, M.C., 2000. Vermiculite from pegmatitic phlogopitic gabbro, Central Turkey. 37th Annual (Wy-2-K$^+$) Meeting, The Clay Minerals Society, June 24-29, 2000, Chicago-U.S.A., Abstracts, p. 116.

Toksoy-Köksal, F., Türkmenoğlu, A., İçöz, S., and Göncüoğlu, M.C., 1999. Vermiculitization of phlogopites within metagabbro, Central Turkey. EUROCLAY'99, Conference of the European Clay Groups Associations, September 5-9, 1999, Krakow-Poland, Abstracts, p. 138.

Tribuzio, R., Tiepolo, M., and Thirlwall, M.F., 2000. Origin of titanian pargasite in gabbroic rocks from the Northern Apennine ophiolites (Italy): insights into the late-magmatic evolution of a MOR-type intrusive sequence. Earth and Planetary Science Letters, 176, 281-293.

Tribuzio, R., Tiepolo, M., Vannucci, R., and Bottazzi, P., 1999. Trace element distribution within olivine-bearing gabbros from the Northern Apennine ophiolites (Italy): Evidence for post-cumulus crystallization in MOR-type gabbroic rocks. Contributions to Mineralogy Petrology, 134, 123-133.

Tüysüz, O., Dellaloğlu, A., and Terzioğlu, N., 1995. A magmatic belt within Neotethyan suture zone and its role in the tectonic evolution of northern Turkey. Tectonophysics, 243(1/2), 173-191.

Van Achterbergh, E., Grifffin, W.L., and Stiefenhofer, J., 2001. Metasomatism in mantle xenoliths from the Letlhakane kimberlites: estimation of element fluxes. Contributions to Mineralogy and Petrology, 141,397-414.

Van Kooten, G.K., 1980. Mineralogy, petrology, and geochemistry of an ultrapotassic basaltic suite, Central Sierra Nevada, California, U.S.A. Journal of Petrology, 21(4), 651-684.

Velde, D., 1979. Trioctahedral micas in melilite-bearing eruptive rocks. Carn. Ins. Washington Yerab., 78, 468-475.

Verhulst, A., Balaganskaya, E., Kirnarsky, Y., and Demaiffe, D., 2000. Petrological and geochemical trace elements and Sr–Nd isotopes characteristics of the Paleozoic Kovdor ultramafic, alkaline and carbonatite intrusion Kola Peninsula, NW Russia. Lithos, 51, 1–25.

Vieten, K., and Hamm, H.-M., 1978. Additional notes "on the calculation of the crystal cehmical formula of clinopyroxenes and their contents of Fe^{3+} from microprobe analyses. Neues Jahrbuch fur Mineralogie, Monatshefte, 71-83.

Volfinger, M., and Robert, J.-L., 1980. Structural control of the distribution of trace elements between silicates and hydrothermal solutions. Geochimica et Cosmochimica Acta, 44, 1455-1461.

Volfinger, M., Robert, J.-L., Vielzeuf, D., and Neiva, A.M.R., 1985. Structural control of the chlorine content of OH-bearing silicates (micas and amphiboles). Geochimica et Cosmochimica Acta, 49, 37-48.

Wagner, C., and Velde, D., 1986. The mineralogy of K-richterite bearing lamproites. American Mineralogist, 71, 17–37.

Wang, Z., Sun, S., Li, J., and Hou, Q., 2002. Petrogenesis of tholeiite associations in Kudi ophiolite (western Kunlun Mountains, northwestern China): implications for the evolution of back-arc basins. Contributions to Mineralogy and Petrology, 143, 471–483.

Wang, Z.H, Sun, S., Hou, Q.L., and Li, J.L., 2001. Effect of melt-rock interaction on geochemistry in the Kudi ophiolite (western Kunlun Mountains, northwestern China): implication for ophiolite origin. Earth and Planetary Science Letters,191(1/2), 33-48.

Wass, S.Y., 1979. Fractional crystallization in the mantle of late-stage kimberlitic liquids - evidence in xenoliths from the Kiama area, N.S.W, Australia. In: Boyd, F.R., Meyer, H.O.A. (eds.), The Mantle Sample: Inclusions in Kimberlites and Other Volcanics. Am. Geophys. Union, Washington, U.S.A., 366-373.

Waters, F.G., and Erlank, A.J., 1988. Assesment of the vertical extent and distribution of mantle metasomatism below Kimberley, SouthAfrica. Journal of Petrology, Special Publication Lithosphere Issue, 185-204.

White, W.M., 1995. Geochemical tracers of mantle processes. Review of Geophysics, 33, 19-24.

Wilson, M., 1989. Igneous Petrogenesis. A Global Tectonic Approach. Unwin Hyman, London, 466 p.

Winchester, J.A., and Floyd, P.A., 1977. Geochemical discrimination of different magma series and their differentiation products using immobile elements. Chemical Geology, 20, 325–342.

Wones, D.R., and Eugster, H.P., 1965. Stability of biotite: experiment, theory and applications. American Mineralogist, 50, 1228-1272.

Wood, D.A., 1978. Major and trace element varaitions in the Tertiary lavas of eastern Iceland and their significance with respect to the Iceland Geochemical Anomaly. Journal of Petrology, 19, 393-436.

Wood, D.A., 1980. The application of a Th-Hf-Ta diagram to problems of tectonomagmatic classification and to establishing the nature of crustal contamination of basaltic lavas of the British Tertiary volcanic province. Earth and Planetary Science Letters, 50, 151-162.

Woodhead, J., Eggins, S., and Gample, J., 1993. High field strength and transition element systematics in island arc and back-arc basin basalts: evidence for multiphase melt extraction and a depleted mantle wedge. Earth Planetary Science Letters, 114, 491-504.

Woodland, A.B., Kornprobst, J., McPherson, E., Bodinier, J.-L., and Menzies, M.A., 1996. Metasomatic interactions in the lithospheric mantle: Petrologic evidence from the Lherz Massif, French Pyrenees. Chemical Geology, 134, 83-112.

Wulff-Pedersen, E., Neumann, E.-R., and Jensen, B.B., 1996. The upper mantle under La Palma, Canary Islands: formation of Si-K-Na-rich melt and its importance as a metasomatic agent. Contributions to Mineralogy and Petrology, 125, 113-139.

Wyllie, P.J., and Sekine, T., 1982. The formation of mantle phlogopite in subduction zone hybridization. Contributions to Mineralogy and Petrology, 79, 375-380.

Yalınız, M.K., 1996. Petrology of the Sarıkaraman Ophiolit (Aksaray-Turkey). Ph.D. Thesis in Geological Engineering, Middle East Technical University, Ankara, 270 p. (unpublished).

Yalınız, M.K., and Göncüoğlu, M.C., 1998. General geological characteristics and distribution of the Central Anatolian Ophiolites. Hacettepe Üniversitesi Yerbilimleri Dergisi, 20, 19-30. (in Turkish).

Yalınız, M.K., and Göncüoğlu, M.C., 1999. Clinopyroxene compositions of the isotropic gabbros from the Sarıkaraman Ophiolite: New evidence on supra-subduction zone type magma genesis in Central Anatolia. Turkish Journal of Earth Sciences, 8, 103-111.

Yalınız, M.K., Floyd, P.A., and Göncüoğlu, M.C., 1996. Supra-subduction zone ophiolites of Central Anatolia: geochemical evidence from the Sarıkaraman Ophiolite, Aksaray, Turkey. Mineralogical Magazine, 60, 697-710.

Yalınız, M.K., Floyd, P.A., and Göncüoğlu, M.C., 2000a. Geochemistry of volcanic rocks from the Çiçekdağ Ophiolite, Central Anatolia, Turkey, and their inferred tectonic setting within the northern branch of the Neotethyan Ocean. In: Bozkurt, E., Winchester, J.A., and Piper, J.D.A. (eds.), Tectonics and Magmatism in Turkey and the Surrounding Area. Geological Society of London, Special Publication, 173, 203-218.

Yalınız, M.K., Floyd, P.A., and Göncüoğlu, M.C., 2000b. Petrology and geotectonic significance of plagiogranite from the Sarıkaraman Ophiolite (central Anatolia, Turkey). Ofioliti, 25(1), 31-37.

Yalınız, M.K., Göncüoğlu, M.C., and Özkan-Altıner, S., 2000c. Formation and emplacement ages of the SSZ-type Neotethyan ophiolites in Central Anatolia, Turkey: palaeotectonic implications. Geological Journal, 35, 53-60.

Yalınız, M.K., Aydın, N.S., Göncüoğlu, M.C., and Parlak, O., 1999. Terlemez quartz monzonite of Central Anatolia (Aksaray-Sarıkaraman): age, petrogenesis and geotectonic implications for ophiolite emplacement. Geological Journal, 34, 233-242.

Yavuz, F., Gültekin, A.H., Örgün, Y., Çelik, N., Çelik-Karakaya, M., and Şaşmaz, A., 2002. Mineral chemistry of barium- and titanium-bearing biotites in calc-alkaline volcanic rocks from the Mezitler area (Balıkesir-Dursunbey), western Turkey. Geochemical Journal, 36, 563-580.

Yaxley, G.M., Crawford, A.J., and Green, D.H., 1991. Evidence for carbonatite metasomatism in spinel peridotite xenoliths from western Victoria, Australia. Earth and Planetary Science Letters, 107, 305-317.

Yılmaz, Y., Tüysüz, O., Yiğitbaş, E., Genç, S.C., and Şengör, A.M.C., 1997. Geology and tectonic evolution of the Pontides. In: Robinson, A.G. (ed.), Regional and Petroleum geology of the Black Sea and surrounding region. American Association of Petroleum Geology, Memorial, 68, 183-226.

Yılmaz-Şahin, S., and Boztuğ, D., 1997. Petrography and whole-rock chemistry of the gabbroic, monzogranitic and syenitic rocks from the Cicekdag region, N of Kırsehir, Central Anatolia, Turkey. In: Boztug, D., Yılmaz-Şahin, S., Otlu, N., and Tatar, S. (eds.), Proceeding of TÜBİTAK-BAYG/NATO-D PROGRAM on Alkaline Magmatism (Theoretical Consideration and Field Excursion in Central Anatolia), 2-10 October, 1997, Dept. of Geology, Cumhuriyet University, Sivas-Turkey, 29-42.

Yılmaz-Sahin, S., and Boztuğ, D., 1998. Petrogenesis of the Çiçekdağ Igneous Complex, N of Kırşehir, Central Anatolia, Turkey. Turkish Journal of Earth Sciences, 7, 185-200.

Yogodzinski, G.M., Kay, R.W., Volynets, O.N., Kolosov, A.V., and Kay, S.M., 1995. Magnesian andesite in the western Aleutian Komandorsky region: implications for slab melting and processes in the mantle wedge. Bulletin of Geological Society of America, 107, 505-519.

Yogodzinski, G.M., Volynets, O.N., Koloskov, A.V., Seliverstov, N.I., and Matvenkov, V.V., 1994. Magnesian andesites and the subduction component in a strongly calc-alkaline series at Piip Volcano, Far western Aleutians. Journal of Petrology, 35, 163-204.

Yogodzinski, G.M., Lees, J.M., Churikova, T.G., Dorendorf, F., Woerner, G., and Volynets, O.N, 2001. Geochemical evidence for the melting of subducting oceanic lithosphere at plate edges. Nature, 409, 500-504.

Zanetti, A., Mazzucchelli, M., Rivalenti, G., and Vannucci, R., 1999. The Finero phlogopite-peridotite massif: an example of subduction-related metasomatism. Contributions to Mineralogy and Petrology, 134,107-122.

Zanetti, A., Vannucci, R., Bottazzi, P., Oberti, R., and Ottolini, L., 1996. Infiltration metasomatism at Lherz as monitored by systematic ion-microprobe investigations close to a hydrous dike. Chemical Geology, 134, 113-133.

Zinngrebe, E., and Foley, S.F., 1995. Metasomatism in mantle xenoliths from Gees, West Eifel, Germany: evidence for the genesis of calc-alkaline glasses and metasomatic Ca-enrichment. Contributions to Mineralogy and Petrology, 122, 79-96.

VITA

Fatma (TOKSOY) KÖKSAL was born in Abadan, ANKARA on January 06, 1972. She received her B.S. degree in 1994 and M.S. degree in 1998 from the Middle East Technical University.

She worked in Incorporated Joint Stock Company of Kalebodur Ceramic Industries, Çanakkale, Turkey in 1995. She has been research assistant since 1997 in the Department of Geological Engineering, Middle Technical University. Her main areas of interest are mineralogy and petrology of magmatic rocks.

She began her Ph.D. studies at the Department of Geological Engineering, Middle Technical University in 1998. She was awarded research fellowships by DAAD (Germany) for two times (2 months between October-December 2001, 6 months between May 2002-October 2002), and by TUBİTAK (NATO-A2) (Turkey) (4 months between November 2002-February 2003) to study in Potsdam University, Germany. She was also awarded travel grants to participate international congress by TÜBİTAK in 1999, and by the Clay Minerals Society in 2000. Moreover, she was awarded by TÜBİTAK during 1996-1997 to continue her M.S. study.

She has 5 papers and 1 abstract, 3 of papers and 1 abstract in international and 2 of papers in national journals. She has 5 presentations at international and 1 presentations at national conferences. A paper is in review in an international journal. She was editor of two proceeding books.

She has been married since 1999.